EXAMINING THE PRESENCE OF ARCHING ACTION IN EDGE-STIFFENED BRIDGE DECK CANTILEVER SLAB OVERHANGS SUBJECTED TO A STATIC AND FATIGUE WHEEL LOAD

By:

Chad Klowak

A Thesis
submitted to the Faculty of Graduate Studies of the University of Manitoba
in partial fulfillment of the requirements
for the degree of

Doctor of Philosophy

Department of Civil Engineering
University of Manitoba
Winnipeg, Manitoba, Canada

This Thesis is dedicated to my beautiful wife Sarah for her loving support throughout my many years as a student. We have come along way together in the last twelve years together with our marriage, the building of our dream log home, and the birth of our two baby girls Kenzie and Presley. It is also dedicated to Kenzie and Presley for their time spent sitting by me at the computer for their curiosity and assistance. I am an extremely lucky man to have been blessed with three precious ladies and the time I have with them. Finally, I would like to dedicate this work to my parents, Steve and Arlene Klowak, and express my sincere gratitude for their persistence and faith in me when I wanted to give up school so many years ago. Without my parents I would not be living my dreams today.

ACKNOWLEDGEMENTS

I would like to thank my supervisor Dr. Aftab Mufti for his ideas, guidance, supervision, and financial support, throughout the course of this project. I would also like to thank him for his mentorship and that something that he saw in me 14 years ago when he asked me to become an engineer for the W.R. McQuade Heavy Structures Laboratory. Dr. Mufti provided the financial support with the assistance from the ISIS Canada Resource Centre. I would like to express my gratitude to Dr. Baidar Bakht for his co-supervision and thoughtful advice on all aspects related to the research program and presentation of data.

I would also like to thank the technical staff of the W.R. McQaude Heavy Structures Laboratory. Mr. Moray McVey and Mr. Grant Whiteside provided the technical assistance during the construction and Mr. Brendan Pachal for aiding with the demolition and removal of the full-scale innovative bridge deck. Testing assistance was provided by Mr. Cody Scaletta and is respectfully appreciated. I would also like to kindly acknowledge the assistance provided by Mr. Amir Ghatefar with the finite element modelling aspect of the project.

The editing assistance of Mr. David Amorim is greatly appreciated. I would like to graciously thank my advisory committee Dr. Dagmar Svecova and Dr. Douglas Thompson for taking the time to review my work and provide their input into the study as well. Finally, I express my thanks to Dr. David Cleland for travelling across the pond to serve as my external examiner.

ABSTRACT

Engineers proposed the idea that arching action present may be present in bridge deck cantilever slab overhangs, stiffened along their longitudinal free edge via a traffic barrier, subjected to a wheel load. The experimental research program consisted of the design, construction, and static as well as fatigue destructive testing of a full-scale innovative bridge deck slab complete with two traffic barrier walls.

The observed experimental data provided extremely interesting findings that indicated a very strong presence of arching action in edge-stiffened cantilever slab overhangs subjected to static and fatigue wheel loads. Deflection profiles indicated curvatures that contradict classical flexural behavior. Large tensile strain magnitudes on the bottom reinforcing mat in all cantilever test locations as well as cracking patterns dictate behavior typical to arching action. Top transverse strains measured did not agree with flexural theory and patterns confirmed earlier research finding that the quantity of top transverse reinforcement may be reduced. Compressive strains measured on the top surface of the cantilever contradicted flexural theory and confirmed the presence of arching action. Punching shear modes of failure observed in all test locations also strengthened the argument for the presence of arching action. Theoretical and analytical modeling techniques were able to validate and confirm the experimental test results.

Based on experimental research findings and analytical modeling researchers were able to confirm a major presence of arching action in edge-stiffened cantilever slab overhangs subjected to static and fatigue wheel loads. Recommendations include a proposed reduction in top transverse reinforcement provided in the adjacent internal panel due to the presence arching action that could contribute to a significant initial capital cost savings. Based on the research findings, the report also suggests potential provisions to design codes that take into account the presence of arching action. Further research and theoretical modeling is still required to better understand the presence of arching action in edge-stiffened cantilever slab overhangs. Additional testing and a demonstration project complete with civionics and structural health monitoring will aid engineers in the implementation of the break-through findings highlighted in this study.

TABLE OF CONTENTS

LIST OF FIGURES

1. INTRODUCTION

2. LITERATURE REVIEW

3. EXPERIMENTAL PROGRAM

4. EXPERIMENTAL RESULTS

5. ANALYTICAL MODELS

6. CONCLUSIONS & RECOMMENDATIONS

LIST OF TABLES

2. LITERATURE REVIEW

3. EXPERIMENTAL PROGRAM

4. EXPERIMENTAL RESULTS

5. ANALYTICAL MODELS

LIST OF SYMBOLS

2. LITERATURE REVIEW

S_c	Cantilever Span
M_x	Moment intensities in the x direction
M_y	Moment intensities in the y direction
PC	Total moment at the root of the cantilever
P	Total load
C	Transverse distance from the root of the cantilever
A_L	Area under the curve to the left side of the transverse free edge f the cantilever
A_R	Area under the curve to the right side of the transverse free edge of the cantilever
A'	Numerical coefficient that depends on location of the load
π	Mathematical constant pi
x	Distance along the x direction
y	Distance along the y direction
B	Numerical coefficient A' divided by 2
S	Internal panel span
D	Numerical coefficient similar to B determined from rigorous analysis
x_{edge}	Distance from the concentrated load to the nearest free edge
X	Distance at the reference point at the root of the cantilever to the nearest transverse free edge equal to $x + x_{edge}$

5. ANALYTICAL MODELS

σ_c^{ef}	Concrete effective stress
ε^{eq}	Concrete equivalent uniaxial strain
σ_{ci}	i^{th} uniaxial concrete strain
E_{ci}	i^{th} uniaxial concrete modulus of elasticity
f'^{ef}_c	Concrete peak compressive effective stress
f'^{ef}_t	Concrete peak tensile effective stress
ε_c	Concrete compressive strain
ε_t	Concrete tensile strain
f'_c	28 day concrete uniaxial cylinder strength
a	Ratio of concrete principle/normal stresses
σ_{c1}	Concrete principle/normal stress in direction one
σ_{c2}	Concrete principle/normal stress in direction two
f_{co}	Initial concrete stress at the beginning of the non-linear stress versus strain curve

ε_{cp}	Concrete plastic strain at the maximum concrete stress
$\varepsilon_{eq}{}^{p}$	Equivalent concrete plastic strain
L_c	Length scale parameter for transforming concrete strains to displacements
w_d	Softening concrete compressive displacement
τ	Bond shear stress for reinforcing bars
τ_{max}	Maximum bond shear stress for reinforcing bars
τ_f	Failure bond shear stress for reinforcing bars
s	Slip displacement
s_1	Slip displacement at maximum bond stress
s_2	Slip displacement 2 at maximum bond stress
s_3	Slip displacement at bond failure
$\delta_{u(Theoretical)}$	Ultimate or maximum deflection due to theoretical ultimate load
$P_{u(Theoretical)}$	Theoretical ultimate load
M_{rc}	Un-factored transverse bending moment in the cantilever span
M_{ri}	Un-factored transverse bending moment in the internal panel
P	Concentrated wheel load
B_c	Coefficient for determining bending moment in cantilever span
B_i	Coefficient for determining bending moment in internal panel
x	Distance along the *x* direction
y	Distance along the *y* direction
y_c	Distance along cantilever in the *y* direction
y_i	Distance along internal panel in the *y* direction
n	Number of cycles to fatigue failure
c	Constant for determining fatigue life
P	Applied cyclic fatigue load
P_u	Ultimate static load

1. INTRODUCTION

1.1 Overview

This thesis is comprised of 6 Chapters. It begins with an introduction that briefly highlights the current condition of today's transportation infrastructure, specifically bridge deck slabs. The opening chapter also discusses the motivation and hypothesis for conducting this research project as well as the objectives and scope of work. Chapter 2 summarizes bridge deck cantilever slab state-of-the-art. Definitions and fundamentals on the mechanics of behaviour and methods of design and analysis for cantilever slab overhangs are presented. Previous research which has provided valuable insight and the interest to re-investigate the presence of arching action in cantilever overhangs is reviewed. The experimental testing program is explained in Chapter 3. It includes the structural details of the bridge deck slab, testing scheme, test set-up, and testing procedures. More specifically, it describes the details related to the construction, instrumentation, and methods of testing a full-scale bridge cantilever slab overhangs to failure. Preliminary experimental test results are summarized in Chapter 4. The results are presented as they relate to the static and fatigue behaviour of the cantilevers. Results are classified with respect to deflection, strain measurements, crack patterns and crack widths, and modes of failure. Chapter 5 provides uses various analytical tools and modeling to confirm the experimental findings and determines if current engineering theory provides the same results. Chapter 6 provides a summary of the major research findings and a number of important conclusions along with supporting arguments. The chapter concludes with some recommendations for future work related to the completion of this research project.

1.2 Background

The aging and deterioration of highway infrastructure throughout North America is a well-known and documented problem. The majority of today's highway infrastructure network in Canada was constructed between 1950 and 1965 following World War II (Eden et al. 2004). At that time, bridges were typically designed for a service life of 50 years. Consequently, a large percentage of bridges are now at, or approaching, the end of their design service life.

Bridge deck slabs, perhaps, are the most important component of a bridge's superstructure. They are directly subjected to the loads induced by passing traffic. They are also the component of a bridge's superstructure that is the most exposed to environmental effects (Figure 1-1(a)). One of the major contributors to the deterioration of concrete bridge deck slabs in colder climates is the penetration of chlorides as a result of the application de-icing chemicals or other ice retarding agents (Figure 1-1(b)). Chloride penetration into the concrete deck accelerates the deterioration of the internal reinforcing steel. Concrete bridges in marine environments also deteriorate at an increased rate due to exposure to salt water. Steady increases in allowable truck weights have also proven to be a contributing factor to the deterioration of highway bridges. Many existing bridges were designed for a service life of 50 years. Many case studies have demonstrated that concrete bridge deck slabs have not been able to withstand the environmental and service conditions that they are subjected to. It is well known and documented that bridge deck slabs across Canada have required rehabilitation or complete replacement prior to their 50 year projected service life.

Figure 1-1(a): Winter conditions common to many Canadian highway bridges

Figure 1-1(b): Deterioration caused by the corrosion of internal steel reinforcement in a cantilever overhang

1.3 Motivation and Hypothesis

Research conducted by Gant and Newhook (1999), summarized in Chapter 2, revealed findings that led Klowak and Mufti (2007) to re-investigate the presence of arching-action in un-stiffened bridge deck cantilever slab overhangs subjected to a concentrated or wheel load. The results obtained from the static and fatigue destructive tests conducted by Klowak (2007), presented in Chapter 2, initiated researchers to question earlier testing performed by Drysdale (1982) and Bakht and Agarwal (1995) that confirmed flexural theories still used today to design and analyze cantilever slabs. A brief description of tests conducted by Drysdale (1982) and Bakht and Agarwal (1995) are provided in Chapter 2.

It is well known and documented that the internal panels of bridge deck slabs, when subjected to wheel loads induced by passing traffic, exhibit arching-action behavior in response to applied concentrated loads (Figure 1-2). Mufti and Bakht hypothesized and proposed the idea that the cantilever slab overhang of a bridge deck exhibits a component of arching-action when subjected to a wheel load (Figure 1-3). The thought or idea behind the rational was that the cantilever slab does not "feel", behave, or act differently if it is supported from above or below. The only exception or difference between an internal panel and a cantilever overhang is that the cantilever overhang is subjected to dead loads of the traffic barrier which may act like an inverted supporting girder (from above). Figure 1-4 illustrates an idealization of a bridge deck slab supported by multiple girders. Consider the outer panel of the bridge deck slab. The theory behind the hypothesis can essentially be phrased as a question: Does the outer panel or cantilever span of the bridge deck "know" or

"feel" how it is being supported (i.e. with the exception of the dead weight of the barrier wall)? Is there a physical difference between the two different idealizations presented in Figure 1-4)?

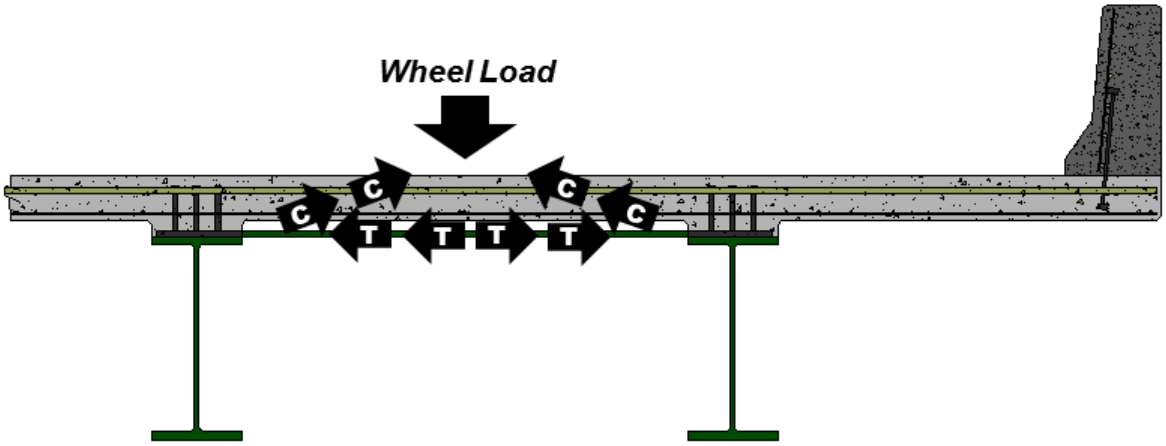

Figure 1-2: Arching-action typical to the internal panel of bridge deck slabs

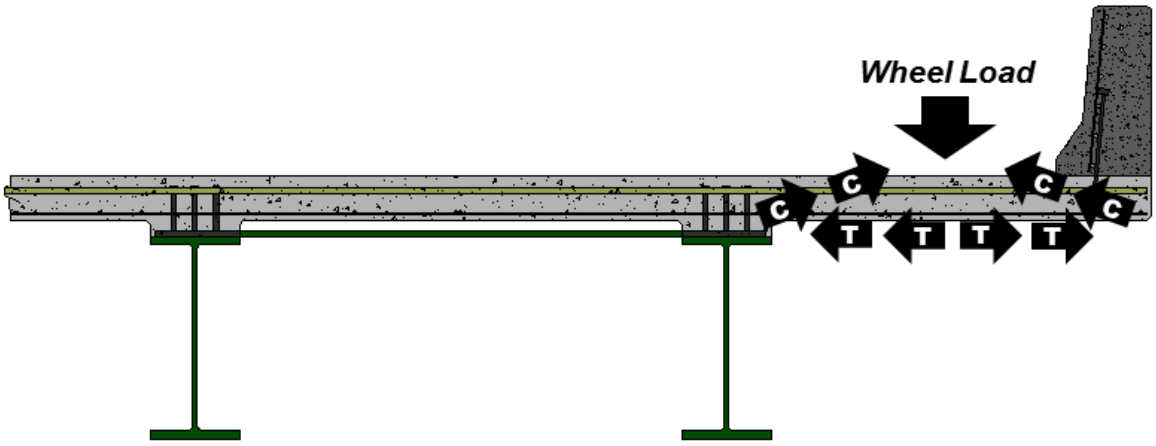

Figure 1-3: Hypothesis of arching-action behavior present in cantilever slab overhangs subjected to a wheel load

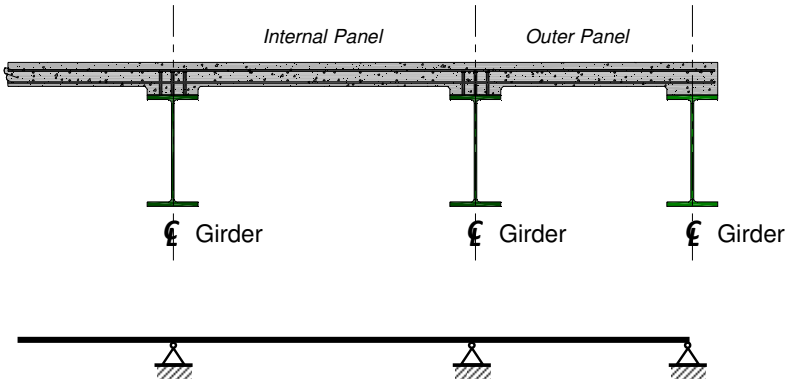

(A) Idealization of Outer Panel Supported by Bridge Girder

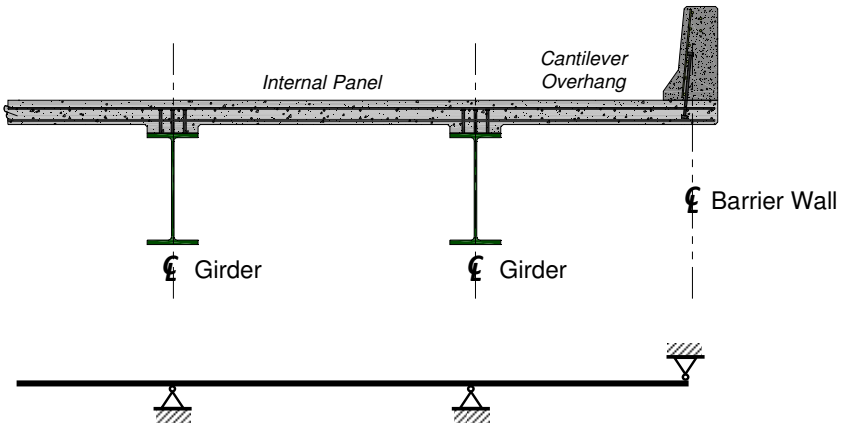

(B) Idealization/Hypothesis of Outer Panel or Cantilever Overhang Supported By Traffic Barrier Wall

Figure 1-4: Idealization and hypothesis of a bridge deck cantilever slab overhang slab supported by traffic barrier wall

1.4 Objectives

The primary objective of this research was to investigate the static and fatigue behaviour of edge-stiffened cantilever slab overhangs, typical to girder bridges, subjected to a wheel load.

The heaviest loads that a cantilever overhang will see in its life time are from the wheel loads from passing traffic or a collision or impact of the barrier wall.

Wheel loads from tractor trailers or heavy trucks tend to be the most critical. Current analysis and design is based on the assumption that the load effects and the response of a bridge deck cantilever slab overhangs is purely flexural. The flexural effects are not only limited to the overhangs, but also extend into the adjacent internal panel of the bridge deck slab. Several objectives related to examining the presence of arching-action in bridge deck cantilever slabs were established and are summarized as follows:

- Establish if the response of a cantilever slab overhang subjected to a static monotonic wheel (concentrated) load is purely flexure or if arching-action is present;
- Ascertain if the response of a cantilever slab overhang subjected to a cyclic fatigue wheel (concentrated) load is purely flexure or if arching-action is present;
- Determine the load induced effects on the internal panel when the cantilever slab overhang is subjected to a static monotonic and fatigue cyclic wheel (concentrated) load;
- Investigate analytic tools for predicting the theoretical behaviour of bridge deck cantilevers subjected to a wheel (concentrated) load;
- Determine, if possible, magnitudes of arching-action and flexural responses to applied monotonic static and cyclic fatigue wheel loads; and
- Look at the possibility of proposing possible design alternatives or changes to current cantilever design methods.

1.5 Potential Structural Engineering and Economic Applications

Based on static and fatigue destructive testing conducted by Klowak (2007), and Gant and Newhook (1999) on un-stiffened cantilever slab overhangs, it was appropriate to investigate the presence of arching-action in a cantilever slab overhang stiffened with a traffic barrier wall. Consequently, if the presence of arching-action can be confirmed, there may be design or analysis alternatives that may have engineering and economic applications. Klowak (2007) suggested that the top transverse reinforcing bars may be terminated half way to the next adjacent girder since negative moments are not distributed completely to the adjacent girder. Such a design change would result in a large reduction in capital costs for the reinforcement required for bridge deck cantilever slab overhangs. The research conducted for this experimental program aims to confirm that conclusion so that appropriate changes may be made to bridge codes. Recent increases in the price of reinforcing steel along with the acceptance of fibre reinforced polymers (FRPs) have made these two different reinforcing materials very competitive. As engineers begin to consider the life cycle cost of using materials such as FRPs, they can design and construct bridge deck slabs that are far more durable than in the past. If arching-action plays a dominant role in the behaviour of bridge deck cantilever slab overhangs subjected to wheel loads, there may be design changes that may have economic impacts as well.

1.6 Scope of Work

The scope of work involved for this research project encompassed many different aspects of structural engineering. The work included:

- The structural design, construction and static as well as fatigue destructive testing of a full-scale reinforced concrete bridge deck slab reinforced with steel and GFRP reinforcement for the purposes of investigating the presence of arching-action in cantilever overhangs
- The complete design and installation of a civionics system prior to testing for monitoring deflections, strains, and crack widths;
- The design and construction of a load frame including a hydraulic actuator capable of failing such a reinforced concrete bridge deck slab under static monotonic and cyclic fatigue loading conditions;
- The design of a testing scheme to ensure that different test locations would not affect the behavior of another;
- The complete analysis of all experimental data; and
- The use of analytical tools that incorporate classical engineering analysis methods and finite element methods to investigate the goals associated with examining the presence of arching-action.

All of the above tasks were required to successfully complete the experimental program of investigating the presence of arching-action in cantilever slab overhangs subjected to static and fatigue wheel loads. The tasks described above provided extensive training in the design of innovative structures using FRPs and the experience necessary to implement the evolving practice of civionics and structural health monitoring. The scope of work was an excellent learning experience for any young, intermediate, or even senior engineer pursuing or having career in structural or bridge engineering.

2. LITERATURE REVIEW

Some terms associated with bridge deck cantilevers may be uncommon to some readers, thus, the chapter begins with a definition of a bridge deck cantilever and associated terms. It then discusses the behaviour mechanisms and methods of analysis for cantilever slabs. A brief overview of FRP materials is presented. Related research conducted at Dalhousie University is described before providing a design example for an unstiffened bridge deck cantilever at the end of the chapter to demonstrate current design methods.

2.1 Definition of a Bridge Deck Cantilever Slab Overhang

It is customary in bridge analysis to refer to the longitudinal direction as the direction of traffic flow on the bridge. The longitudinal direction is parallel to the girders of a slab-on-girder bridge. The transverse direction is taken as the direction perpendicular to the flow of traffic. For the purposes of the remaining discussion, the *x*- and *y*- axes are defined as the longitudinal and transverse directions respectively.

> A ***BRIDGE DECK CANTILEVER***, also referred to as a ***cantilever slab*** **or** ***cantilever overhang***, is typically the portion of a concrete deck slab that projects transversely beyond the outermost girders of a girder bridge. These overhangs are usually provided for economic reasons and aesthetics (Mufti et al., 1996).

Several other terms and geometries are associated with the behaviour of bridge deck cantilevers. They should be described, with the help of Figure 2-1, prior discussing the methods of analysis for cantilever overhangs.

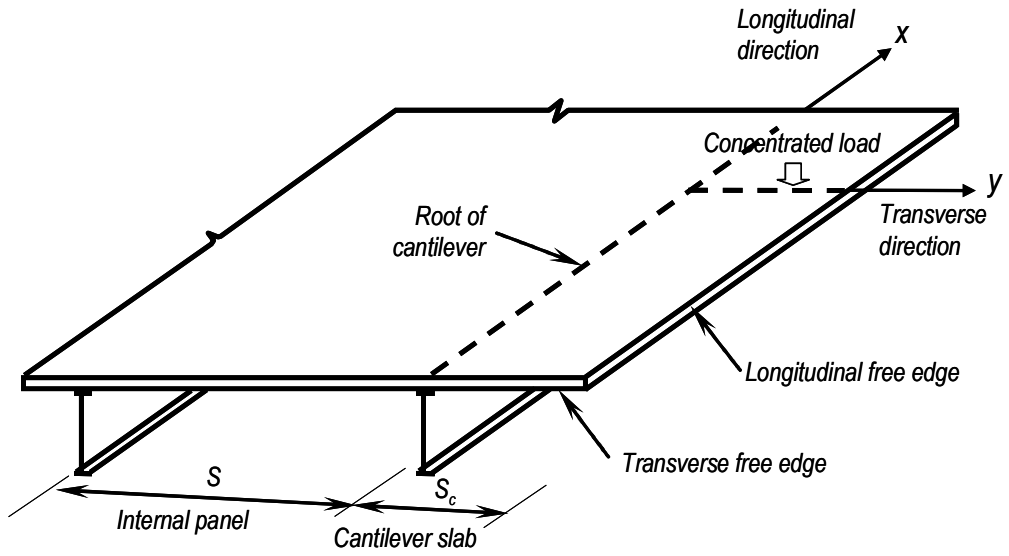

Note: Published with the permission of Mufti et. al. (2008)

Figure 2-1: Typical notations of a bridge deck cantilever slab overhang

The ***root*** of a cantilever, simply stated, is the support of a cantilever. It provides some measure of restraint against rotation and vertical deflection. These restraints may individually be infinite or finite. The root of a cantilever, as it relates to bridges, is the outermost girder.

The free edges of a bridge deck cantilever overhang are parallel and perpendicular to the root or the outermost girder. The ***transverse free edge*** is the edge of the slab perpendicular to the girder (root) and the ***longitudinal free edge*** is the edge parallel to the girder (root).

The ***cantilever span*** is defined as the transverse distance between the longitudinal free edge and the root. The cantilever span is denoted as, $S_{c,}$ in Figure 2-1. Some design codes require that the root of the cantilever be taken as the outer edge of the girder, if the girder is constructed of concrete. This practice is only justifiable if the cantilever slab is assumed to be fully fixed against rotation at its root. For the purposes of this report, the root is defined as the center-line of the girder.

2.2 Methods of Analysis

It is customary in deck slab analysis to refer to moments and shears on a per-unit-length basis; these quantities are called ***moment intensities*** and ***shear intensities*** and they have the units of force-length/length and force/length, respectively. The moment intensities along the *x* direction are denoted as M_x and the moment intensities acting in the *y* direction are denoted as M_y. The moment intensities in the *y* direction are usually more significant in cantilever slabs and are referred to either as transverse moment intensity or cantilever moment intensity. Consistent with the terminology or sign convention used in textbooks on plate analysis, the moment intensity causing tension in the top fibres of the cantilever is regarded as negative. On the other hand, moment intensity causing tension in the bottom fibres is defined as positive.

If the transverse free edges of a cantilever are far enough away from the applied load that they do not affect the behaviour or load distribution, the cantilever is considered a ***cantilever of infinite length***.

When one of the transverse free edges of a cantilever is close enough to the applied load to have an influence on its behaviour, the cantilever is said to be a ***cantilever of semi-infinite length***.

The ***internal panel*** can be described as the portion of a bridge deck slab which is located between the outermost girder and the girder immediately adjacent to it. When a load is applied to a cantilever, the effects due to the load are not limited to the cantilever overhang. Effects are also distributed to the internal panel. On a multi-girder bridge, these effects are only significant in the internal panel adjacent to the cantilever.

Cantilevers sometimes vary in thickness linearly in the transverse direction. The variation in thickness is referred to as the ***thickness ratio***. The two depths considered in determining the thickness ratio are the thickness at the root and the thickness at the tip. The methods of analysis described in the following sections are based on classical plastic plate theory and are highlighted in more detail by Mufti et al. (2008).

2.2.1 Behaviour of a Cantilever of Infinite Length

The discussion of this section relates to the behaviour of the cantilever overhang if the cantilever is considered to be infinite in length when it is subjected to a concentrated load. Figure 2-2 illustrates the distribution of moment intensities, M_y, at the root of the cantilever and at a location between the concentrated load and the root. The patterns of moment intensities at the two sections are similar. They are bell-shaped with a well-defined, but not

sharp, peak. In the longitudinal direction, the moment intensity drops from the peak and gradually reduces to zero. The peak moment intensity is greater at the root than the peak intensity at the section between the concentrated load and the root. The moment intensity at the root diminishes to zero at a much greater value of x than at the other section. The locations where M_y drops to zero define a boundary of the zone of influence as a result of the concentrated load. It can be appreciated that the zone of influence spreads out in the longitudinal direction as the reference section moves away from the load towards the root of the cantilever.

Figure 2-2 demonstrates that the total area under the curves is equal to the total cantilever moments at the respective sections. The total moment at the root of the cantilever is PC, where P is the total load and C is the transverse distance from the root. The total moment (area under the curve) at a longitudinal section is determined from static equilibrium and is not affected by any other factors. It is dependent only on the magnitude of the load and its distance from the section considered.

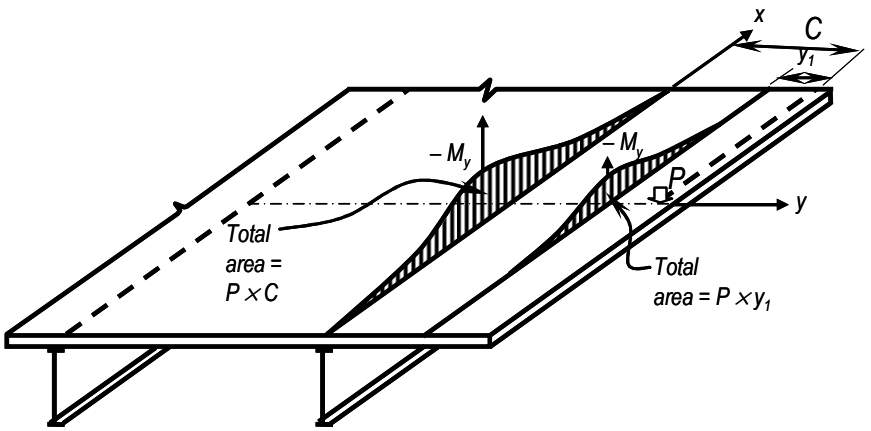

Note: Published with the permission of Mufti et. al. (2008)

Figure 2-2: Distribution of transverse negative moment intensities in the cantilever overhang due to a concentrated load

2.2.1.1 Transverse Negative Moments in the Internal Panel

To examine the distribution of negative moments in the internal panel adjacent to a cantilever overhang, a beam having a simple support at one end and a cantilever overhang beyond the other with a concentrated load on it can be considered. The statically determinant negative moment in the beam varies linearly from zero at the simple support to a maximum moment at the other. There are no other similarities between beam analogy and an actual deck slab. The negative moment intensity, M_y, at a transverse section in the internal panel does not vary linearly along the transverse direction although the total negative moment does.

The ratio of span of the cantilever and span of the internal panel along with the thickness ratio are two factors that affect the transverse variation of the peak intensity moment. The ratio of the two has a more pronounced effect. Three cantilever slabs have spans of the cantilever overhang and internal panel as shown in Figure 2-3. Each is subjected to the loads shown as well. The loads were chosen to induce the same peak moment intensity, M_y, at the root of the cantilever. The variation in peak moment intensities tends to become linear as the span of the cantilever becomes very large related to the span of the internal panel. Alternatively, the distribution in moment intensity becomes non-linear as the cantilever span becomes short compared to the span of the internal panel. It can be said that the increase in span of the internal panel has the beneficial effect of reducing the degree of transverse rotational restraint at the root of the cantilever (girder center-line), leading to a rapid decrease of the peak moment intensity in the internal panel.

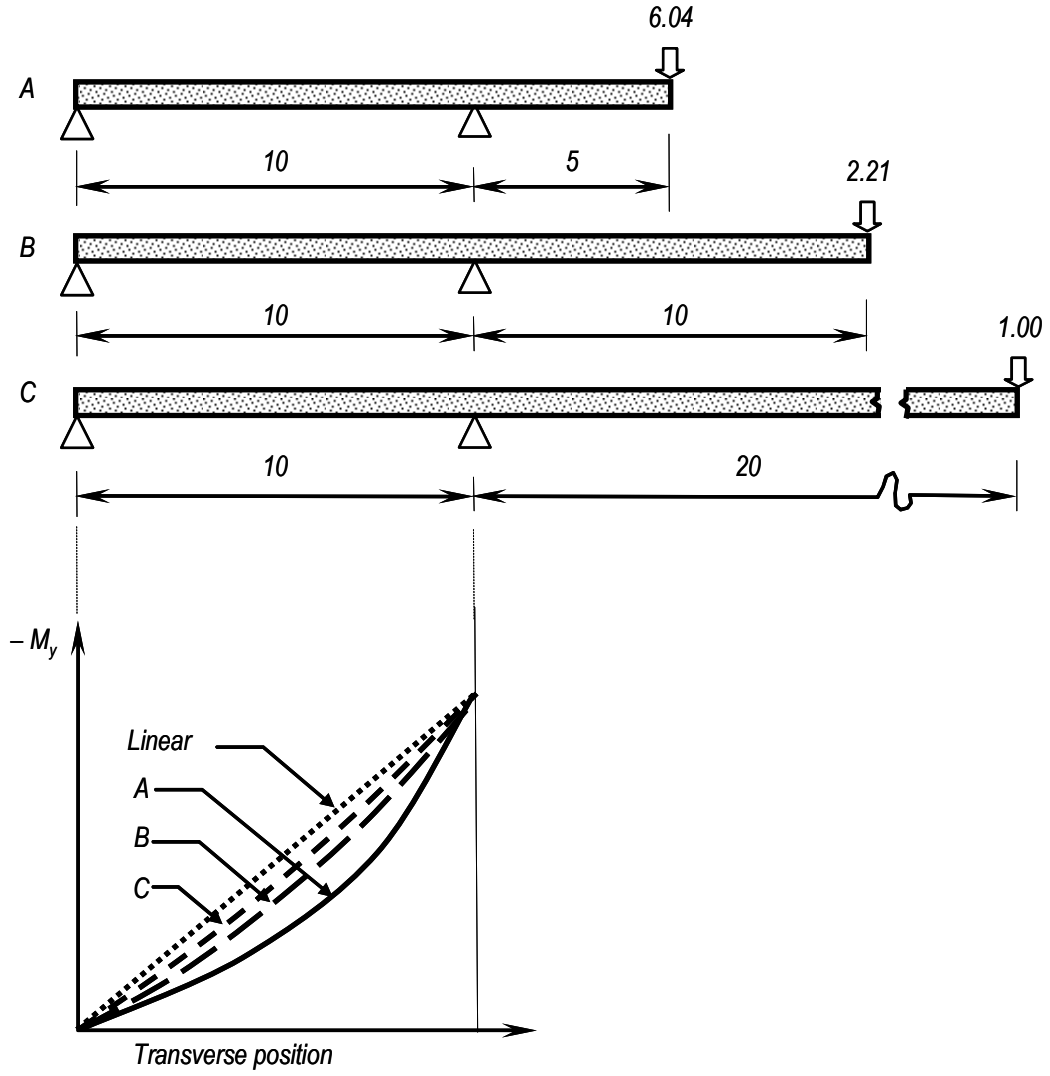

Note: Published with the permission of Mufti et. al. (2008)

Figure 2-3: Distribution of peak negative moment intensities in an internal panel

2.2.2 Behaviour of a Cantilever of Semi-infinite Length

The distribution of transverse negative moments, M_y, due to a concentrated load in the proximity of a transverse free edge is discussed with the assistance of Figure 2-4. The total moment at the root of the cantilever overhang is the area under the curve and is equal to the total moment PC. A transverse free edge can be regarded as dividing a slab of infinite length. The free edge divides the total area under the curve into to areas A_L and A_R with the area A_L being on the left hand side of the transverse free edge. Simply stated, the cantilever of infinite length has now been cut by the transverse free edge and is now considered as a cantilever of semi-infinite length. To satisfy static equilibrium, the moment represented by the area A_L must be redistributed within the curtailed slab. The moment A_L has been reflected back, and this pattern has been confirmed for design purposes by rigorous analysis. The net moments for a cantilever of semi-infinite length are obtained by superimposing the redistributed moments A_L over the moments given by A_R. It is appreciated that the peak moments, M_y, for a slab of semi-infinite length are larger than the peak moments, M_y, for a slab of infinite length (Mufti et al., 1996).

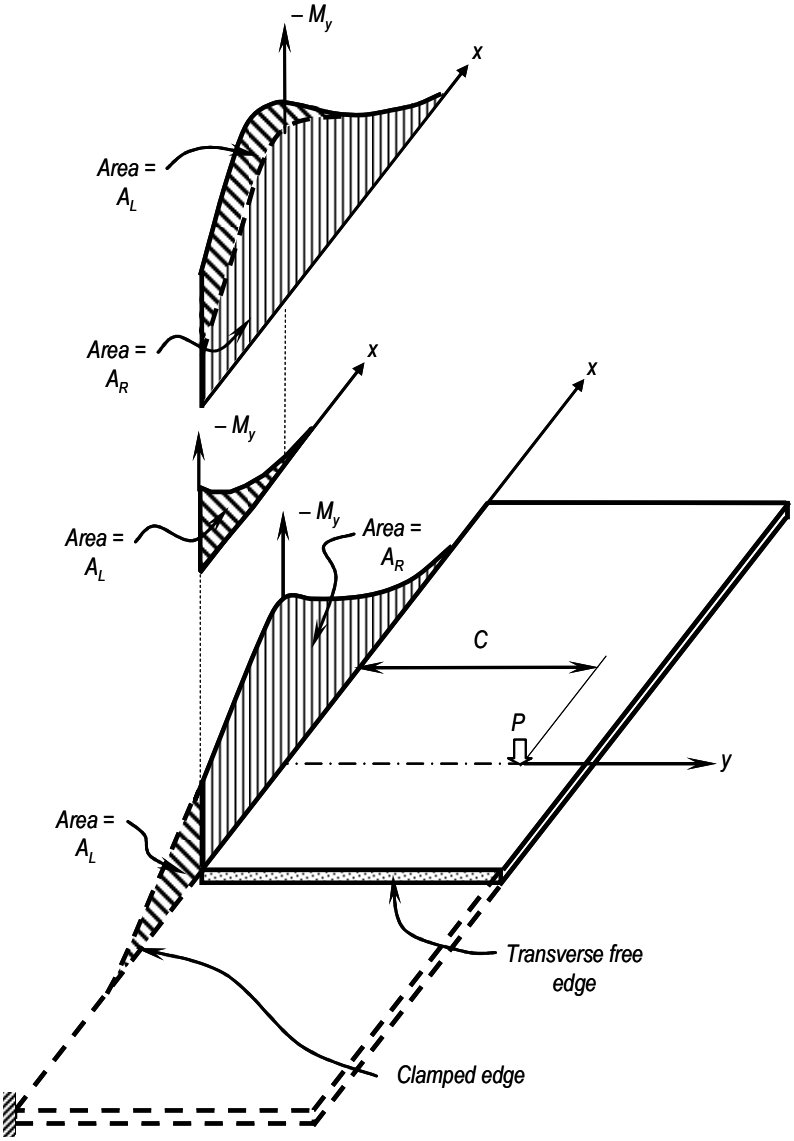

Note: Published with the permission of Mufti et. al. (2008)

Figure 2-4: Distribution of cantilever negative transverse moment intensities in the vicinity of a transverse free edge

2.2.3 Analysis Method for an Unstiffened Cantilever Slab of Infinite Length

A simplified method for determining the cantilever moment intensity, M_y, for a cantilever subjected to a concentrated load was proposed by Bakht and Holland (1976). It is expressed as:

$$M_y = \frac{PA'}{\pi} \frac{1}{\cosh\left(\frac{A'x}{C-y}\right)} \tag{2.1}$$

where A' is a coefficient whose values depend on the location of the load and the reference point with respect to the cantilever root. Other notation as illustrated in Figure 2-5.

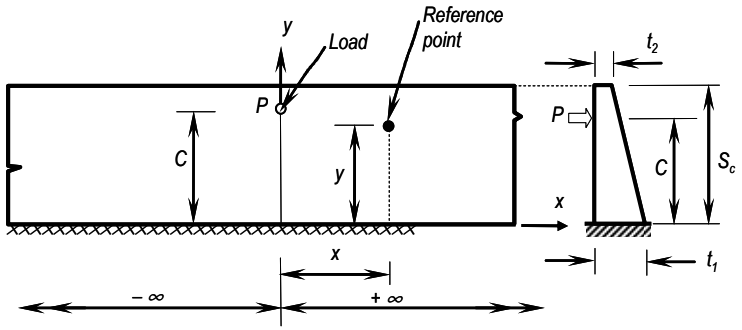

Note: Published with the permission of Mufti et. al. (2007)

Figure 2-5: Notation used for simplified method of analysis for a cantilever of infinite length for determining moment intensity

Graphical charts are provided for magnitudes of A' by Bakht and Holland (1976). Jaeger and Bakht (1990) have shown that it sometimes may be preferred that Equation 2.1 be replaced by an algebraic function. As a result, M_y takes the following form:

$$M_y = -\frac{2PB}{\pi}\left[\frac{(C-y)^4}{\left[(C-y)^2+(Bx)^2\right]^2}\right] \tag{2.2}$$

Where

$$B = \frac{A'}{2} \tag{2.3}$$

Neither equation is preferred over the other in terms of accuracy. Engineers might prefer Equation 2.2 because it may be easier to relate to its algebraic function. The methods used by Bakht and Holland (1976) and Dilger et al. (1990) provide moment intensities for the cantilever. They do not provide information related to the transverse negative moment distribution in the internal panel. In the absence of this information, designers will usually formulate their own empirical rules for determining negative moment reinforcement for the internal panel. The rules are usually based on the assumption that the negative moment intensity varies linearly across the internal panel span.

Mufti et al. (1993) have shown that the internal moment intensity can be attained by either of the following expressions:

$$M_y = \frac{PB}{\pi}\frac{1}{\cosh\left(\frac{2BSx}{C(S-y)}\right)} \tag{2.4}$$

$$M_y = -\frac{2PB}{\pi}\left[\frac{C^4(S-y)^4}{\left[C^2(S-y)^2+S^2(Bx)^2\right]^2}\right] \tag{2.5}$$

The notation used in Equations 2.4 and 2.5 is illustrated in Figure 2-6 where it is shown that the direction of *y* for the cantilever overhang is reversed. Mufti et al. (1993) have provided tables of the constant, *B*, which also depend on the ratio of the internal panel span, *S*, divided by the cantilever span, S_c.

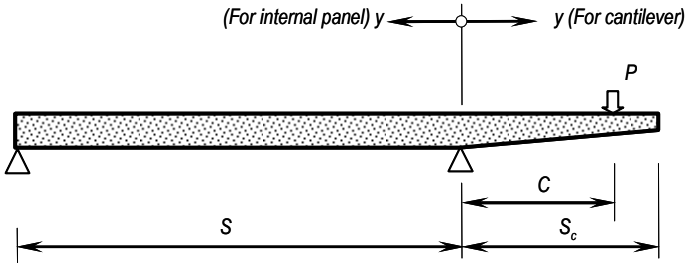

Note: Published with the permission of Mufti et. al. (2008)

Figure 2-6: Definition of transverse co-ordinate *y*

2.2.4 Analysis Method for an Unstiffened Cantilever Slab of Semi-infinite Length

Bakht et al. (1979) have shown that the moment intensity of a fully clamped cantilever overhang due to a concentrated load near a free edge is given by:

$$M_y = \frac{PB}{\pi}\left[\frac{1}{\cosh\left(\frac{2BSx}{C(S-y)}\right)} + D\,e^{(-KX/S_c)}\right] \tag{2.6}$$

where K is determined from the following equation:

$$K = \frac{BD\,S_c}{C}\left[\frac{1}{\tan^{-1}\left[\exp(-2B\,x_{edge}/C)\right]}\right] \tag{2.7}$$

In Equations 2.6 and 2.7, D is a coefficient which is similar to B and obtained from rigorous analysis, x_{edge} is the distance from the concentrated load to the nearest transverse edge, and X is the distance of the reference point at the root to the nearest transverse free edge equal to $x+x_{edge}$ (Figure 2-7).

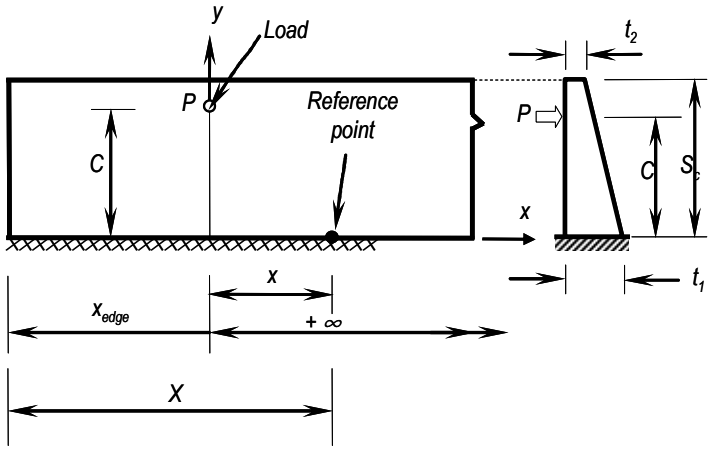

Note: Published with the permission of Mufti et. al. (2008)

Figure 2-7: Notation used for simplified method of analysis for a cantilever of semi-infinite length

2.2.5 Cantilever slabs with Edge-Stiffening (Stiffened Longitudinal Free Edge)

It is obvious that the stiffening of the longitudinal free edge of a cantilever slab will spread the effect of concentrated loads in the longitudinal direction and will improve the distribution

of moment, M_y (i.e. reduce its peak intensity). Overall statics requires that a reduction in the peak moment, $M_{y,}$ will lead to an increase in the values of M_y elsewhere. This is an important observation because in the case of multiple concentrated loads, the edge-stiffening may not reduce the peak value of M_y as much as it would for a single concentrated load.

Bahkt (1981) and Tadros et. al. (1994) have confirmed that Equations 2.1, 2.2, 2.4, and 2.5 are also applicable to cantilever slabs with edge-stiffening provided that the loads applied are at least a distance of three times the span of the cantilever, S_c, away from any transverse free edge. The values of coefficient, $B,$ depend upon the ratio of flexural rigidity of the edge stiffening and that of the cantilever slab (Mufti et. al. 2008).

Tadros et. al. (1994) have proven that that the increase of flexural rigidity of the edge stiffening beyond a certain point has little influence in the distribution of transverse negative moments in both the cantilever and the internal panel. Fortunately, the limiting flexural rigidity corresponds to concrete barrier walls commonly employed in bridge deck cantilever slabs referred to as New Jersey or "F-shaped" barrier walls.

2.3 Arching Action (AA) and Compression Membrane Action (CMA)

Arching action (AA) or compressive membrane action (CMA) in reinforced concrete slabs occurs as a result of the great difference between the tensile and compressive strengths of concrete. Cracking of the concrete causes a migration of the neutral axis which is

accompanied by in-plane expansion of the slab at its boundaries. If this natural tendency to expand is restrained, the development of arching action enhances the strength of the slab.

In a one-way spanning slab (common to bridge deck slabs supported by steel or concrete bridge girders) the deck is made composite with the girders via shear studs or stirrups. Upon the application of a concentrated load (wheel load), the deck will deform and stresses will develop according to flexural theory which will initiate a longitudinal flexural crack in the concrete between the girders. It is well known that when the deck cracks, it wants to expand or displace outward in both transverse and longitudinal directions causing the girders and edge beams to displace outwards away from the point of load application. It is the bottom transverse reinforcement or external steel straps that assist the top flanges of the girders to provide a lateral restraining force to the concrete bridge deck slab which develops arching or compressive membrane forces within the slab itself (Figure 2-8). After cracking has taken place, the arching action forces enable the deck slab to sustain forces even though the deck has little flexural capacity remaining. The degree of lateral restraint provided will determine the ultimate load at which the deck will fail in punching shear. The arching action in the longitudinal direction near the transverse free edge of the deck slab is restrained by a transverse composite edge beam. The ultimate load may be several times greater than the load that causes flexural cracking and failure.

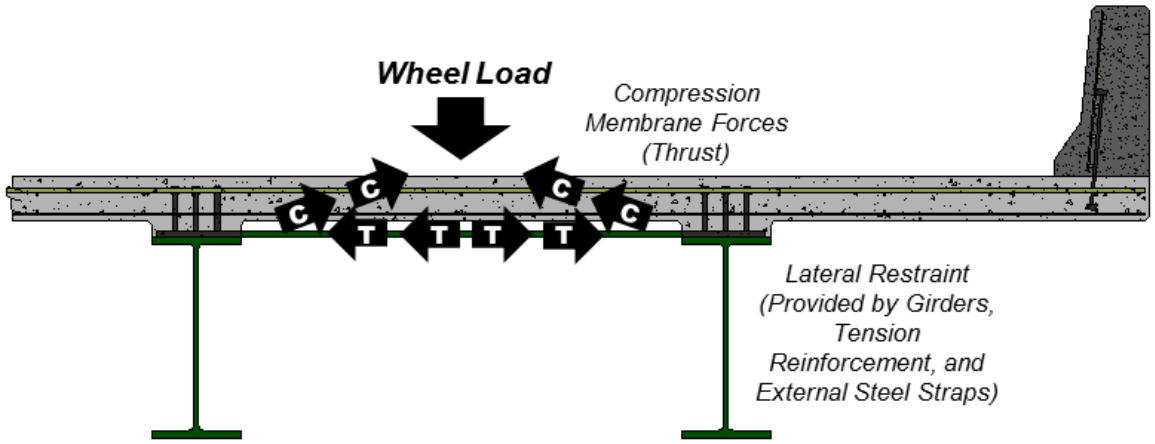

Figure 2-8: Cross-section of a steel free bridge deck illustrating compression membrane action

It is a well-established phenomenon that if a reinforced concrete bridge deck slab that is supported in such a way that lateral displacement is restricted or restrained at its edges or supports, it will fail at a load several times greater than an equivalent simply supported slab.

Consider a restrained, under-reinforced, strip slab behaving in pure flexure. As failure approaches, the neutral axis at mid-span and at the supports moves towards the compression face providing a relatively small compressive stress block at failure. Pure flexure is accompanied by expansion of the concrete below the neutral axis. If the expansion or extension is restricted by restraints at the boundaries (longitudinal supporting bridge girders) compressive forces in the plane of the slab develop as well as moment restraint. Thus failure due to pure flexure cannot occur. The presence of the boundary restraints implies that the neutral axis must be close to the middle of the slab. The resulting compressive stress block is now considerably larger than in the case of pure flexure. Therefore, the ultimate moment and hence failure or collapse load becomes considerably larger. The mode of failure is

transformed from ductile to brittle. This phenomenon is known as compressive membrane action (CMA). Figure 2-9 illustrates the variation in size of the compression stress block in a restrained strip slab. In Figure 2-9, the hogging moments at the support are more critical and the resulting stress block is smaller.

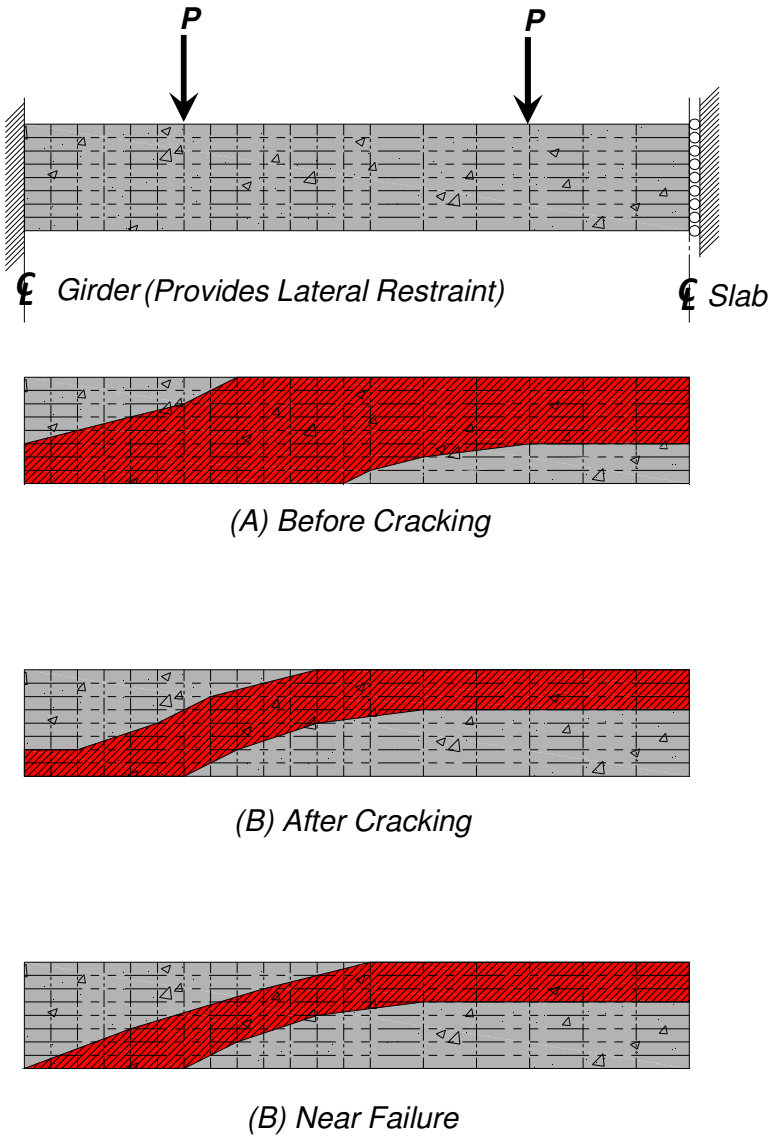

Figure 2-9: Principle stress trajectories in an axially restrained slab strip; Compressive zone is shaded red (Lahlou and Waldo, 1992)

Restraint at the edges of the concrete bridge deck slab can be derived from a compression membrane force and/or fixed boundary action. The compression membrane force is generated by the in-plane and the fixed boundary conditions which produces a moment at the boundary. Both are generated due to the presence of the supporting girders (Figure 2-10).

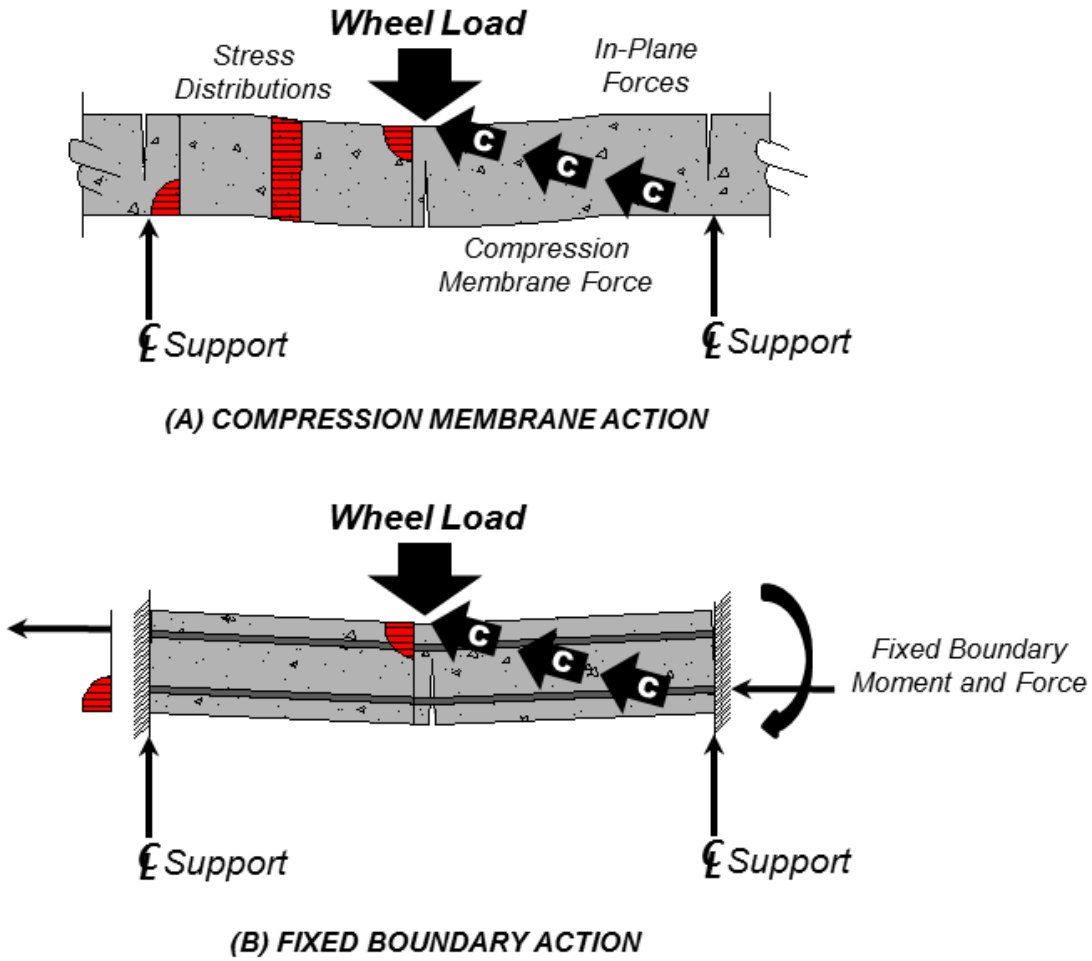

Figure 2-10: Idealized restrained bridge deck slab

Compression membrane action manifests itself in bridge deck slabs as shown in Figure 2-8. It relies on the non-linearity of concrete (cracking and different stress versus strain relationships in tension and compression) to occur. If a slab is un-cracked or has the same

stress versus strain relationship in tension and compression, compression membrane action cannot develop or occur. For example, cracks do not occur in metals as they tend to deflect and yield rather than crack and thus membrane action does not occur (Figure 2-11).

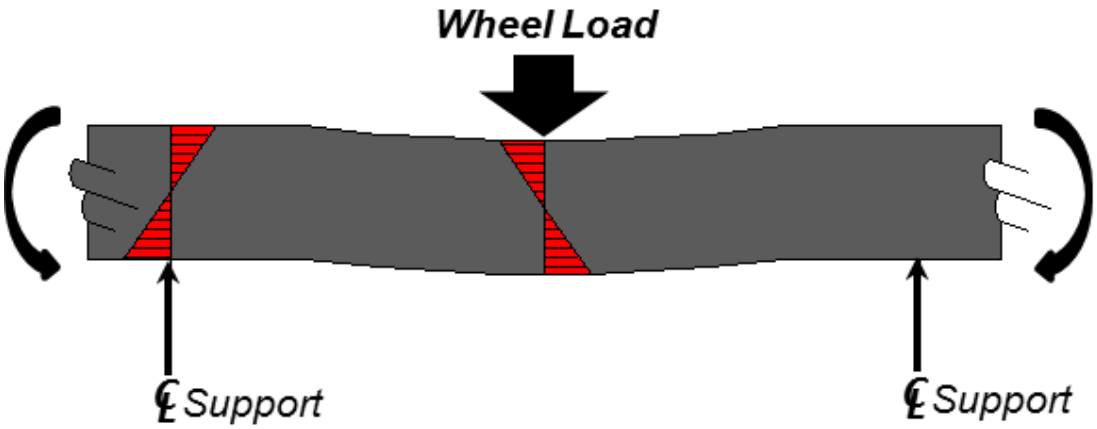

Figure 2-11: Slab with the same stress versus strain relationship in tension and compression (e.g. metals)

Compression membrane action can occur in a cracked un-reinforced concrete slab but fixed boundary conditions require tension reinforcement and rotational restraint (provided by girder flanges) at the boundaries. The progression to failure with boundary restraints as described by Hewitt and Batchelor, 1975 is:

- Fixed boundary condition (if reinforced and restrained against rotation at the boundary);
- Cracking;

- Compressive membrane action (if unreinforced) or compressive membrane action plus fixed boundary action (if reinforced and restrained against rotation at the boundaries); and
- Failure.

2.4 Current Bridge Deck Cantilever Slab Overhang Design Methods

2.4.1 Limit State Design

Limit state design (LSD), also referred to as load and resistance factor design (LRFD), refers to design methods practiced by structural engineers and is specified by current modern design codes. A limit state is a condition of a structure beyond which it no longer fulfills the relevant design criteria. Two principle limit states that engineers typically use in the design process are the ultimate limit state (ULS) and the serviceability limit state (SLS).

2.4.1.1 The Ultimate Limit Sate

Bridge engineers currently design bridge deck cantilever overhangs for the ULS which corresponds to the maximum or ultimate load that a bridge might be expected to experience in its life time. However, cantilever slab overhang design is typically governed by impact on the barrier wall which is an Extreme Limit State (ELS) as defined by AASHTO (2014). Designing for ULS is essentially using linear elastic assumptions to simplify the design for the ultimate strength when structures are typically behaving in a non-linear manner. This

design process is conducted by factoring the appropriate loads on the structure and determining the factored resistance (usually moment or shear). Engineers apply appropriate material resistance factors and determine the factored material resistance. The design is completed by ensuring that the factored resistances are greater than the factored moment and shear intensities due to factored loads usually in the form of Equation 2.8:

$$\text{Factored Resistance} \geq \text{Effect of Factored Loads} \tag{2.8}$$

$$\phi R \geq \alpha_D D + \Psi(\alpha_L L) \tag{2.9}$$

Where ϕ *resistance factor*, which accounts for the fact that the real strength (resistance) of the element may be greater or less than the nominal resistance due to variations in dimensions, material properties, etc.

α_D, α_L *load factors*, which account for the possibility that loads larger than those anticipated may act on the structure, the uncertainty involved in predicting loads and the approximations in the analysis of the effects of the loads on the structure

Ψ *load combination factor*, which accounts for the reduced probability of a number of loads reaching their specified values simultaneously

D, L *dead load(s) and live load(s),* which a Dynamic Load Allowance (DLA)

2.4.1.2 The Serviceability Limit Sate

The serviceability limit state (SLS) refers to the loading that a bridge cantilever overhang is expected to experience under normal service conditions. At the SLS, the bridge should not experience excessive deformation or deflection, cracking, or excessive vibration due to live loads such as passing vehicles. It should be noted that with FRP materials, the SLS usually governs the design process.

2.4.2 Design Loads

2.4.2.1 Dead Loads

Dead loads that must be considered in the design of a bridge deck cantilever slab overhang are the self-weight of the concrete, asphalt wearing surface (if any), and the traffic barrier wall. A cross-section of a typical bridge deck slab supported by steel girders and the idealization of dead loads is shown in Figure 2-12. Appropriate dead load design factors and their reference with respect to the CAN/CSA S6-06 Canadian Highway Bridge Design Code (CHBDC, 2006) are summarized in Table 2-1

Table 2-1: Dead load design factors for bridge deck cantilever slab overhangs

Component	Dead Load Factor (α_D)	Reference
Concrete deck slab	*1.2*	*Table 3.5.1(b); Permanent Loads: Maximum Values of Load Factors for ULS; pg. 50; CHBDC 2006*
Asphalt wearing surface	*1.5*	*Table 3.5.1(b); Permanent Loads: Maximum Values of Load Factors for ULS; pg. 50; CHBDC 2006*
Concrete traffic barrier	*1.2*	*Table 3.5.1(b); Permanent Loads: Maximum Values of Load Factors for ULS; pg. 50; CHBDC 2006*

2.4.2.2 Live Loads

The most critical live load that a bridge deck cantilever slab overhang will experience in its service life is the wheel load from passing trucks. The design truck for the CAN/CSA S6-06 CHBDC 2006 is the CL-625 truck design truck (Figure 2-13). The maximum wheel load measures 87.5 kN in magnitude. The maximum distance to the outermost wheel from the center-line of the outermost girder is defined by the assumption that the distance from the curb or barrier wall to the center-line of the tandem wheel load is 600 mm (Figure 2-13). Appropriate live load design factors and dynamic load allowances and their reference with respect to the CAN/CSA S6-06 CHBDC are summarized in Table 2-2 and 2-3.

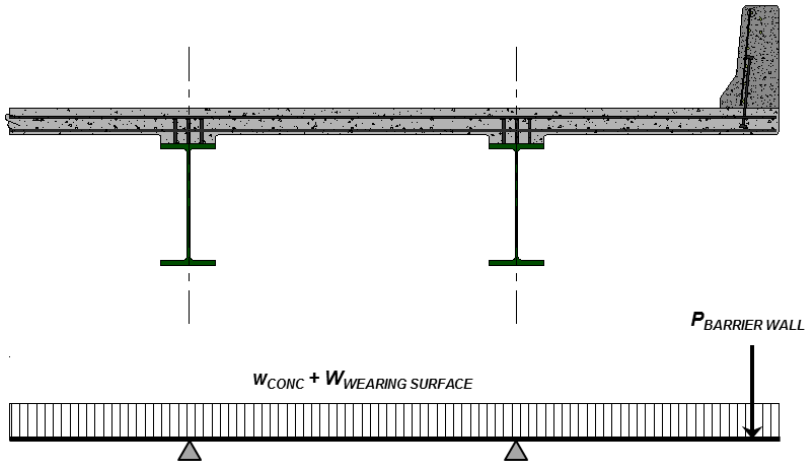

Figure 2-12: Idealization of dead loads for a typical bridge deck cantilever slab overhang

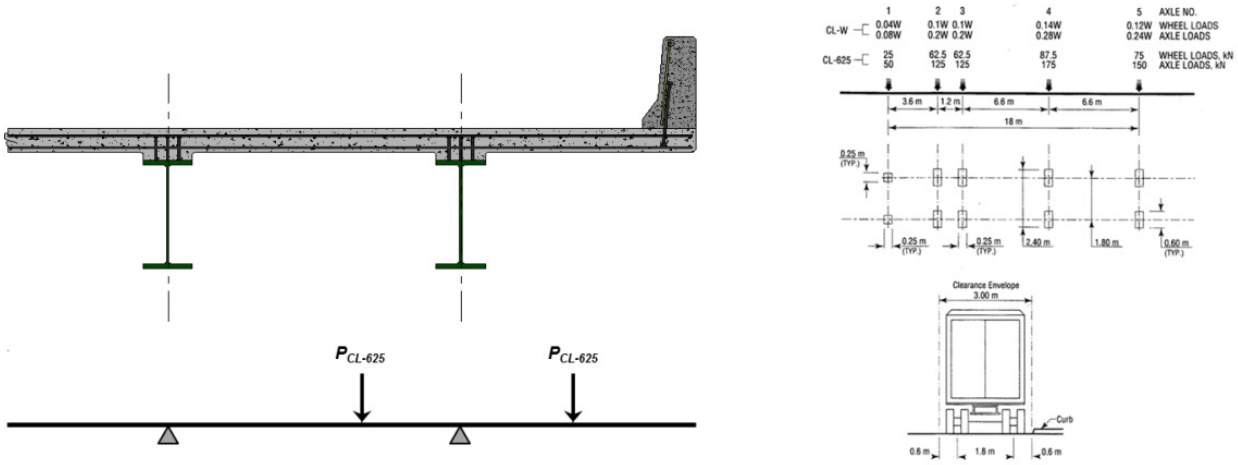

Figure 2-13: Schematic of the CL-625 design truck for the design of a bridge deck cantilever slab overhang

Table 2-2: Live load design factors for bridge deck cantilever slab overhangs

Description	Live Load Factor (α_L)	Reference
Single wheel load from CL-625 design truck	*1.7*	*Table 3.5.1(a); Load factors and load combinations; pg. 49; CHBDC 2006*

Table 2-3: Dynamic load allowances for bridge deck cantilever slab overhangs

Description	Dynamic Load Allowance (DLA)	Reference
Deck Joint	*0.5*	*Clause 3.8.4.5.3; Dynamic Load Allowance; pg. 56, CHBDC 2006*
One axle of the CL-625 truck is used	*0.4*	*Clause 3.8.4.5.3; Dynamic Load Allowance; pg. 56, CHBDC 2006*
Two axles of the CL-625 truck are used	*0.3*	*Clause 3.8.4.5.3; Dynamic Load Allowance; pg. 56, CHBDC 2006*
Three axles of the CL-625 Truck are used, except for axles 1, 2, and 3, or more than three axles are used	*0.25*	*Clause 3.8.4.5.3; Dynamic Load Allowance; pg. 56, CHBDC 2006*

2.4.2.3 Impact Loads on the Traffic Barrier

Bridge deck cantilever slab overhangs must also be designed to withstand impact loads from passing traffic. The CHBDC 2006 speifies in detail how bridge engineers shall design cantilever slab overhangs for such impact loads. The engineer must first determine the traffic barrier exposure index *(B_e)* given by the following formula:

$$B_e = \frac{(AADT_1)K_h K_c K_g K_s}{1000} \quad (2.3)$$

Where $AADT_1$ *average annual daily traffic* for the first year after construction

K_h *highway type factors*, based on the number of lanes and design speeds (Table 12.5.2.1.2(a); pg 554, CHBDC 2006)

K_c *highway curvature factors*, which account for radii of curves and the location of the barrier wall (Table 12.5.2.1.2(b); pg 554, CHBDC 2006)

K_g *highway grade factors*, which account for percentage of grade on travel lanes (Table 12.5.2.1.2(c); pg 554, CHBDC 2006)

K_s *superstructure height factors*, which take into account the height of the bridge deck above deep or shallow water and/or the land use below (Table 12.5.2.1.2(d); pg 555, CHBDC 2006)

Based on the barrier exposure index B_e, the percentage of trucks based on the $AADT_1$, design speeds, and the barrier clearance, the engineer can then determine the optimum performance level for the given traffic barrier found in tables 12.5.2.1.3(a) to 12.5.2.1.3(c). Design impact loads for traffic barriers based on performance level are given in Table 2-4 and the configuration of these loads is shown in Figure 2-14. It is important to note the the barrier wall performance levels are determined by the authority having jurisdiction over the bridge and not the design engineer.

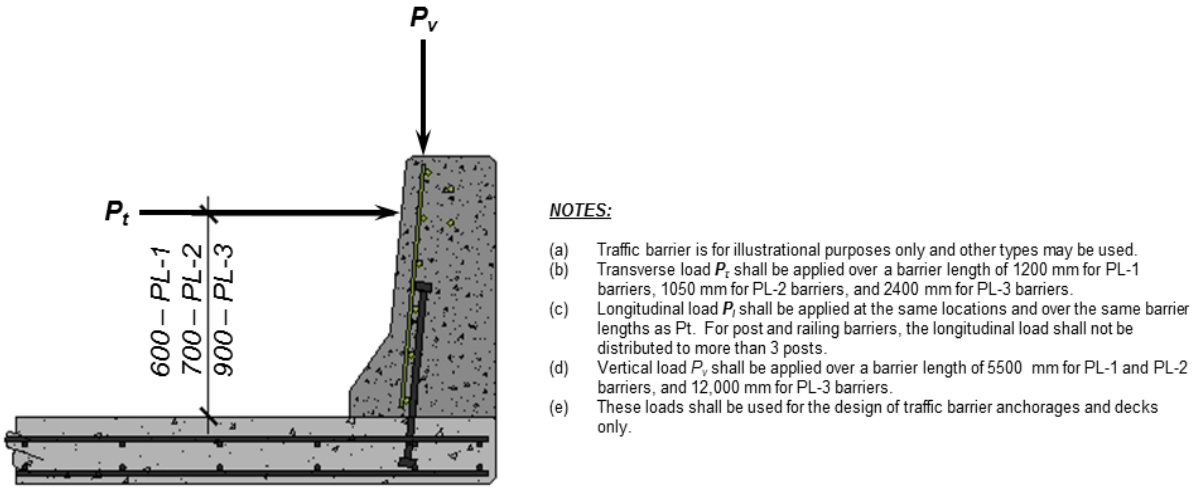

Figure 12-14: Schematic of magnitude and location of impact loads from CHBDC CL-625 design truck on railings or barrier walls

Table 2-4: Impact loads on traffic barrier walls

Performance Level	Transverse Load [kN]	Longitudinal Load [kN]	Vertical Load [kN]
PL-1	*50*	*20*	*10*
PL-2	*100*	*30*	*30*
PL-3	*210*	*70*	*90*

2.4.3 Flexural Design of Cantilever Slab Overhangs

Today, bridge deck cantilever slab overhangs are designed and analyzed as one-way slabs with a width of 1000 mm. Based on the loads outlined in Section 2.4.3, the design engineer can perform simplified hand calculations, or use a more refined method of analysis such as a computer program, to determine the factored bending moment for the cantilever slab overhang.

A design engineer can simply determine the factored moment due to dead loads from beam diagrams and formulae found in any analysis textbook or design handbook. A simplified formula, based on the flexural behavior of cantilever slabs, for determining the moment due to truck wheel loads can be found in the CHBDC 2006 and is given by:

$$M_y = \frac{2PA}{\pi} \frac{1}{\left[1+\left(\frac{Ax}{C-y}\right)^2\right]^2} \qquad (2.4)$$

Where A *a coefficient* obtained from Figure 5.7.1.6 of the CHBDC 2006 based on the ratio of load distance from the root of the cantilever divided by the cantilever span, thickness of the cantilever, and whether or not the cantilever has edge stiffening

x, y *coordinates* to the location of the applied load as defined in Figure 5.7.1.6.1(a) of the CHBDC 2006

The relevant design moment intensity is obtained by multiplying M_y, as obtained above, by (1 + DLA). The factored design moment intensity is the sum of moment due to factored dead loads plus the factored moment due to wheel loads from the CL-625 design truck. The bridge engineer must then ensure that the factored moment resistance of the 1000 mm wide section is greater and/or equal to the moment due to the factored loads given by:

$$\phi M_r \geq M_f = M_{fDL} + M_{fLL} \tag{2.5}$$

The CHBDC 2006 states in Clause 3.8.8.1 that loads due to impact of the barrier wall or rails shall not be considered to act simultaneously with the curb load nor with wheel loads due to the CL-625 design truck. Therefore, at the ULS, the cantilever slab must also be able to a resist a moment caused by the impact of a CL-625 design truck. A simple analysis, based on the loads described in Section 2.4.3, shall be carried out to determine cantilever slab moments due to an impact load. The design engineer must ensure that the factored moment resistance is greater or equal to the moment caused by an impact load given by:

$$\phi M_r \geq M_{fIMPACT} \tag{2.6}$$

2.5 Related Research

This section briefly highlights past research which has led to today's current flexural design practices for bridge deck cantilever slab overhangs. It also presents more recent research conducted on un-stiffened bridge deck cantilever slab overhangs which prompted the further

research discussed in this study regarding edge-stiffened bridge deck cantilever slab overhangs subjected to a concentrated wheel load.

2.5.1 Past Research

In their book, "Recent Advances in Bridge Engineering" Mufti, Bakht and Jaeger (2008) have noted: "Internal arching action is limited to that portion of the deck slab which is subjected to live load that is transversely contained between the outermost girders and which is subjected to live loads also located within these bounds. The load effects induced by loads on the cantilever overhangs are *believed* to respond to a purely flexural behaviour." In the textbook, the authors were following common wisdom, which was supported by McMaster University tests (Drysdale, 1982), in which a mirror-image model of a cantilever deck slab with only one girder was tested (Figure 2-15). This project was sponsored by Ministry of Transportation of Ontario (MTO) and B. Bakht was the project engineer. The cantilever deck slab model at McMaster University did indeed fail in bending giving credence to the belief that there is no arching action in cantilever deck slab overhangs. Figure 2-16, reproduced from Drysdale (1982), shows the cracking pattern at failure in the slab under a single concentrated load. The roughly semi-circular cracks with their apexes pointing towards the root of the cantilever are consistent with a flexural failure in a cantilever slab.

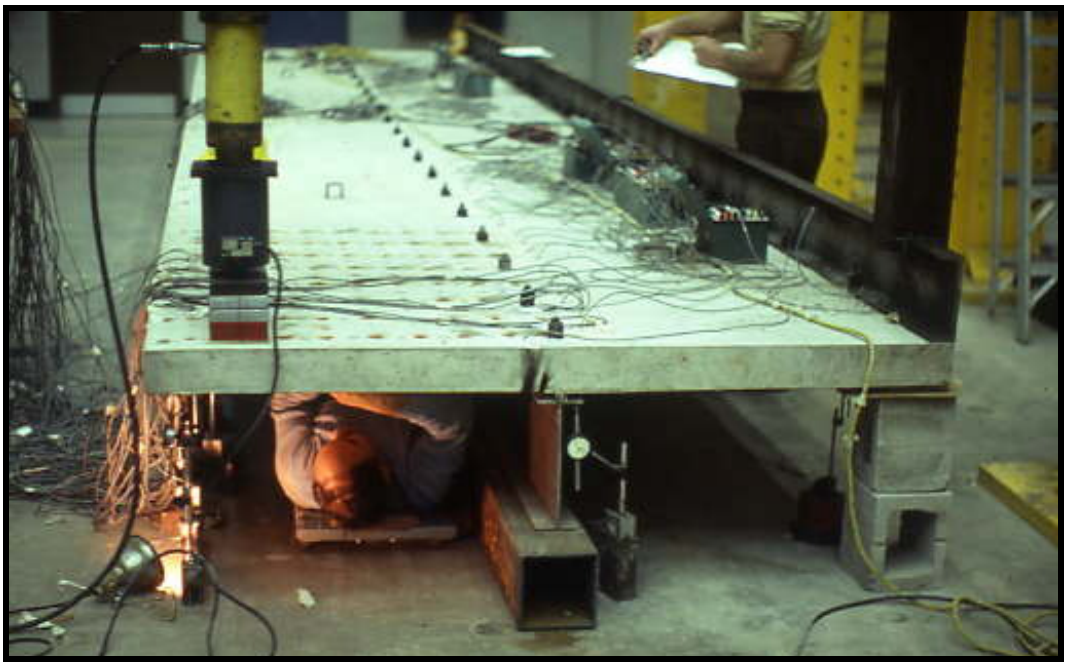

Figure 2-15: Photograph illustrating experimental test set-up for mirror-image model of a cantilever deck slab with only one girder (Drysdale, 1982)

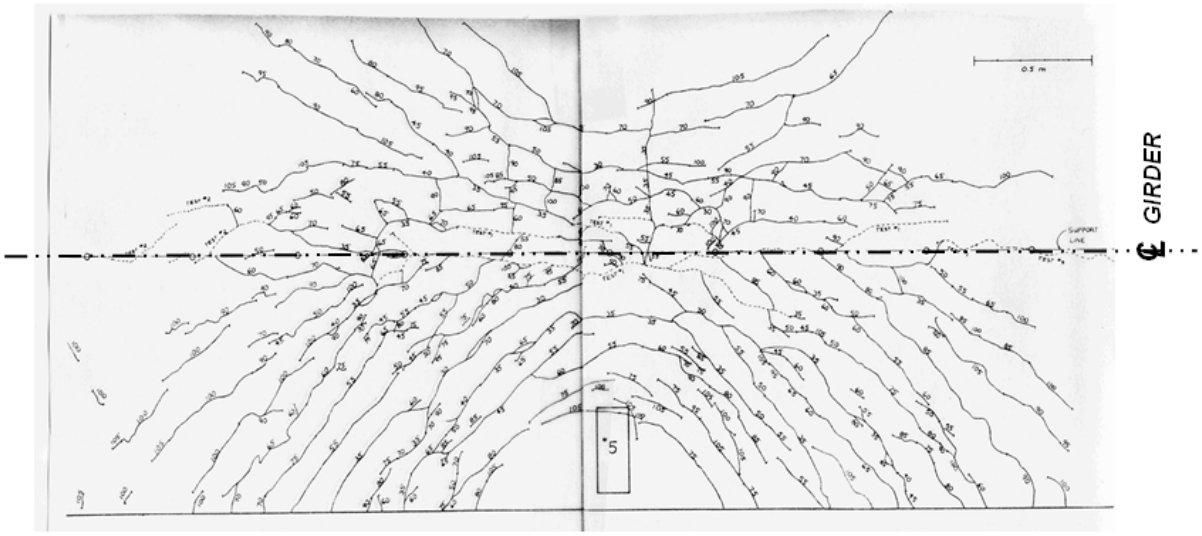

Figure 2-16: Crack patterns in cantilevers subjected to a concentrated load (Drysdale, 1982)

The absence of arching-action in cantilever deck slabs was also confirmed by tests on cantilever slab models without any reinforcement. One such test was reported by Bakht and

Agarwal (1995) who tested a half-scale model of a skew deck slab without any reinforcement. The plan view of the half scale model in Figure 2-17 illustrates that the deck slab had a cantilever overhang with a span of 400 mm. The photograph of the slab held in the vertical direction by a crane shows that the cantilever slab failed in bending leading to an approximately semi-circular area detaching itself from the rest of the deck slab. The observation again confirmed the absence of arching action in cantilever deck slabs. Note that the edges of the deck slab were vertical at the failure line. This observation is consistent with the assumption of the yield-line theory, according to which the plastic failure is assumed to take place at each yield line through the entire depth of the slab.

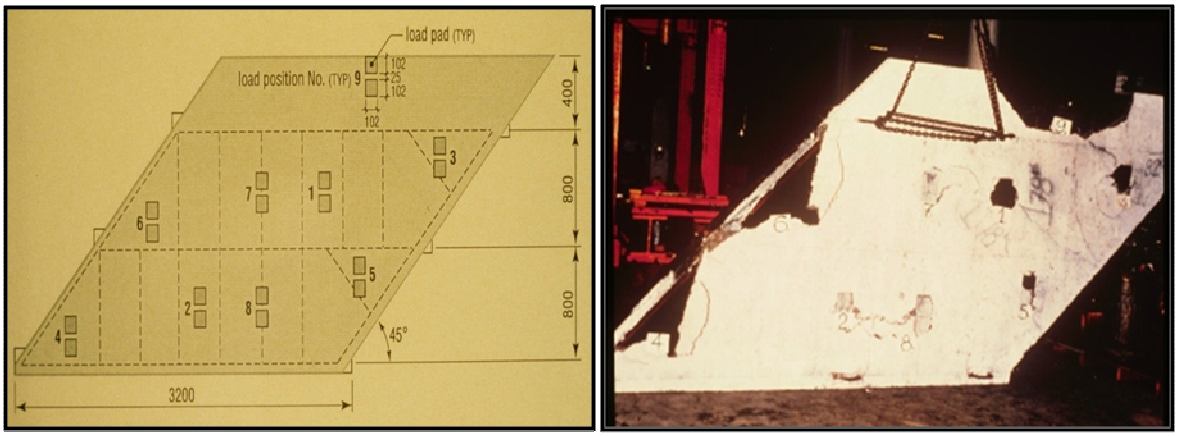

Figure 2-17: A half-scale model of a skew deck slab on three girders showing the flexural mode of failure consistent with yield line theory at test position no. 9 (Bakht & Agarwal, 1995)

In 1999, Gant and Newhook at Dalhousie University tested cantilever deck slabs with and without bottom reinforcement. They found that the failure load in the cantilever deck slab with bottom reinforcement was approximately two times greater than the failure load for the same cantilever slab without bottom reinforcement (Figure 2-18). In light of this

information, Mufti and Bakht 2004 decided to reinvestigate the arching-action in cantilever deck slab overhangs.

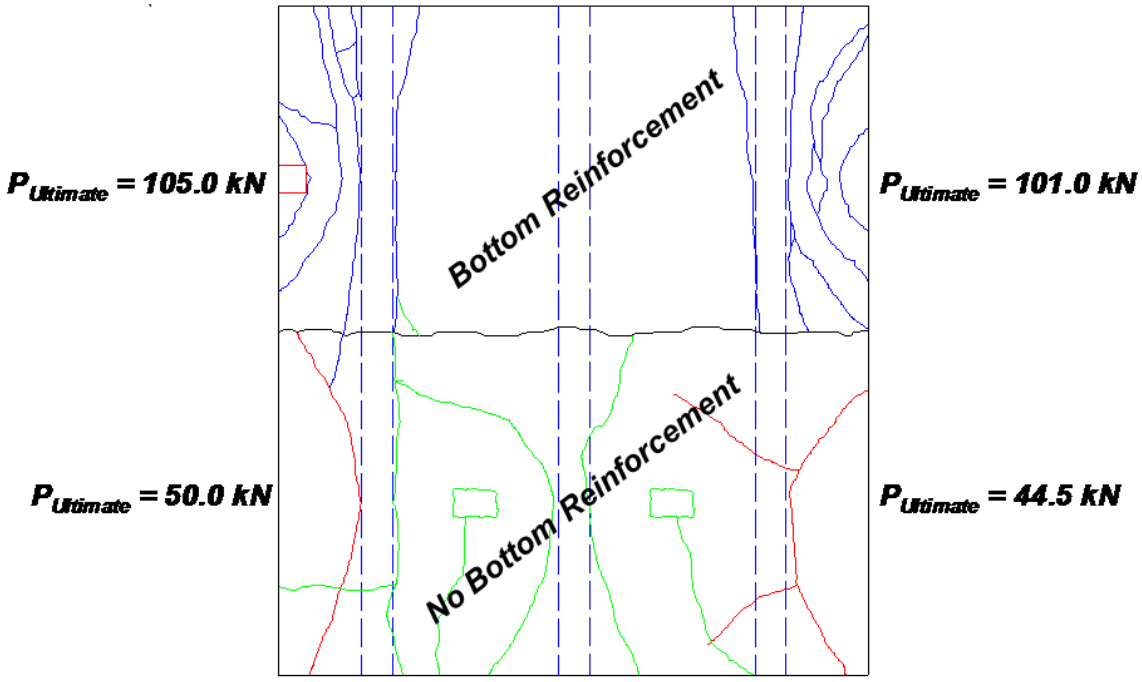

Figure 2-18: Crack patterns and failure loads for static cantilever tests (Gant & Newhook, 1999)

Upon reflection, it became obvious to Mufti and Bakht that the mirror-image model of the cantilever slab with only one central girder did not have enough restraint in the transverse direction to develop any arching action. The same was the case with the cantilever slab without any reinforcement. Therefore, an extensive experimental program was undertaken at the University of Manitoba to re-investigate the presence or possibility of arching-action in bridge deck cantilever slab overhangs subjected to concentrated loads. The following two sections briefly describe some of the findings.

2.5.2 Arching-action in Un-stiffened Cantilever Slab Overhangs

Klowak (2007) conducted testing on a full-scale cast-in-place innovative bridge deck slab that included two cantilevers. The following sections will present design and construction details, some of the test results from the cantilever testing, and will provide arguments that suggest that there may be arching-action present in bridge deck cantilever slab overhangs.

2.5.2.1 Bridge Deck Slab and Cantilever Reinforcement Details

The transverse negative moment reinforcement chosen for the cantilevers consisted of conventional deformed reinforcing steel, CFRP, and GFRP bars in order to provide a comparison and investigation between the three different reinforcing materials for bridge deck cantilevers. The top transverse reinforcing bars were divided into three 3000 mm sections (Figure 2-19).

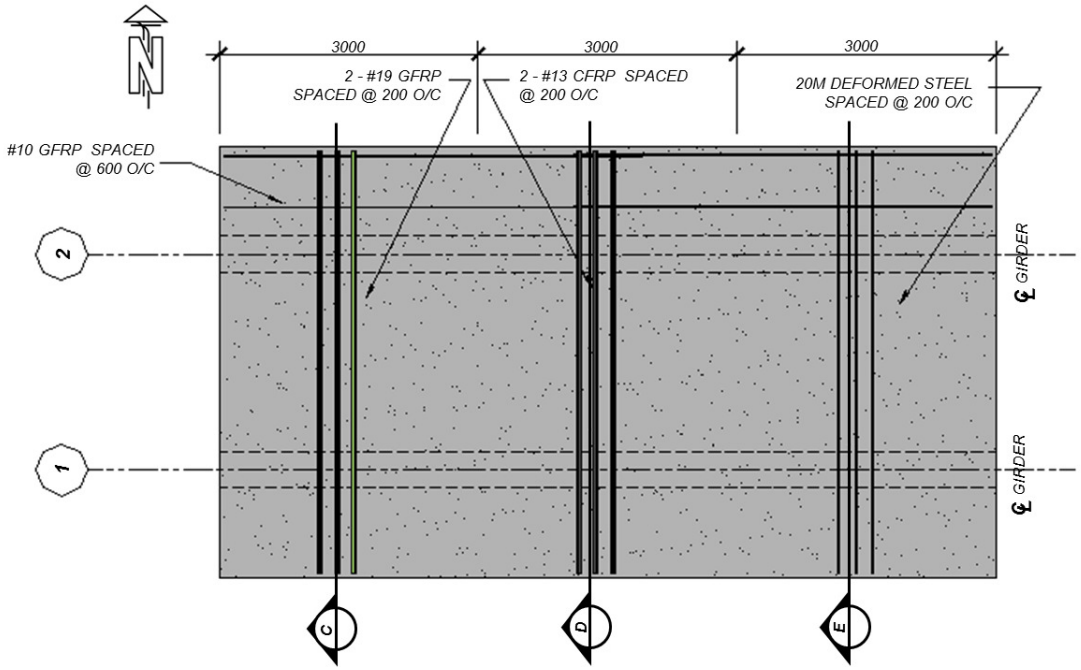

Figure 2-19: Plan view of un-stiffened cantilever slab overhang reinforcement (Klowak, 2007)

The east cantilever section of the bridge deck was reinforced with conventional deformed reinforcing steel consisting of 20M top transverse reinforcing bars spaced at 200 mm center-to-center. The central cantilever section of the deck was reinforced with two top transverse #13 CFRP spaced at 200 mm center-to-center. The west section contained two top transverse #19 GFRP bars at a spacing of 200 mm center-to-center. The top longitudinal reinforcing bars were uniform throughout the entire length of the bridge deck and were comprised of #10 GFRP spaced at 600 mm center-to-center. A very important characteristic of the cantilever slabs was that all three sections contained identical bottom mats of reinforcement consisting of #10 GFRP at 200 mm center-to-center in the transverse direction and #10 GFRP spaced at 600 mm center-to-center in the longitudinal direction (Figure 2-20).

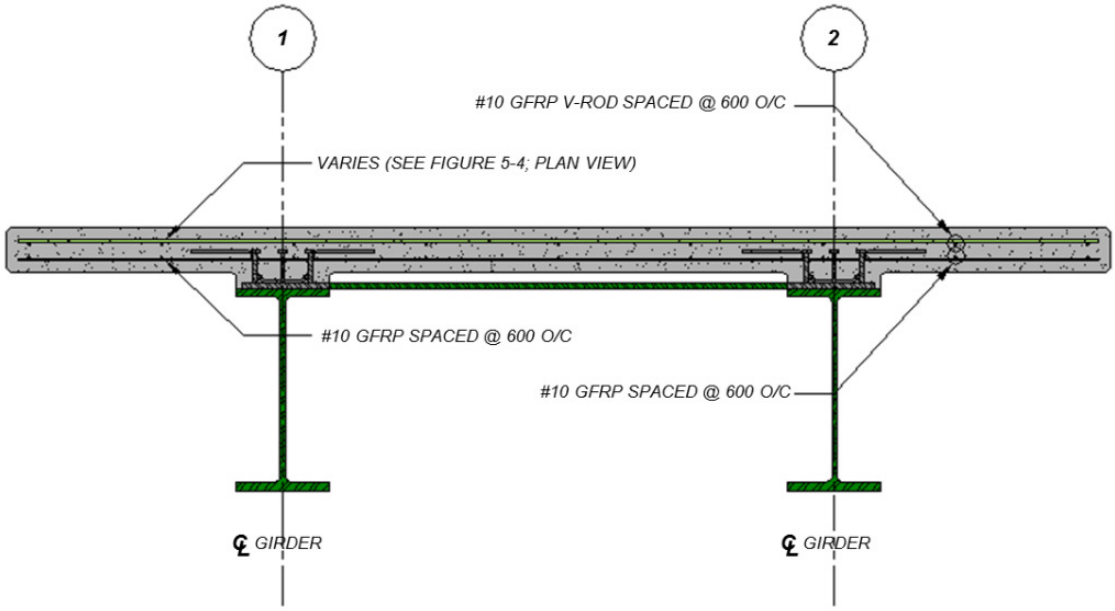

Figure 2-20: Typical cross-section of un-stiffened cantilever slab overhang showing internal reinforcement (Klowak, 2007)

2.5.2.2 Test Set-up & Testing Scheme

The preparatory work for the static and fatigue destructive testing of the full-scale experimental bridge deck slab consisted of providing support for the superstructure (i.e. the steel girders and concrete deck), setting up the steel load frame, moving the load frame into each desired position, and setting up instrumentation and connecting it to a data acquisition system. It should be noted that the set-up for each of the six test locations was the same. Figure 2-22 illustrates the test-set-up for the testing program.

The testing scheme was comprised of six different test locations. Each cantilever section, reinforced with top transverse CFRP, steel and GFRP, was subjected to one static monotonic test to failure and one fatigue cyclic test to failure. The static tests were conducted on the

north cantilever and the fatigue tests were conducted on the south cantilever (Figure 2-21). For the purposes of this report only static test results are briefly discussed.

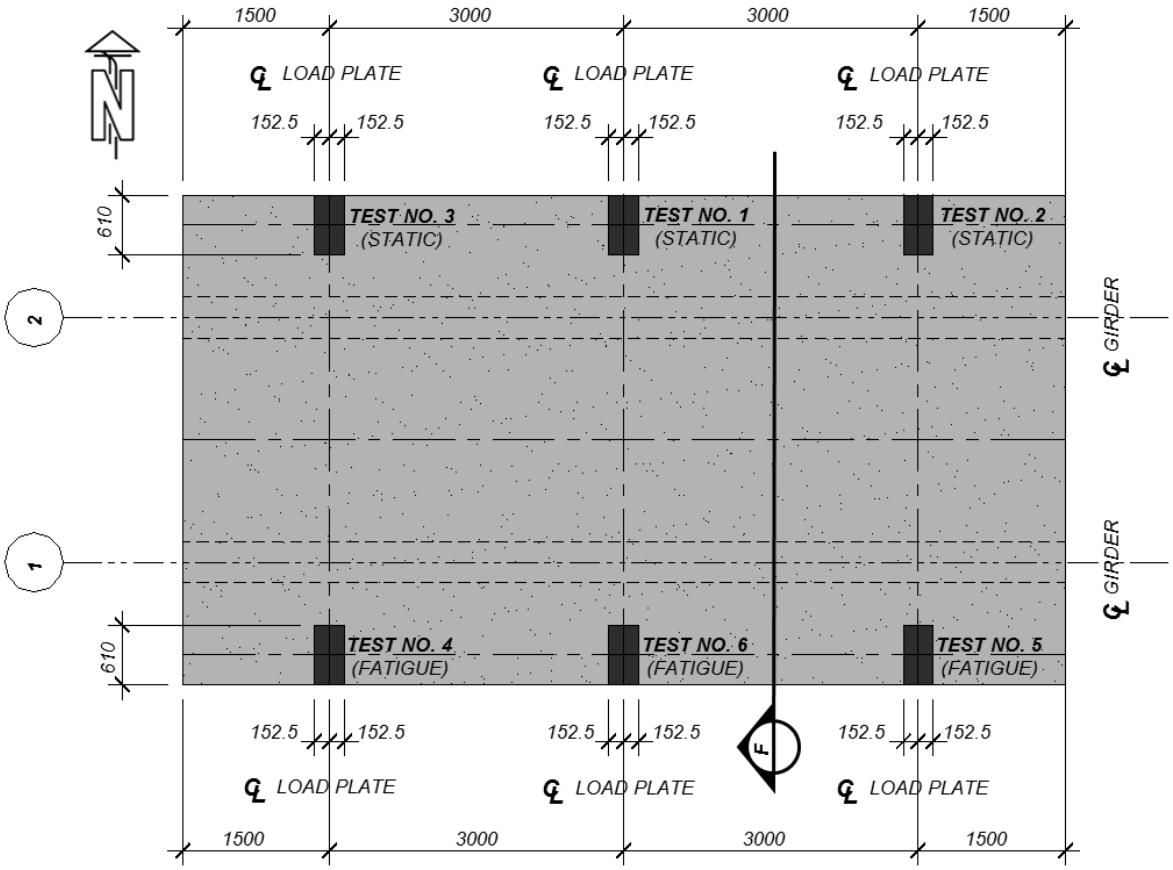

Figure 2-21: Static and fatigue test locations for un-stiffened cantilevers (Klowak, 2007)

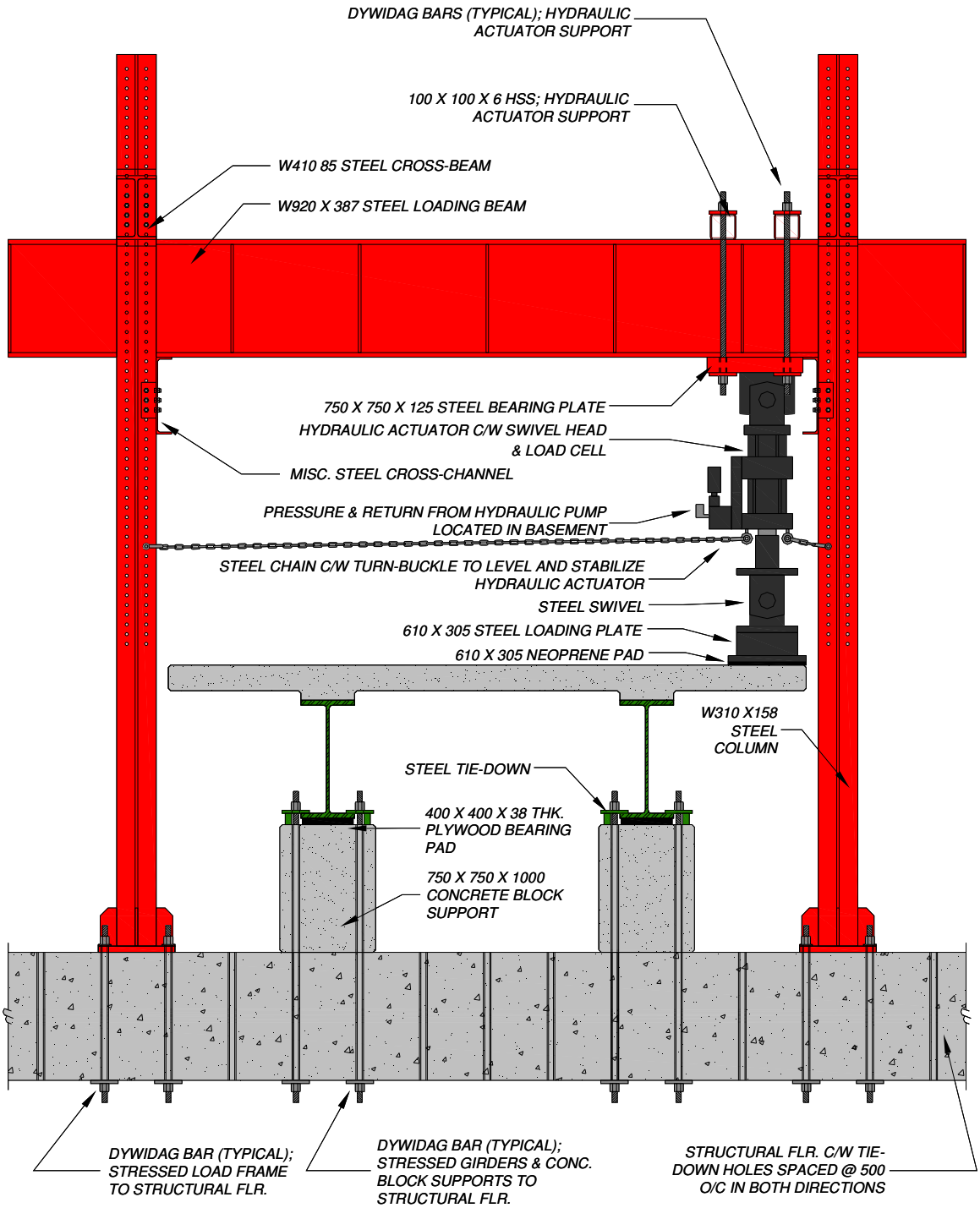

Figure 2-22: Test set-up for static and fatigue destructive testing of cantilevers (Klowak, 2007)

2.5.2.3 Static Modes of Failure

The three cantilever slab, under static load, at all three test locations exhibited a punching type failure similar to that of an internal panel of a bridge deck. The shape of the punch cone was approximately a half circle compared to a full circle punch cone typical of an internal panel.

Static failure of the central cantilever reinforced with top transverse CFRP occurred at an ultimate load of 294 kN. The punch angle in the east direction along the center-line of the loading plate was determined to be approximately 7° and 27° along the center-line of the loading plate in the south direction (towards girder). Top and bottom views of the failure are shown in Figures 2-23(a) and 2-23(b) respectively.

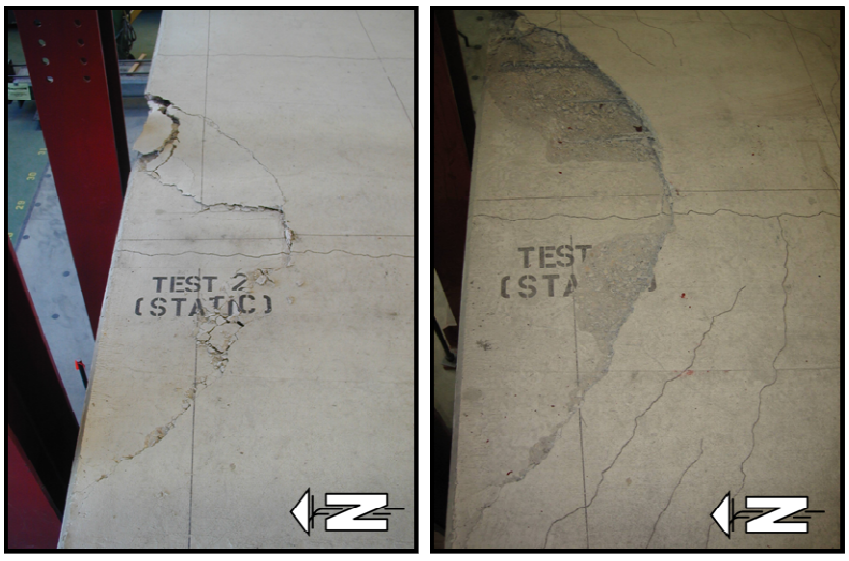

Figure 2-23(a): Top view of semi-circular punching type failure for the cantilever section with top transverse CFRP reinforcement subjected to static monotonic loading (Klowak, 2007)

Figure 2-23(b): Bottom view of semi-circular punching type failure for the cantilever section with top transverse CFRP reinforcement subjected to static monotonic loading (Klowak, 2007)

The cantilever with top transverse steel reinforcement failed an ultimate load of 301 kN. The punch angles along the center-line of the loading plate in the east and south (towards girder) directions of the steel reinforced cantilever were roughly 15° and 28° respectively (Figure 2-24(a) and 2-24(b)).

The final cantilever section that was tested under a static monotonic load until failure was the cantilever section with top transverse GFRP. The punch angle along the center-line of the loading plate in the east direction was determined to be approximately 9° and roughly 36° in the south direction (towards girder). Figure 2-25(a) and Figure 2-25(b) illustrate the semi-circular punching type failures from the top and bottom view of the cantilever respectively.

Figure 2-24(a): Top view of semi-circular punching type failure for the cantilever section with top transverse steel reinforcement subjected to static monotonic loading (Klowak, 2007)

Figure 2-24(b): Bottom view of semi-circular punching type failure for the cantilever section with top transverse steel reinforcement subjected to static monotonic loading (Klowak, 2007)

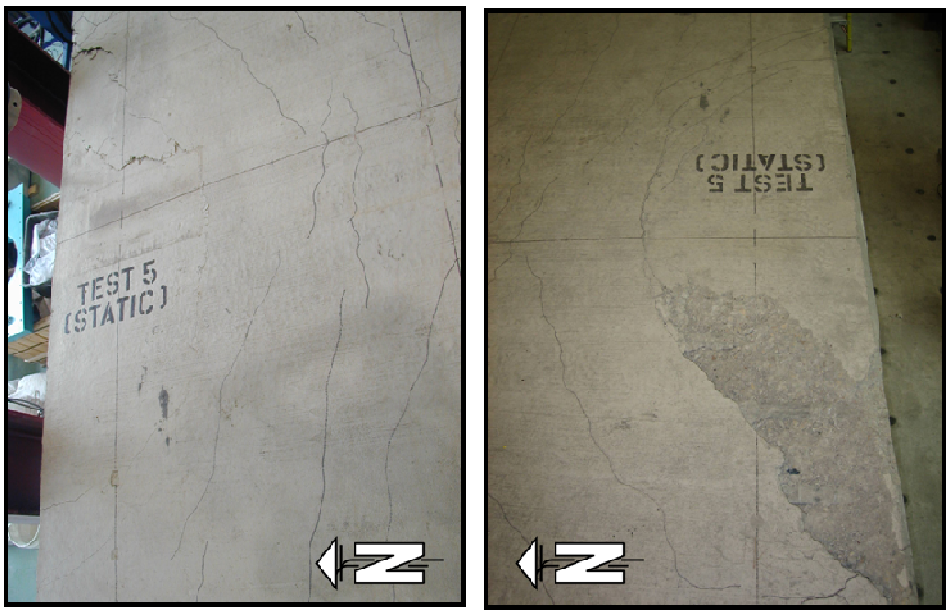

Figure 2-25(a): Top view of semi-circular punching type failure for the cantilever section with top transverse GFRP reinforcement subjected to static monotonic loading (Klowak, 2007)

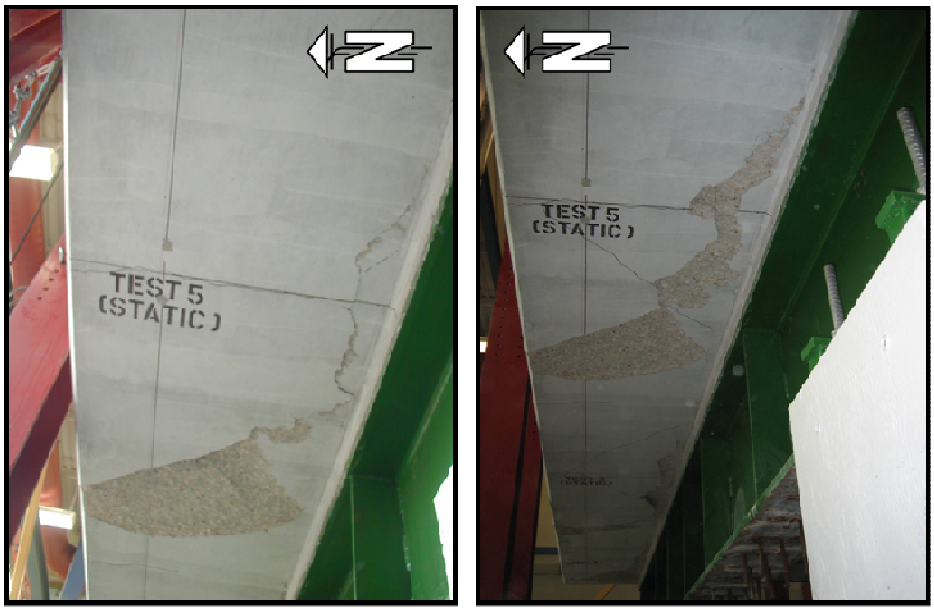

Figure 2-25(b): Bottom view of semi-circular punching type failure for cantilever section with top transverse GFRP reinforcement subjected to static monotonic loading (Klowak, 2007)

2.5.2.4 Discussion

The ultimate un-factored nominal moment capacity for a 1000 mm wide section of the central cantilever section reinforced with top transverse CFRP was determined to be 154.9 kN*m/m with a corresponding strain in the concrete of 3500 με. The ultimate un-factored nominal moment capacities of the cantilever sections with top transverse steel and GFRP for a 1000 mm wide section were established as 82.7 and 142.2 kN*m/m respectively (Figure 2-26(a)). Both cantilever sections also had a corresponding strain in the concrete of 3500 με. Based on a 1000 mm wide section of the cantilevers, it is shown that the cantilever with top transverse steel was under reinforced because the steel yielded prior to the concrete crushing. On the other hand, both cantilever sections with FRP reinforcement were over-reinforced because the section failed prior to the CFRP and GFRP reinforcement achieving their respective ultimate strains of 9320 and 15870 με (Figure2-26(b)). It is noted that all of the output generated from the ***M_r Moment Capacity*** program was checked using hand calculations.

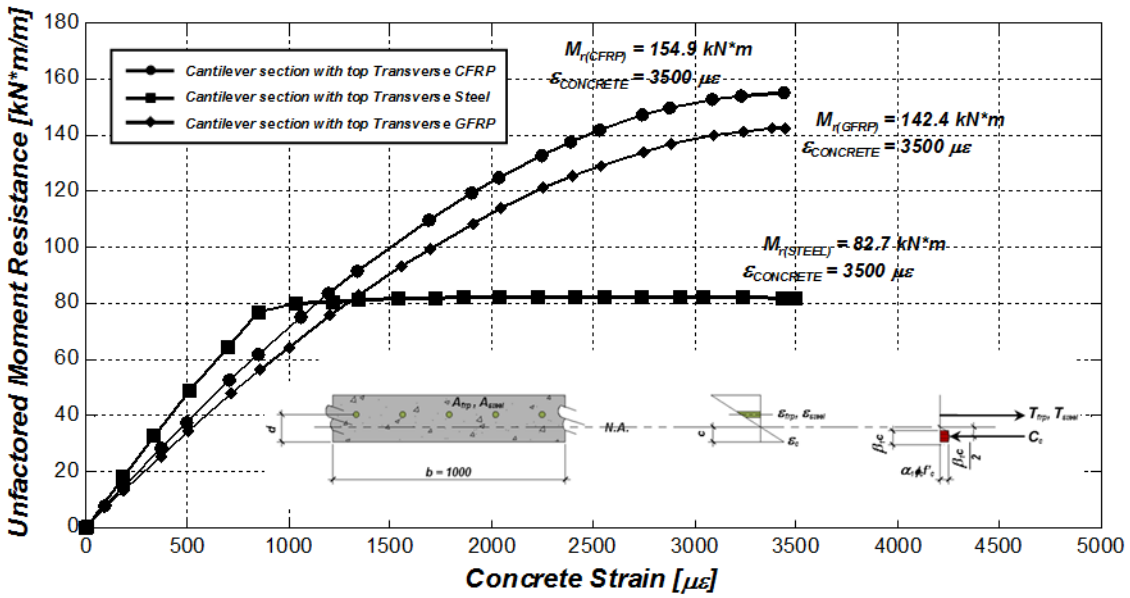

Figure 2-26(a): Plot of un-factored nominal moment resistance versus concrete strain for a 1000 mm wide section of all the cantilever sections based on strain compatibility (Klowak, 2007)

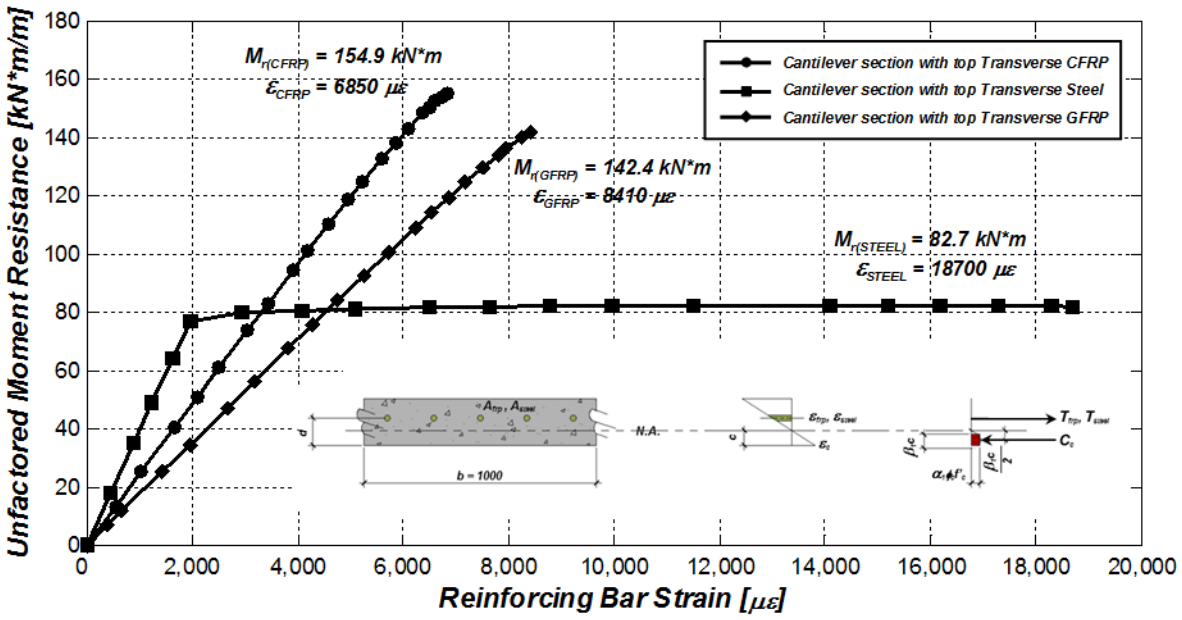

Figure 2-26(b): Plot of un-factored nominal moment resistance versus reinforcing bar strain for a 1000 mm wide section of all the cantilever sections based on strain compatibility (Klowak, 2007)

The experimental results indicated that the cantilever sections with top transverse CFRP, steel and GFRP failed at the ultimate static loads of 286, 301, and 294 kN respectively when they were subjected to a simulated wheel load on the extreme free edge of the cantilever. It is necessary at this point to make the following argument:

> *"If the behaviour of the different cantilever sections was completely and purely flexural, it is obvious that the ultimate load of the two cantilever sections with top transverse CFRP and GFRP should have failed at a higher ultimate load than the cantilever section with top transverse steel reinforcement. The static modes of failure, which consisted of a half frustum of a punch cone, were inconsistent with yield line theory in which the failure plane should be vertical and full depth. The argument presented is that the behaviour of the cantilever overhang of a bridge deck slab, when subjected to a wheel load, is not purely flexural. Arching-action may be present in bridge deck cantile ver slab overhangs (Klowak, 2007)."*

3. EXPERIMENTAL PROGRAM

The experimental program can be divided into six major categories, which include topics related to structural details, testing scheme, test set-up, instrumentation, static testing procedure, and fatigue testing procedure.

3.1 Structural Details

The following sub-sections describe the structural details of the bridge deck slab that was tested in the W.R. McQuade Heavy Structures Laboratory. Details specific to the steel girders that supported the deck, as well as the concrete dimensions and specifications, are discussed. Reinforcement details and specifications for the cantilever overhangs, internal panel, traffic barrier walls, edge beams, and haunches are also provided.

3.1.1 Steel Girder Details

The bridge deck was supported by two W920 X 387 steel girders spaced at 2500 mm center-to-center (Figure 3-1(a)). The girders measured 9000 mm in length with 19 mm thick web stiffeners spaced as shown in Figure 3-1(b). Steel Nelson studs that measured 22 mm in diameter and 200 mm in length were welded to the top flange of each girder. They were spaced at 400 mm center-to-center longitudinally and 110 mm transversely to facilitate composite action between the deck slab and the supporting steel girders (Figure 3-1(c)). The end diaphragms consisted of two back-to-back 102 X 102 X 13 mm thick steel angles for top

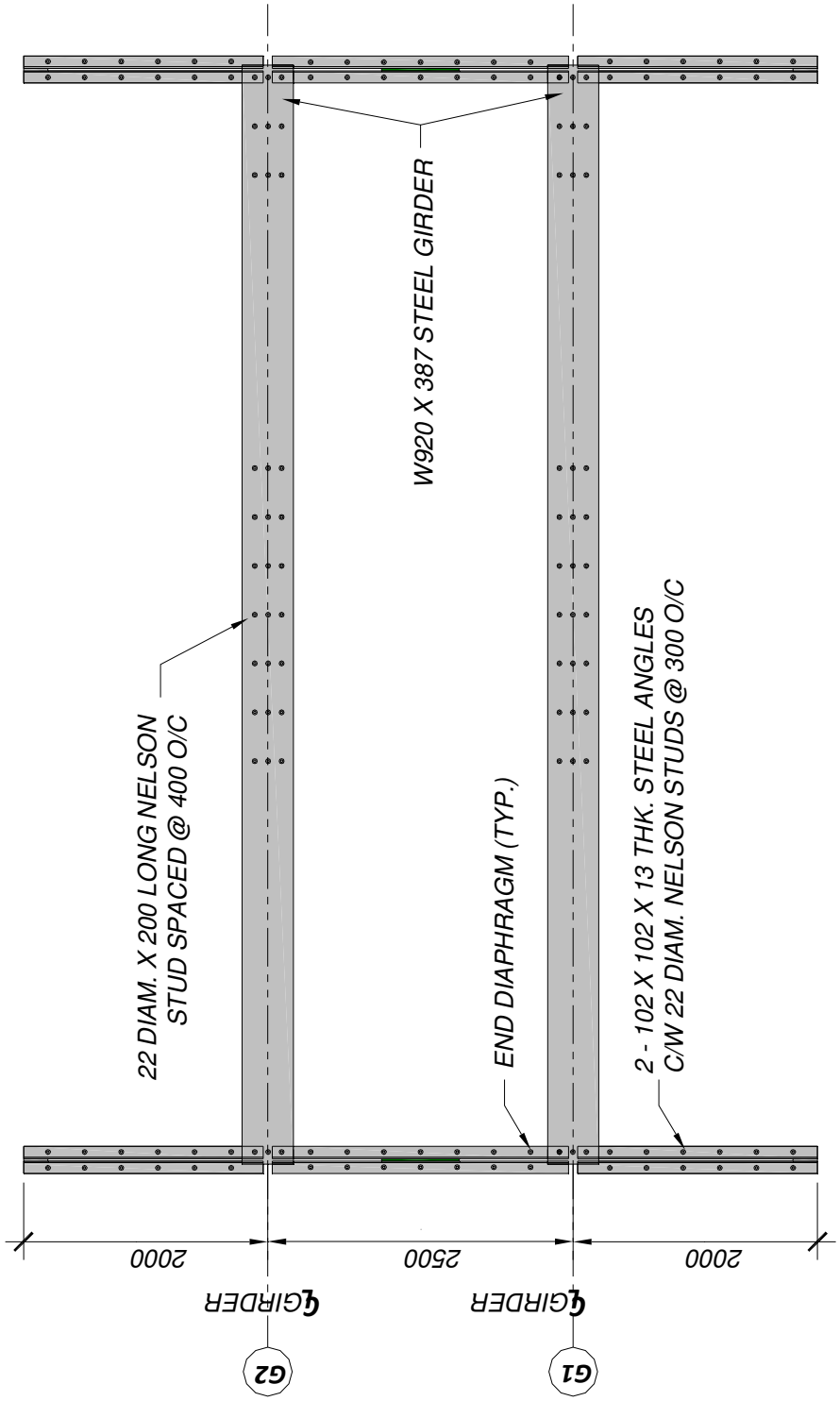

Figure 3-1(a): Plan view of steel girders and end diaphragms

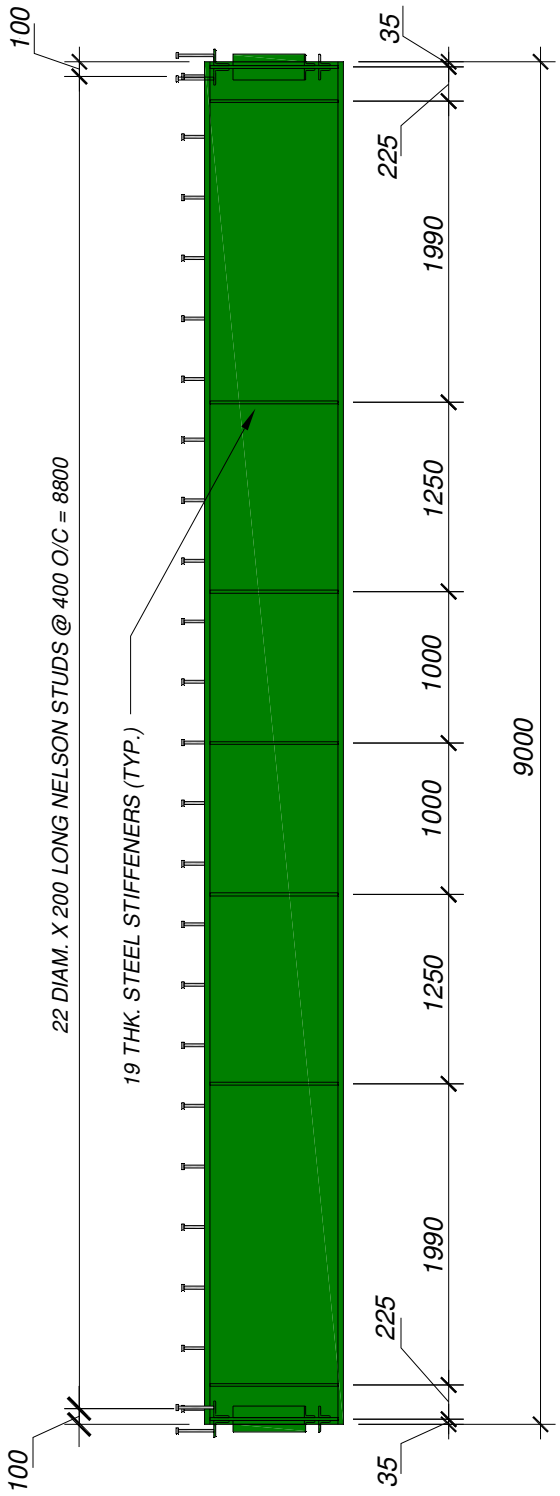

Figure 3-1(b): Elevation view of the steel girders and end diaphragms

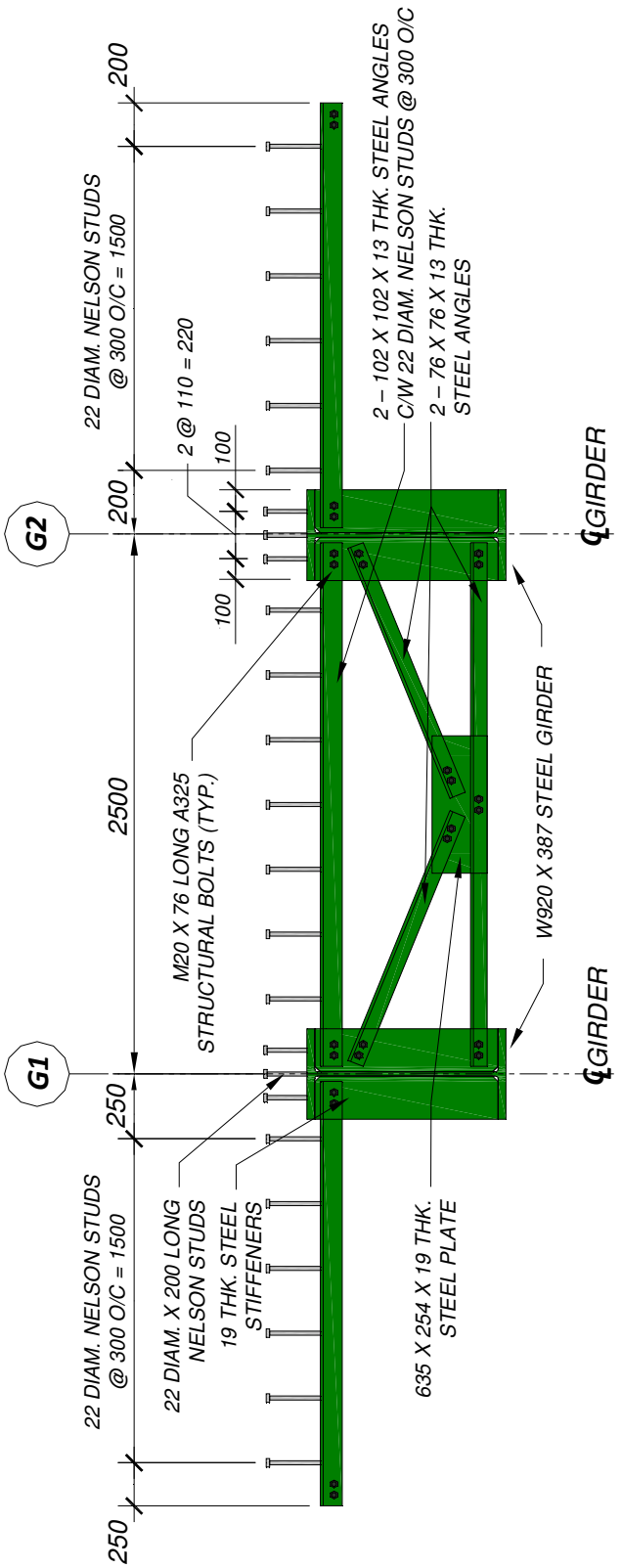

Figure 3-1(c): End view of the steel girders and end diaphragms

Figure 3-2(a): Photograph of end diaphragm

Figure 3-2(b): Photograph of steel girders after the removal of cantilever formwork

members, and back-to-back 76 X 76 X 13 mm thick steel angles for the diagonal and bottom members (Figure 3-1(c)). Steel Nelson studs measuring 22 mm in diameter and 250 mm in length were welded to the top back-to-back angles in order facilitate composite action for the two transverse free edge beams discussed in Section 3.1.2.1. The diagonal and bottom members of the diaphragm were connected by a 635 X 254 X 19 mm thick steel plate as shown in Figure 3-2(a). A photograph steel girders is shown in Figure 3-2(b).

3.1.2 Concrete Details

The concrete details, for the purpose of this report, are divided into two different categories: bridge deck slab concrete details and traffic barrier wall concrete details. The details discussed are specific to the bridge deck itself (i.e. cantilever overhangs, the internal panel, and edge beams). Concrete dimensions and details pertaining to the traffic barrier wall are also described in the following sections.

3.1.2.1 Bridge Deck Slab Concrete Details

The bridge deck, for the purpose of this report, consists of the cantilever overhangs, the internal panel, edge beams located at the two transverse free edges, and the haunches located over the girders. A photograph illustrating the placement of the concrete is shown in Figure 3-3. The bridge deck was a continuous cast-in-place concrete deck measuring 9150 mm in length and 6500 mm in width (Figure 3-4(a)). The deck slab thickness was 200 mm and it included 75 mm deep haunches over each of the steel girders. The internal panel of the deck

and cantilever overhangs had a span of 2500 and 2000 mm respectively from the center-lines of each of the girders (Figure 3-4(b)). Two edge beams measuring 220 mm in width and 335 mm in depth were cast along the transverse free edges of the deck slab (Figure 3-4(c)). The total volume of concrete required for the bridge deck slab and the haunches was approximately 12 cubic meters and required the use of two different concrete trucks to supply it. The concrete from the first truck was cast on the north half of the deck and the concrete from the second truck was poured on the south half of the deck. The specified concrete strength for the bridge deck slab was 35 MPa. Specified concrete parameters are outlined in Table 3-1. The concrete properties obtained from cylinder testing are outlined in Table 3-2. One cylinder from the north half of the bridge deck slab was instrumented with a longitudinal and transverse 50 mm concrete strain gauge for determining a stress-strain relationship as well as an experimental modulus of elasticity and Poisson's ratio (Figure 3-5).

Figure 3-3: Photograph of concrete placement for experimental bridge deck slab

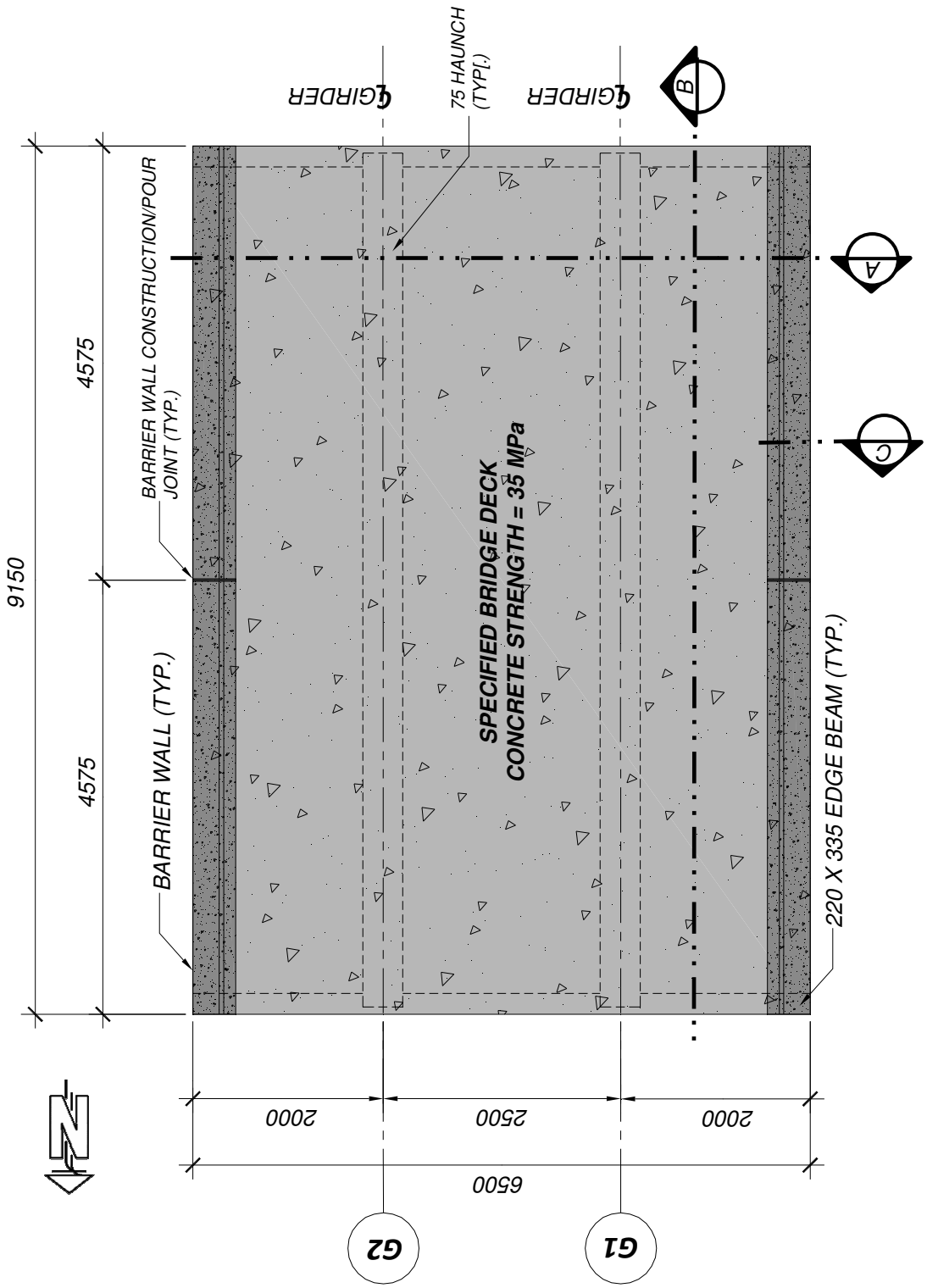

Figure 3-4(a): Plan view of the bridge deck slab concrete details

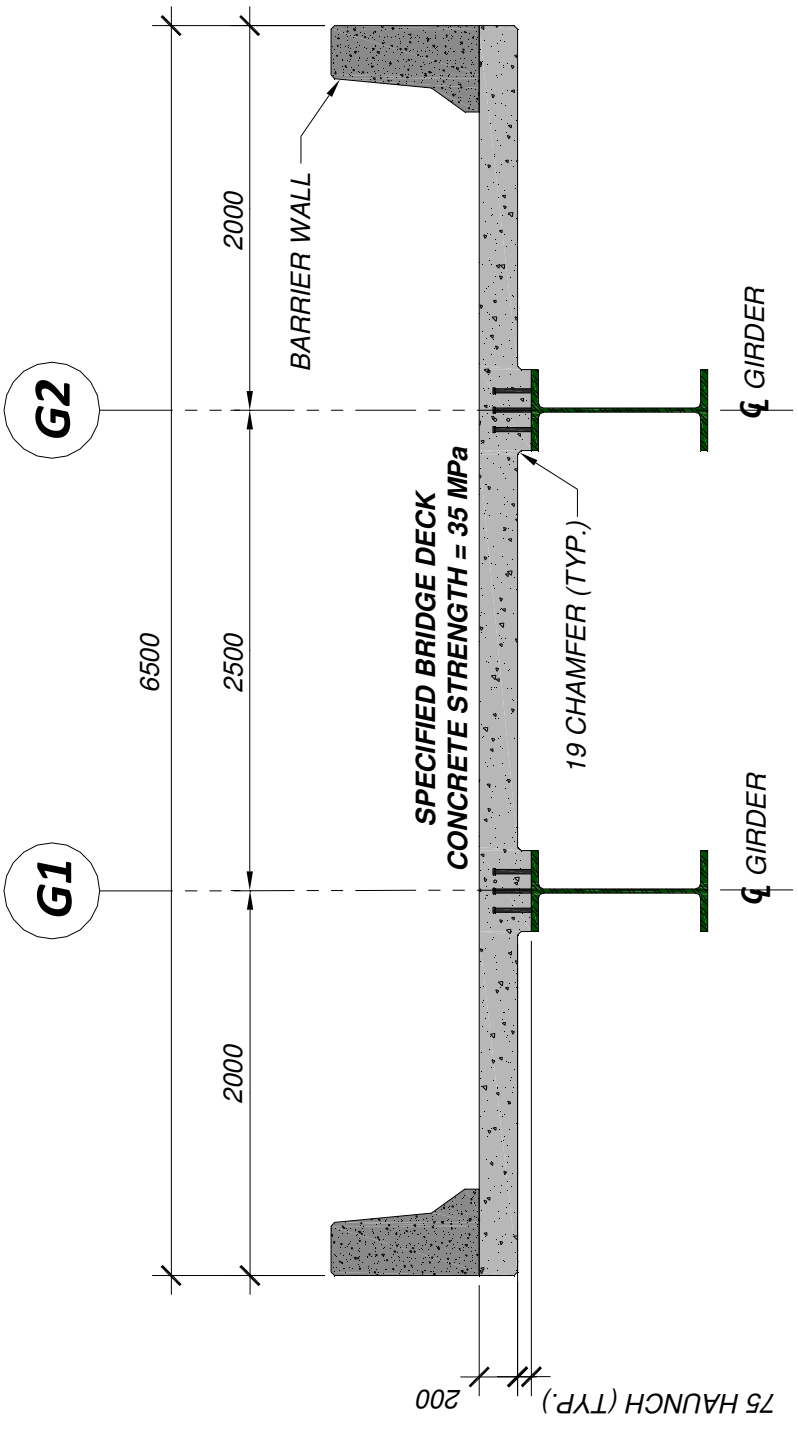

Figure 3-4(b): Transverse cross section of the bridge deck slab concrete details (Cross section "A" from Figure 3-4(a))

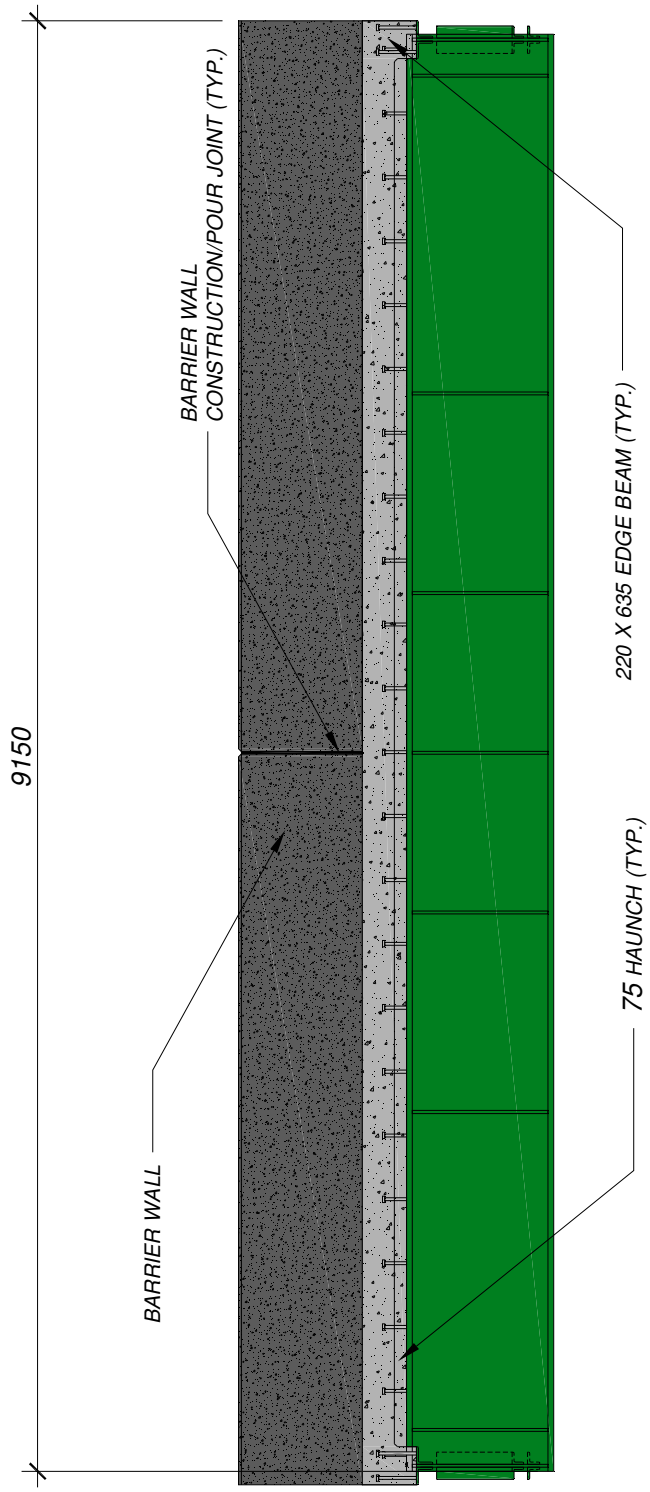

Figure 3-4(c): Longitudinal cross section of the bridge deck slab concrete details (Cross section "B" from Figure 3-4(a))

Table 3-1: Specified concrete parameters for bridge deck slab

Design Strength [MPa]	Cement Type	Max. Aggregate [mm]	Slump [mm]	Air Content [%]
35	*10 Normal*	*20*	*100*	*5 to 8*

Table 3-2: Bridge deck slab concrete mechanical properties obtained from testing of concrete cylinders

Pour Date	Test Date	Age of Test [Days]	Compressive Strength (f_c') [MPa]	Tensile Strength (f_r) [MPa]	Modulus of Elasticity (E) [MPa]	Remarks
01.30.2008	*02.27.2008*	*28*	*38.0*	*3.7*	*27740*	*Truck No. 1; placed on North half of deck*
01.30.2008	*02.27.2008*	*28*	*34.8*	*3.5*	*26546*	*Truck No. 2; placed on South half of deck*
01.30.2008	*10.09.2008*	*240*	*40.4*	*3.8*	*29713*	*Truck No. 2; placed on South half of deck*
01.30.2008	*03.04.2010*	*792*	*41.1*	*3.8*	*29906*	*Truck No. 2; placed on South half of deck*
01.30.2008	*11.30.2010*	*1062*	*45.1*	*4.0*	*30977*	*Truck No. 1; placed on North half of deck*
01.30.2008	*01.13.2011*	*1106*	*45.8*	*4.1*	*31160*	*Truck No. 1; placed on North half of deck*

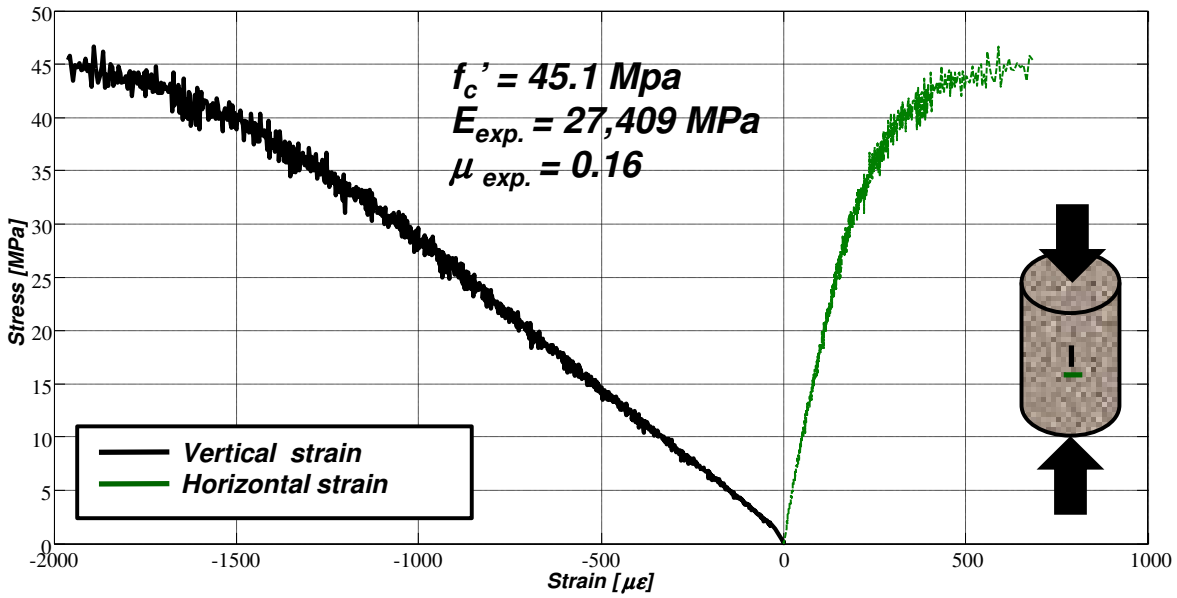

Figure 3-5: Plot of concrete longitudinal stress versus longitudinal and transverse strain for concrete cylinder compression testing

3.1.2.2 Traffic Barrier Wall Concrete Details

In order to simulate traffic barrier walls representative of those found on actual bridges, the barrier walls were cast with a pour joint at mid-span of the longitudinal length of the test bridge deck. The traffic barrier walls for the test bridge deck were cast in two different stages and connected via steel dowels and included and typical pour joint detail discussed in Section 3.1.3.4 (Figure 3-3(a)). The length of the barrier walls between the pour joints was 4575 mm. The overall height of the barrier wall was 775 mm and the width at the base was 450 mm. The face of the barrier walls that would be subjected to an impact from passing traffic had to different angles as shown in Figure 3-6. The specified concrete strength was identical to the strength of the deck and was 35 MPa. Specified concrete parameters are outlined in Table 3-3. The concrete properties obtained from cylinder testing are given in Table 3-4. A photograph illustrating the formwork and barrier wall construction is shown in Figure 3-7.

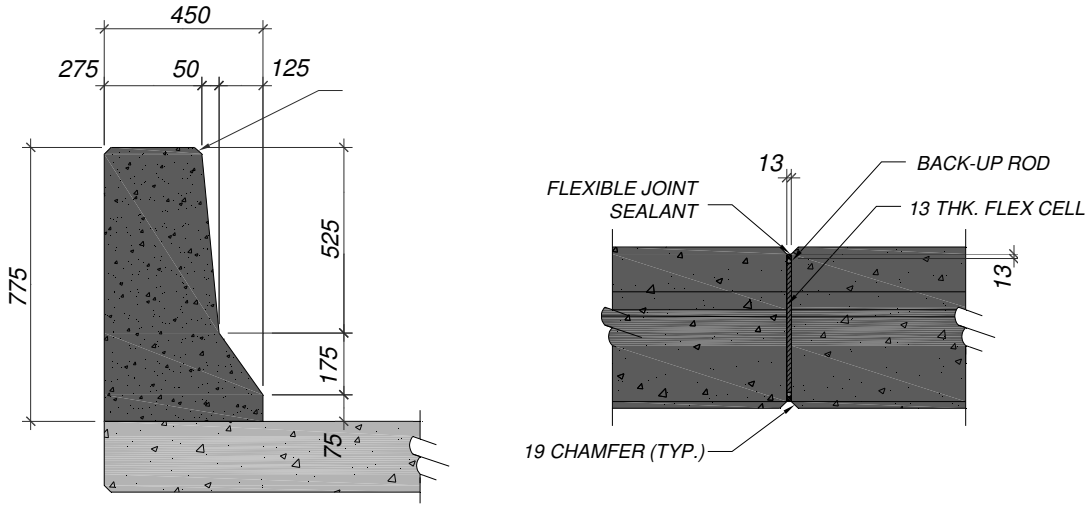

Figure 3-6: Barrier wall concrete details (Cross section "C" from Figure 3-4(a))

Table 3-3: Specified concrete parameters for traffic barrier wall

Design Strength [MPa]	Cement Type	Max. Aggregate [mm]	Slump [mm]	Air Content [%]
35	*10 Normal*	*20*	*100*	*5 to 8*

Table 3-4: Traffic barrier wall concrete mechanical properties obtained from testing of concrete cylinders

Pour Date	Test Date	Age of Test [Days]	Compressive Strength (f_c') [MPa]	Tensile Strength (f_r) [MPa]	Modulus of Elasticity (E) [MPa]	Remarks
04.15.2008	*05.13.2008*	*28*	*37.5*	*3.7*	*27557*	*North Barrier (East & West Side)*
05.24.2008	*06.21.2008*	*28*	*36.9*	*3.6*	*27335*	*South Barrier (East & West Side)*
01.30.2008	*10.09.2008*	*140*	*42.6*	*3.9*	*30313*	*South Barrier (East & West Side)*
01.30.2008	*03.04.2010*	*690*	*43.1*	*3.9*	*30448*	*South Barrier (East & West Side)*
01.30.2008	*11.30.2010*	*1062*	*43.9*	*4.0*	*30661*	*North Barrier (East & West Side)*
01.30.2008	*01.13.2011*	*954*	*43.2*	*3.9*	*30474*	*North Barrier (East & West Side)*

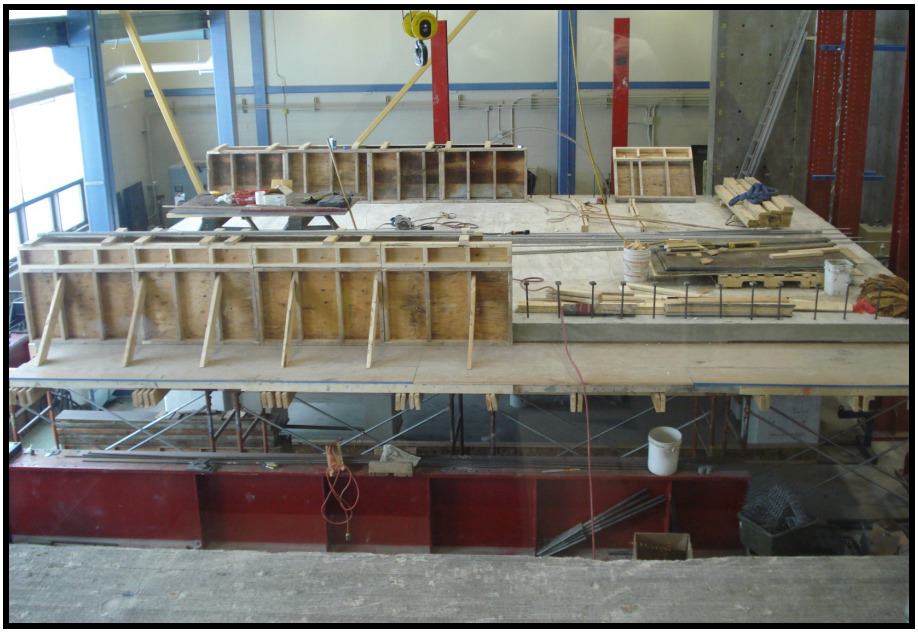

Figure 3-7: Photograph of traffic barrier wall construction

3.1.3 Reinforcement Details

The experimental bridge deck, although cast monolithically, was divided into two different sections (Figure 3-8). The north half of the bridge was comprised of a corrosion/steel free GFRP hybrid innovative design and the south half of the deck used conventional deformed steel reinforcement designed based on the empirical design method outlined in the CAN/CSA S6-06 CHBDC 2006 (Figure 3-9(a)). The following two sub-sections describe in detail the reinforcing details for the entire bridge deck which included internal panel reinforcement, cantilever overhang reinforcement, and reinforcement provided in the edge beams located at the transverse free edges of the bridge deck. For practical purposes, the reinforcement description will be described in terms of bottom reinforcement, top reinforcement, and reinforcement provided in the transverse free edge beams.

Figure 3-8: Photograph of internal GFRP and steel reinforcement prior to concrete placement

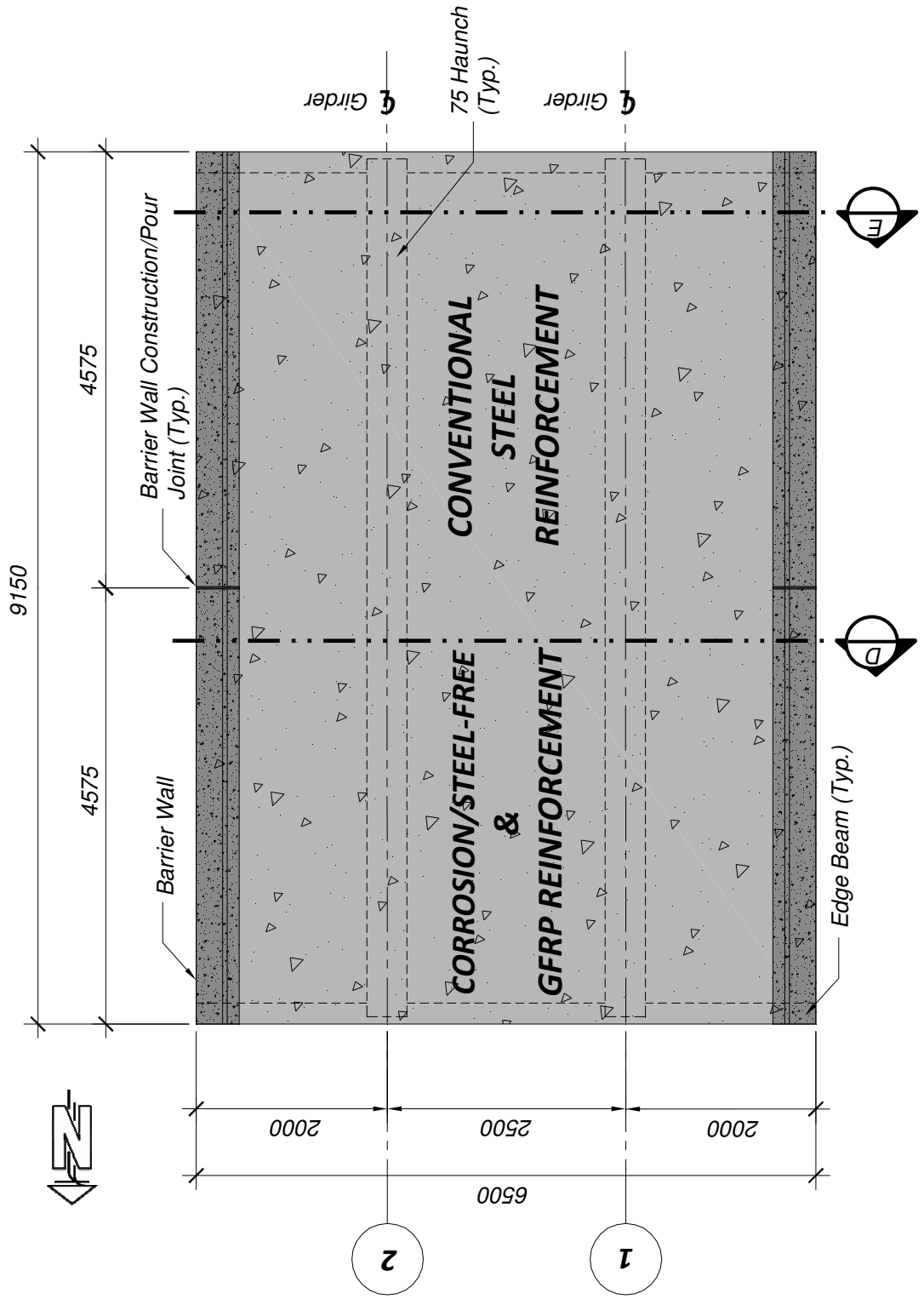

Figure 3-9(a): Plan view of bridge deck reinforcement

3.1.3.1 Bridge Deck Slab Reinforcement Details

The primary bottom reinforcement for internal panel reinforcement for the corrosion/steel-free GFRP hybrid half of the deck was comprised of external steel straps spaced at 1200 mm center-to-center measuring 25 X 50 mm complete with three 22 mm diameter Nelson studs. Reinforcement used for crack control consisted of No. 10 internal bottom GFRP bars spaced at 500 mm center-to-center in both the transverse and longitudinal directions (Figure 3-9(b)). The clear cover to the underside of the bottom transverse GFRP bars was 25 mm. The bars were placed in such a manner to ensure that there was a longitudinal bar located exactly at half of the internal panel span (longitudinal center line of the applied load and parallel to girders) and 2375 mm from the north free edge of the bridge deck slab (transverse center line of the applied load and perpendicular to the girders).

The bottom internal panel reinforcement for the conventionally steel reinforced half of the deck was comprised of bottom 15M deformed steel bars spaced at 300 mm in both the transverse and longitudinal directions (Figure 3-9(c)). The bars were placed in such a manner to ensure that there was a longitudinal bar located exactly at half of the internal panel span (longitudinal center line of the applied load and parallel to girders) and 2375 mm from the north free edge of the bridge deck slab (transverse center line of the applied load and perpendicular to the girders). The clear cover from the underside deck to the underside of the bottom transverse bars was 32 mm.

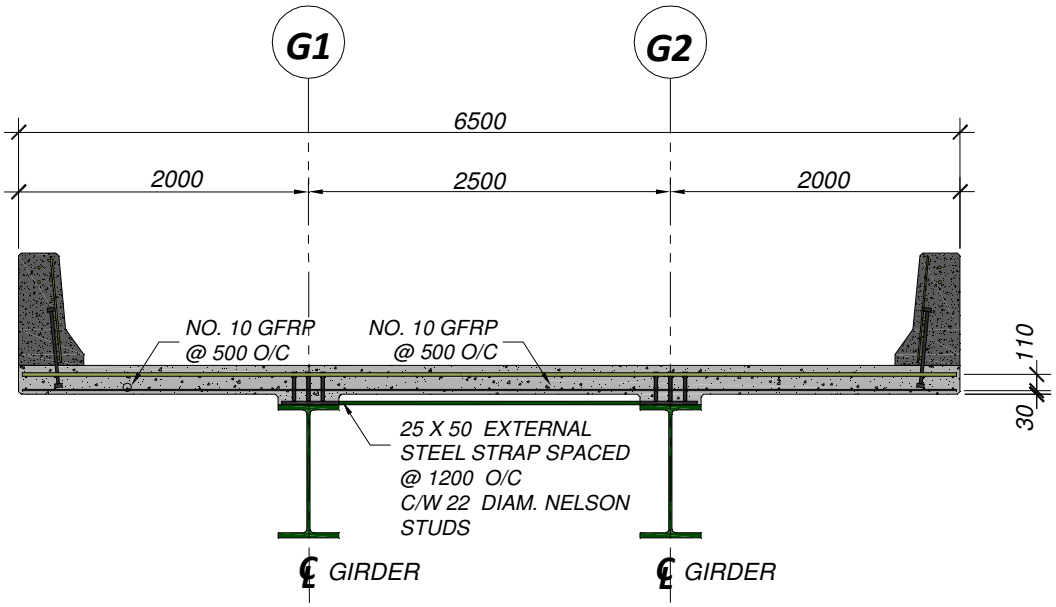

Figure 3-9(b): Typical cross section illustrating the bottom reinforcement details for section with GFRP reinforcement (Cross section "D" from Figure 3-9(a))

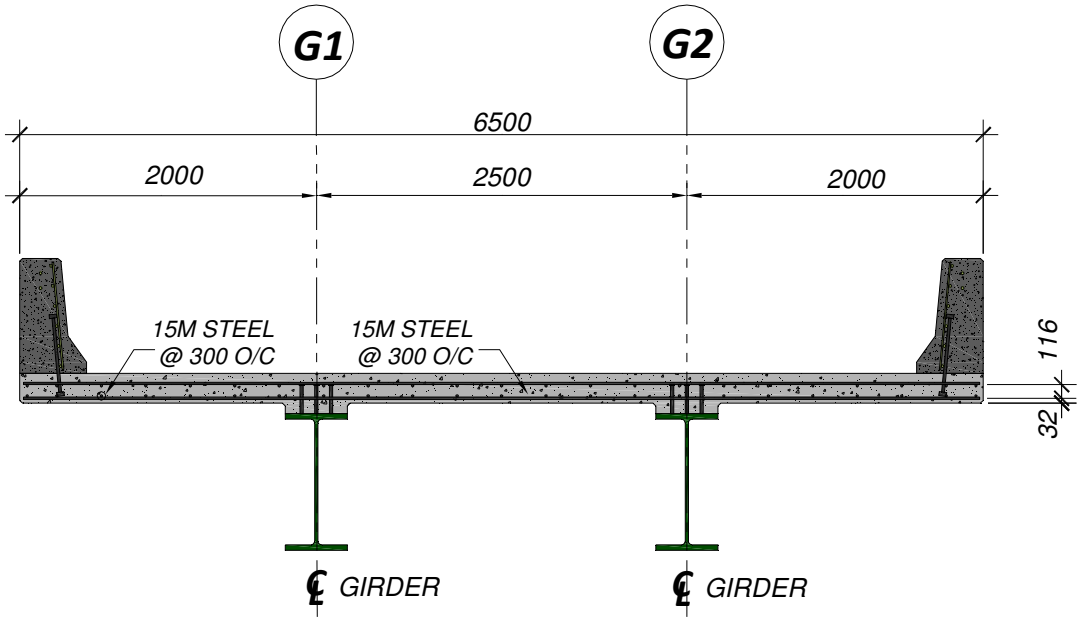

Figure 3-9(c): Typical cross section illustrating the bottom reinforcement details for the section with steel reinforcement (Cross section "E" from Figure 3-9(a))

Top longitudinal GFRP reinforcement consisting of No. 10 GFRP bars 4925 mm in length were spaced at 500 mm center-to-center and were tied using FRP approved tie wire to the underside of the top transverse GFRP bar. Top transverse GFRP reinforcement required to resist negative moments, typical to cantilever slab overhangs, consisted of No. 25 GFRP bars spaced at 175 mm center-center (Figure 3-9(d)). Due to a specification error provided to the manufacturer the bars were not continuous in length for the entire transverse width of the of the bridge deck slab. The bars measured 4425 mm in length and 3700 mm in length (i.e. with a lap splice length of 1250 mm) and the location of the splices were alternated every 175 mm such that every second bar contained a splice for each cantilever side of the bridge deck slab. The clear cover from the top surface of the concrete slab to the center-line of the top transverse bars measured 60 mm.

The top longitudinal steel bars measured 4925 mm in length and were spaced at 300 mm center-to-center and were tied to the underside of the top transverse bars using conventional steel rebar tie wire. Additional top transverse 15M steel bars measuring 6400 mm in length were added at a spacing of 100 mm center-to-center resulting in top transverse 15M steel bars spaced at 100 mm center-to-center to resist negative moments (Figure 3-9(e)).

Table 3-5 provides the complete reinforcing schedule for all reinforcement found in the bridge deck slab. Figures 3-10 through 3-12 show the stress versus strain plots for all of the bridge deck reinforcement obtained from static tensions tests conducted on the No. 10 GFRP bars, No. 25 GFRP bars, and 15M deformed steel bars.

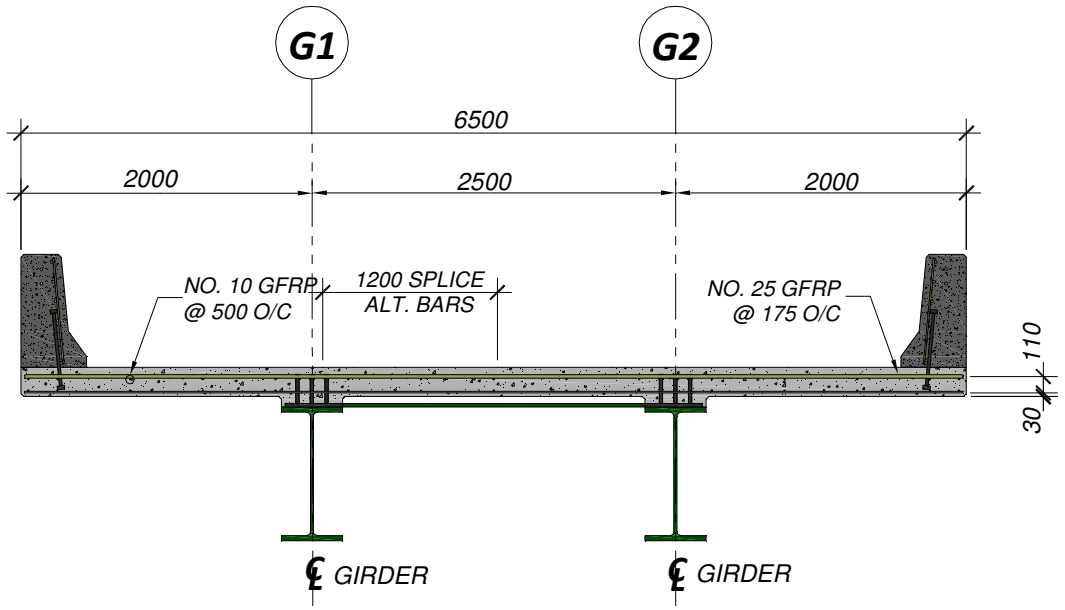

Figure 3-9(d): Typical cross section illustrating the top reinforcement details for section with GFRP reinforcement (Cross section "D" from Figure 3-9(a))

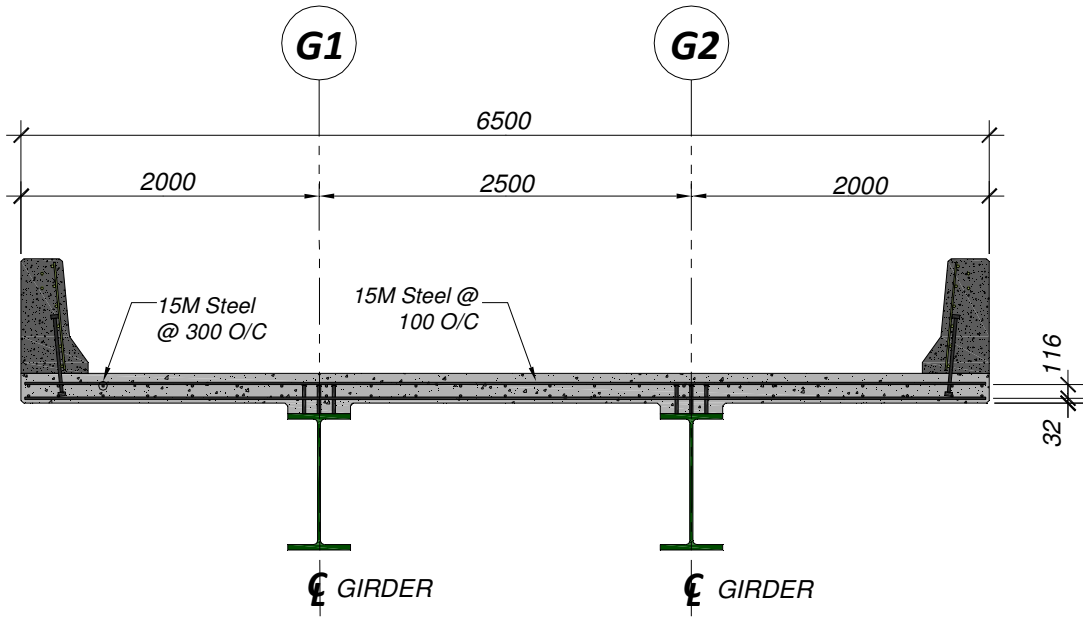

Figure 3-9(e): Typical cross section illustrating the top reinforcement details for the section with steel reinforcement (Cross section "E" from Figure 3-9(a))

The reinforcement for the edge beams located at the north and south transverse free edges of the deck slab consisted of four additional 15M steel transverse bars (two on the top and two on the bottom) as well as stirrups (Figure 3-15). The stirrups were comprised of 15M steel bars with a long leg on the top of the stirrup to aid in achieving composite action between the concrete slab and the steel angles (Figure 3-16).

Figure 3-10: Photograph showing transverse steel bars and stirrups located in transverse edge beam

Table 3-5: Bridge deck slab reinforcing bar schedule

Bridge Deck Bottom Reinforcement								
Location	**Type**	**Material**	**Size**	**Spacing [mm]**	**Diameter [mm]**	**Area [mm^2]**	**Length [mm]**	**No. of Bars**
GFRP Corrosion/Steel-Free	*External Steel Strap*	*Steel*	*-*	*1200*	*-*	*1250.0*	*2250*	*5*
GFRP Corrosion/Steel-Free	*Btm. Transverse*	*GFRP*	*No. 10*	*500*	*9.5*	*71.3*	*6400*	*10*
GFRP Corrosion/Steel-Free	*Btm. Longitudinal*	*GFRP*	*No. 10*	*500*	*9.5*	*71.3*	*4925*	*11*
Steel Reinforced	*Btm. Transverse*	*Steel*	*15M*	*300*	*16.0*	*200.0*	*6400*	*16*
Steel Reinforced	*Btm. Longitudinal*	*Steel*	*15M*	*300*	*16.0*	*200.0*	*4925*	*22*
Bridge Deck Top Reinforcement								
Location	**Type**	**Material**	**Size**	**Spacing [mm]**	**Diameter [mm]**	**Area [mm^2]**	**Length [mm]**	**No. of Bars**
GFRP Corrosion/Steel-Free	*Top Transverse*	*GFRP*	*No. 25*	*175*	*9.5*	*506.5*	*4425*	*26*
GFRP Corrosion/Steel-Free	*Top Transverse*	*GFRP*	*No. 25*	*175*	*9.5*	*506.5*	*3700*	*26*
GFRP Corrosion/Steel-Free	*Top Longitudinal*	*GFRP*	*No. 10*	*500*	*9.5*	*71.3*	*4925*	*14*
Steel Reinforced	*Top Transverse*	*Steel*	*15M*	*300*	*16.0*	*200.0*	*6400*	*46*
Steel Reinforced	*Top Longitudinal*	*Steel*	*15M*	*300*	*16.0*	*200.0*	*4925*	*22*
Edge Beam Reinforcement								
Location	**Type**	**Material**	**Size**	**Spacing [mm]**	**Diameter [mm]**	**Area [mm^2]**	**Length [mm]**	**No. of Bars**
GFRP Corrosion/Steel-Free	*Transverse*	*GFRP*	*15M*	*-*	*16.0*	*200.0*	*6400*	*4*
GFRP Corrosion/Steel-Free	*Stirrups*	*GFRP*	*15M*	*300*	*16.0*	*400.0*	*-*	*22*
Steel Reinforced	*Transverse*	*Steel*	*15M*	*300*	*16.0*	*200.0*	*6400*	*4*
Steel Reinforced	*Stirrups*	*Steel*	*15M*	*300*	*16.0*	*400.0*	*-*	*22*

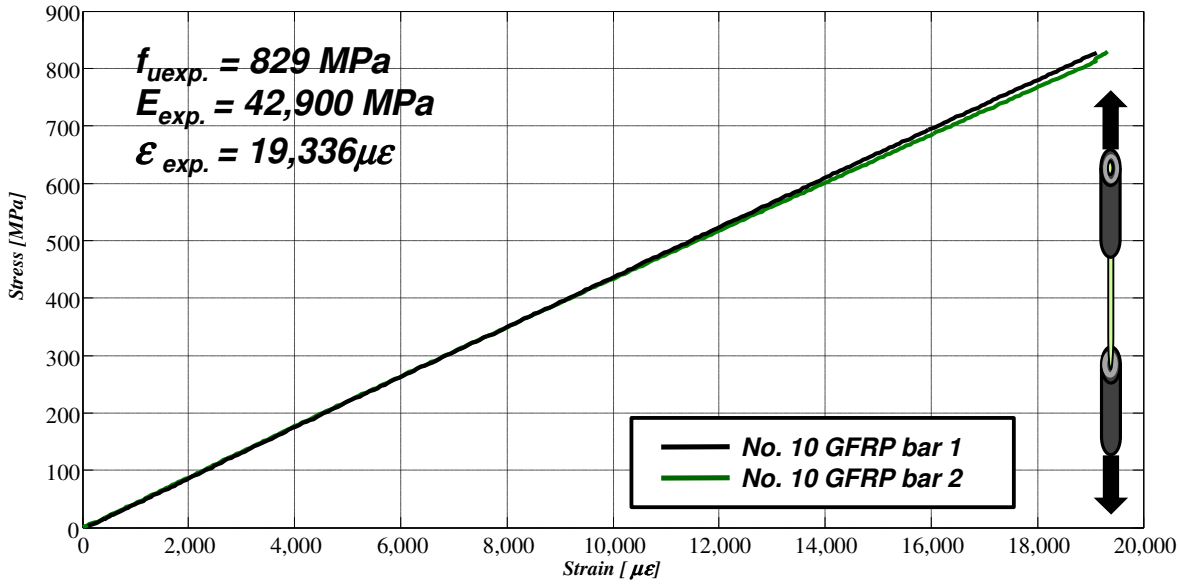

Figure 3-11: Plot of stress versus strain for no. 10 GFRP reinforcing bars

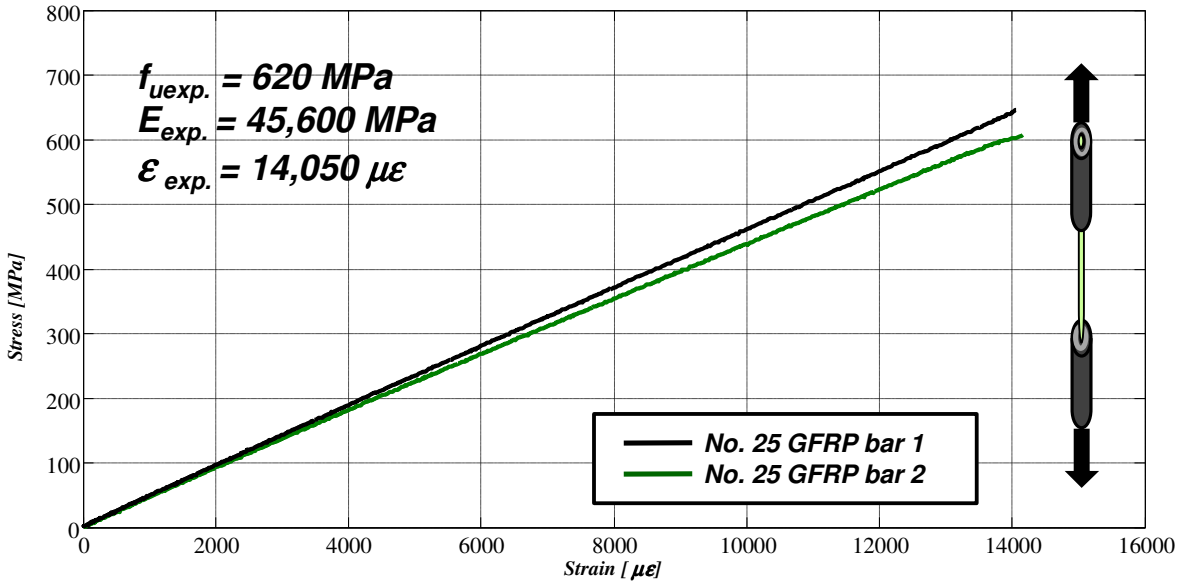

Figure 3-12: Plot of stress versus strain for no. 25 GFRP reinforcing bars

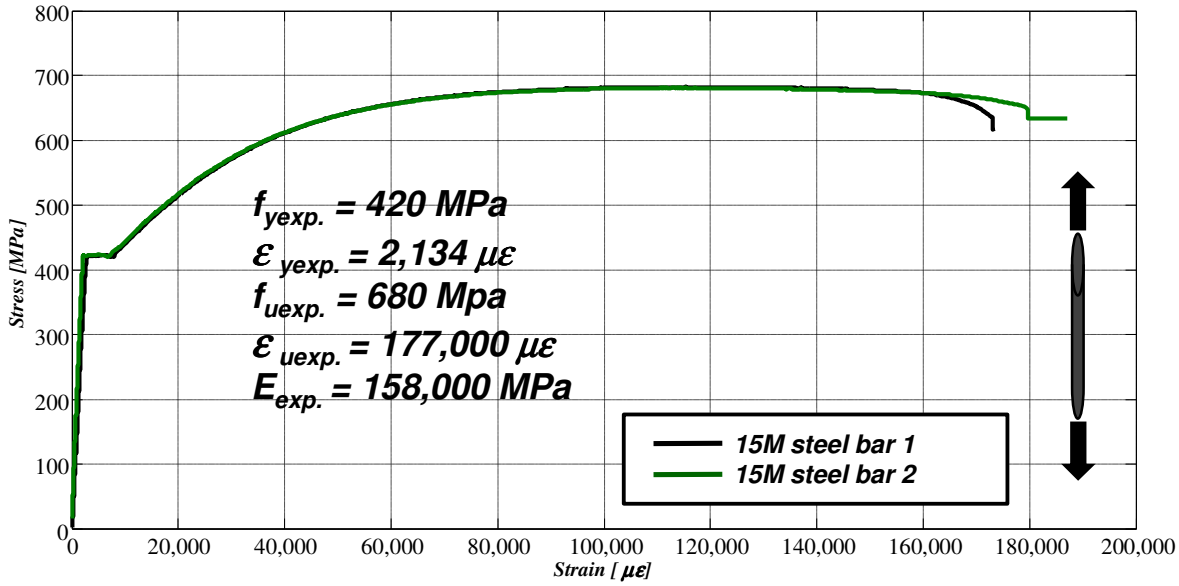

Figure 3-13: Plot of stress versus strain for 15M steel reinforcing bars

3.1.3.3 Traffic Barrier Reinforcement Details

The barrier wall design and construction was the same for both cantilever sections and consisted of both steel and GFRP reinforcement. Reinforcement for the traffic barrier walls involved reinforcement for two different pour joints (i.e. barrier wall to cantilever slab, and barrier wall construction/pour joint) as well as internal reinforcement. The barrier is usually cast at a later date than the cantilever slab and thus requires a method of connection able to withstand impact loads from passing traffic. The connection detail for the barrier wall to cantilever slab consisted of 19 mm diameter double headed anchor studs that measured 550 mm long spaced at 300 mm center-to-center. The heads on the studs measured 25 mm in thickness and 50 mm in diameter. The connection at the barrier wall construction/pour joint consisted of three 25 mm diameter smooth steel dowels that were 600 mm in length and spaced at 250 mm center-to-center (Figure 3-13). Internal reinforcement consisted of 6 no.

19 longitudinal GFRP bars spaced equally over the height of the barrier wall (approx. 135 mm). No. 10 GFRP vertical reinforcing bars were provided at a spacing of 150 mm center-to-center. Two additional No. 19 GFRP bars were provided at the locations shown in Figure 3-14). Table 3-6 provides the reinforcing bar schedule for the traffic barrier walls.

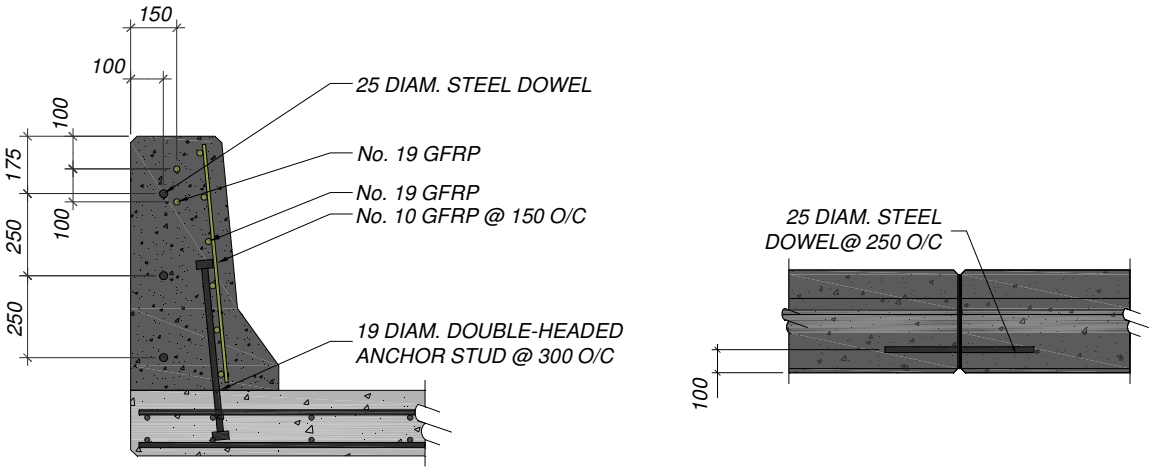

Figure 3-14: Barrier wall concrete details (Cross section "C" from Figure 3-3(a))

Table 3-15: Photograph of traffic barrier wall construction showing reinforcement

Table 3-6: Traffic barrier wall reinforcing schedule

Traffic Barrier Wall Reinforcement								
Location	**Type**	**Material**	**Size**	**Spacing [mm]**	**Diameter [mm]**	**Area [mm^2]**	**Length [mm]**	**No. of Bars**
Barrier Wall-to-Cantilever Slab	*Double Headed Steel Anchor Studs*	*Steel*	*-*	*300*	*19.0*	*283.3*	*550*	*62*
Barrier Wall Construction Joint	*Steel Dowels*	*Steel*	*-*	*250*	*25.4*	*505.5*	*600*	*6*
Barrier Wall	*Horiz. Longitudinal*	*GFRP*	*No. 19*	*135*	*19.0*	*283.3*	*4875*	*32*
Barrier Wall	*Vertical*	*GFRP*	*No. 10*	*150*	*9.5*	*71.3*	*700*	*128*

3.2 Testing Scheme

There were a total of six test locations for the bridge deck slab described in the previous sections. The fatigue testing conducted on the internal panel of this bridge deck slab is beyond the scope of this report. Therefore, the testing scheme for the cantilever slab overhangs was comprised of four different test locations. Each cantilever section was subjected to one static monotonic test to failure and one cyclic fatigue test to failure. The static tests were conducted on the west cantilever and the fatigue tests were conducted on the east cantilever (Figure 3-15(a)). The load plate for the static and fatigue tests conducted cantilever section with GFRP reinforcement was located 2325 mm from north transverse free edge. The load plate for the static and fatigue tests conducted on the cantilever section with steel reinforcement was located 2325 mm from south transverse free edge. The steel load plate, measuring 305 X 610 mm (standard dual tire foot print for a CL-625 design truck), for the static and fatigue tests conducted on the cantilever sections was located 600 mm from the inside face of the traffic barrier wall to the longitudinal center line (parallel to the girders) of the steel plate foot print as outlined in the CAN/CSA S6-06 CHBDC 2005 (Figure 3-15(b)).

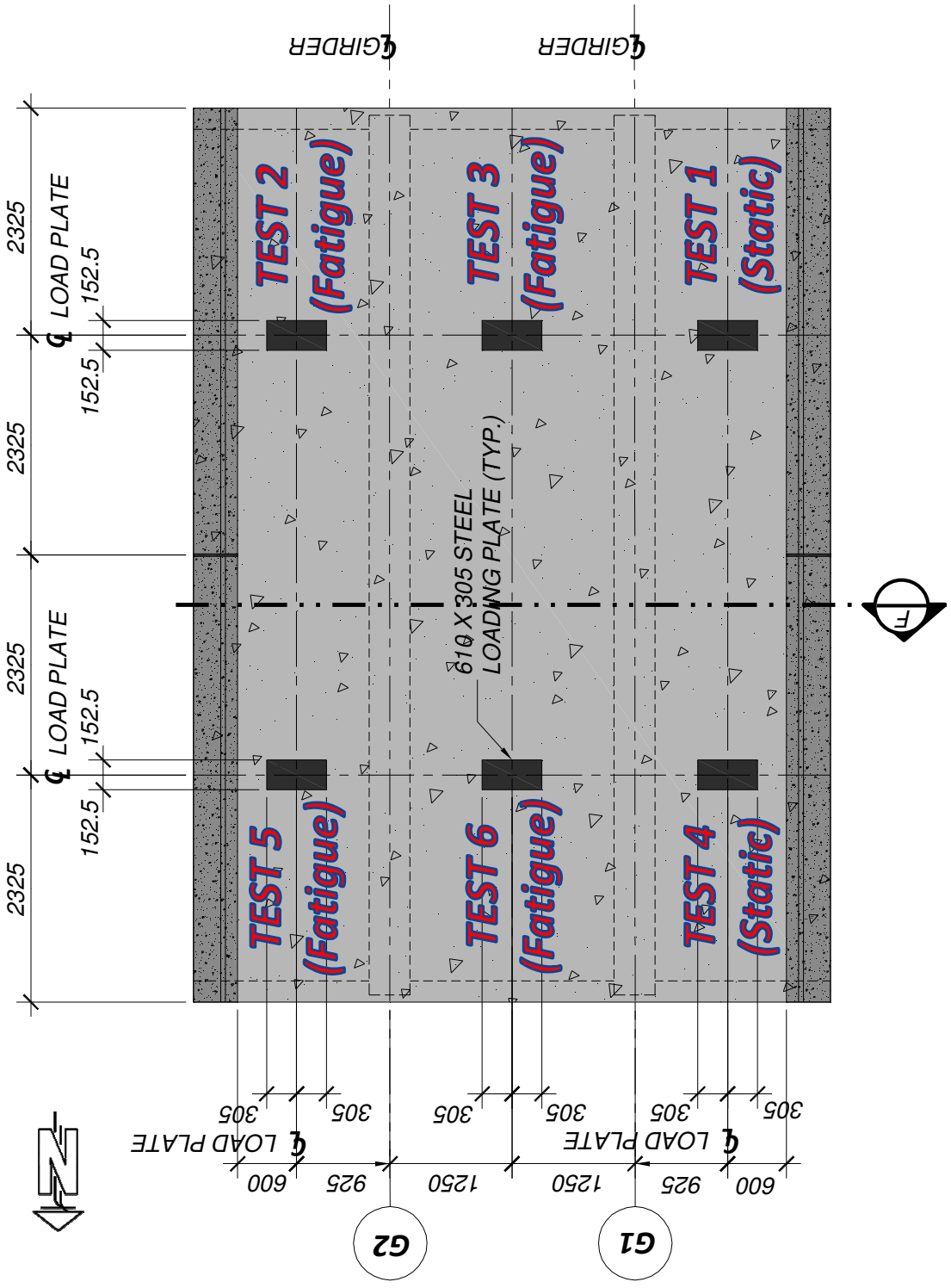

Figure 3-16(a): Plan view of testing scheme

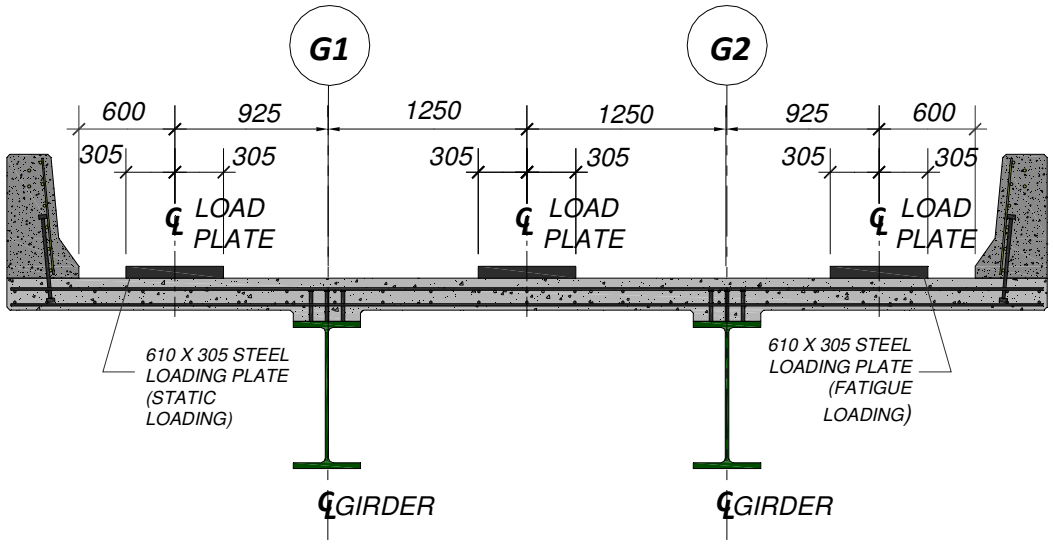

Figure 3-16(b): Typical cross section illustrating transverse location of steel loading plate (Cross section "F" from Figure 3-16(a))

3.3 Test Set-up

The preparatory work for each static and destructive test of the full-scale experimental bridge deck cantilever overhangs consisted of providing support for the superstructure (i.e. the steel girders and concrete deck). It involved the design and construction of the steel load frame, re-locating or moving the load frame to test each cantilever section, as well as setting up instrumentation and connecting it to a data acquisition system. It should be noted that the set-up for each of the four test locations was identical. To avoid repetition, a generalized description of the set-up is outlined in the following sub-sections pertaining to the details of how the superstructure was supported, details of the load frame, and the instrumentation required to provide important information about the performance and behaviour of each of the different cantilever sections. Figure 3-17 shows the full-scale test set-up.

3.3.1 Superstructure Support

Four concrete blocks measuring 750 X 750 X 1000 mm in depth were used to support the steel girders and the bridge deck slab. Plywood bearing pads that measured 400 X 400 X 38 mm thick were placed between the concrete block supports and steel girders. In order to avoid any up-lift on the adjacent girder when a cantilever was loaded, steel tie-downs were used along with high-strength Dywidag bars to post-tension both girders and the concrete supporting blocks to the structural floor.

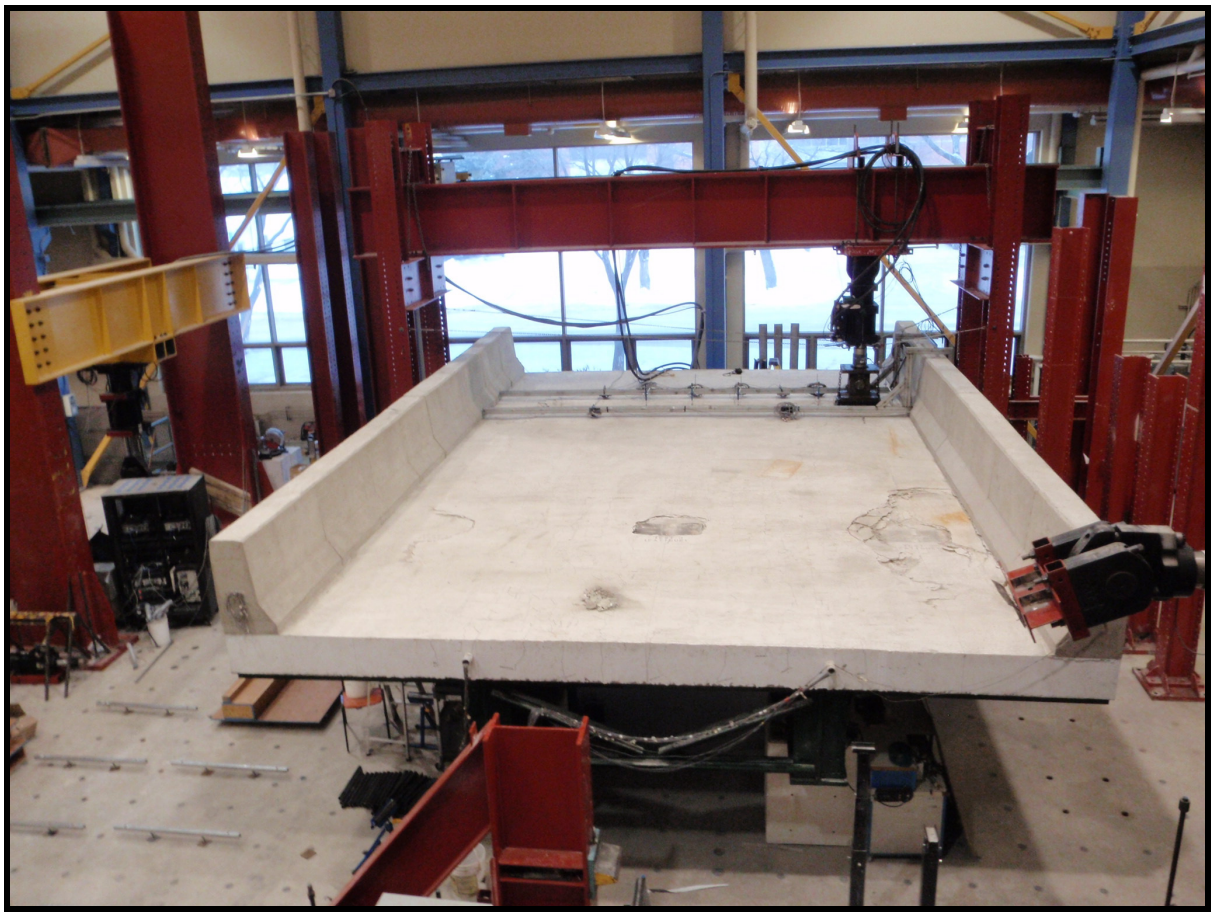

Figure 3-17: Photograph of test set-up for static and fatigue destructive testing of cantilevers

3.3.2 Load Frame and Loading Apparatus Details

The load frame was used for all four test locations and was comprised of the following components:

- 4 - W310 X 158 steel columns
- 2 - W410 X 86 steel cross-beams
- 2 - Miscellaneous steel cross-channels
- 1 - W920 X 387 steel loading beam

The four W310 X 158 steel columns were post-tensioned to the structural floor using high-strength Dywidag bars at the locations shown in figures 3-17(a) and (b). The W920 X 387 steel loading beam was bolted to the W410 X 86 steel cross-beams and miscellaneous steel channels with 16 19 20 mm diameter A325 structural bolts. The W410 X 86 steel cross-beams and miscellaneous steel channels were bolted to the W310 X 158 steel columns with a total of 48 25 mm A325 structural bolts.

A Materials Testing System (MTS) servo-hydraulic actuator, with a maximum capacity of 1000 kN, connected to a hydraulic pump located in the corner of the structures lab was used to load the cantilevers. The actuator was equipped with a swivel head; however, an additional swivel was placed below the actuator to accommodate rotation of the cantilever. A steel loading plate with a footprint of 610 mm in length and 305 mm in width was placed on top of a neoprene pad to simulate a wheel load from a CL-W design truck Steel chains

equipped with the appropriate shackles and turn-buckles were used to level and stabilize the actuator. A photograph showing the generalized view of the test set-up is pesented in Figure 3-17.

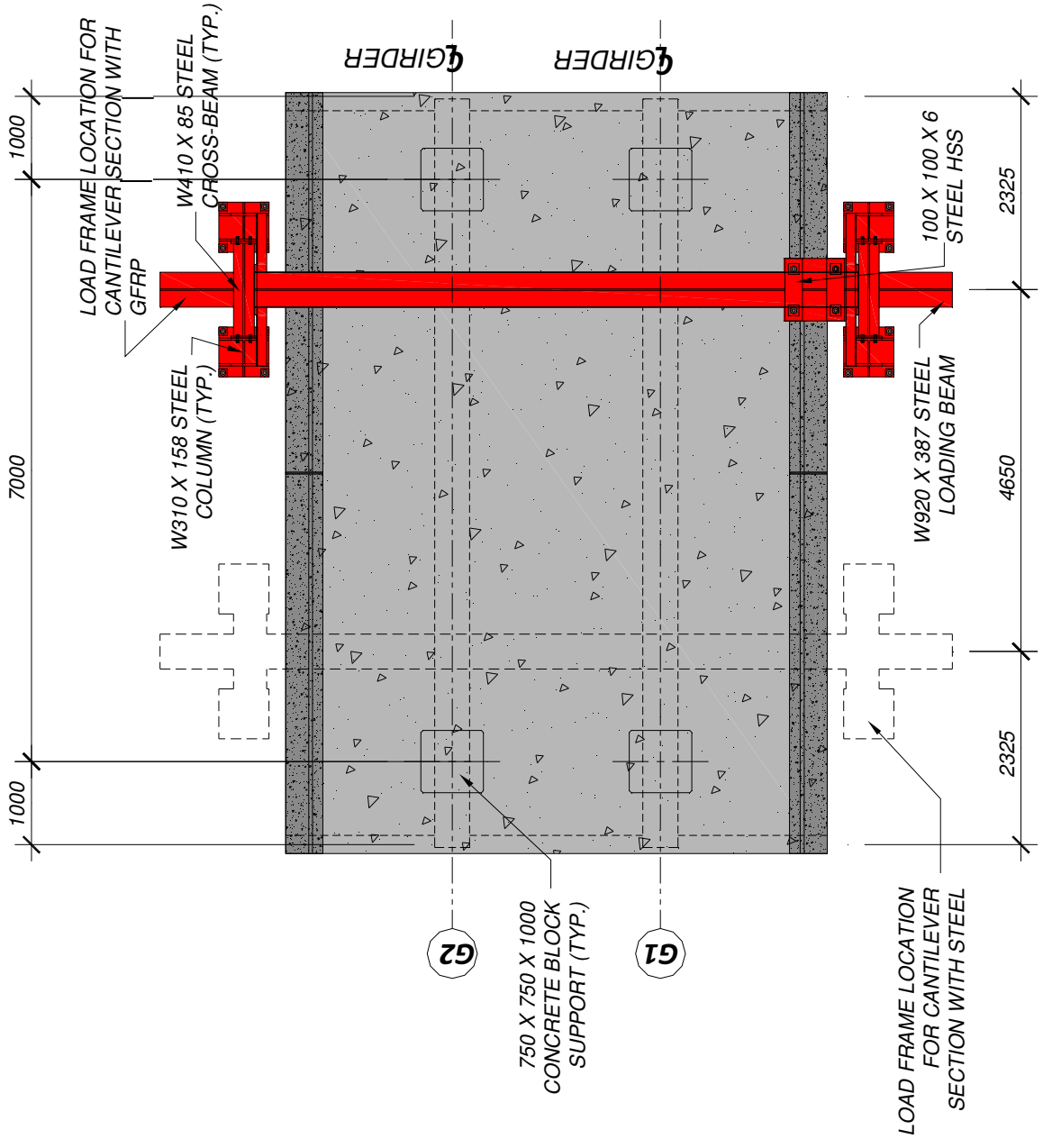

Figure 3-18(a): Plan view of full-scale test set-up illustrating superstructure support and load frame

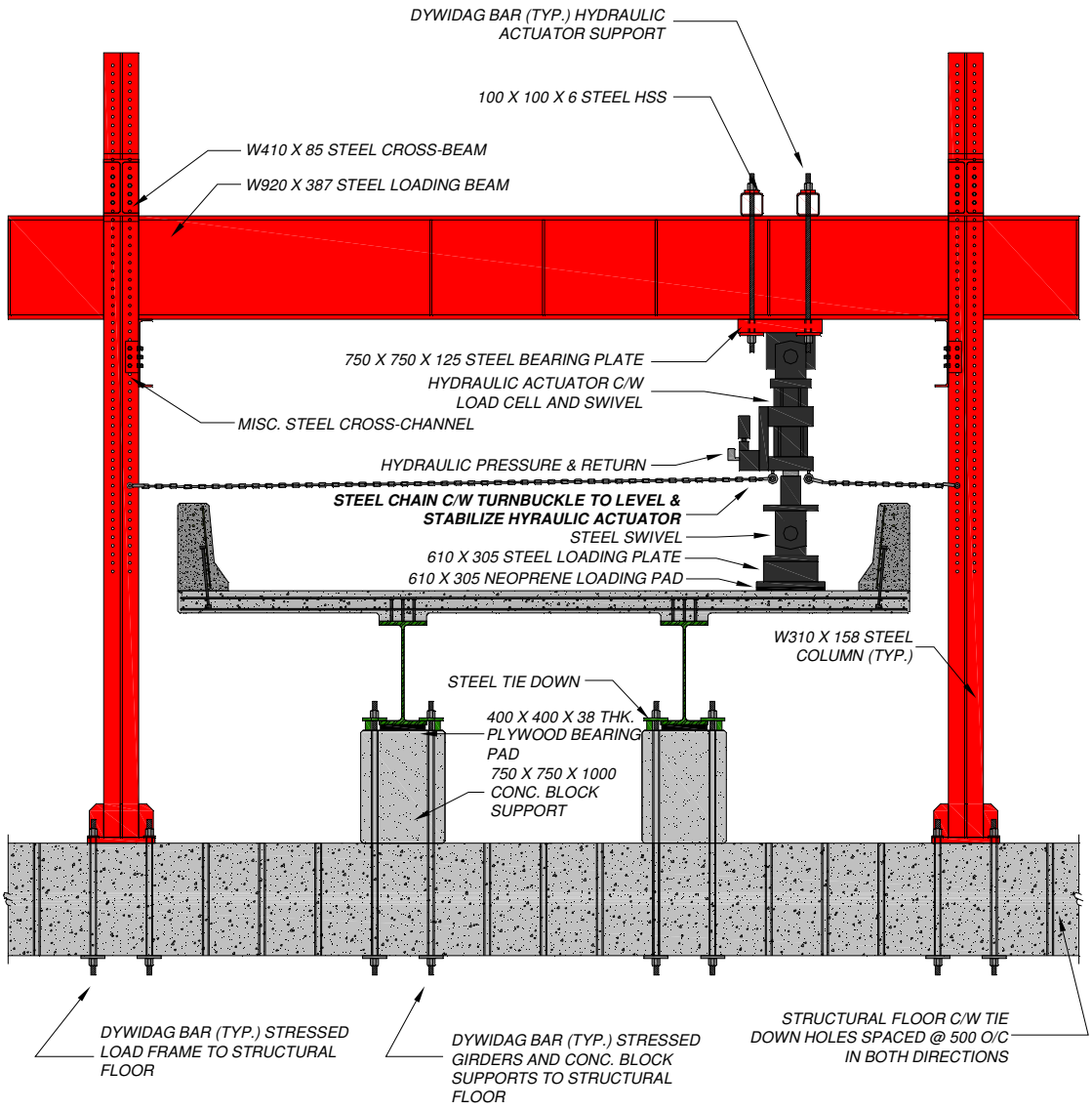

Figure 3-18(b): Typical cross-section of full-scale test set-up illustrating superstructure support and load frame

3.4 Instrumentation Details

Instrumentation for all of the static and fatigue test locations was required to record the magnitude of applied load, cantilever and internal panel displacements, strains in the top transverse reinforcing bars, strains in the bottom transverse and longitudinal reinforcing bars,

and crack widths. Instrumentation for all for test locations was identical. Concrete strain gauges were added for the static and fatigue tests conducted on the cantilever reinforced with GFRP. A detailed description of the various types of instrumentation used in the research program is outlined in the following four sub-sections.

3.4.1 Load Measurement

The 1000 kN load cell attached to the hydraulic actuator was connected to a data acquisition system which displayed the magnitude of the applied load during the various tests. The load magnitude was recorded at a rate of 2 Hz for all of the static tests and 4 Hz for the fatigue tests. A frequency of 4 Hz was adequate because the cyclic loading rate for the fatigue tests was only 0.2 Hz, thus resulting in 20 readings per cycle.

3.4.2 Displacement Measurement

Vertical deflections of the cantilever slab overhangs and the internal panel were measured using linear variable displacement transducers (LVDTs). They were measured along the center-line of the load plate in the transverse (perpendicular to girders) direction. A total of seven LVDTs were supported by clamps attached to a steel uni-strut supported by miscellaneous steel angles placed over the girder center-lines. They were supported in that manner to facilitate an accurate measurement of the cantilever and the internal panel displacements relative to the deflections of the steel girders. Deflections along the center-line of the load plate in the transverse direction were measured at the extreme longitudinal

free edge, halfway between the load plate and the longitudinal free edge, at the longitudinal center-line of the load plate, halfway between the load plate and the girder, and at quarter-points in the internal panel (Figure 3-19). All of the displacement transducers were connected to the data acquisition system via extension cables. Deflection measurements were recorded at a rate of 2 Hz and 4 Hz for the static and fatigue tests respectively. A photograph illustrating the locations and rack used to mount them is shown in Figure 3-20.

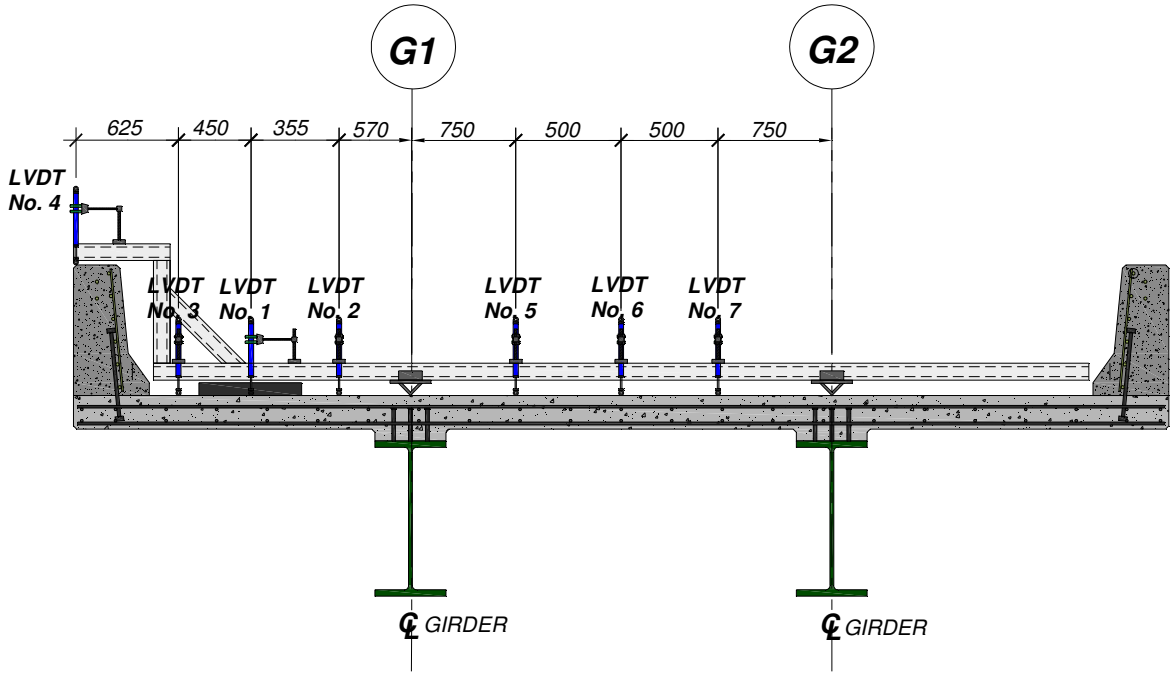

Figure 3-19: Schematic illustrating the LVDT supporting apparatus used to measure deflections of the cantilever and internal panel relative to the girders

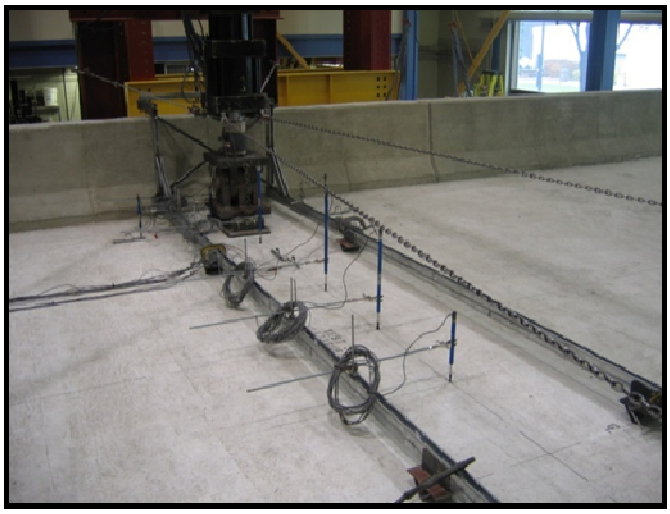

Figure 3-20: Photograph illustrating the LVDT supporting apparatus used to measure deflections of the cantilever and internal panel relative to the girders

3.4.3 Strain Measurement

A total of 154 electronic strain gauges were installed on internal reinforcing bars for measuring strain magnitudes. A large number were used because it was essential to understand the behaviour of the cantilever overhang, internal panel, and barrier wall due to the applied load on the cantilever slab overhang. Strain gauges were installed on the top transverse reinforcing bars, bottom longitudinal and transverse reinforcing bars, as well as on longitudinal reinforcing bars located in the traffic barrier wall. The following sub-sections describe the number and location of the strain gauges as they related to each individual test.

3.4.3.1 Top Transverse Reinforcing Bar Strain Measurement

65 (45 per test location) electronic strain gauges (6 mm gauge length) were installed at various locations along the length of five different top transverse reinforcing bars. Symmetry

was assumed in order to obtain the maximum amount of information with respect to transverse and longitudinal negative bending moment intensities. To avoid repetition for static and fatigue test locations, it is noted that the only difference between strain gauge locations for the cantilevers reinforced with steel and GFRP was the transverse reinforcing bar spacing (perpendicular to girders) between instrumented bars. The transverse spacing (parallel to girders) was identical for all four test locations. The transverse spacing of the strain gauges located on the top transverse reinforcing bars in the cantilevers was essentially 500 mm center-to-center (Figure 3-21 and 3-22). The spacing varied in the internal panel slightly as shown. The spacing in the longitudinal direction for cantilevers reinforced with steel and GFRP was 300 mm center-to-center and 350 mm center-to-center respectively (Figure 3-21 and 3-22). For all of the test locations the first bar was located under the transverse center line of the applied load. The adjacent reinforcing bars moving away from the transverse center line of the applied load towards the transverse free edges were also instrumented. All of the strain gauge wires were cable tied to the underside of the top reinforcing bars and exited the deck via rigid PVC conduit installed in the haunches.

3.4.3.2 Bottom Transverse and Longitudinal Reinforcing Bar Strain Measurement

40 (12 per steel test location and 8 per GFRP test location) 6 mm long electronic strain gauges were installed on the bottom transverse and longitudinal reinforcing bars for all cantilever test locations. The instrumentation of the bottom reinforcing bars was crucial for aiding the researchers in determining the presence of arching-action. Research conducted by Klowak 2007 did not include the instrumentation of bottom reinforcing bars. Gauge

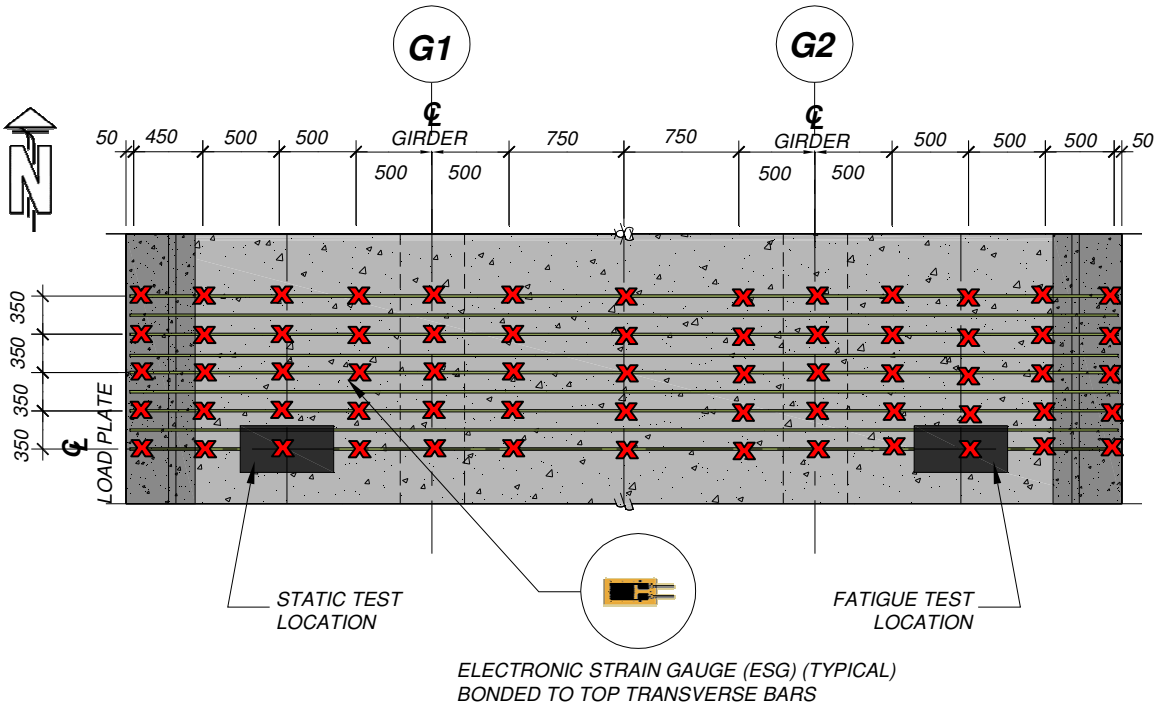

Figure 3-21: Schematic illustrating top transverse reinforcing bar strain gauge locations for the cantilever section with GFRP reinforcement

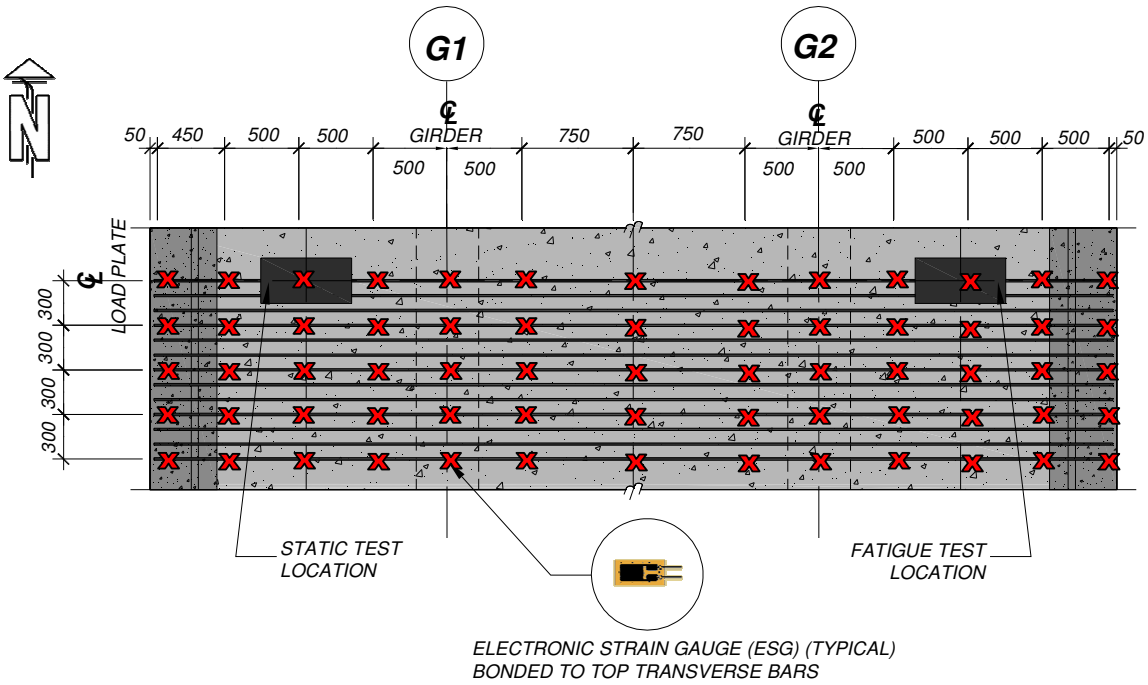

Figure 3-22: Schematic illustrating top transverse reinforcing bar strain gauge locations for the cantilever section with steel reinforcement

locations were the same for the static and fatigue testing of a given cantilever section. However, strain gauge spacing did vary between the two different cantilever sections because the bottom reinforcing ratios were different between the cantilever sections reinforced with steel and GFRP. Gauges were placed on the underside of three of the bottom transverse reinforcing bars and two of the longitudinal reinforcing bars at the locations shown in Figure 3-23 for the cantilever with steel reinforcement. Strain gauges were located on two of the bottom transverse bars and three of the longitudinal bars at the locations illustrated for the cantilever section reinforced with GFRP for the static and fatigue test locations (Figure 3-24). All of the strain gauge wires were cable tied to the underside of the bottom reinforcing bars and exited the deck through the rigid PVC conduit installed in the haunches.

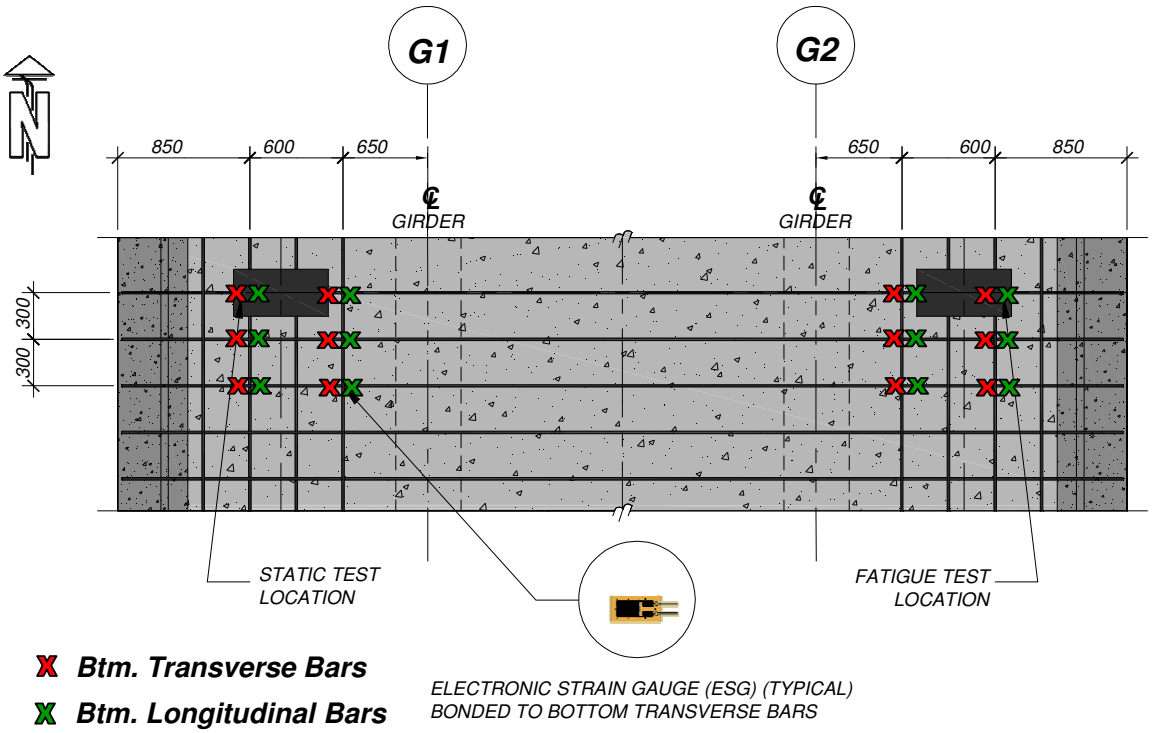

Figure 3-23: Schematic illustrating bottom transverse and longitudinal reinforcing bar strain gauge locations for the cantilever section with steel reinforcement

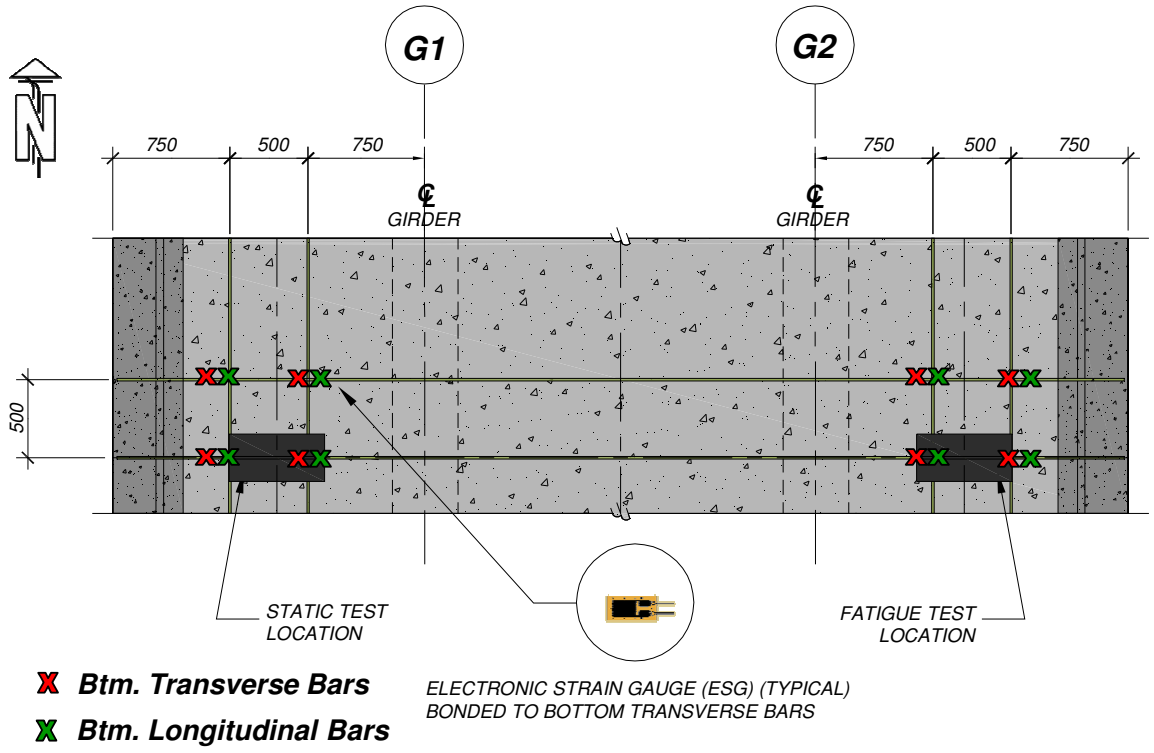

Figure 3-24: Schematic illustrating bottom transverse and longitudinal reinforcing bar strain gauge locations for the cantilever section with GFRP reinforcement

3.4.3.3 Top of Cantilever Slab Overhang Concrete Surface Strain Measurement

After observations from the static and fatigue testing of the cantilever with steel reinforcement, researchers decided to place 50 mm long concrete strain gauges on the top surface of the cantilever slab in close proximity of the steel loading plate. The gauges were placed as close as possible to the loading steel loading plate orientated such that they would measure strain magnitudes in the transverse direction, or the direction in which flexural strains due to negative moments should be present. Researchers felt that gauges in the location shown in Figure 3-25 would greatly increase the understanding of the cantilevers

behaviour. Observations with respect to strain magnitudes would also aid in determining the presence of arching-action.

Figure 3-25: Photograph illustrating location of a concrete strain gauge placed in the transverse direction on the top surface of the cantilever slab overhang near the steel loading plate

3.4.3.4 Barrier Wall Longitudinal Reinforcing Bar Strain Measurement

A total of 16 (4 per test location) 6 mm electronic strain gauges were installed on the longitudinal GFRP reinforcing bars located in the traffic barrier wall. The gauges were installed at the transverse center line of the applied load. Researchers felt instrumenting the barrier wall would aid in determining if it carried load as a structural member or acted like a supporting girder from above. The strain gauge locations were the same for all four test locations and are shown in Figure 3-26.

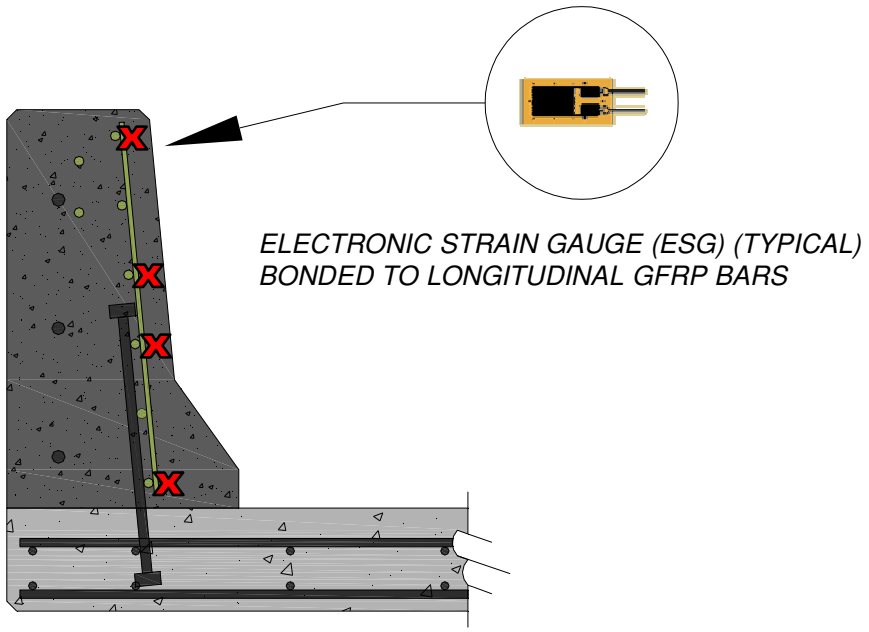

Figure 3-26: Schematic illustrating strain gauge locations on longitudinal GFRP reinforcement in the traffic barrier wall (typical all test locations)

3.3.3.4 Crack Measurement

Pi gauges with a gauge length of 200 mm were used to measure crack widths for static and fatigue loading destructive testing. The pi gauge locations for all four tests were identical. Two pi gauges were placed over the girder to measure crack widths due to flexure in the region of maximum negative moment. Two additional pi gauges were placed on the underside of the cantilever located below the loading plate to monitor static and fatigue crack widths based on crack patterns observed by Klowak 2007. All of the pi gauges were connected to the data acquisition system via extension cables and recorded static and fatigue crack widths at 2 Hz and 4 Hz respectively. Photographs showing the pi gauges installed on the underside of the cantilever slab overhang and on the top concrete surface over the girder are presented in Figures 3-27(a) and 3-27(b) respectively.

Figure 3-27(a): Photograph showing pi gauge locations on the underside of the cantilever slab overhand under the loading plate (typical all test locations)

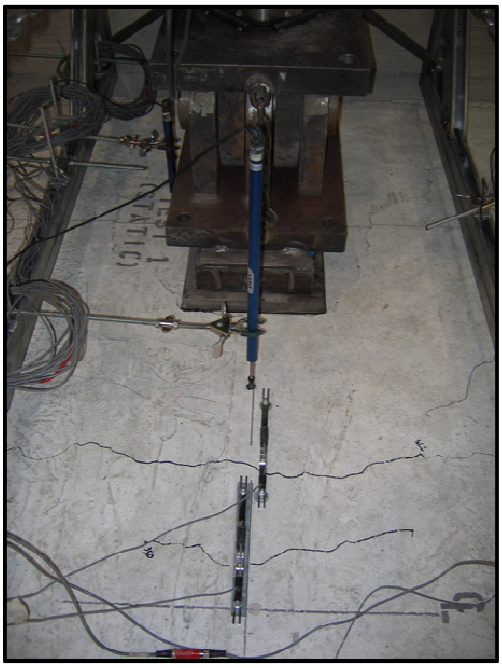

Figure 3-27(b): Photograph showing pi gauge locations on the top concrete surface over the girder (typical all test locations)

3.5 Test Procedure for Static Monotonic Destructive Tests

The test procedure was the same for both of the static monotonic destructive tests conducted on the two different cantilever sections with only a few differences. The only alteration in the procedure was unforeseen problems with the hydraulics and the observed failure loads.

3.5.1 Test Procedure for Static Monotonic Destructive Test Conducted on the Cantilever Section with Steel Reinforcement

The load was monotonically increased at a rate of 1 mm per minute up to a maximum load of 110 kN (slightly higher than typical service loads) where it was held constant to allow for inspection of the cantilever section. The load was then removed. This process was repeated 10 times to stabilize the cantilever section before proceeding to failure. After completing the pre-load cycles, the load was monotonically increased up to a load of 500 kN. At loads of 50, 100, 150, 200, 250, 300, 350, 400, 450, and 500, the load was held constant for several minutes in order to allow for inspection of cracks and damage. After reaching a load of 500 kN, it was deemed to be unsafe for further inspection and the load was increased monotonically until failure. After failure, the load was removed and a final inspection of the cantilever section was conducted, which included damage assessment, crack mapping, and appropriate photography.

For the cantilever section with steel reinforcement, the load was removed three times prior to failure. The load was removed twice (at 265 kN and 400 kN) during the static test conducted on the cantilever section with steel reinforcement in order to relocate two different pi gauges

to ensure that they were spanning the appropriate cracks. Upon reaching the ultimate load of 772 kN, the hydraulics suddenly interlocked for an unknown reason resulting in a sudden drop of load to approximately 0 kN. After hydraulic power was restored, the cantilever with steel reinforcement was again loaded at the same loading rate until achieving a maximum load of 727 kN at which time a punching type shear failure was observed (discussed in Chapter 4 & 5) with a sudden drop in load to 510 kN.

3.5.2 Test Procedure for Static Monotonic Destructive Test Conducted on the Cantilever Section with GFRP Reinforcement

The load was monotonically increased at a rate of 1 mm per minute up to a maximum load of 110 kN (slightly higher than typical service loads) where it was held constant to allow for inspection of the cantilever section. The load was then removed. This process was repeated 10 times to stabilize the cantilever section before proceeding to failure. After completing the pre-load cycles, the load was monotonically increased up to 400 kN. At levels of 50, 100, 150, 200, 250, 300, 350, 400, the load was held constant for several minutes in order to allow for inspection of cracks and damage. The load was removed at 400 kN in order to re-loacte a pi gauge on the underside of the cantilever to capture a longitudinal crack. The cantilever was then re-loaded and an inspection was conducted at 450 kN. The load was then increased and prior to reaching a load of 500 kN a punching shear type failure was observed at a load of 486 kN. Researchers decided to continue with the application of load until the punching shear type failure was exaggerated and it was decided to halt the test. After failure, the load was removed and a final inspection of the cantilever section was conducted, which included damage assessment, crack mapping, and appropriate photography.

3.5 Test Procedure for Fatigue Cyclic Destructive Tests

The test procedure was the same for both of the cyclic fatigue destructive tests conducted on the two different cantilever sections. The magnitude of the applied cyclic fatigue load for each of the respective cantilever sections was chosen based on the static ultimate load obtained from the static test conducted previously on the two different cantilever sections.

3.5.1 Test Procedure for Fatigue Cyclic Destructive Tests Conducted on the Cantilever Section with Steel Reinforcement

The magnitude of the applied fatigue cyclic load was chosen to be 62 % (high enough load to cause fatigue failure; based on experience from previous fatigue testing) of the static ultimate load observed from the static test. The load was monotonically increased up to the maximum of 480 kN and was held constant at 50, 100, 150, 200, 250, 300, 350, 400, 450, and 480 kN to allow inspection of the cantilever section for damage and cracks. After inspection and confirmation that the pi gauges were spanning the appropriate cracks, and that all of the other instrumentation was functioning correctly, the load was removed. After completing the first cycle up to 480 kN, the load was removed. The load was then monotonically increased up to 242.5 kN and a sine wave loading program was initiated with a range of ±237.5 kN. As a result, the cantilever was subjected to a sine wave loading pattern with a frequency of 0.2 Hz, a maximum load of approximately 480 kN, and a minimum load of 5 kN. The frequency of 0.2 Hz was chosen because it was pre-determined that the frequency should remain constant throughout the entire test. It was recognized that the deflection would increase throughout the fatigue life and the actuator would require a greater stroke (greater oil flow requirement) as

the cantilever fatigued which would require a slower frequency of applied load. After the failure of the cantilever section, a final careful inspection was performed to assess damage, take photographs, and map crack patterns.

3.5.2 Test Procedure for Fatigue Cyclic Destructive Tests Conducted on the Cantilever Section with GFRP Reinforcement

The magnitude of the applied fatigue cyclic load was chosen to be 62 % (high enough load to cause fatigue failure; based on experience from previous fatigue testing) of the static ultimate load observed from the static test. The load was monotonically increased up to the maximum of 305 kN and was held constant at 50, 100, 150, 200, 250, and 305 kN to allow inspection of the cantilever section for damage and cracks. After inspection and confirmation that the pi gauges were spanning the appropriate cracks, and all of the other instrumentation was functioning correctly, the load was removed. After completing the first cycle up to 305 kN, the load was removed. The load was then monotonically increased up to 155 kN and a sine wave loading program was initiated with a range of ±150 kN. As a result, the cantilever was subjected to a sine wave loading pattern with a frequency of 0.2 Hz, a maximum load of approximately 305 kN, and a minimum load of 5 kN. The frequency of 0.2 Hz was chosen because it was pre-determined that the frequency should remain constant through-out the entire test. It was recognized that deflection would increase throughout the fatigue life and the actuator would require a greater stroke (greater oil flow requirement) as the cantilever fatigued which would require a slower frequency of applied load.

The cantilever with GFRP reinforcement did not fail under the loading conditions described above. After it was subjected to 2,000,000 cycles at a frequency of 0.2 Hz, researchers decided to halt the fatigue test and test the cantilever section under a static monotonic load to failure. The load was monotonically increased up to 450 kN and was held constant at 350, 400, 450 kN to inspect for further damage and new cracks. Upon reaching a load of 450 kN, it was deemed to be unsafe for further inspection and the load was increased monotonically until failure which occurred at 520 kN.

4. EXPERIMENTAL RESULTS

The experimental test results for the static and fatigue destructive testing of the bridge deck cantilevers reinforced with steel and GFRP are grouped into seven different categories. The categories consist of results dealing with:

- Deflections;
- Strain in top transverse reinforcing bars;
- Strain in bottom transverse and longitudinal reinforcing bars;
- Strain in the top surface of concrete;
- Strains in barrier wall longitudinal reinforcing bars;
- Strain compatibility below the loading plate;
- Crack widths; and
- Modes of failure

4.1 Deflections

The experimentally observed deflections are divided into five different categories. The following five sub-sections (4.1.1 to 4.1.5) deal with the static load versus deflection, static transverse deflection profiles, fatigue load versus deflection, fatigue transverse deflection profiles, and fatigue deflections versus the number of cycles required to fail the cantilever slab overhang.

4.1.1 Static Load versus Deflection

The static load versus deflection results for the two cantilever sections are presented in this section. The deflections presented in this section were measured at the transverse and longitudinal center line of the loading plate (as close as possible to the loading plate). The assumption that the deflection under the extremely rigid steel loading plate was uniform was employed to facilitate placement of the LVDT on the top surface of the cantilever slab overhang. The deflection observed at this location is illustrated in the load versus deflection plots.

Ten cycles up to a maximum load of 110 kN were applied to pre-load the cantilever and simulate service load conditions, prior to monotonically loading the cantilever with steel reinforcement to failure. A maximum deflection of 0.5 mm was measured under the loading plate. The cantilever with steel reinforcement had an ultimate load of 772 kN and a maximum deflection of 16.7 mm under the loading plate while subjected to monotonic load increasing monotonically at a rate of 1.0 mm per minute (Figure 4-1). At the load of 772 kN the hydraulics became interlocked and the load was removed suddenly. After the hydraulic power was restored, the cantilever with steel reinforcement was reloaded until failure. It achieved a load of 727 kN and a maximum deflection of 16.5 mm under the loading plate at the time of failure. The load-deflection curve was linear up to a load of approximately 150 kN, at which time during the test, a transverse crack on the underside of the cantilever under the applied load was found. The load-deflection curve was non-linear between 150 kN and the ultimate load of 772 kN. At a load of approximately 265 kN and 400 kN the load was

removed to re-locate pi gauges to ensure that they were located over appropriate cracks. A punching shear type failure was observed at 727 kN followed by a sudden drop in the load to 510 kN. Load was still applied resulting in a plateau in the load-deflection curve until it was decided to halt the test because researchers felt the punch cone was being held up by internal reinforcement of the cantilever slab and the barrier wall to slab connection. Upon removal of the load, a permanent deflection of 12.1 mm was observed.

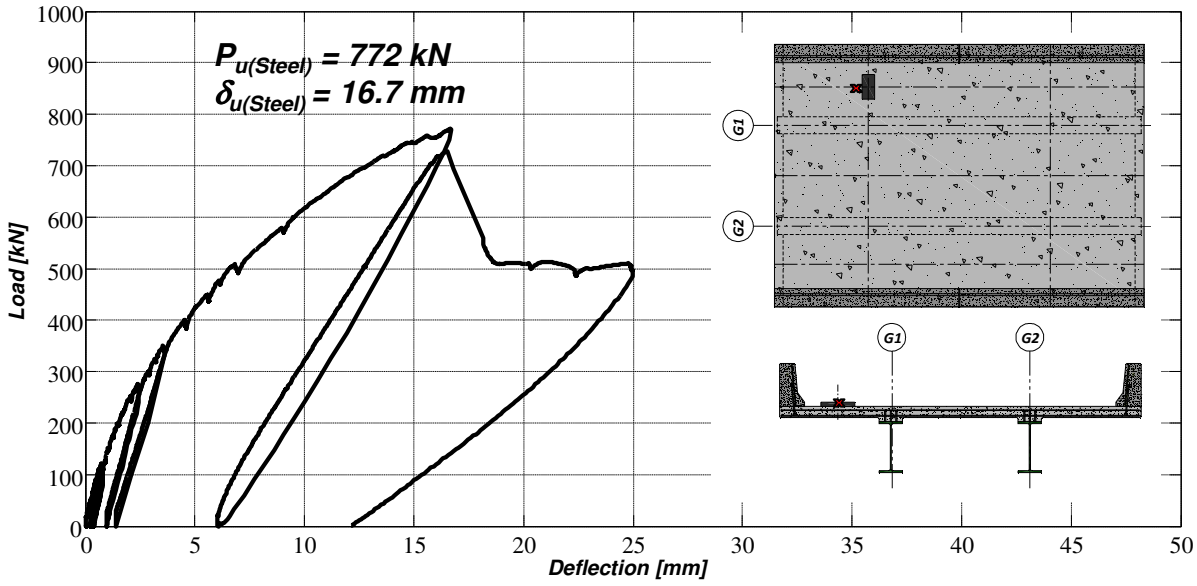

Figure 4-1: Plot of load versus deflection for the cantilever section with steel reinforcement subjected to static monotonic loading

Ten cycles up to a maximum load of 110 kN were applied to simulate service conditions and pre-load the cantilever with GFRP reinforcement, before monotonically loading the cantilever until failure. A maximum deflection of 0.8 mm was recorded under the loading plate. The cantilever with GFRP reinforcement failed at a maximum deflection of 10.9 mm under the loading plate at the load of 487 kN under monotonic loading conditions at a rate of

1 mm per minute (Figure 4-2). The load-deflection curve was linear up to a load of approximately 110 kN, at which time during the test, a transverse crack on the underside of the cantilever under the applied load was observed. The load was removed after reacging 400 kN to re-locate a pi gauge on the underside of the cantilever to ensure that it would measure an appropriate crack width. The cantilever with GFRP reinforcement did not exhibit a sudden drop in load or a significant noise after the punching shear type failure. The load gradually decreased as the punch cone type failure was exaggerated. A permanent deflection of 26.9 mm was measured.

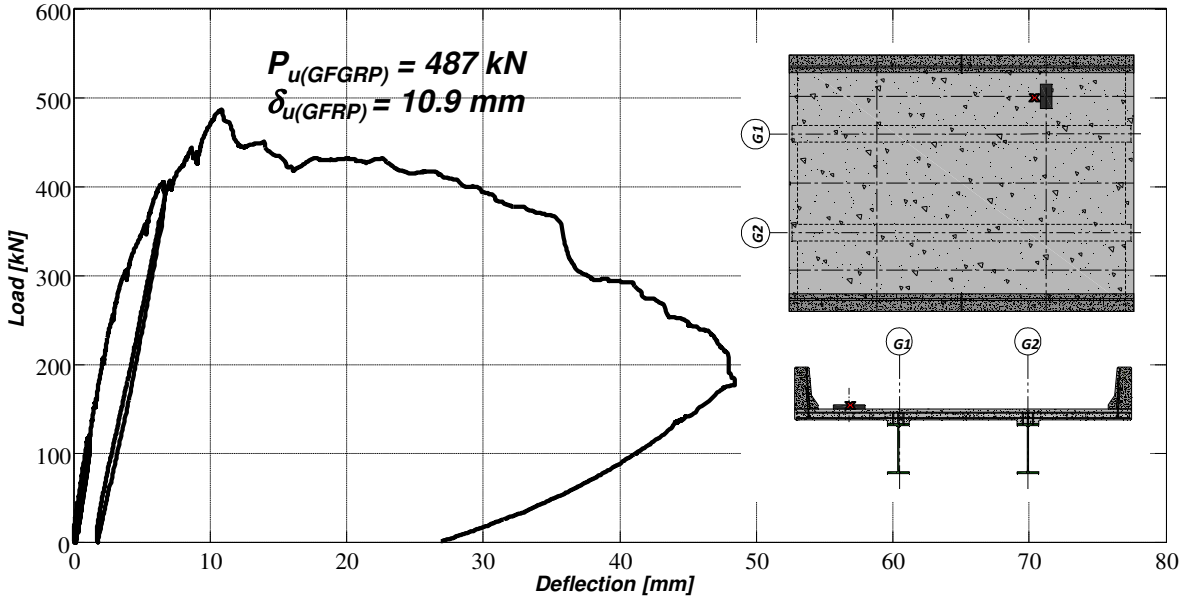

Figure 4-2: Plot of load versus deflection for the cantilever section with GFRP reinforcement subjected to monotonic static loading

It can be seen in Figure 4-3 that until the initiation of the crack on the underside of both cantilever sections, the two cantilever sections behaved in a very similar matter. Under service loads, the cantilever with steel reinforcement exhibited smaller deflections which are

most likely due the higher stiffness and quantity of steel compared to that of the GFRP. Until reaching a load of 300 kN, both cantilevers had very similar behaviour. Beyond 300 kN, the behaviour was significantly different because the cantilever reinforced with conventional steel displayed a much steeper curve indicating a greater stiffness. The increase in stiffness of the cantilever with steel reinforcement can be attributed to both stiffer top transverse reinforcement ratio and a far greater bottom reinforcing ratio when compared to the cantilever reinforced with GFRP. The major difference in the load-deflection behaviour between the two cantilever sections was the ultimate load. The cantilever sections with steel and GFRP reinforcement failed at the ultimate loads of 772 kN and 487 kN respectively. The argument for the difference in ultimate loads can be attributed to the bottom reinforcing ratios and will be discussed in greater detail in chapter 5.

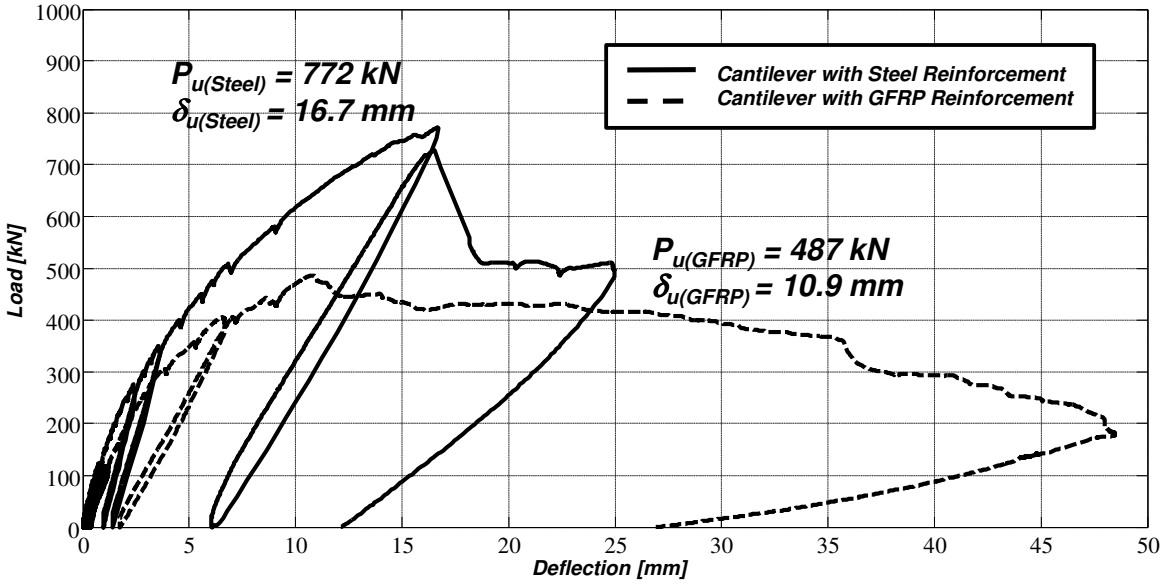

Figure 4-3: Plot of Load versus deflection for both of the cantilever sections subjected to static monotonic loading

4.1.2 Transverse Deflection Profiles under Static Load

The maximum deflection of the central cantilever with steel was measured at the free edge just prior to failure and was 21.32 mm. The deflections for loads of 90, 214, 428, and 772 kN for the cantilever with steel reinforcement are shown in Table 4-1 and plotted in Figure 4-4. The internal panel experienced a maximum upward deflection of -2.74 mm at the mid-span of the internal panel at the ultimate load of 772 kN (just prior to failure).

Table 4-1: Static transverse deflection profiles for the cantilever section with steel reinforcement

Load [kN]	Transverse Distance Along Deck [mm]								
	0	625	1075	1430	2000	2750	3250	3750	4500
90	*0.84*	*0.27*	*0.48*	*0.03*	*0.00**	*0.01*	*-0.01*	*-0.01*	*0.00**
214	*2.65*	*1.67*	*1.64*	*0.51*	*0.00**	*-0.02*	*-0.08*	*-0.05*	*0.00**
428	*7.46*	*6.05*	*5.14*	*1.93*	*0.00**	*-0.44*	*-0.55*	*-0.28*	*0.00**
772	*21.32*	*19.60*	*16.68*	*5.21*	*0.00**	*-2.63*	*-2.74*	*-1.69*	*0.00**

**Deflections over girder center-lines were assumed to be zero*

Table 4-2: Static transverse deflection profiles for the cantilever section with GFRP reinforcement

Load [kN]	Transverse Distance Along Deck [mm]								
	0	625	1075	1430	2000	2750	3250	3750	4500
90	*1.52*	*0.69*	*0.77*	*0.20*	*0.00**	*0.00*	*0.00*	*-0.01*	*0.00**
214	*4.05*	*2.83*	*2.32*	*1.00*	*0.00**	*-0.02*	*0.01*	*-0.01*	*0.00**
428	*11.12*	*9.41*	*8.16*	*3.19*	*0.00**	*-0.81*	*-0.37*	*-0.02*	*0.00**
487	*13.57*	*12.08*	*10.85*	*4.07*	*0.00**	*-1.11*	*-0.51*	*-0.02*	*0.00**

**Deflections over girder center-lines were assumed to be zero*

The maximum deflection of the cantilever with GFRP reinforcement, was recorded at the free edge at a load of 487 kN just prior to failure, was 13.57 mm. The deflections for loads of 90, 214, 428, and 487 kN for the cantilever with GFRP are shown in Table 4-2 and plotted

Figure 4-5. The internal panel had a maximum upward deflection of -1.11 mm at the quarter-span nearest to the applied load of the internal panel at a load of 487 kN (just prior to failure).

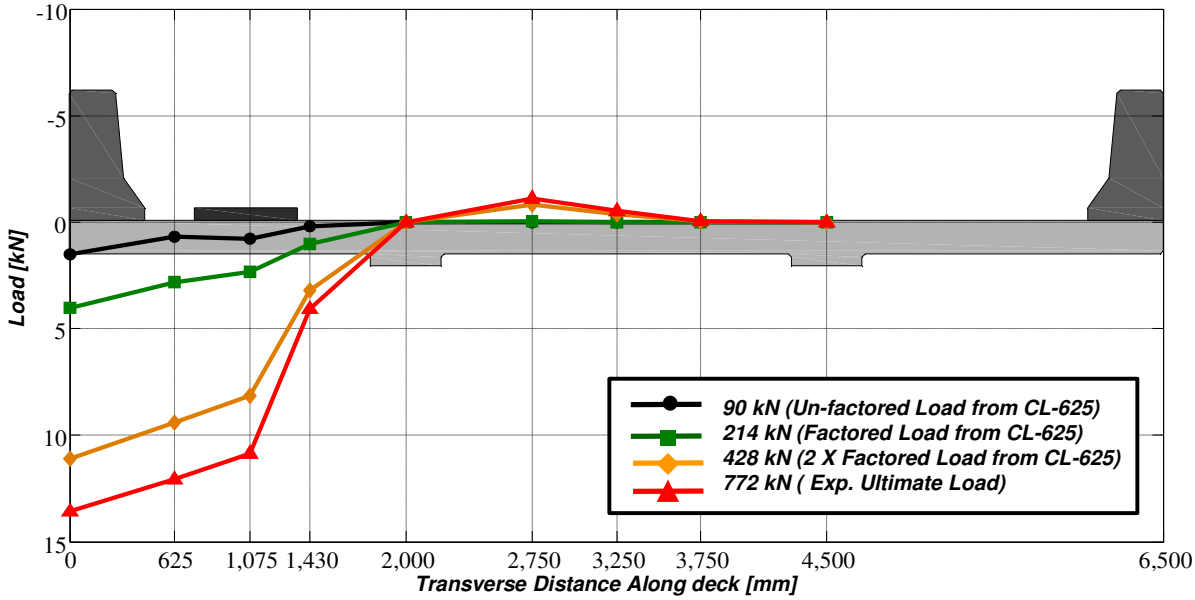

Figure 4-4: Transverse deflection profiles for the cantilever section with steel reinforcement subjected to static load

At lower loads such as 90 kN (un-factored wheel load or service load from an CL-625), both cantilever sections showed a larger localized deflection under the loading plate as if the barrier wall were acting as a supporting girder (Figure 4-3 and 4-5). However, at higher loads approaching failure, both cantilevers transitioned from positive curvature to negative curvature in the vicinity of the load plate, which indicates that at the higher loads, shear may be more dominant than bending, as is the case with arching-action. In both cantilever sections, the barrier wall is deflecting because it does not have end supports. The curvature under the loading plate suggests that the cantilever slab is bending between the barrier wall and the external girder.

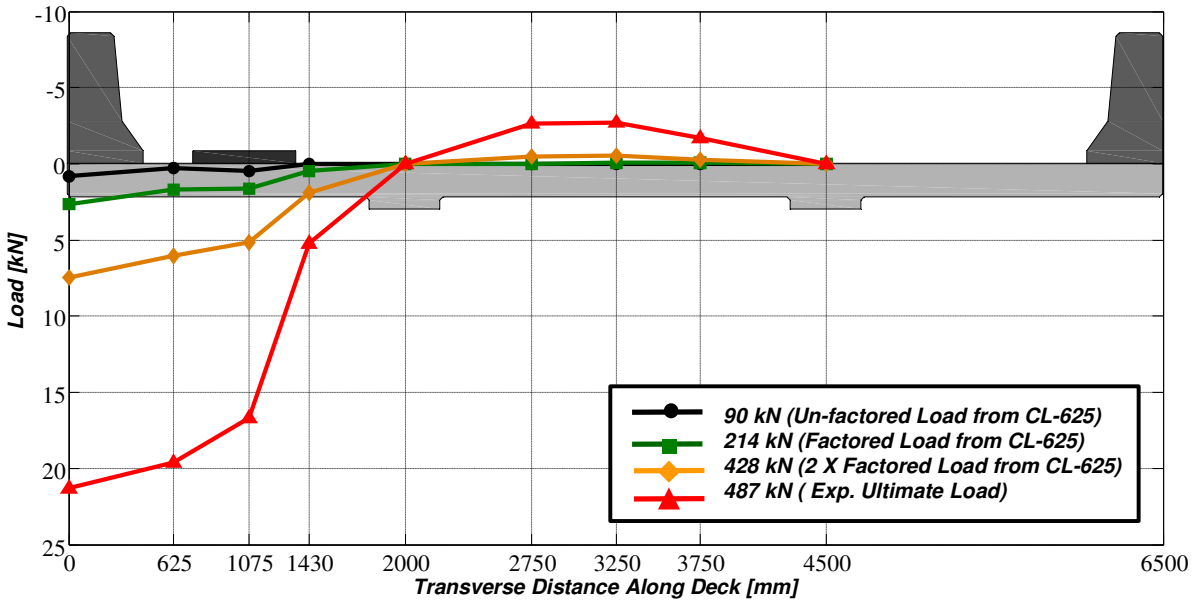

Figure 4-5: Transverse deflection profiles for the cantilever section with GFRP reinforcement subjected to a static load

4.1.3 Fatigue Load versus Deflection

The first fatigue test was conducted on the cantilever section reinforced with steel. The magnitude of load chosen for the fatigue test of the cantilever reinforced with steel was 62.2 % of the ultimate load achieved from the static test which corresponds to a load of 480 kN. The average deflection due to each individual cycle was observed to be 5.5 mm. The energy dissipated for the cycles plotted is relatively equal and is represented by the area between the loaded and unloaded portion of load-deflection curve for each of the given cycles. The amount of energy dissipation that occurred in the last 17 cycles was far greater than that observed earlier in the loading history. The cantilever with steel reinforcement failed after completing 514,647 at which stage a punching shear type failure was observed. The

cantilever test location could no longer sustain load as shown in Figure 4-6. A permanent deflection of 60.4 mm was present upon removal of the fatigue cyclic load.

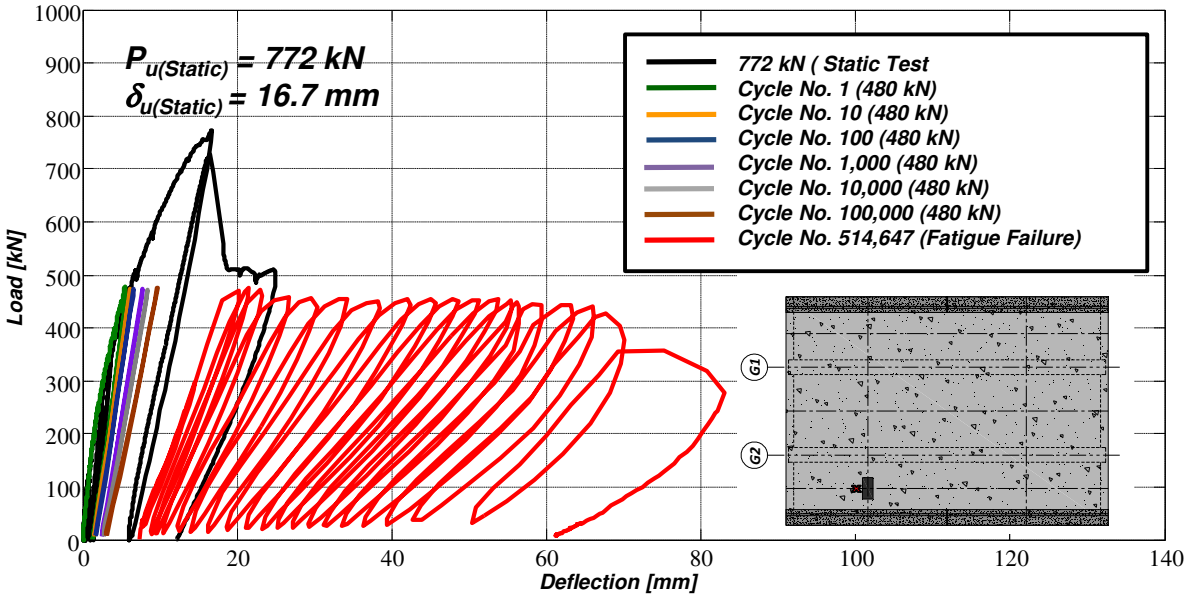

Figure 4-6: Plot of load versus deflection for the cantilever with steel reinforcement subjected to fatigue cyclic loading

The second fatigue test was conducted on the cantilever section reinforced with GFRP. The magnitude of load chosen for the test was 305 kN or 62.6 % of the ultimate load observed from the static test previously conducted. Figure 4-7 shows a steady increase in the deflection, with increasing number of cycles. The average maximum deflection for each cycle was measured to be approximately 4.6 mm. However, the cantilever with GFRP reinforcement did not fail after completing 2,000,000 cycles. Upon completing 2,000,000 cycles a static monotonic test was conducted to failure. The cantilever with GFRP reinforcement failed an ultimate load of 513 kN and a maximum deflection of 15.4 mm. A punching shear type failure was observed followed by a sudden drop in the load to 430 kN.

The load was not removed to investigate post ultimate behavior which can be seen by the descending portion of the load-deflection curve. It was decided to stop the test because researchers felt the punch cone was being held up by internal reinforcement of the cantilever slab and the barrier wall to slab connection. Upon removal of the load a permanent deflection of 25.2 mm was observed.

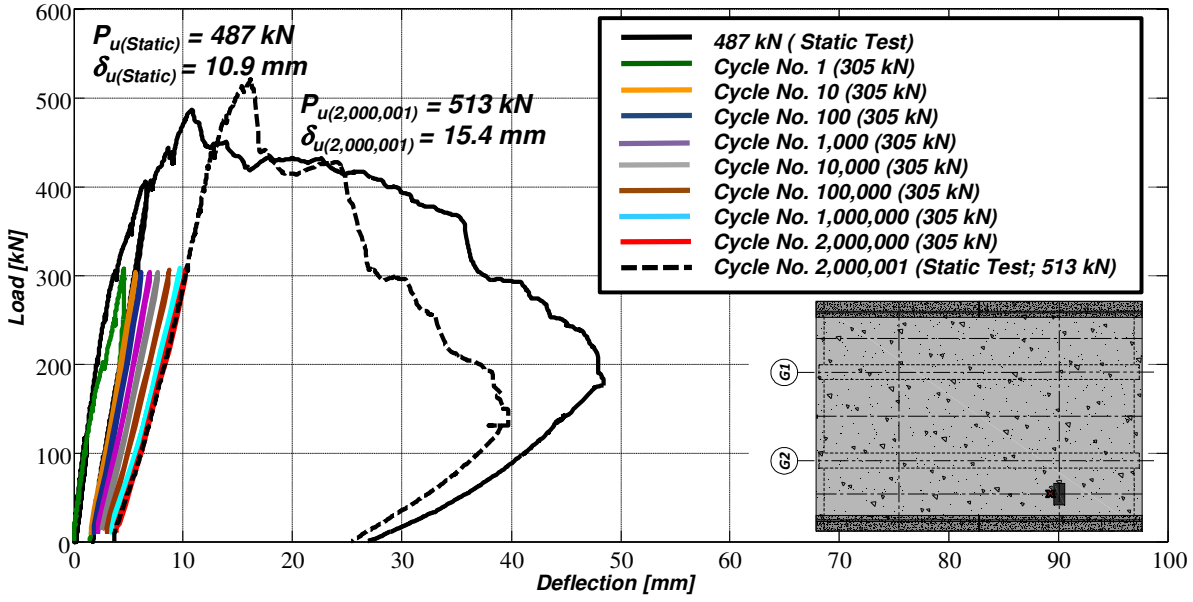

Figure 4-7: Plot of load versus deflection for the cantilever with GFRP reinforcement subjected to fatigue cyclic loading

4.1.4 Transverse Deflection Profiles under Fatigue Load

The maximum deflection of 21.7 mm was observed at the free edge of the cantilever with steel reinforcement just prior to failure after completing 514,647 cycles at the average applied fatigue cyclic load of 480 kN. The deflections for the static loads of 480 and 772 kN (static failure) and cycle number 1, 10, 100, 1,000, 10,000, 100,000, 514,647 for the

cantilever and the internal panel are shown in Table 4-3 and plotted in Figure 4-8. The internal panel did show approximately the same response or influence from the applied load on the cantilever as a result of the fatigue cyclic load compared to the upward deflection seen during the static test. A maximum upward deflection of -2.60 mm was observed at the quarter-span of the internal panel closest to the applied load compared to the maximum upward deflection of -2.74 mm measured from the static test.

Table 4-3: Transverse deflection profiles for the cantilever section with steel reinforcement under fatigue load

Cycle No.	Transverse Distance Along Deck (x) [mm]								
	0	625	1075	1430	2000	2750	3250	3750	4500
Static Test (480 kN)	8.93	7.42	6.24	2.33	0.00*	-0.76	-0.64	-0.40	0.00*
1	4.56	3.94	4.18	1.18	0.00*	-0.74	-0.34	-0.21	0.00*
10	5.19	4.73	4.84	1.50	0.00*	-0.90	-1.02	-0.26	0.00*
100	5.66	5.16	5.31	1.58	0.00*	-0.95	-1.01	-0.31	0.00*
1,000	6.91	5.90	6.45	1.72	0.00*	-1.06	-0.89	-0.49	0.00*
10,000	9.15	6.58	7.09	1.73	0.00*	-1.22	-0.77	-0.48	0.00*
100,000	13.33	10.86	9.67	4.76	0.00*	-2.39	-1.36	-0.40	0.00*
515,647 (Failure)	21.70	21.50	18.70	2.70	0.00*	-2.60	-1.20	-0.44	0.00*
Static Test (772 kN)	21.32	19.60	16.68	5.21	0.00*	-2.63	-2.74	-1.69	0.00*

**Deflections over girder center-lines were assumed to be zero*

A maximum deflection of the cantilever with GFRP reinforcement was observed at the free edge of the cantilever to be 13.19 mm after completing 2,000,000 cycles at the average applied fatigue cyclic load of 305 kN. The deflection profiles for the static loads of 305 kN and 487 kN (static failure) and cycle number 1, 10, 100, 1,000, 10,000, 100,000, 1,000,000, 2,000,000, and static cycle 2,000,001 for the cantilever are shown in Table 4-4 and are plotted Figure 4-9. The maximum upward deflection of -1.76 mm was observed at the mid-span of the internal panel after completing 2,000,000 cycles. A maximum deflection of

18.26 mm was observed at the ultimate static load of 513 kN at the free edge and the maximum upward deflection did not exceed the observed magnitude of -1.76 measured after 2,000,000 cycles.

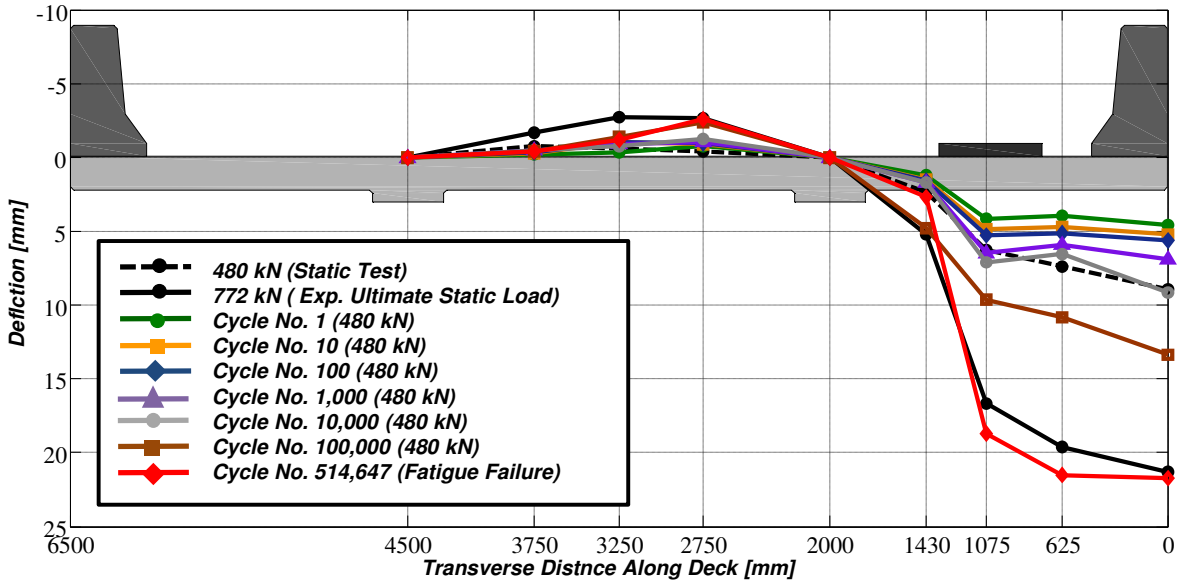

Note: *Transverse deflection profiles for the static test and the fatigue test are plotted at the same locations along the bridge deck for comparison purposes*

Figure 4-8: Transverse deflection profiles for the cantilever section with steel reinforcement under fatigue load

Deflection profiles for the entire fatigue loading history illustrate a transition from positive curvature to negative curvature in the vicinity of the load plate. Therefore, as the cantilever sections undergo damage from fatigue loading they exhibit the same behaviour observed from the static tests. Damage due to shear may be more dominant than damage due to bending, as is the case with the arching-action present in the internal panel of bridge decks.

Table 4-4: Transverse deflection profiles for the cantilever section with GFRP reinforcement under fatigue load

Cycle No.	Transverse Distance Along Deck (x) [mm]								
	0	625	1075	1430	2000	2750	3250	3750	4500
Static Test (305 kN)	8.11	6.56	5.58	2.23	0.00*	-0.52	-0.22	-0.01	0.00*
1	5.90	5.23	4.54	1.58	0.00*	-0.05	-0.64	0.01	0.00*
10	7.98	6.84	5.65	1.87	0.00*	-0.58	-1.28	-0.06	0.00*
100	8.78	7.45	6.21	2.21	0.00*	-0.62	-1.44	-0.12	0.00*
1,000	9.82	8.36	6.96	2.58	0.00*	-0.94	-1.94	-0.02	0.00*
10,000	10.73	9.11	7.69	3.09	0.00*	-0.80	-1.88	-0.04	0.00*
100,000	11.67	10.16	8.70	3.55	0.00*	-0.83	-1.98	-0.04	0.00*
1,000,000	12.70	11.43	9.70	5.59	0.00*	-0.87	-1.78	-0.39	0.00*
2,000,000	13.19	12.80	10.26	6.38	0.00*	-0.97	-1.76	-0.49	0.00*
2,000,001 (Static Test; 513 kN)	18.26	18.74		8.04	0.00*	-1.58	-1.76	-0.78	0.00*
Static Test (487 kN)	13.56	12.08	10.85	4.07	0.00	-1.11	-0.51	-0.02	0.00*

**Deflections over girder center-lines was assumed to be zero*

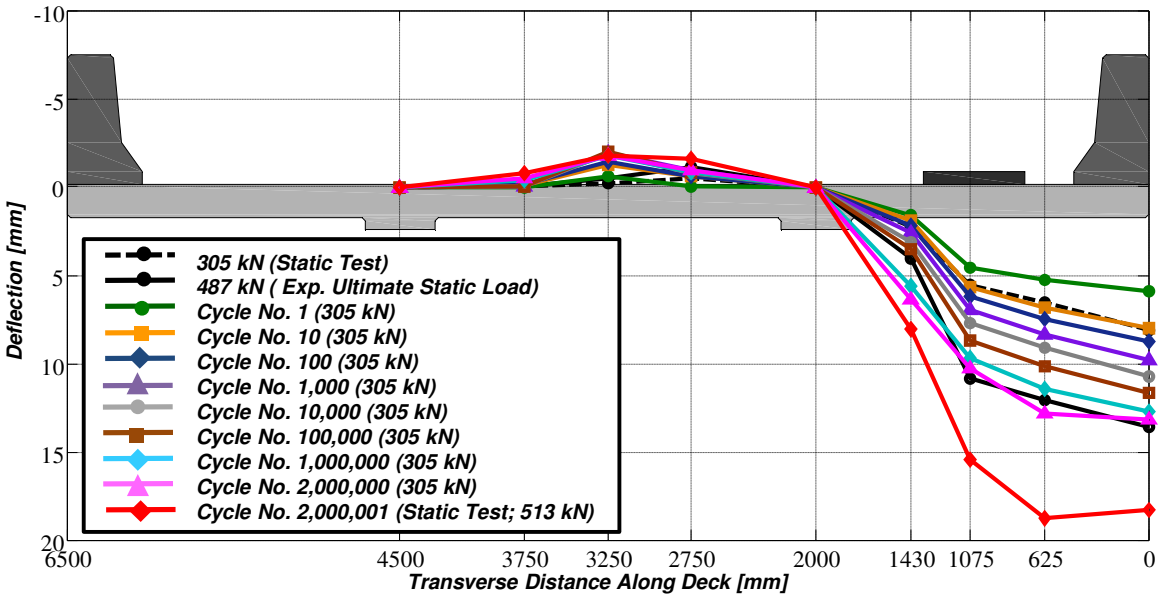

Note: *Transverse deflection profiles for the static test and the fatigue test are plotted at the same locations along the bridge deck for comparison purposes*

Figure 4-9: Transverse deflection profiles for the cantilever section with GFRP reinforcement under fatigue load

4.1.5 Fatigue Deflection versus Number of Cycles

The cantilever reinforced with steel failed after completing 514,647,777 cycles at the average applied fatigue cyclic load of 480 kN or 62.2 % of the static ultimate load observed from the static test (Figure 4-10). The maximum deflection measured under the loading plate at the maximum load for each particular cycle was plotted against the number of cycles for the free edge and under the load plate. It can be seen that for approximately the first 10,000 cycles or 2 % of the fatigue life of the cantilever (relative to the entire fatigue life observed of 514,647 cycles) the deflection versus cycle behaviour was non-linear. The deflection verses cycles behaviour was relatively linear for the following 490,000 cycles or approximately 95 % of the cantilever's fatigue life.

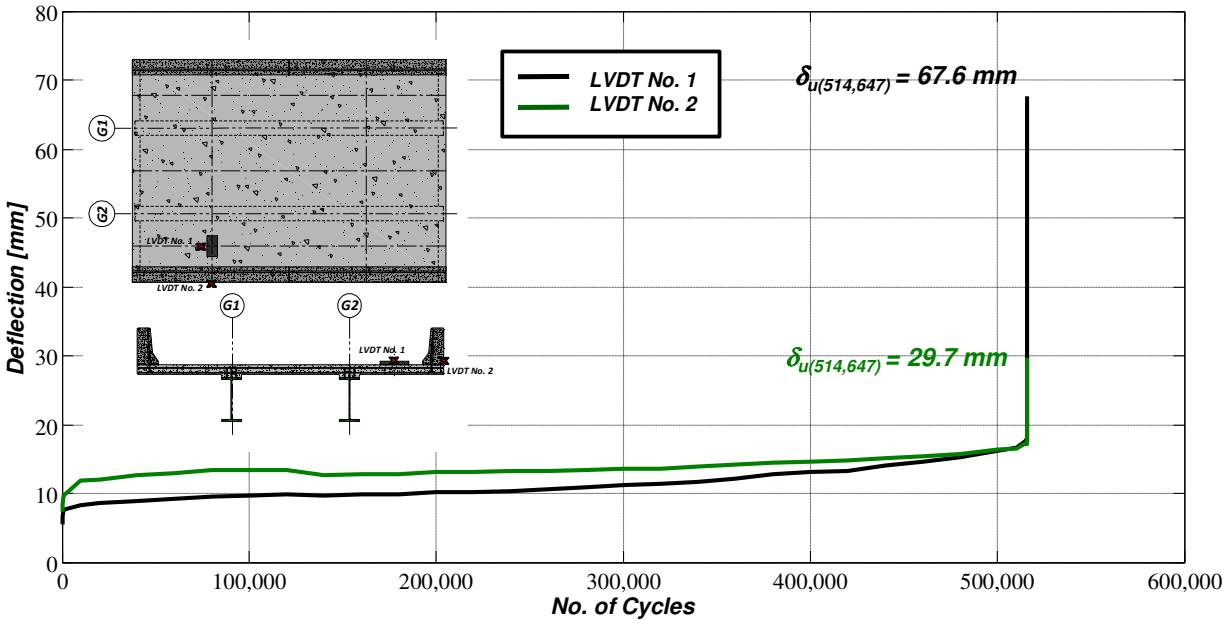

Figure 4-10: Plot of maximum deflection versus number of cycles for the cantilever with steel reinforcement subjected to fatigue cyclic loading

The deflection rapidly increased in the last 14,647 cycles, or 3 % of the cantilever's fatigue life, as the cantilever approached failure, before failing at the maximum deflection of approximately 67.6 mm. A significant observation was that the deflection under the load plate increased and surpassed the deflection measured at the free edge during the final 4,647 cycles as the cantilever approached fatigue failure (Figure 4-11), strengthening the argument for the presence of arching action.

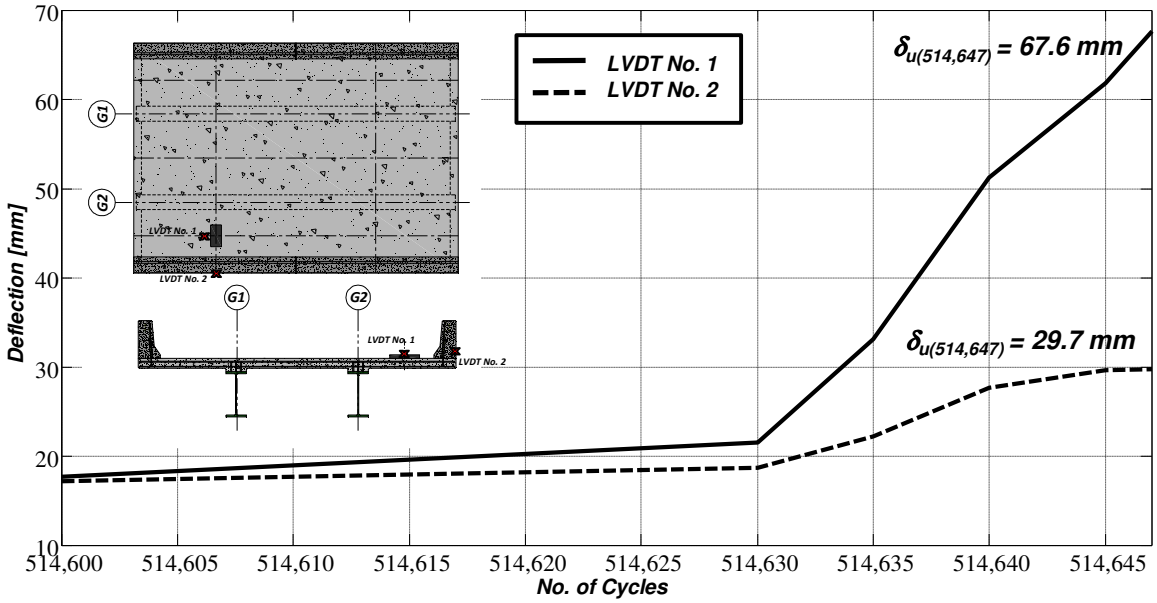

Figure 4-11: Plot of maximum deflection versus number of cycles for the cantilever with steel reinforcement subjected to fatigue cyclic loading for the final 4,647 cycles

The cantilever section reinforced with GFRP did not fail under the applied fatigue load, which comprised of 2,000,000 cycles at the average applied fatigue cyclic load of 305 kN or 62.6 % of the static ultimate load observed from the static test (Figure 4-12). The maximum deflection under the loading plate recorded at maximum load for each particular cycle plotted

against the number of cycles, shows that for approximately the first 100,000 cycles that the deflection behavior was non-linear, reaching a deflections of about 11.7 mm and 8.7 mm at the free edge and under the loading plate respectively. The deflection behavior was relatively linear with a slight increase, throughout the remaining 1,900,000 cycles. The maximum observed deflection at the free edge after completing 2,000,000 cycles was 13.2 mm and was measured to be 10.3 mm under the loading plate.

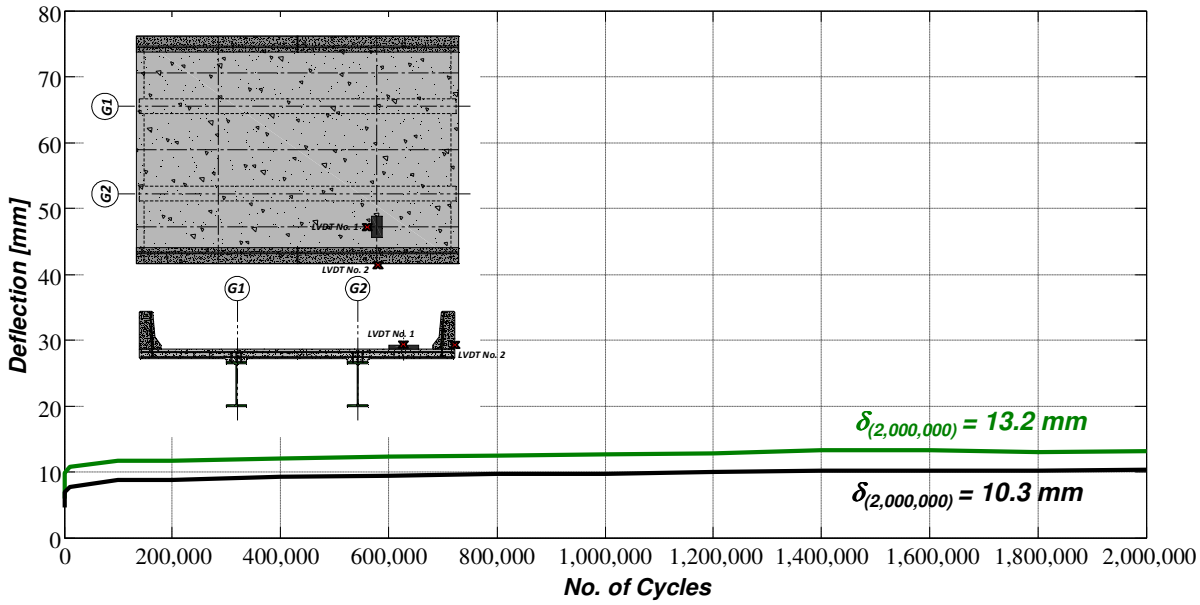

Figure 4-12: Plot of maximum deflection versus number of cycles for the cantilever with GFRP reinforcement subjected to fatigue cyclic loading

Figure 4-13 compares deflections under the loading plate, for each cycle plotted against the number of completed cycles for both of the cantilever sections. The vertical axis was adjusted to illustrate the rapid transition from linear to non-linear deflection behavior observed as the cantilever with steel reinforcement failed under fatigue loading conditions. The cantilever with GFRP reinforcement did not fail under cyclic fatigue loading conditions

and thus made it difficult to directly compare the fatigue performance of the two cantilevers with respect to deflection under the loading plate. Figure 4-14 is the same load-deflection data plotted on a log scale. It demonstrates that the slope for the measured deflection versus number of completed cycles is experimentally identical for both cantilever sections for the free edge and under the loading plate respectively. The relationship between deflection and the number of completed cycles will be discussed in greater detail in Chapter 5.

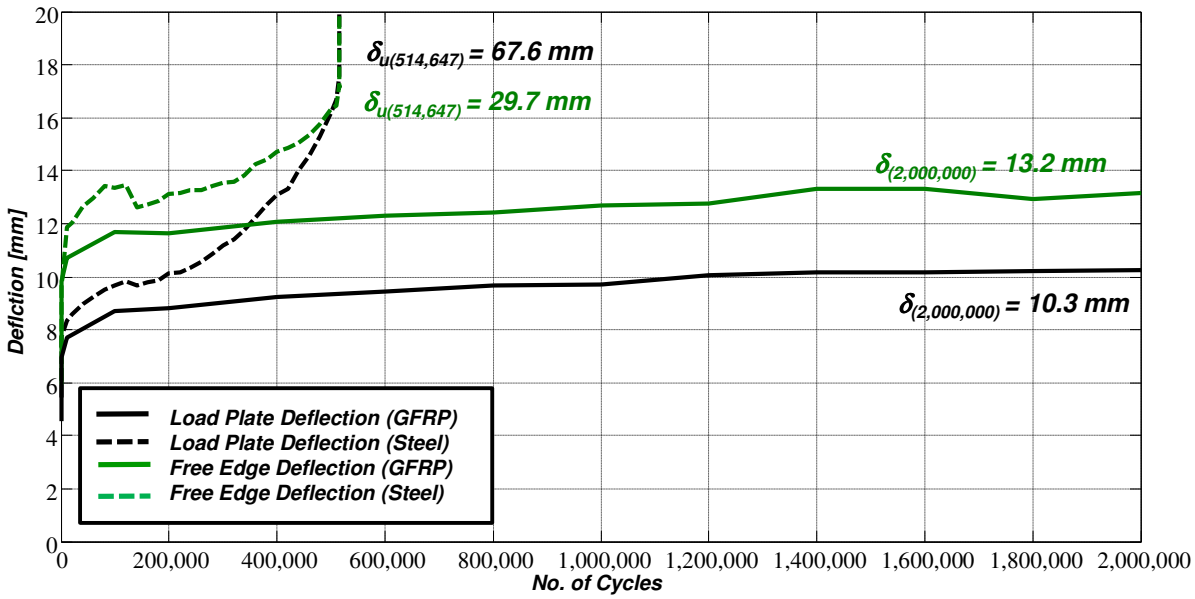

Figure 4-13: Plot of maximum deflections under the load plate and free edge versus number of cycles for both cantilever sections subjected to fatigue cyclic loading

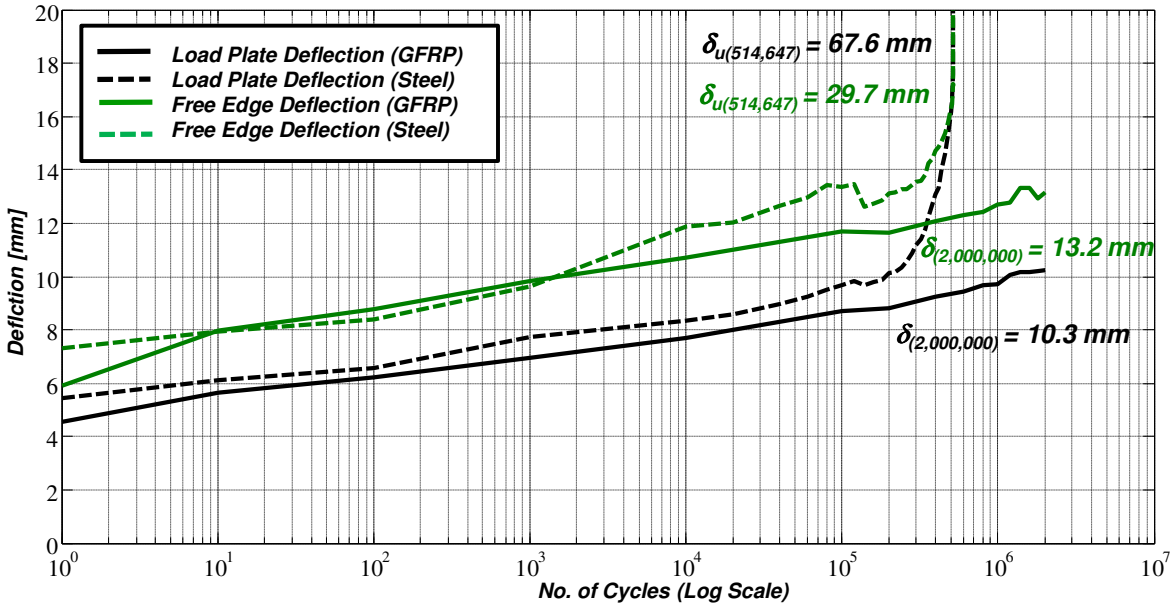

Figure 4-14: Plot of maximum deflection under the load plate and free edge versus number of cycles (log scale) for both cantilever sections subjected to fatigue cyclic loading

4.2 Strains

Results associated with strains are divided into four different categories. The categories deal with strain results obtained for (a) the top transverse reinforcing bars; (b) the bottom transverse and longitudinal reinforcing bars; (c) longitudinal reinforcing bars in the traffic barrier wall; and (d) concrete strain results measured on the top surface of the GFRP reinforced cantilever. Discussed in each of the following sub-sections (4.2.1 to 4.2.4) is the static load versus strain behaviour, static top reinforcing bar transverse strain profiles, fatigue load versus strain behaviour, fatigue top reinforcing bar transverse strain profiles, and strain magnitudes related to the number of cycles required to fail a particular cantilever section (maximum and cumulative).

4.2.1 Top Transverse Reinforcing Bar Strain Related Test Results

4.2.1.1 Static Load versus Strain Test Results

The maximum observed strains over girder center line and adjacent to the applied load along transverse center line of the applied load are presented in this section. Load-strain curves are plotted for the strain gauge over the girder center line and adjacent to the load plate for the cantilever section with steel reinforcement (Figure 4-15).

Ten cycles up to a maximum load of 110 kN were applied to pre-load the cantilever with steel reinforcement before monotonically loading the cantilever until failure. Maximum strains of 37 and 7 με were recorded over the center-line of the girder and adjacent to the loading plate from (1500 mm from the free edge) respectively (Figure 4-15). The cantilever with steel reinforcement failed at a maximum strain of 2166 με and an ultimate load of 772 kN under monotonic loading conditions at a rate of 1 mm per minute. The maximum strains of 2166 με (adjacent to the loading plate) and 1912 με (over the girder centerline) were measured at their respective locations just prior to failure. The load-strain curve was linear up to a load of approximately 150 kN, at which time a transverse crack on the underside of the cantilever was discovered under the applied load. The strain gauge adjacent to the loading plate did not show significant strains until approximately 400 kN, at which time longitudinal cracks on the top surface of the cantilever slab were visible. At an approximate load of 150 kN, the load was removed a second time to change the location of a pi gauge on the top surface of the cantilever to measure crack widths on the top surface of the

cantilever. After removal of the load, a permanent strain of 506 με was observed over the center-line of the girder. Data after unloading was unavailable for the strain gauge adjacent to the loading due to its failure of the strain gauge.

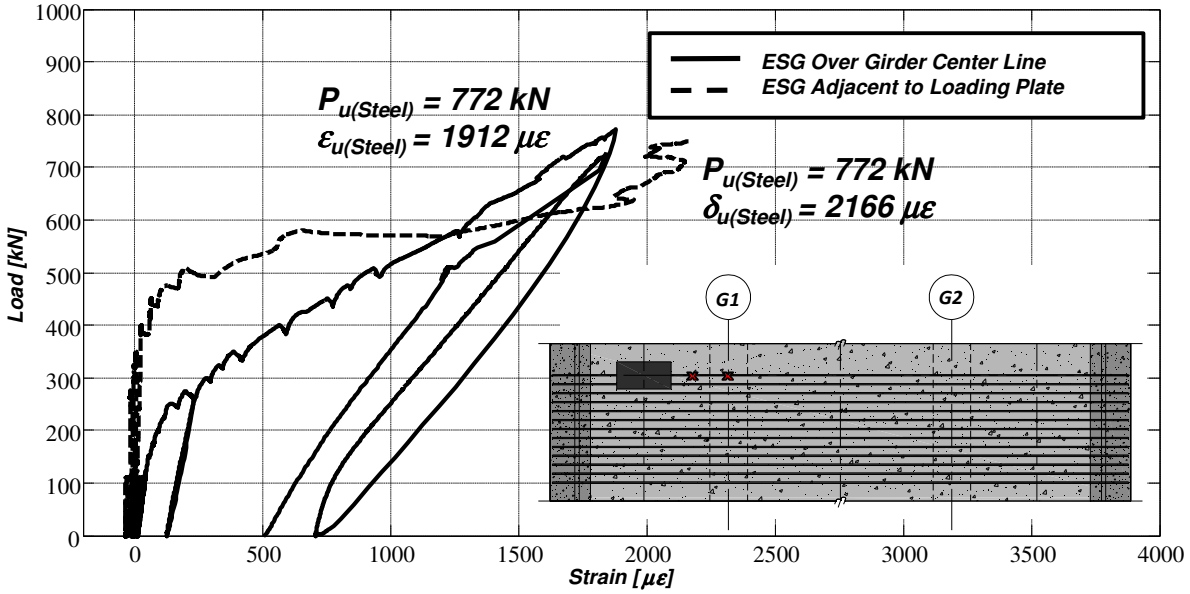

Figure 4-15: Plot of load versus top transverse reinforcing bar strain for the cantilever with steel reinforcement subjected to a static monotonic load

Prior to monotonically loading until failure, 10 cycles up to a maximum load of 110 kN were applied to pre-load the cantilever with GFRP reinforcement. Maximum strains of 41 and 3 με were observed over the center-line of the girder and 1500 mm from the free edge respectively (Figure 4-16). The cantilever with GFRP reinforcement failed at a maximum strain of 1332 με located 1500 mm from the free edge and 1328 με over the girder center line. It failed at an ultimate load of 487 kN under static monotonic loading conditions at a rate of 1 mm per minute. The strains of 1332 and 2565 με correspond to 9.5 % and 18.3 % of the ultimate strains for a No. 25 GFRP bar. The load strain-curve was linear up to a load

of approximately 120 kN, at which time during the test a transverse crack appeared on the underside of the cantilever under the applied. At a load of approximately 405 kN, longitudinal cracks over the girder were observed. Permanent strains over the girder center line were observed to be 488 με after removal of the load. Strains adjacent to the load were not measured due to the damage of the strain gauge.

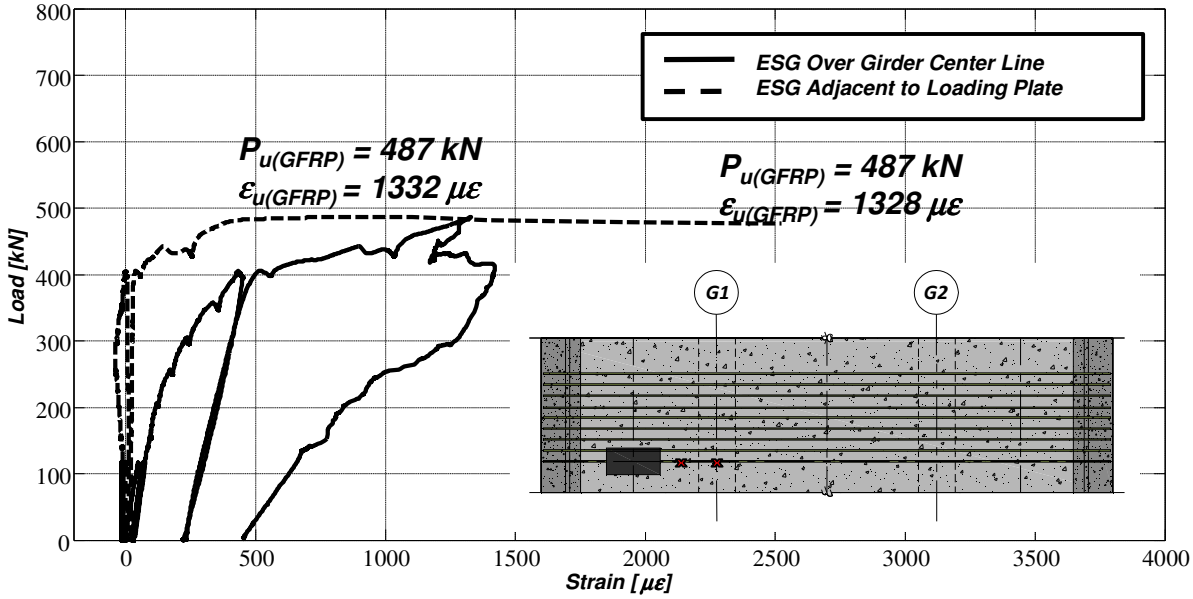

Figure 4-16: Plot of load versus top transverse reinforcing bar strain for the cantilever with GFRP reinforcement subjected to a static monotonic load

4.2.1.2 Top Transverse Reinforcing Bar Strain Profiles under Static Load

The strains in the top transverse bars for loads of 90, 214, and 428 kN, and the ultimate load of 772 kN are shown in Table 4-5 and plotted in Figure 4-17. At lower loads such as 90 kN (un-factored wheel load including a DLA for an CL-625), the maximum strain along the top transverse steel bar located below the load plate was recorded to be 33 με over the girder

center-line. At a load of 214 kN (factored wheel load including DLA), the maximum strain still occurred over the center-line of the girder and was measured to be 104 με.

Table 4-5: Top transverse reinforcing bar strain profiles along the transverse center-line of the applied load for the cantilever section with top transverse steel reinforcement subjected to static monotonic loading

Load [kN]	Transverse distance along deck [mm]								
	50	500	1000	1500	2000	2500	3250	4000	4500
90	*4*	*6*	*-25*	*7*	*33*	*28*	*12*	*4*	*1*
214	*12*	*9*	*-95*	*-5*	*104*	*71*	*26*	*6*	*-1*
428	*77*	*9*	*-95*	*43*	*875*	*536*	*79*	*14*	*-8*
772	*139*	*21*	*311*	*2166*	*1912*	*1402*	*206*	*18*	*-36*

Note: All strains are in micro-strain

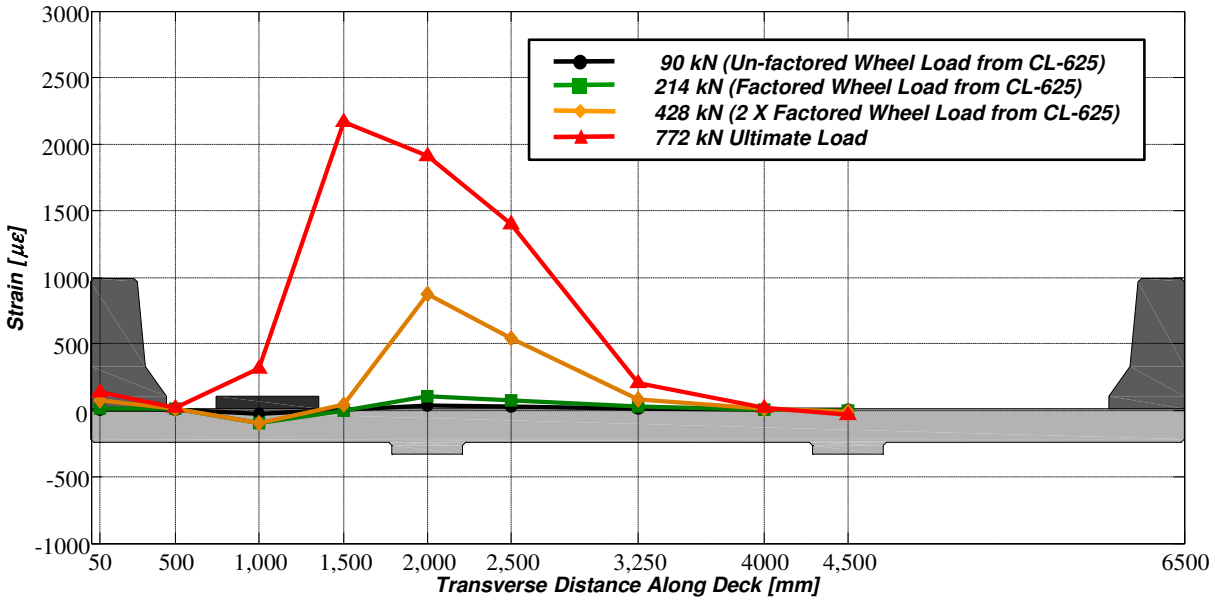

Figure 4-17: Top transverse reinforcing bar strain profiles along the center-line of the applied load for the cantilever section with steel reinforcement subjected to static monotonic loading

At higher loads such as the twice the factored load (428 kN), the maximum tensile strain was still located over the girder center line and was measured to be 875 με. Interestingly, even at a load of 428 kN, compressive strain magnitudes were measured under the loading plate

which contradict classical flexural theory. At the ultimate load of 772 kN, the maximum strain shifted away from the girder center line and towards the loading plate achieving a maximum tensile strain of 2166 με.

The maximum tensile strain along the top transverse reinforcing bar located under the loading plate for the cantilever with GFRP was measured to be 37 με for an applied static load of 90 kN (Table 4-6 and Figure 4-18). At 214 kN, the maximum tensile strain was observed to be 132 με (0.9 % of the bars ultimate strain) and was located over the girder centerline. Also at 214 kN, compressive strain magnitudes were measured in the vicinity of the loading plate. Just prior to failure at a load of 487 kN, the maximum tensile strain along the top transverse bars was located closer to the edge of the loading plate (1500 mm from the free edge) and was recorded to be 2565 με or 18.3 % of the ultimate strain for the GFRP reinforcing bar.

Table 4-6: Top transverse reinforcing bar strain profiles along the transverse center-line of the applied load for the cantilever section with top transverse GFRP reinforcement subjected to static monotonic loading

Load [kN]	Transverse distance along deck [mm]								
	50	500	1000	1500	2000	2500	3250	4000	4500
90	*3*	*1*	*-24*	*1*	*37*	*20*	*8*	*4*	*0**
214	*18*	*-1*	*-78*	*-28*	*132*	*29*	*24*	*9*	*0**
428	*267*	*194*	*387*	*267*	*794*	*787*	*43*	*19*	*0**
487	*384*	*198*	*892*	*2565*	*1332*	*1013*	*50*	*24*	*0**

**Strains in top transverse over adjacent girder center line were not measured due to channel limitations*
Note: All strains are in micro-strain

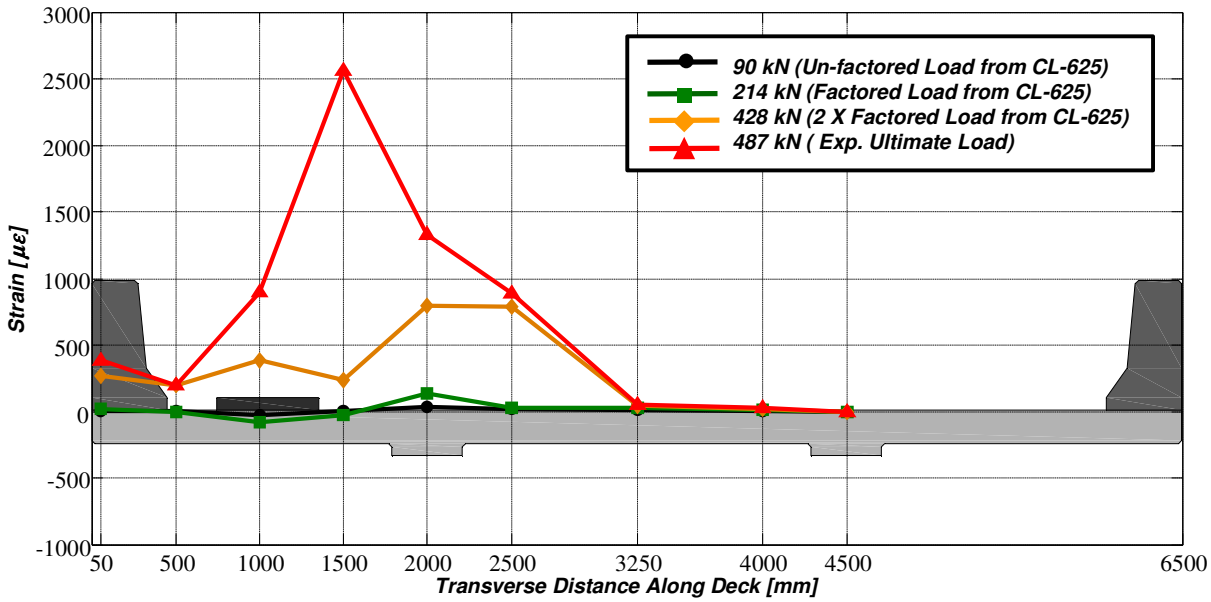

Figure 4-18: Top transverse reinforcing bar strain profiles along the center-line of the applied load for the cantilever section with GFRP reinforcement subjected to static monotonic loading

The maximum strain at lower loads occurs in both cantilever sections over the center-line of the girder. However, at higher loads approaching the ultimate load, the maximum strain occurred 1500 mm from the free edge (140 mm from the edge of the loading plate). Both cantilever sections also exhibited compressive strains at lower loads in the vicinity of the loading plate. Strains recorded in the internal panel of both cantilever sections subjected to static monotonic loading indicate that the tensile stresses in the top transverse bars under the applied load on the cantilever are not distributed to the next adjacent girder in the manner suggested by flexural or bending analysis. Tensile strains observed in the internal panel of both cantilever sections indicates that the tensile strains are negligible beyond halfway to the next adjacent girder, even at ultimate loads.

4.2.1.3 Fatigue Load versus Strain Test Results

The cantilever with steel reinforcement was the first to be tested under fatigue cyclic loading conditions. The magnitude of load chosen for the fatigue tests was 480 kN or 62.2% of the ultimate load obtained from the static test conducted previously. The fatigue load versus strain curves are presented in two different figures. Figure 4-19(a) shows load-strain plots for the strain gauge located on the top transverse bar 2000 mm from the free edge (girder center line); and Figure 4-19(b) is a load-strain plot for the strain gauge on the top transverse bar 1500 mm from the free edge (adjacent to the loading plate or 140 mm from the edge of the loading plate). The strains in the top transverse steel over the girder center line kept growing throughout the early fatigue life. However, as the failure and cracking became more localized around the loading plate, the strain over the girder tended to stabilize and get smaller (Figure 4-19(a)). Figure 4-19(b) shows that a maximum strain tensile of 2003 με was recorded just prior to fatigue failure at 514,647 cycles. It can be seen from the plot that the amount of energy lost through accumulated strain in the top transverse steel bars increased with the number of cycles indicating that the bars are subjected to fatigue. The amount of dissipated energy is represented by the area between the loading and unloading curves. The important observation made was that the strain in the top transverse steel bars near the applied load increased throughout the fatigue life of the cantilever and failure occurred when the absolute strain in the bars was approximately equal to the strain at the same location measured during the static test.

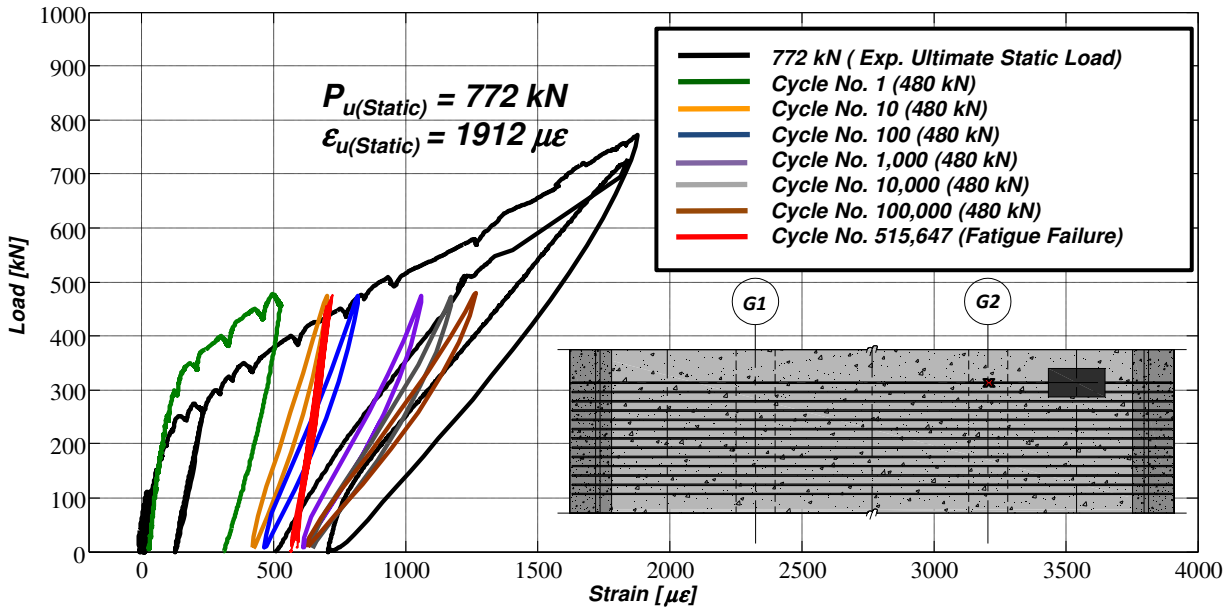

Figure 4-19(a): Plot of load versus top transverse reinforcing bar strain over the girder center-line for the cantilever with steel reinforcement subjected to a fatigue cyclic load

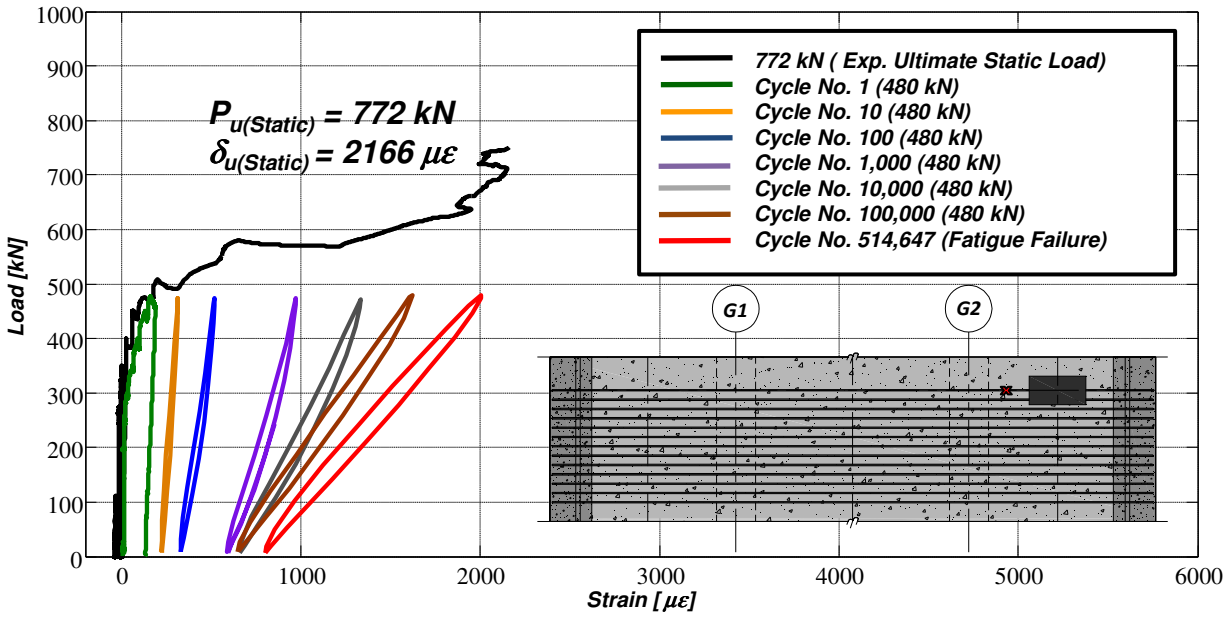

Figure 4-19(b): Plot of load versus top transverse reinforcing bar strain adjacent to the loading plate for the cantilever with steel reinforcement subjected to a fatigue cyclic load

The second fatigue test was conducted on the cantilever section reinforced with GFRP. The magnitude of load chosen for the test was 62.6 % (305 kN) of the ultimate load observed from the static test. The load versus strain results are presented for gauges 2000 mm from the free edge of the cantilever (girder center line) and adjacent to the loading plate (140 mm from the loading plate edge) in Figure 4-20(a) and 4-20(b) respectively. The increase in absolute strain was relatively negiligable over the 2,000,000 cycles, and it can be seen that the amount of energy loss with the increase in number of cycles was approximately equal for each of the cycles plotted. The maximum strain in the top transverse GFRP bars measured over the girder center-line after completing 2,000,000 cycles was 797 με. The strain over the girder center-line did increase throughout the entire loading history. The ultimate strain measured over the girder center line during the final static test was 1358 με, showing that the gauge over the girder center line experienced the maximum strain that was observed at that location from the static test conducted earlier. The fatigue strains measured adjacent to the loading plate also demonstrated a steady increase in magnitude throughout the 2,000,000 cycle loading history. The maximum strain observed was approximately 775 με after completing 2,000,000 cycles. Upon conducting the static test, the maximum or ultimate strain observed was 1689 με. Again, the strain observed during the final static test was nearly the same as the strains measured during the initial static test conducted on the opposite cantilever.

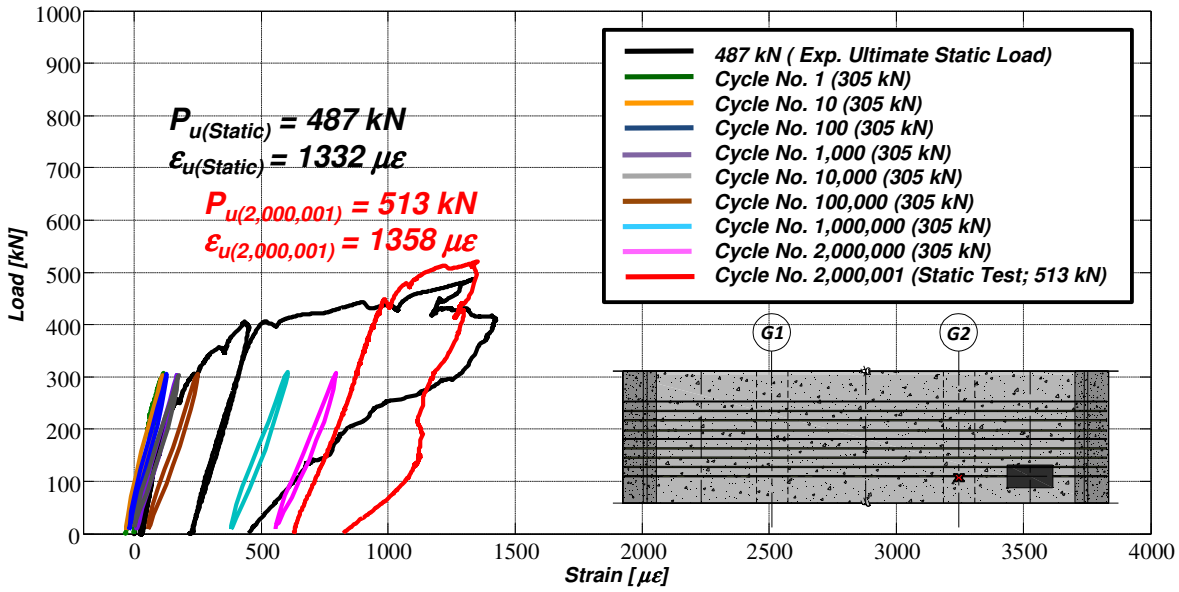

Figure 4-20(a): Plot of load versus top transverse reinforcing bar strain over the girder center-line for the cantilever with GFRP reinforcement subjected to a fatigue cyclic load

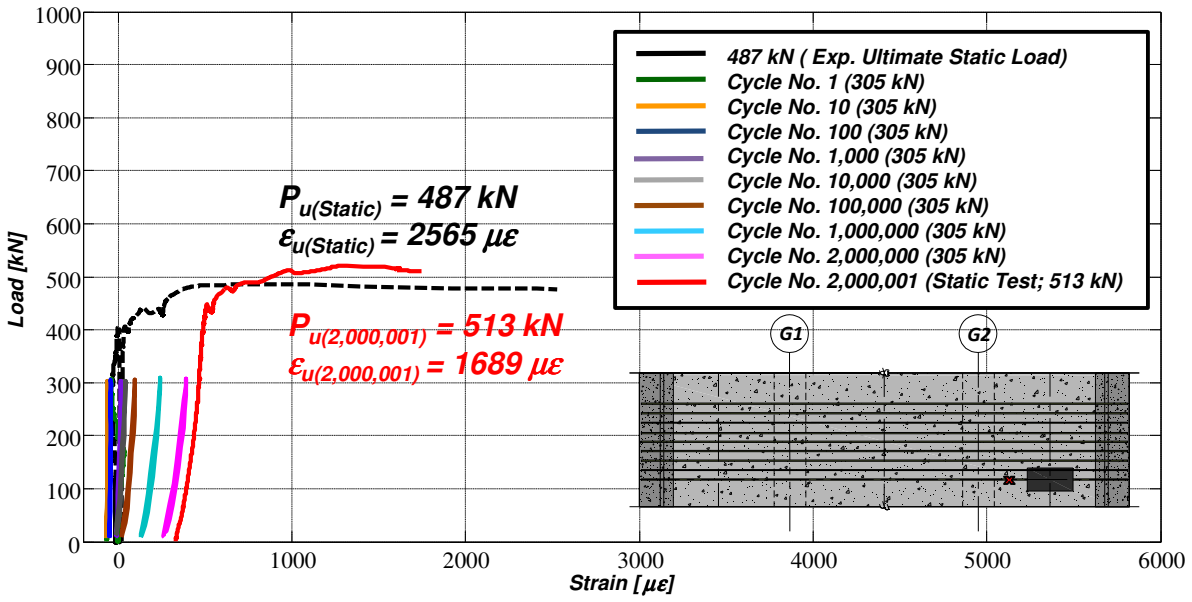

Figure 4-20(b): Plot of load versus top transverse reinforcing bar strain adjacent to the loading plate for the cantilever with GFRP reinforcement subjected to a fatigue cyclic load

4.2.1.4 Top Transverse Reinforcing Bar Strain Profiles under Fatigue Load

The maximum strain of 2003 με was recorded for the cantilever with steel reinforcement at a distance of 1500 mm from the free edge of the cantilever (approximately 140 mm from the edge of the loading plate) after completing 514,647 cycles (Table 4-7 and Figure 4-21).

Table 4-7: Top transverse reinforcing bar strain profiles along the center-line of the applied load for the cantilever section with steel reinforcement subjected to fatigue cyclic loading

No. of Cycles	Transverse distance along deck [mm]								
	50	500	1000	1500	2000	2500	3250	4000	4500
Static Test (P = 480 kN)	99	3	-3	176	1051	675	84	12	-11
1	-8	11	80	257	499	163	-22	-2	5
10	-12	11	80	387	702	314	80	-3	4
100	-12	16	82	444	819	522	138	-7	6
1,000	-7	32	100	588	1061	971	244	34	9
10,000	6	55	130	643	1173	1334	270	84	14
100,000	121	264	407	1352	1266	1625	275	256	317
514,647	299	451	561	2003	678	485	292	269	323
Static Test (P = 772 kN)	139	21	311	2166	1912	1402	206	18	-36

Note: All strains are in micro-strain

The maximum strain along the top transverse bars occurred over the girder center-line for approximately the first 1,000 cycles. However, for the following a 90,000 or so cycles, the maximum strain occurred 2500 mm from the free edge in the internal panel. The absolute strain over the girder center-line became stable or decreased during the final 214,647 cycles, most likely do to the localized cracking and punching type failure observed.

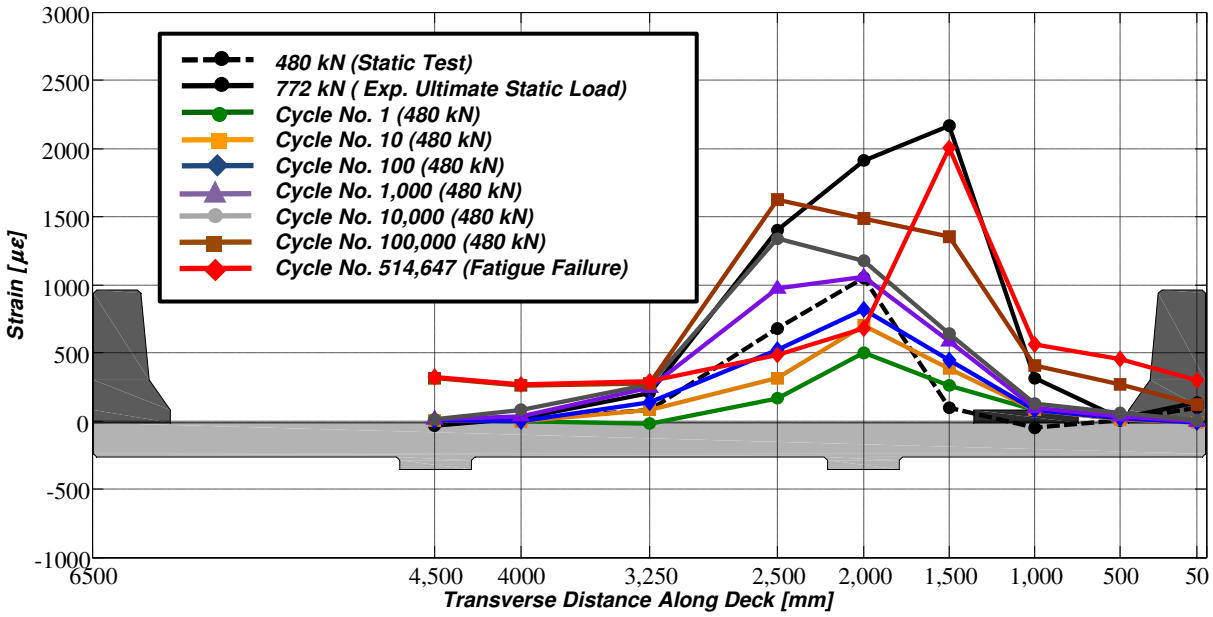

Figure 4-21: Top transverse reinforcing bar strain profiles along the center-line of the applied load for the cantilever section with steel reinforcement subjected to fatigue cyclic loading

The cantilever with GFRP reinforcement did not fail after completing 2,000,000 cycles, after which the maximum in the top transverse bar was 797 με and was located over the girder center line (Table 4-8 and Figure 4-22). During the static test to failure, the maximum strain was found to be 1000 mm from the free edge and was measured to be 1348 με. An important observation made was that, like the static tests conducted previously, the strain magnitudes in the top transverse bars for both cantilever sections was negligible midway to the adjacent girder. The negligible strain magnitudes indicate that negative moment stresses in the internal panel due to a concentrated load on the cantilever are not distributed to the adjacent girder as conventional flexural theory dictates. Also, the maximum strains found in the top transverse bars shifted away from the girder center with increased fatigue cycles indicating that a localized punching type failure was approaching.

Table 4-8: Top transverse reinforcing bar strain profiles along the center-line of the applied load for the cantilever section with GFRP reinforcement subjected to fatigue cyclic loading

No. of Cycles	Transverse distance along deck [mm]								
	50	500	1000	1500	2000	2500	3250	4000	4500
Static Test (P = 305 kN)	46	23	-58	-34	237	61	31	8	0*
1	-1	1	-69	23*	115	98	29	1	0*
10	-3	-2	7	59*	111	114	25	1	0*
100	-3	4	60	94*	128	148	25	-15	0*
1,000	6	2	191	180*	170	197	30	-14	0*
10,000	-51	-42	249	210*	176	188	-27	-24	0*
100,000	-111	-37	350	300*	251	272	-34	-36	0*
1,000,000	-63	54	644	624*	604	597	84	42*	0*
2,000,000	-310	127	749	775*	797	493	-27	-14*	0*
Static Test (P = 487 kN)	-273	200	1348	1287*	1226	826	7	4*	0*
2,000,001 (Static Test; P = 513 kN)	-273	200	1348	1287*	1226	826	7	4*	0*

**Strains were not measure at this location and were assumed to be negligible*
Note: All strains are in micro-strain

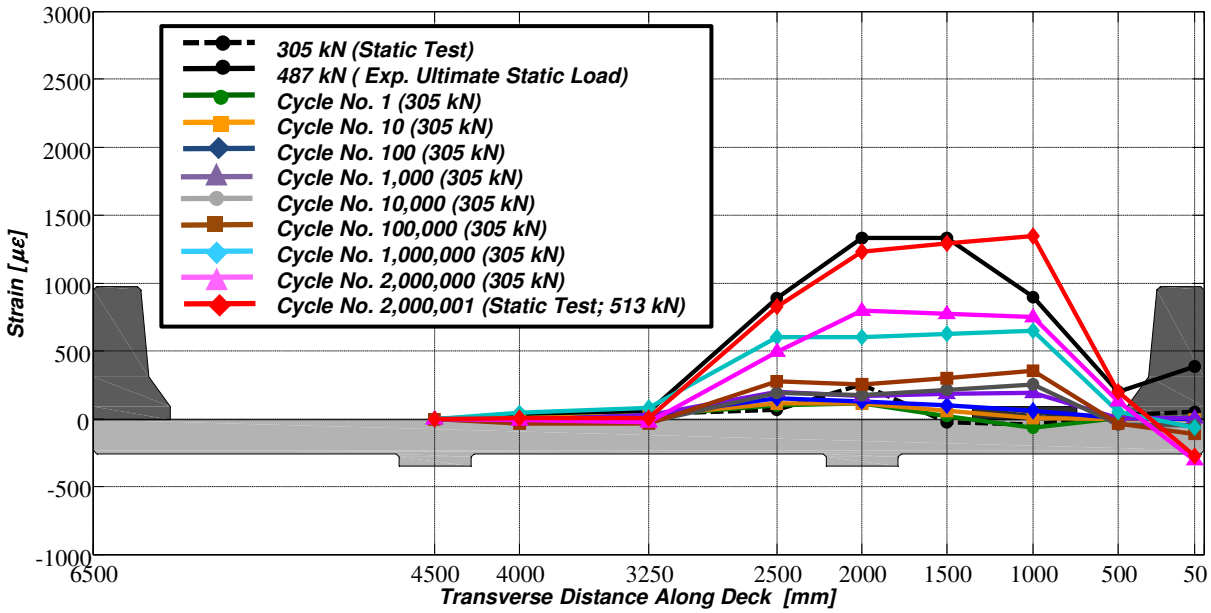

Figure 4-22: Top transverse reinforcing bar strain profiles along the center-line of the applied load for the cantilever section with GFRP reinforcement subjected to fatigue cyclic loading

4.2.1.5 Fatigue Strain versus Number of Cycles

The strains measured along the top transverse reinforcing bars can be divided into two different components, the absolute strains and cumulative strains. Absolute strain for the purposes of this thesis is the magnitude of the strain at any given cycle corresponding to any magnitude of applied load. Cumulative strain is the permanent non-recoverable strain remaining after the removal of the load.

Figures 4-23 and 4-24 show the absolute and cumulative strains plotted against the number of applied cycles for the cantilever section with steel reinforcement over the girder center-line and near the edge of the loading plate (1500 mm from the free edge) respectively. The absolute strain measured in the top transverse bar over the girder center-line increased steadily throughout the fatigue life of the cantilever and was observed to be 678 με at the time of failure. The maximum strains over the girder reached magnitudes of approximately 1500 με but dropped off during the final 214,647 cycles. The absolute strain measured 1500 mm from the free edge of also increased over the 514,647 cycles. The strains near the edge of the loading plate increased substantially from approximately 200 με to 2003 με over the fatigue life of the cantilever. Cumulative strains along the top transverse bar, 1500 mm from the free edge of the cantilever and over the girder center-line, were recorded to be 723 με and 509 με respectively.

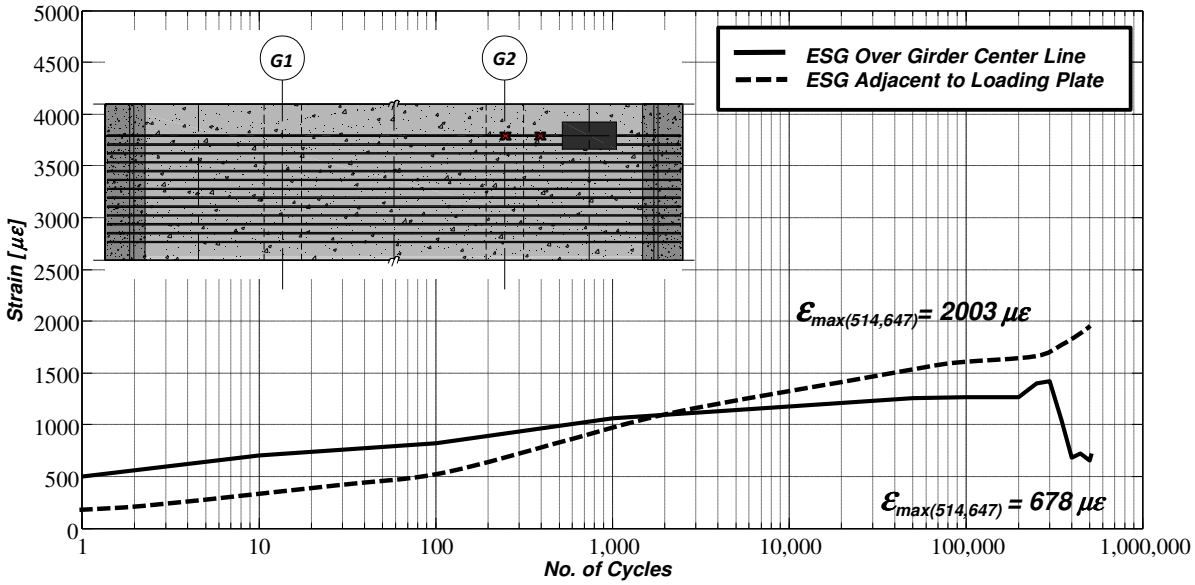

Figure 4-23: Plot of maximum strain over the girder center-line and near the applied load versus number of cycles for the cantilever section steel reinforcement subjected to fatigue cyclic loading

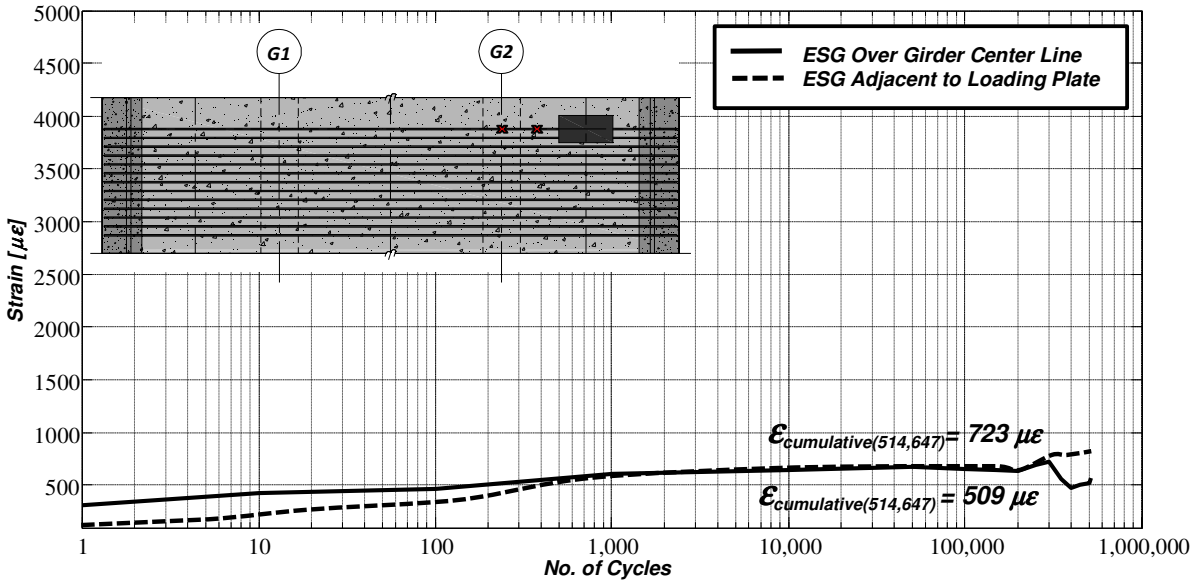

Figure 4-24: Plot of cumulative strain over the girder center-line and near the applied load versus number of cycles for the cantilever section steel reinforcement subjected to fatigue cyclic loading

Strains over the girder centerline and 1500 mm from the longitudinal free edge, for the cantilever section with GFRP reinforcement, increased slightly in magnitude over the applied 2,000,000 cycles. The strains in the top transverse GFRP bar over the girder center line increased gradually from 100 to 797 με and the strain in the bar adjacent to the loading plate increased from 0 to 775 με throughout the remainder of the fatigue test. The cumulative strain patterns for both locations were similar to the absolute values but smaller in magnitude measuring 556 and 213 με over the girder center-line and 1500 mm from the free edge respectively (Figure 4-26).

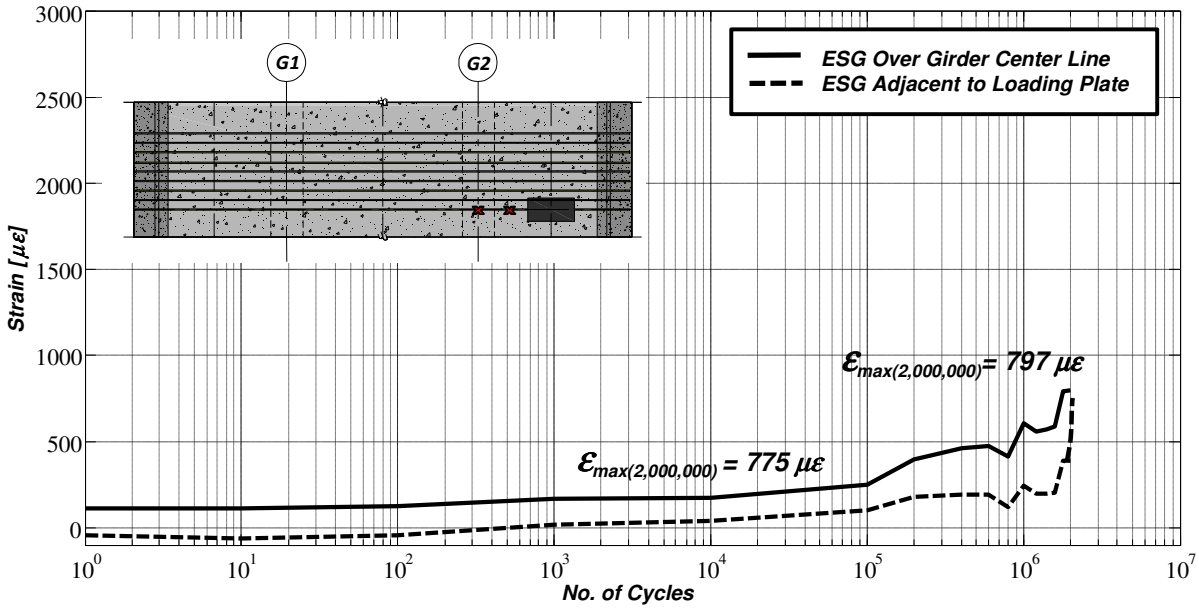

Figure 4-25: Plot of maximum strain over the girder center-line and near the applied load versus number of cycles for the cantilever section GFRP reinforcement subjected to fatigue cyclic loading

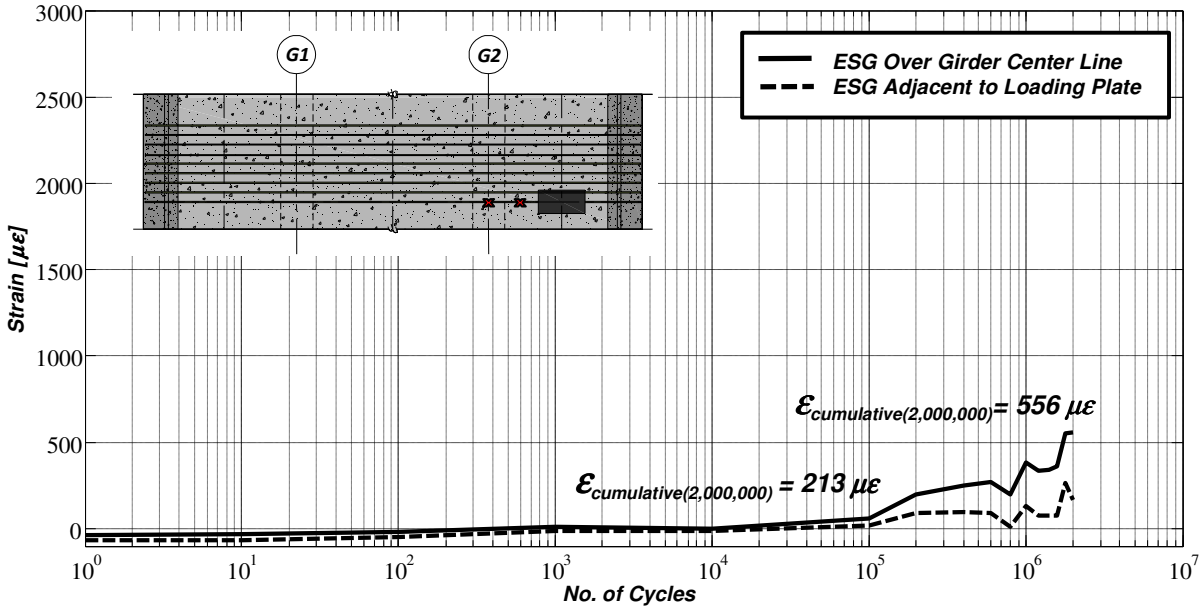

Figure 4-26: Plot of cumulative strain over the girder center-line and near the applied load versus number of cycles for the cantilever section GFRP reinforcement subjected to fatigue cyclic loading

Thus, the magnitude of cumulative strain in the top transverse bar over the girder center line was approximately 4.0 % of the ultimate rupture strain for a #25 GFRP bar. However, the total cumulative strain measured 1500 mm from the free edge of the cantilever (near the edge of the loading plate) was approximately 1.5 % of the total rupture strain for the same size GFRP bar.

4.2.2 Bottom Reinforcing Bar Strains

Test results obtained by Klowak (2007) prompted researchers to install strain gauges on the bottom transverse and longitudinal reinforcing bars. The strains in gauges installed on the bottom transverse reinforcing bars in the vicinity of the applied load for both cantilever

sections were not consistent with those obtained from flexural theory. At no instance in the loading history, for either of the cantilever sections, do the strain gauges on the bottom transverse bar(s) indicate compressive strain magnitudes. Only tensile strains were measured throughout the entire loading history. The following sections present the test results for the bottom transverse and longitudinal steel and GFRP reinforcing bars for the static and fatigue tests.

4.2.2.1 Static Load versus Strain

The strain gauges installed on the bottom transverse and longitudinal reinforcing bars along the transverse center line of the applied wheel load, for the cantilever section with steel reinforcement, measured maximum strain magnitudes of 3283 με and 3355 με (Figure 4-27) respectively. According to small deflection plate theory, these strain gauges should have measured compressive strains. Both strain gauges recorded excessive tensile strain magnitudes.

Strain magnitudes recorded for the cantilever section with GFRP were tensile for the bottom transverse and longitudinal reinforcing bars. The bottom transverse No. 10 GFRP reinforcement was subjected to a tensile strain of 3355 με and the bottom longitudinal bar obtained a maximum strain of 3911 με at the ultimate load of 487 kN (Figure 4-28).

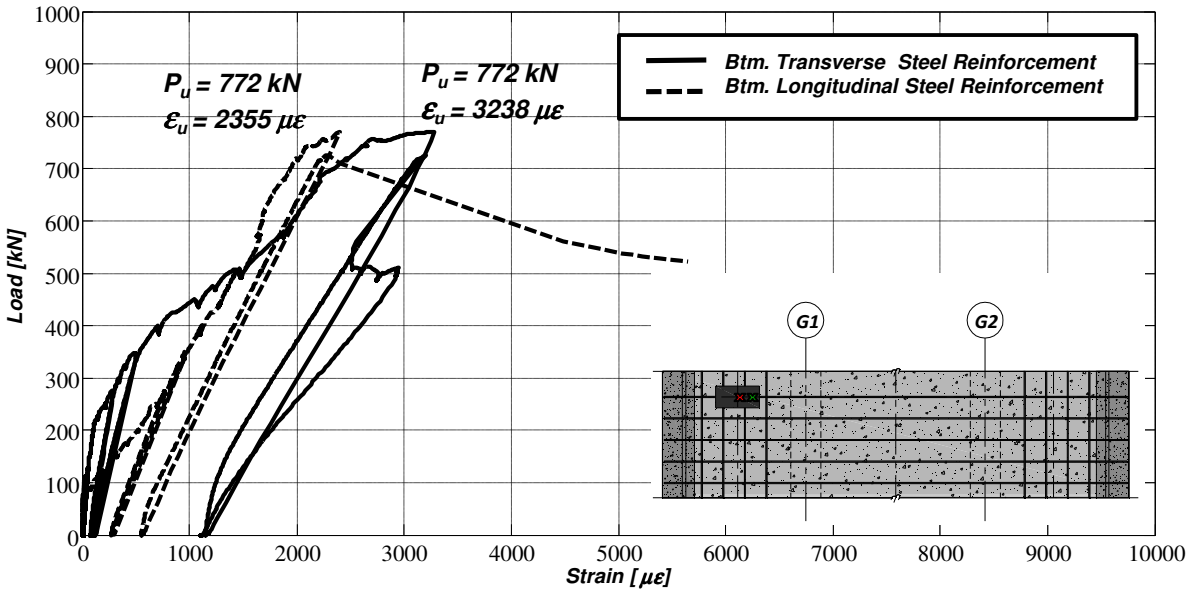

Figure 4-27: Plot of load versus bottom transverse and longitudinal reinforcing bar strain for the cantilever section with steel reinforcement subjected to a static monotonic load

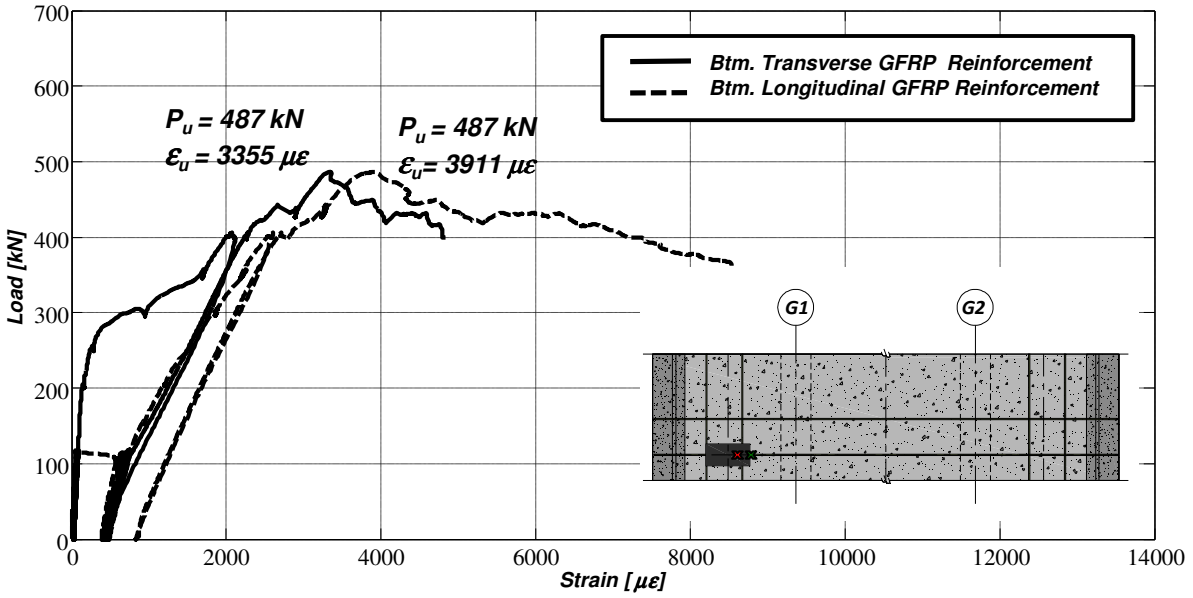

Figure 4-28: Plot of load versus bottom transverse and longitudinal reinforcing bar strain for the cantilever section with GFRP reinforcement subjected to a static monotonic load

4.2.2.2 Fatigue Load versus Strain

Fatigue cyclic loading also led to tensile strains in the bottom bars for both cantilever sections. Strain gauges installed on the bottom transverse steel bar located below the loading plate were only able to provide reliable data for approximately the first 20,895 cycles, when the maximum strain was 1461 με at cycle 20,895 (Figure 4-29). It is difficult to determine if the strain gauge simply stopped functioning or if that particular bottom transverse steel bar ruptured due to fatigue loading as discussed in Section 4.5. The longitudinal steel bar did provide reliable data until failure after 514,647 cycles. The maximum tensile strain observed was 1834 με, as shown in Figure 4-30.

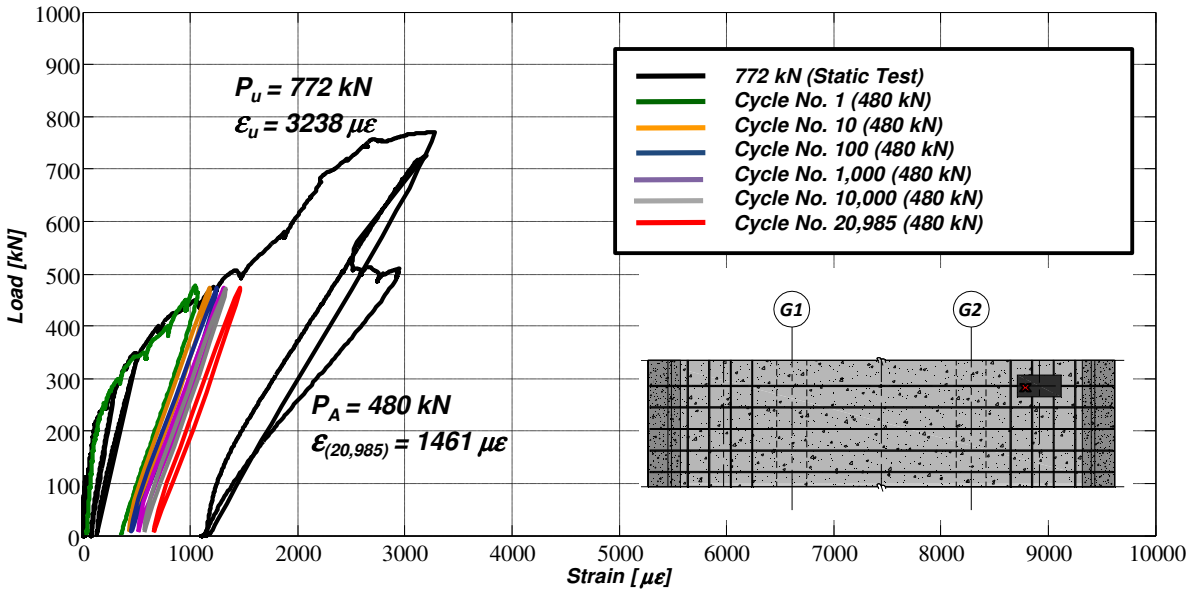

Figure 4-29: Plot of load versus bottom transverse reinforcing bar strain for the cantilever section with steel reinforcement subjected to a fatigue cyclic load

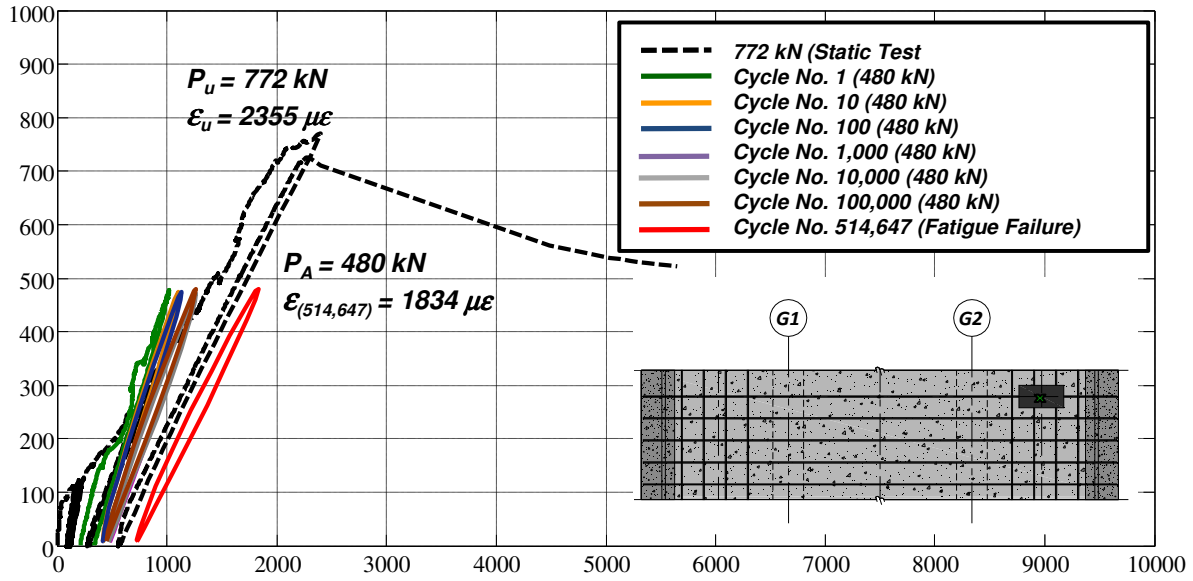

Figure 4-30: Plot of load versus bottom longitudinal reinforcing bar strain for the cantilever section with steel reinforcement subjected to a fatigue cyclic load

The strain gauges installed on the bottom transverse and longitudinal GFRP reinforcement did not provide reliable data beyond 15,020 cycles (Figure 4-31 and Figure 4-32). The strain gauge on the bottom transverse bar ceased to provide data after cycle 8,040. The maximum tensile strain recorded after 8,040 cycles was 2,799 με. Upon inspecting for damage after completing the final static test to failure, the bottom transverse GFRP bar was found to be ruptured. However, it cannot be stated with certainty that this bar ruptured after 8,040 cycles. It may have been possible that the strain gauge stopped working. The bottom longitudinal strain gauge managed to provide data for 15,020 cycles and measured 1585 με at the time of failure of the strain gauge or rupture of that particular bar.

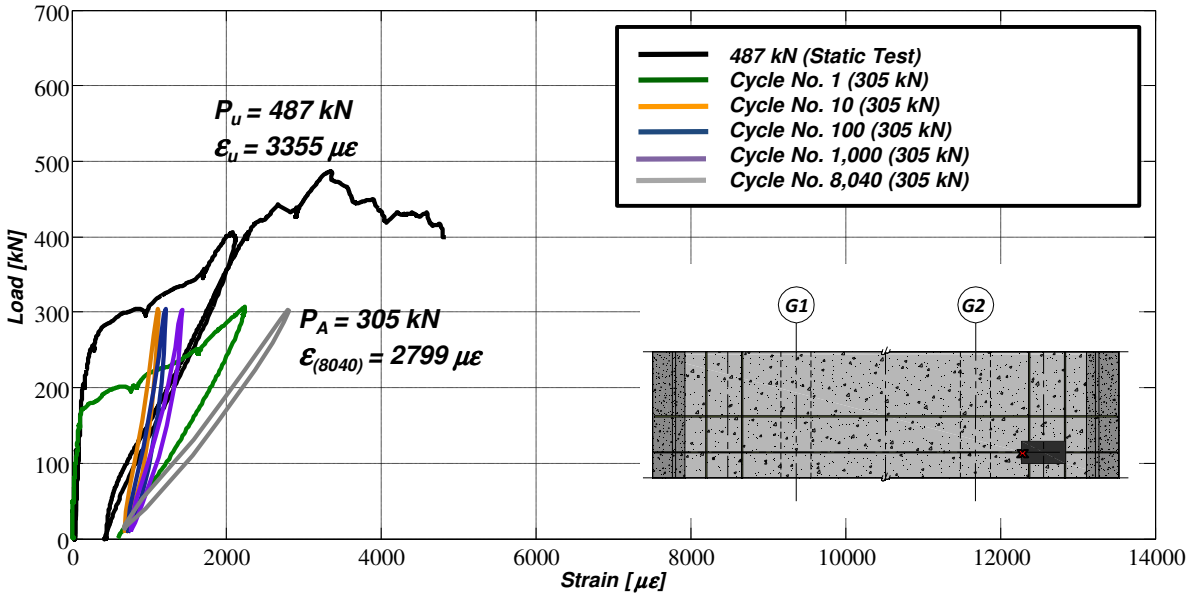

Figure 4-31: Plot of load versus bottom transverse reinforcing bar strain for the cantilever section with GFRP reinforcement subjected to a fatigue cyclic load

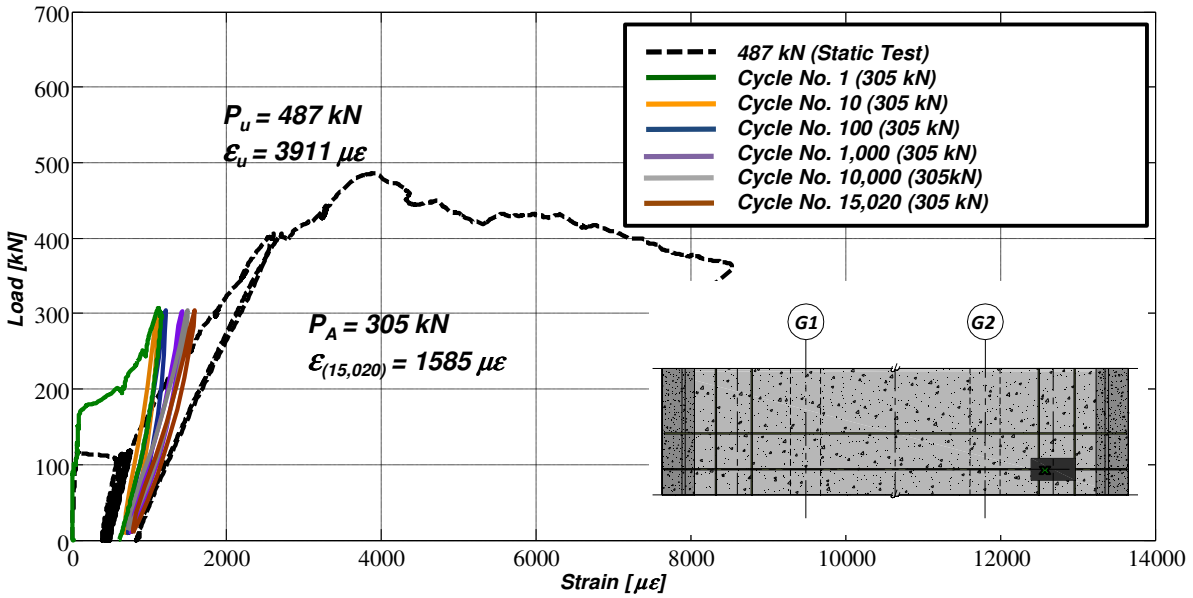

Figure 4-32: Plot of load versus bottom longitudinal reinforcing bar strain for the cantilever section with GFRP reinforcement subjected to a fatigue cyclic load

4.2.2.3 Fatigue Strain versus Number of Cycles

The maximum observed strains, as well as the cumulative strains, in the bottom transverse and longitudinal steel reinforcing bars are plotted in Figure 4-33 against the number of cycles. The maximum strains in the bottom transverse steel reinforcement initially increased until the slope changed near the failure load. At the time of bar rupture or damage to the strain gauge (i.e. at 20,985 cycles) the maximum cumulative strain measured in the bottom transverse steel reinforcement was 684 με. The bottom longitudinal reinforcement in the cantilever section with steel reinforcement provided strain readings until the fatigue failure. The maximum and cumulative strains of 1831 and 722 με were recorded at the time of fatigue failure respectively.

Observed strains in the bottom transverse and longitudinal GFRP bars due to the applied fatigue loading are plotted against the number of completed cycles in Figure 4-34. The small reinforcing ratio may have been the cause of the early rupture of the No. 10 GFRP bars or damage to the strain gauges. Figure 4-34 shows that the maximum and cumulative strains for the bottom transverse GFRP reinforcement after completing 8,040 cycles were 2799 and 722 με respectively. The bottom longitudinal GFRP bar also displayed a longer fatigue life and provided reliable strain data for up to 15,020 cycles. The maximum strain recorded after 15,020 cycles was smaller in magnitude and was observed to be 1585 με. The largest cumulative strain measured in the bottom longitudinal GFRP reinforcement was 795 με.

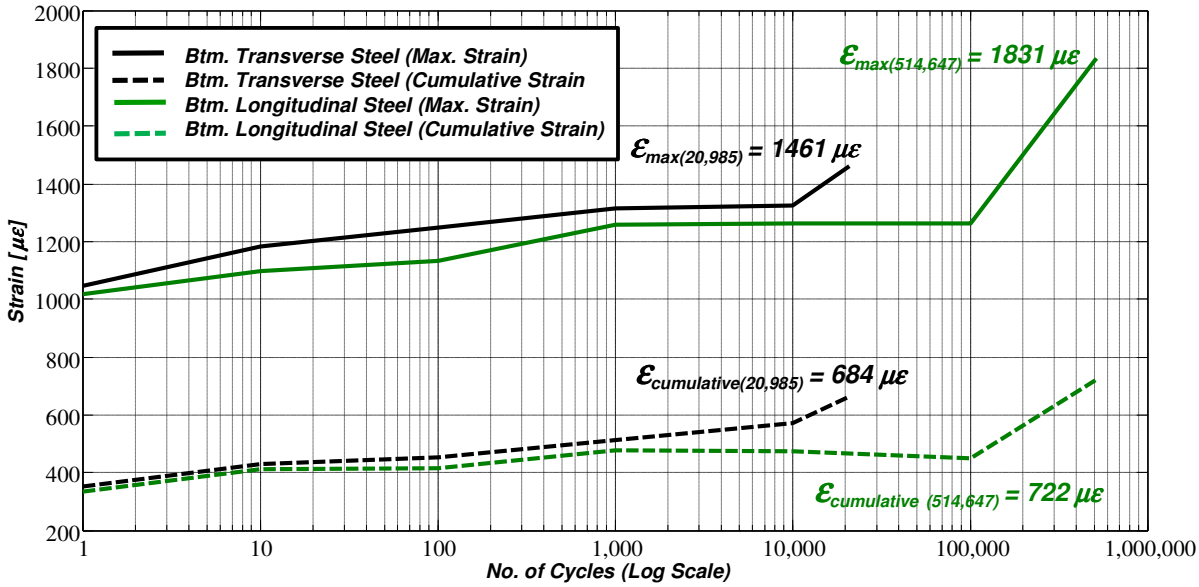

Figure 4-33: Plot of maximum and cumulative strain versus number of cycles for the bottom transverse and longitudinal reinforcing bars for the cantilever section with steel reinforcement subjected to fatigue cyclic loading

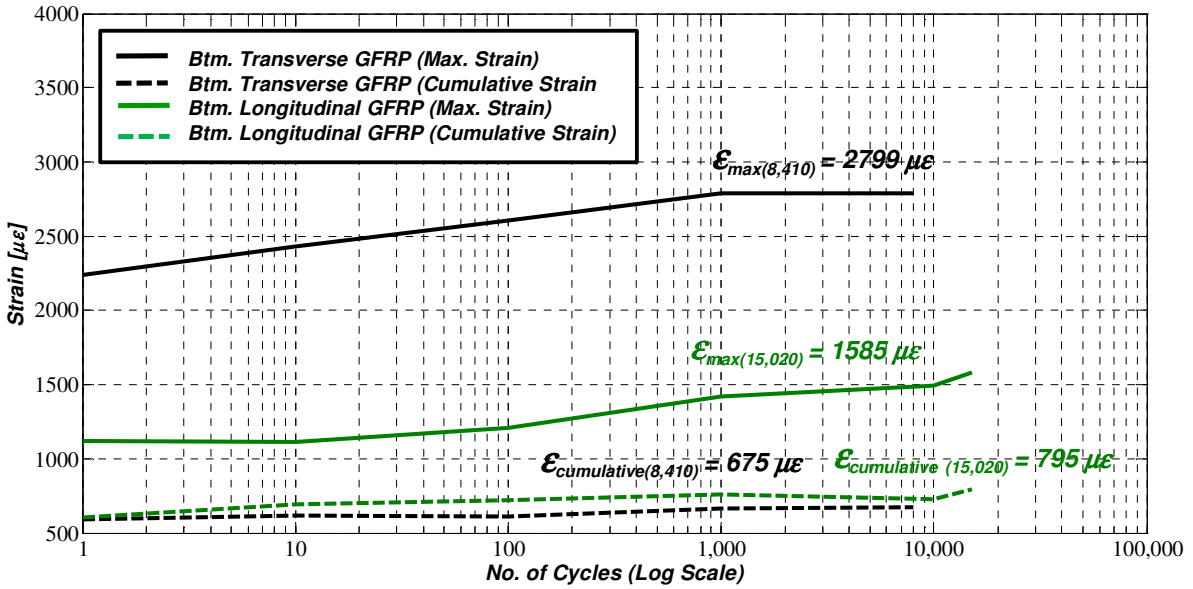

Figure 4-34: Plot of maximum and cumulative strain versus number of cycles for the bottom transverse and longitudinal reinforcing bars for the cantilever section with GFRP reinforcement subjected to fatigue cyclic loading

4.2.3 Top of Concrete Surface Strains

4.2.3.1 Static Load versus Strain

Unfortunately, no concrete gauges were installed on the top surface of the cantilever with steel reinforcement. Additional concrete strain gauges were provided after review of the results from the static and fatigue tests conducted on the cantilever section with steel reinforcement. The strain magnitudes measured on the top surface of the cantilever slab with GFRP reinforcement demonstrate a significant observation. The strain gauge installed next to the loading plate, on the top surface of the cantilever slab overhang, clearly indicates compressive strains in the transverse direction that are significant in magnitude. Flexural behaviour dictates that these strains should have been tensile strains. The compressive strain measured at the ultimate load of 487 kN was -1420 με (Figure 4-35). At no time in the static loading history was the top surface of the concrete in the vicinity of the loading plate subjected to tensile strain magnitudes.

4.2.3.2 Fatigue Load versus Strain

As previously stated, the cantilever with GFRP reinforcement did not fail under fatigue loading conditions. It completed 2,000,000 cycles under a fatigue cyclic load of 305 kN.

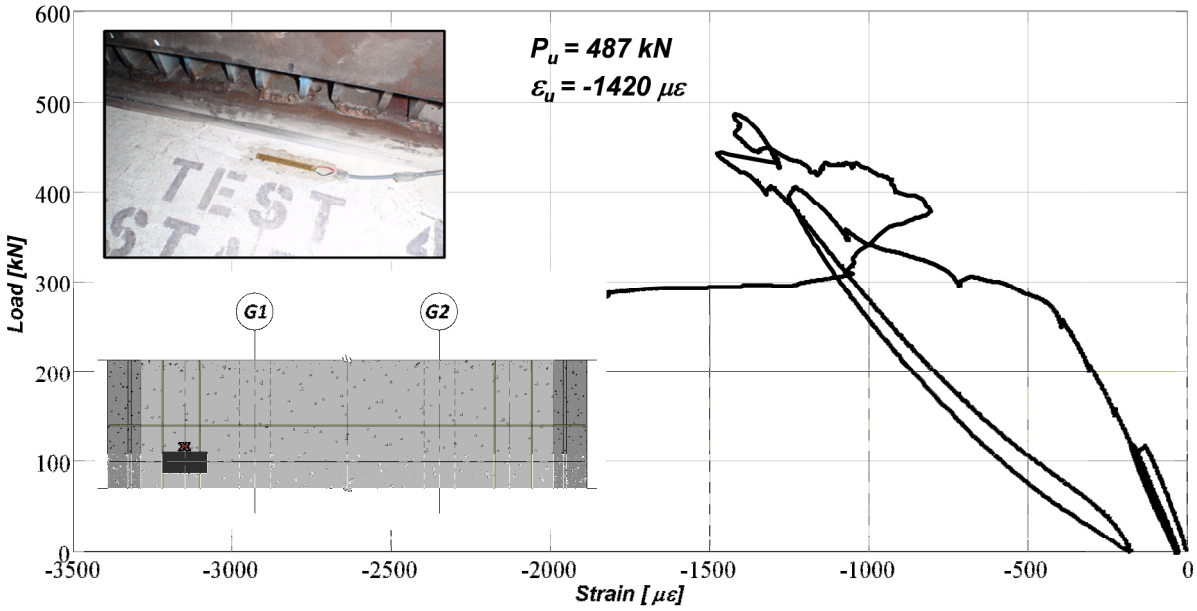

Figure 4-35: Plot of load versus concrete strain in the transverse direction on the top surface of the cantilever slab near the steel loading plate for the cantilever with GFRP reinforcement subjected to a static monotonic load

Figure 4-36 shows a steady increase in the maximum observed compressive strains in the transverse direction in the vicinity of the steel loading plate. The maximum observed compressive strain after 2,000,000 cycles was -492 με. After fatigue testing, the cantilever slab over with GFRP reinforcement was tested under a monotonically increasing load. It failed under a static load of 513 kN and a maximum compressive strain on the top surface of the concrete slab overhang of -1030 με.

The presence of compressive strain on the top surface of the cantilever slab, in the transverse direction, clearly is not consistent with small deflection plate theory and indicates a strong presence of arching action.

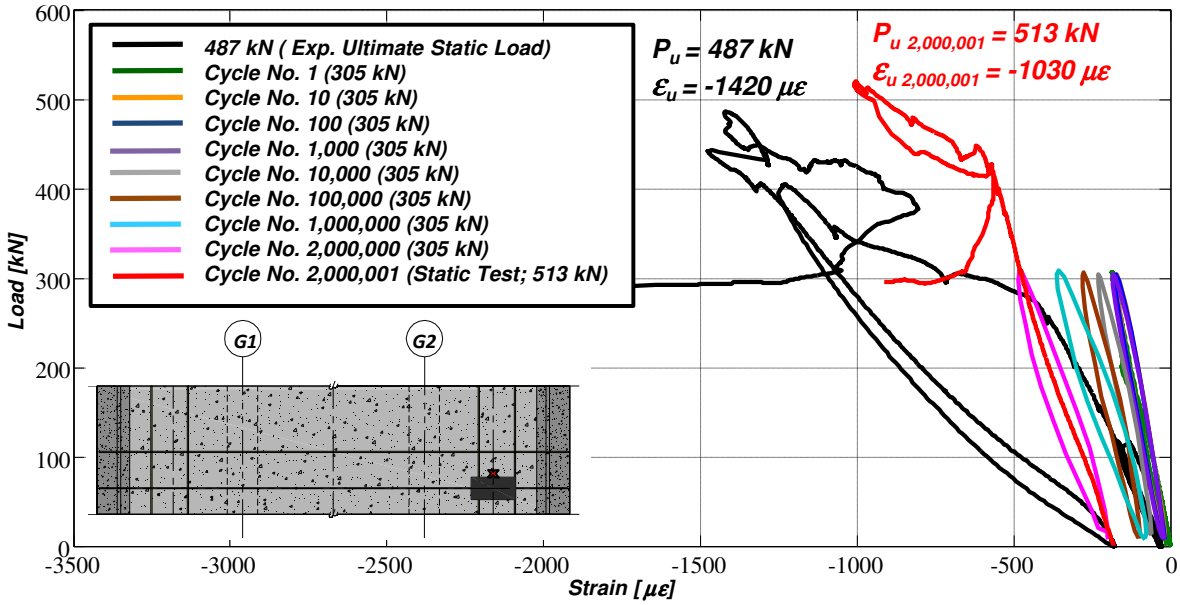

Figure 4-36: Plot of load versus concrete strain in the transverse direction on the top surface of the cantilever slab near the steel loading plate for the cantilever with GFRP reinforcement

4.2.3.3 Fatigue Strain versus Number of Cycles

No concrete fatigue strain data versus the number of cycles can be presented for the cantilever with steel reinforcement because a concrete strain gauge was not installed.

The maximum absolute compressive strain observed after completing 2,000,000 cycles at 305 kN was -492 με (Figure 4-37). The cumulative or permanent plastic strain in the concrete as a result of the fatigue loading conditions was observed to be -200 με. The fatigue strain magnitudes measured on the top surface of the cantilever slab with GFRP reinforcement confirmed observations and behavior from the previously conducted static test. Only compressive strains were measured on the top concrete surface of the cantilever slab over.

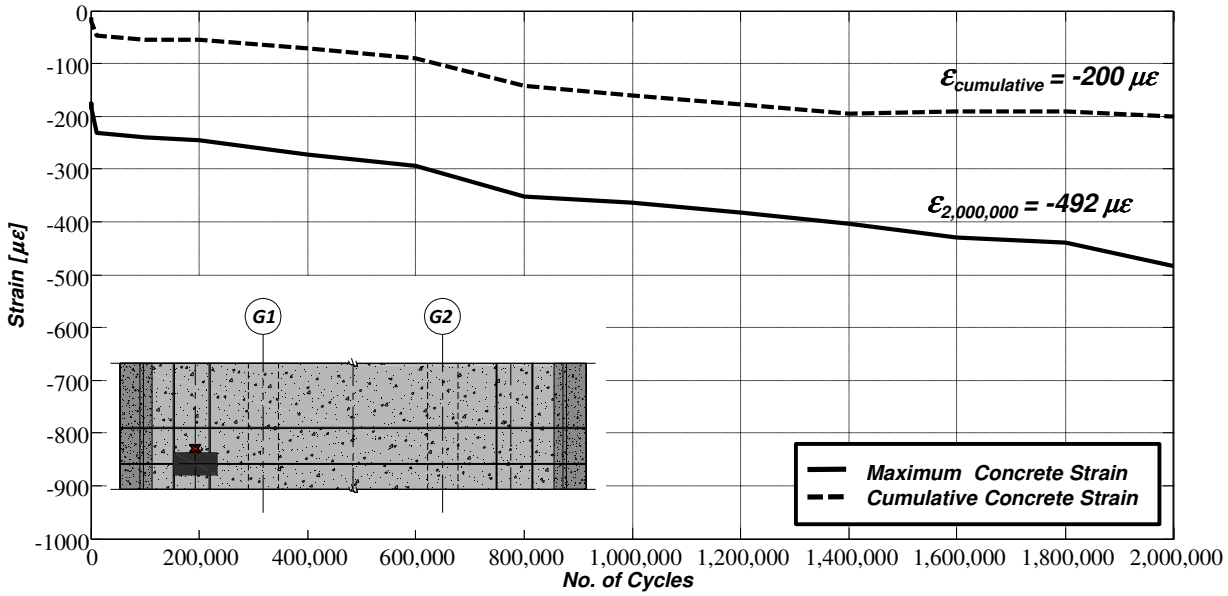

Figure 4-37: Plot of maximum and cumulative concrete strain versus number of cycles in the transverse direction on the top surface of the cantilever slab near the steel loading plate for the cantilever with GFRP reinforcement

4.2.4 Barrier Wall Reinforcing Bar Strains

Strain results obtained from the strain gauges installed in the GFRP bars located in the barrier wall indicated that the barrier is subjected to bending stresses as a result of the applied wheel load on the cantilever slab overhang. The following two sections highlight strain data obtained from the static and fatigue tests conducted on the cantilevers with steel and GFRP reinforcement.

4.2.4.1 Static Load versus Strains

Strains in three out of the four strain gauges'; installed on the No. 19 GFRP longitudinal reinforcement in the traffic barrier wall, are plotted against load in Figure 4-38 and Figure 4-

39. The barrier wall for the cantilever section with steel reinforcement exhibited cracking at approximately 420 kN and the vertical tensile cracks grew longer throughout the duration of the static test. At the ultimate load of 772 kN, The maximum compressive strain in the top bar was -352 με. and The maximum tensile strain in the bottom bar was 1811 με.

The cantilever section with GFRP reinforcement failed at 487 kN compared to the cantilever slab overhang reinforced with steel which failed at 772 kN. It failed at 487 kN and as a result had less cracking. It displayed small tensile cracks that initiated approximately 400 kN and grew only after ultimate failure had occurred due to the post ultimate loading on the cantilever slab overhang. At the ultimate load the maximum compressive strain measured was -333 με and the maximum tensile strain observed was 601 με (Figure 4-39).

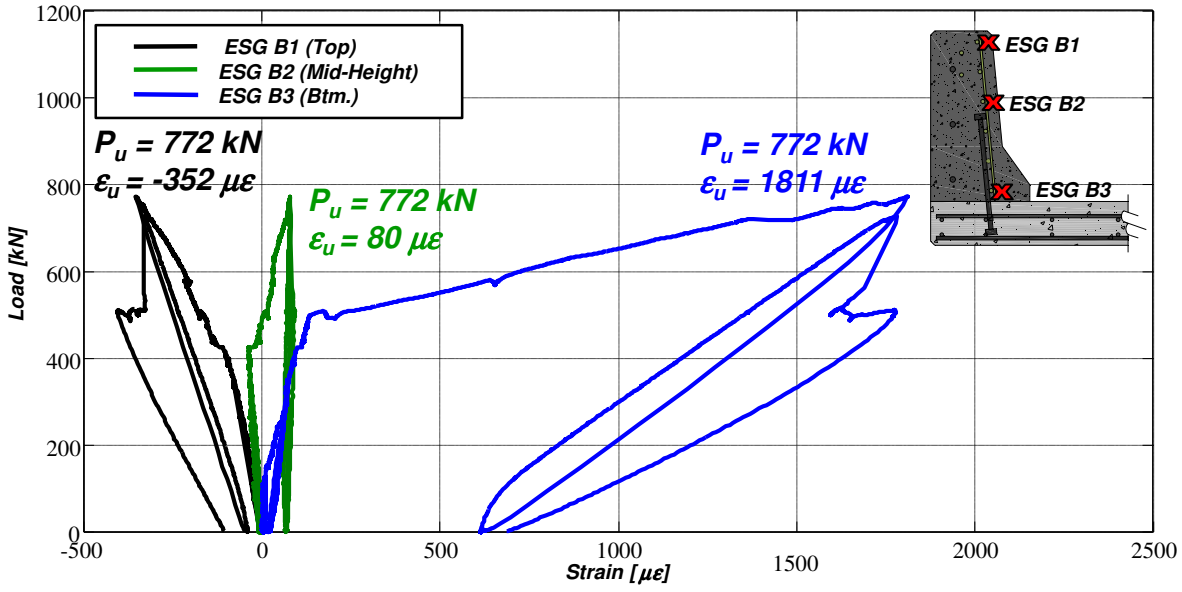

Figure 4-38: Plot of load verses longitudinal reinforcing bar strains in the traffic barrier wall for the cantilever with steel reinforcement subjected to static monotonic loading

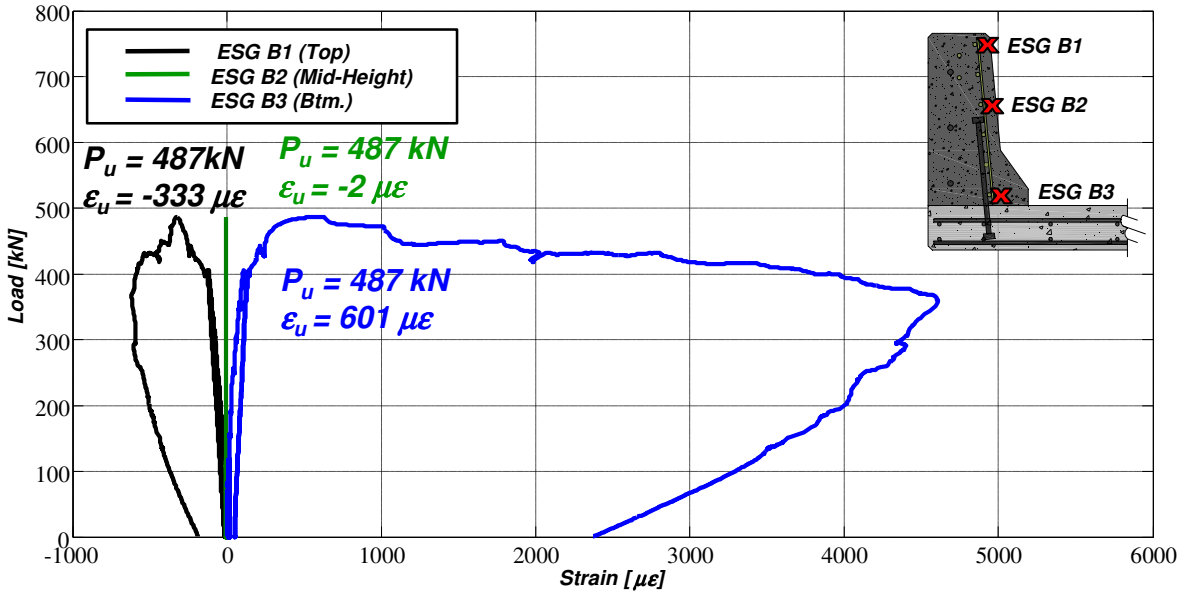

Figure 4-39: Plot of load verses longitudinal reinforcing bar strains in the traffic barrier wall for the cantilever with GFRP reinforcement subjected to static monotonic loading

4.2.4.2 Barrier Wall Static Strain Profiles

The strains in three of the four strain gauges are plotted against their vertical location over the depth of the barrier wall for the cantilevers sections with steel and GFRP reinforcement in Tables 4-9 and Table 4-10 and are plotted in (Figure 4-40 and Figure 4-41). It is interesting to observe that at the lower loads, the strain profile remains virtually linear. At the higher loads, as was the case with the cantilever with steel reinforcement, the neutral axis shifted upwards caused by cracking due to bending stresses in the barrier wall. The lower ultimate load observed for the cantilever with GFRP reinforcement is the primary reason for less cracking and essentially no significant shift in the neutral axis and strain profile (Figure 4-41). Strain magnitudes shown in Table 4-9 and 4-10 clearly demonstrate classical bending

behavior indicating that barrier was acting like an inverted girder from above as engineers' hypothesis suggested.

Table 4-9: Longitudinal Reinforcing bar strain Profiles in the traffic barrier wall for the cantilever with steel reinforcement subjected to static monotonic loading

Depth of Barrier Wall [mm]	Applied Static Load			
	90 (Un-factored Wheel Load) [kN]	214 (Factored Wheel Load) [kN]	428 (2 X Factored Wheel Load) [kN]	772 (Ultimate Load) [kN]
775	*-*	*-*	*-*	*-*
725	*-15*	*-40*	*-125*	*-352*
455	*-11*	*-24*	*-18*	*80*
50	*4*	*38*	*112*	*1811*
0	*-*	*-*	*-*	*-*

Table 4-10: Longitudinal reinforcing bar strain profiles in the traffic barrier wall for the cantilever with GFRP reinforcement subjected to static monotonic loading

Depth of Barrier Wall [mm]	Applied Static Load			
	90 (Un-factored Wheel Load) [kN]	214 (Factored Wheel Load) [kN]	428 (2 X Factored Wheel Load) [kN]	487 (Ultimate Load) [kN]
775	*-*	*-*	*-*	*-*
725	*-10*	*-44*	*-213*	*-333*
455	*-1*	*-2*	*-2*	*-2*
50	*7*	*30*	*195*	*601*
0	*-*	*-*	*-*	*-*

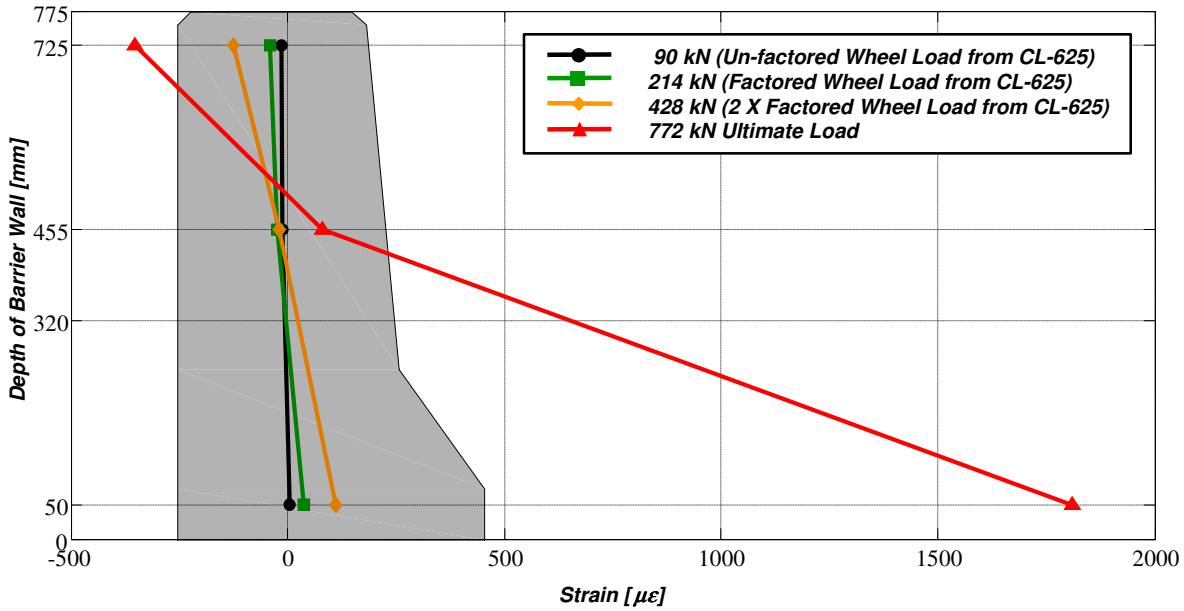

Figure 4-40: Longitudinal reinforcing bar strain profiles in the traffic barrier wall for the cantilever with steel reinforcement subjected to static monotonic loading

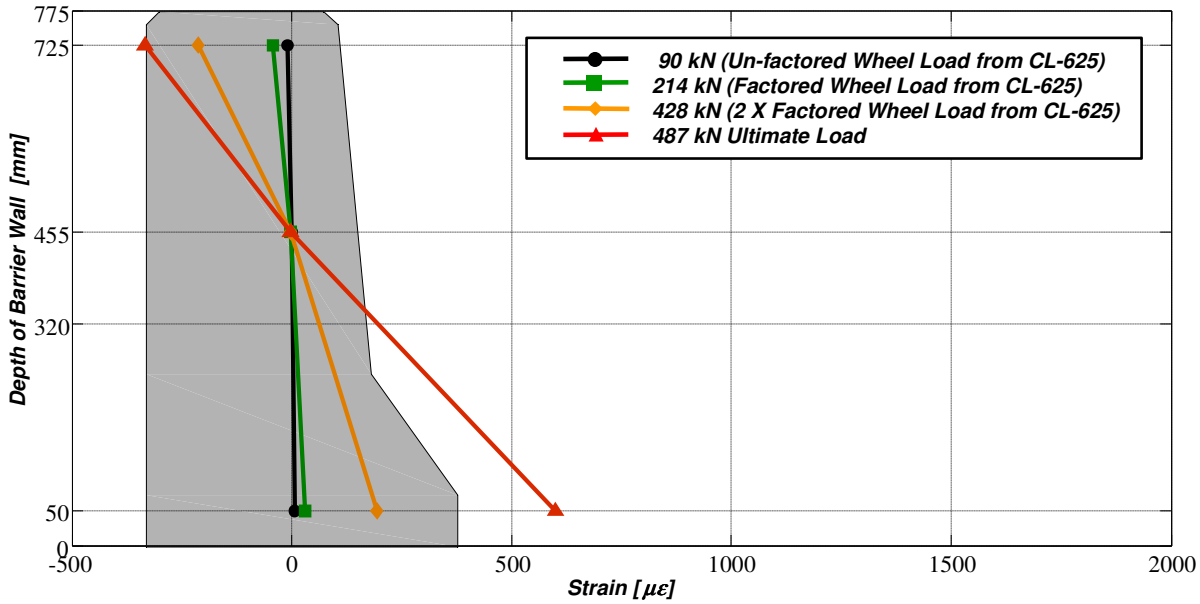

Figure 4-41: Longitudinal reinforcing bar strain profiles in the traffic barrier wall for the cantilever with GFRP reinforcement subjected to static monotonic loading

4.2.4.3 Barrier Wall Fatigue Strain Profiles

The cantilever with steel reinforcement was subjected to an applied fatigue cyclic load of 480 kN. Strain profiles for a load of 480 kN obtained from the initial static test on the opposite cantilever and for cycle 1 indicated a negligible shift in the neutral axis based on the scale of the plot (Table 4-11 and Figure 4-42). The following half of a million cycles indicate that the barrier wall was subjected to significant cumulative strains as a result of the applied cyclic load on the cantilever slab overhang.

Fatigue testing on the cantilever section with GFRP reinforcement indicated no cracking in the barrier wall. The cracking load obtained from the previous static test revealed that the barrier wall cracked at approximately 400 to 420 kN. The fatigue strain profiles for the cantilever section with GFRP reinforcement are shown in Table 4-12 and are plotted in Figure 4-43 and indicate no experimental change in the neutral axis for the entire loading history.

Table 4-11: Longitudinal Reinforcing bar strain Profiles in the traffic barrier wall for the cantilever with steel reinforcement subjected to fatigue cyclic loading

Depth of Barrier Wall [mm]	Fatigue Cycle No. (Applied Fatigue Load P_a = 480 kN)								Static Test (P_u = 772 kN)
	Static Test (P_u = 480 kN)	1	10	100	1,000	10,000	100,000	514,647	
775	-	-	-	-	-	-	-	-	-
725	*-152*	*-127*	*-168*	*-189*	*-219*	*-215*	*-237*	*-500*	*-352*
455	*0*	*47*	*209*	*551*	*1241*	*1368*	*1400*	*1425*	*80*
50	*129*	*476*	*1899*	*2507*	*3489*	*3701*	*3721*	*4675*	*1811*
0	-	-	-	-	-	-	-	-	-

Table 4-12: Longitudinal reinforcing bar strain profiles in the traffic barrier wall for the cantilever with GFRP reinforcement subjected to fatigue cyclic loading

Depth of Barrier Wall [mm]	Fatigue Cycle No. (Applied Fatigue Load P_a = 305 kN)									Initial Static Test (P_u = 487 kN)	Final Static Test (P_u = 513 kN)
	Static Test (P = 305 kN)	1	10	100	1,000	10,000	100,000	1,000,000	2,000,000		2,000,001
775	-	-	-	-	-	-	-	-	-	-	-
725	-79	-79	-86	-86	-81	-179	-174	-180	-298	-333	-481
455	34	1	2	2	3	-8	-15	19	6	-2	55
50	65	44	38	44	57	65	100	140	202	601	390
0	-	-	-	-	-	-	-	-	-	-	-

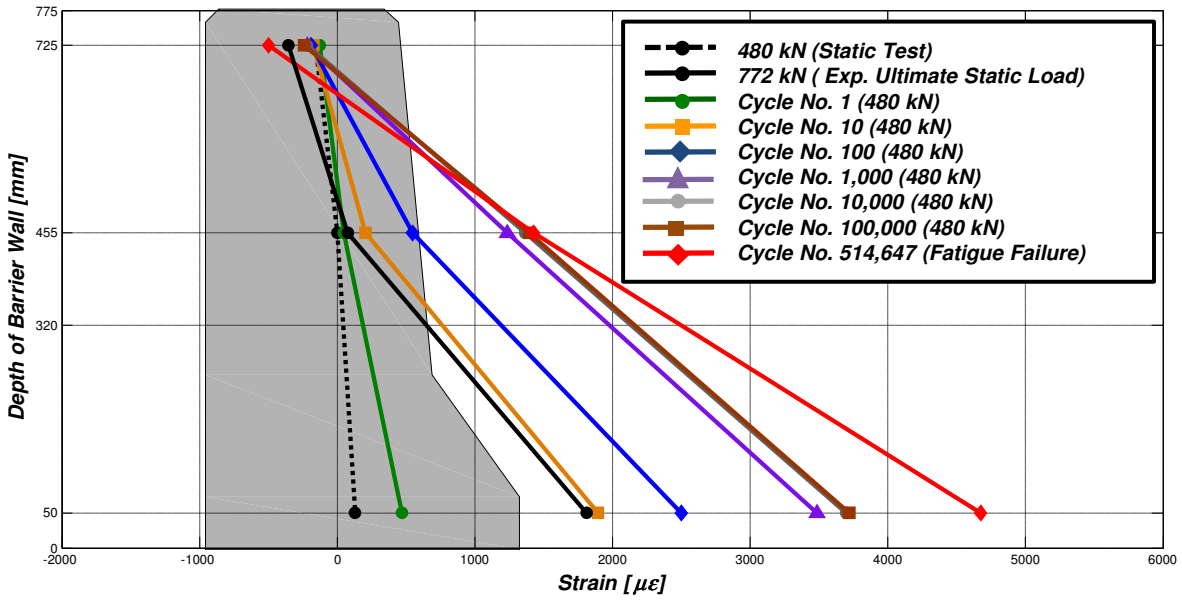

Figure 4-42: Longitudinal reinforcing bar strain profiles in the traffic barrier wall for the cantilever with steel reinforcement subjected to fatigue cyclic loading

Fatigue testing results confirmed the results obtained from the initial static testing. Punching shear failures are localized and the author feels that it is as if the cantilever slab overhang away from the load is supporting the barrier which in return is supporting the free longitudinal free edge of the cantilever in the vicinity of the concentrated wheel load.

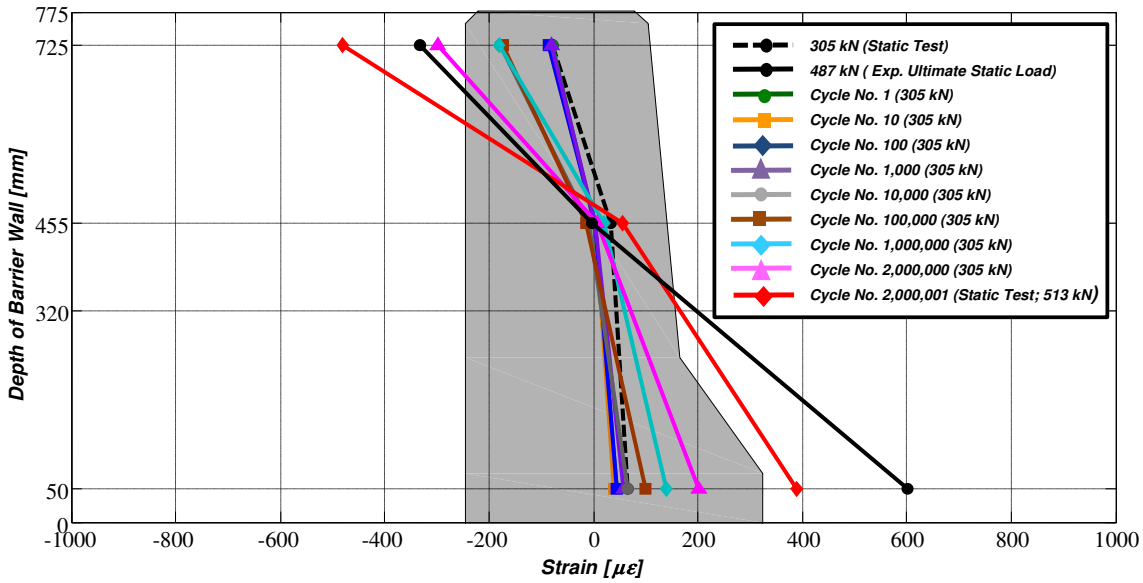

Figure 4-43: Longitudinal reinforcing bar strain profiles in the traffic barrier wall for the cantilever with GFRP reinforcement subjected to fatigue cyclic loading

4.2.5 Strain Compatibility below Wheel Load

The experimental data presented in this section illustrates the strains produced below the loading plate for both cantilever sections. It investigates the strains in the top and bottom transverse reinforcing bars located below the loading plate for both monotonic static tests to failure. For the cantilever section with GFRP reinforcement, it also looks at the static top surface of the concrete strains for the cantilever section with GFRP reinforcement plotted against the depth of the slab. The concept of strain compatibility was used for the cantilever with steel reinforcement and assumes that plane sections remain plane to extrapolate the magnitude of strain on the top surface of the concrete. It is perhaps the most powerful argument and indication of the presence of arching-action in bridge deck cantilever slab overhangs subjected to a wheel load.

4.2.5.1 Static Load versus Strains

The cantilever section with steel reinforcement was not instrumented with a concrete strain gauge to measure concrete strain on the top surface of the cantilever. The gauge on the top transverse steel bar located under the transverse center line of the applied load recorded compressive strains up to a load approximately 500 kN. The maximum compressive strain observed in the top transverse reinforcing bar was -134 με at a load of 360 kN (Figure 4-44). The strain in the top transverse reinforcing bar transitioned from compressive strain magnitudes to tensile strain magnitudes and eventually obtained a maximum tensile strain of 311 με at the ultimate load of 772 kN. The maximum tensile strain measured in the bottom transverse reinforcing bar located below the loading plate was 3238 με at the static ultimate of 772 kN (Figure 4-44).

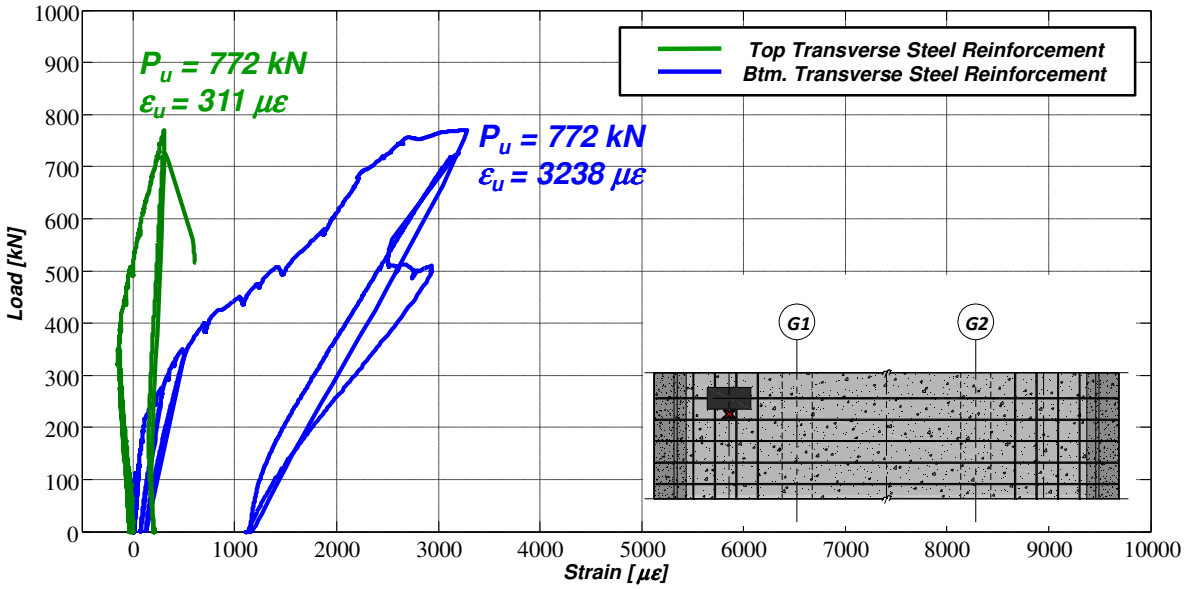

Figure 4-44: Plot of load verses top and bottom transverse reinforcing bar strain for the cantilever with steel reinforcement subjected to static monotonic loading

For the cantilever section with GFRP, the strain measured on the top of the concrete surface measured a maximum compressive strain magnitude of -1420 με at the observed static ultimate load of 487 kN. The concrete strain gauge did not measure tensile strains.

The top transverse GFRP bar located under the transverse center line of the load plate initially measured compressive strain magnitudes up to approximately 300 kN. The maximum compressive strain observed in the top transverse reinforcing bar was -97 με at a load of 280 kN (Figure 4-45). The strain in the top transverse reinforcing bar also changed from compressive to tensile strains and was 892 με at the ultimate load of 487 kN. The tensile strain measured in the bottom transverse GFRP reinforcing bar located below the load plate was 3348 με at the static ultimate of 487 kN.

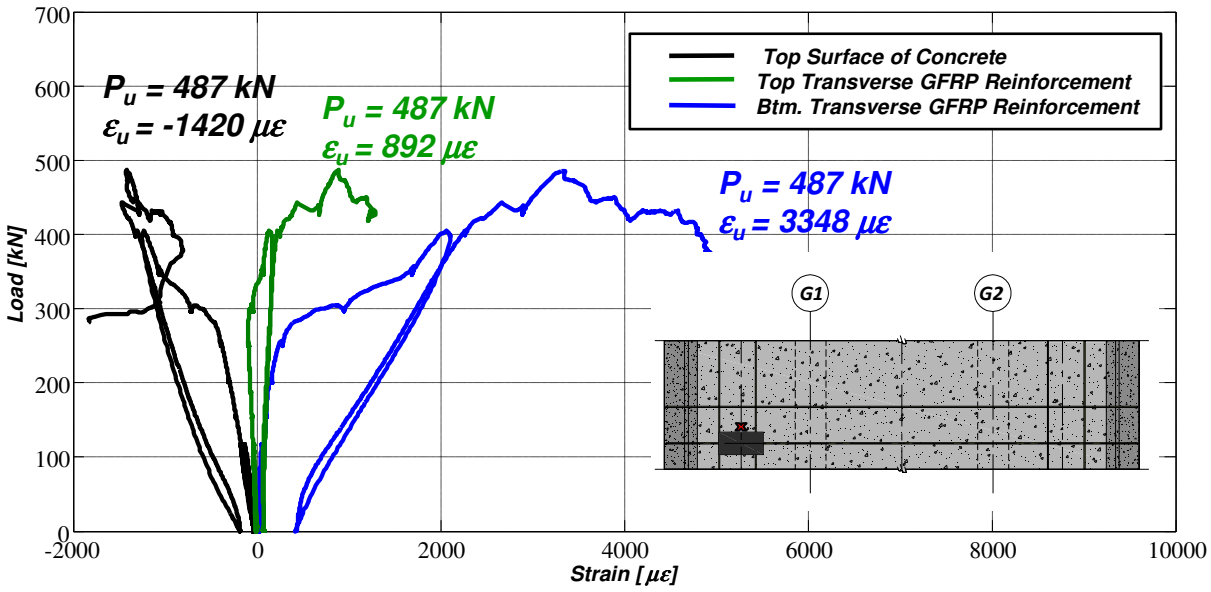

Figure 4-45: Plot of load verses top surface of concrete strain as well as top and bottom transverse reinforcing bar strain for the cantilever with GFRP reinforcement subjected to static monotonic loading

4.2.5.2 Static Strain Compatibility Profiles

The strain values measured for the top and bottom transverse steel reinforcing bars located below the loading plate are shown in Table 4-13 for the loads of 90, 214, 428 and 772 kN. The values for the concrete strain were extrapolated linearly from the top and bottom transverse reinforcing bars based on the assumption that a plane section remains plane. At the experimental ultimate load of 772 kN, the maximum extrapolated strain determined for the concrete was -1050 με and the maximum tensile strain observed in the bottom transverse steel reinforcing bar below the loading plate was 3238 με (Figure 4–46).

Table 4-13: Strain compatibility profile located below the steel loading plate for the cantilever section with steel reinforcement subjected to static monotonic loading

Depth of Cantilever Slab Overhang [mm]	Applied Static Load			
	90 [kN]	214 [kN]	428 [kN]	772 [kN]
0	*-80**	*-185**	*-625**	*-1050**
52	*-25*	*-95*	*-95*	*311*
168	*44*	*115*	*903*	*3238*
200	-	-	-	-

**Values were interpolated based on strain compatibility and assumption that plane sections remain plane*

The observed strains values measured for the top surface of the concrete as well as the top and bottom transverse GFRP reinforcing bars located below the loading plate are shown in Table 4-14 for the loads of 90, 214, 428 and 487 kN. The transverse compressive strains measured on the top surface of the cantilever slab for the cantilever with GFRP reinforcement also confirm the presence of arching action (Figure 4-47).

Table 4-14: Strain compatibility profile located below the steel loading plate for the cantilever section with GFRP reinforcement subjected to static monotonic loading

Depth of Cantilever Slab Overhang [mm]	Applied Static Load			
	90 [kN]	214 [kN]	428 [kN]	487 [kN]
0	*-145*	*-321*	*-1431*	*-1420*
60	*-24*	*-78*	*387*	*892*
170	*71*	*170*	*2540*	*3348*
200	-	-	-	-

At the experimental ultimate load of 487 kN, the maximum measured strain for the concrete was -1420 με. The maximum tensile strains observed in the top transverse and bottom transverse GFRP reinforcing bars below the concentrated wheel load (loading plate) were 892 με and 3348 με respectively (Figure 4–47).

If the cantilever slab overhangs response to the wheel load been flexural, the transverse strains on the top of the slab should have been tensile. Figure 4-46 and Figure 4-47, which illustrate strains in the vicinity of the loading plate, confirm that strains on the top of the slab are compressive and that the strain profile over the depth of the slab is linear. Strain compatibility over the depth of the cantilever slab is valid and it contradicts small deflection plate theory for a cantilever slab overhang subjected to a concentrated wheel load. The presence of arching action is confirmed by the experimental strain results in the vicinity and below the loading plate.

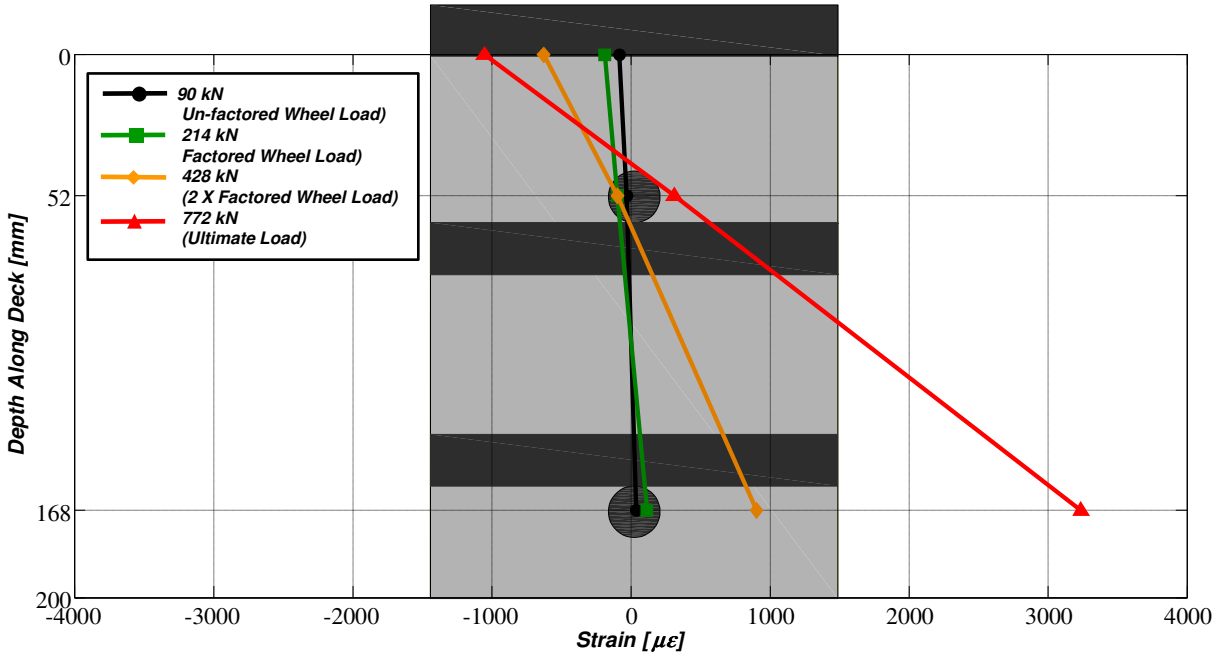

*Values for top surface of concrete were interpolated based on strain compatibility and assumption that plane sections remain plane

Figure 4-46: Plot strain compatibility profiles for the cantilever section with steel reinforcement subjected to static monotonic loading

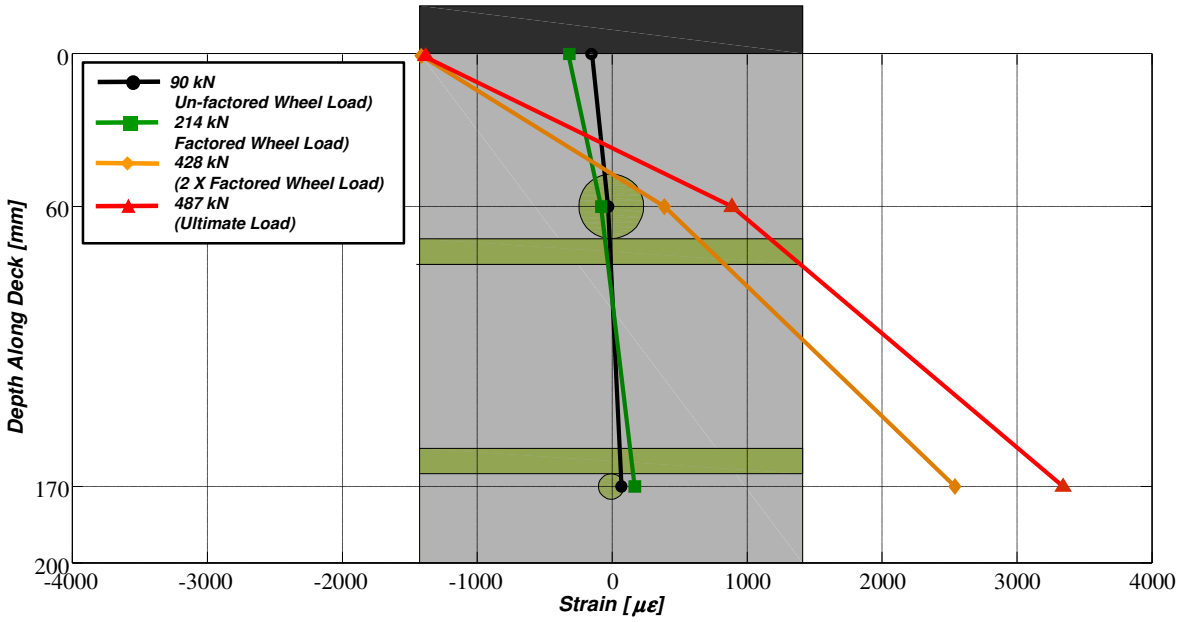

Figure 4-47: Plot strain compatibility profiles for the cantilever section with GFRP reinforcement subjected to static monotonic loading

4.3 Cracking

Observed concrete cracking in the cantilever slab overhangs is divided into five different categories. The following five sub-sections (4.3.1 to 4.3.5) deal with crack mapping under static loads, static load versus crack widths, crack mapping under fatigue loads, fatigue load versus crack widths, and crack width versus the number of cycles required to fail a particular cantilever section.

4.3.1 Crack Mapping under Static Loads

Four different types of cracks appeared under static wheel loads on the cantilever slab overhangs. The first type of crack observed during the static tests was a single transverse crack on the underside of the cantilever located below the loading plate. The underside transverse crack first became apparent in both cantilever sections between the loads of 120 and 130 kN and are labeled as crack type "A" (Figures 4-48 and 4-49). The second type of crack observed was radial cracks that initiated on the underside of the slab, originating from below the loading point, at approximately. 150 kN and continued to grow in length and number until failure. These types of cracks are labelled as crack type "B" (Figures 4-48 and 4-49). The third crack to appear during the static destructive testing of both cantilever sections were longitudinal cracks over the girder and are labelled as type "C". These cracks first became apparent at approximately 280 to 320 kN and continued to grow in width and length until failure and are shown in Figures 4-48 and 4-49).. The final cracks to appear were circumferential cracks on the top surface of the concrete of both cantilever sections

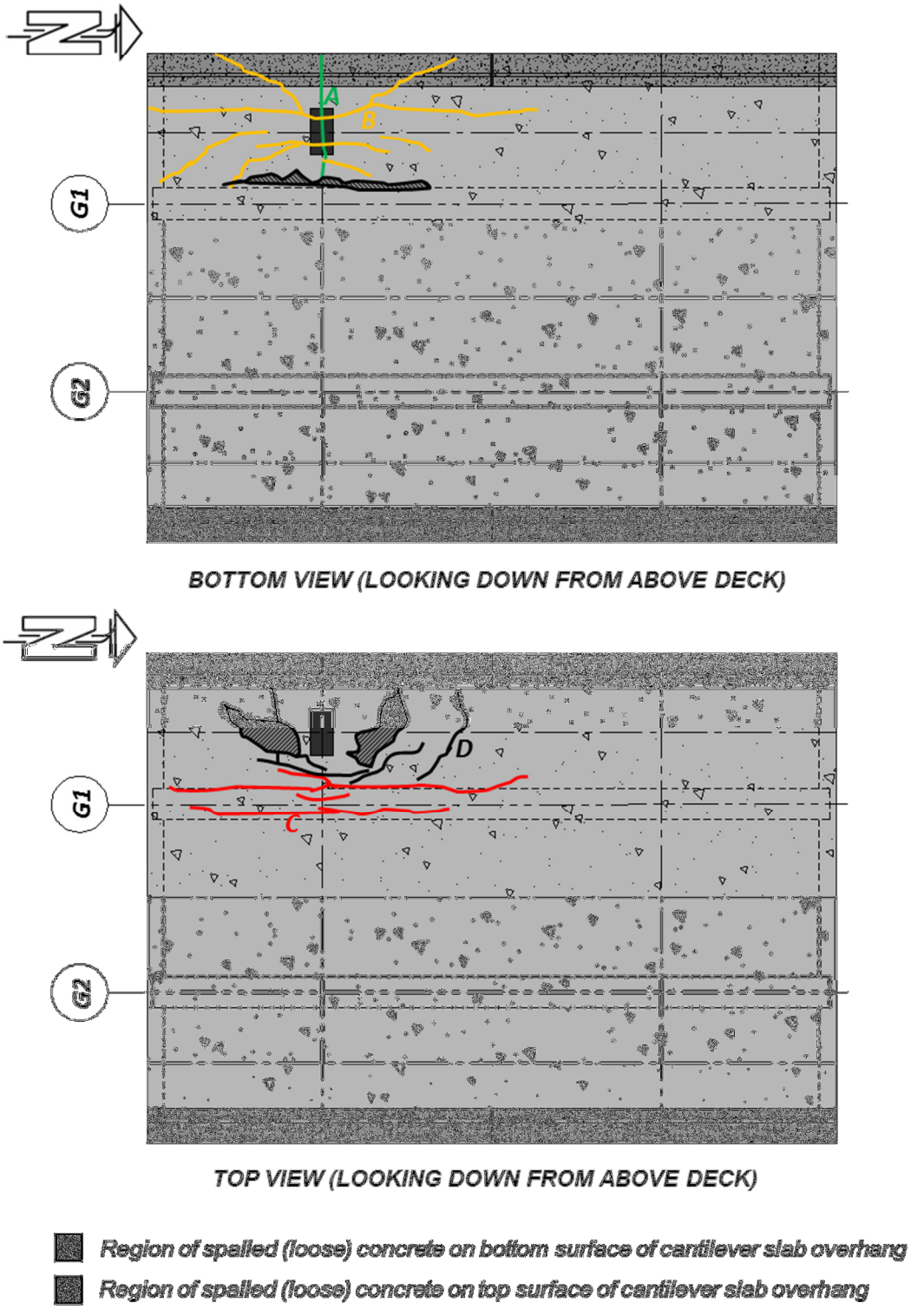

Figure 4-48: Crack patterns for the cantilever section with steel reinforcement subjected to static monotonic loading

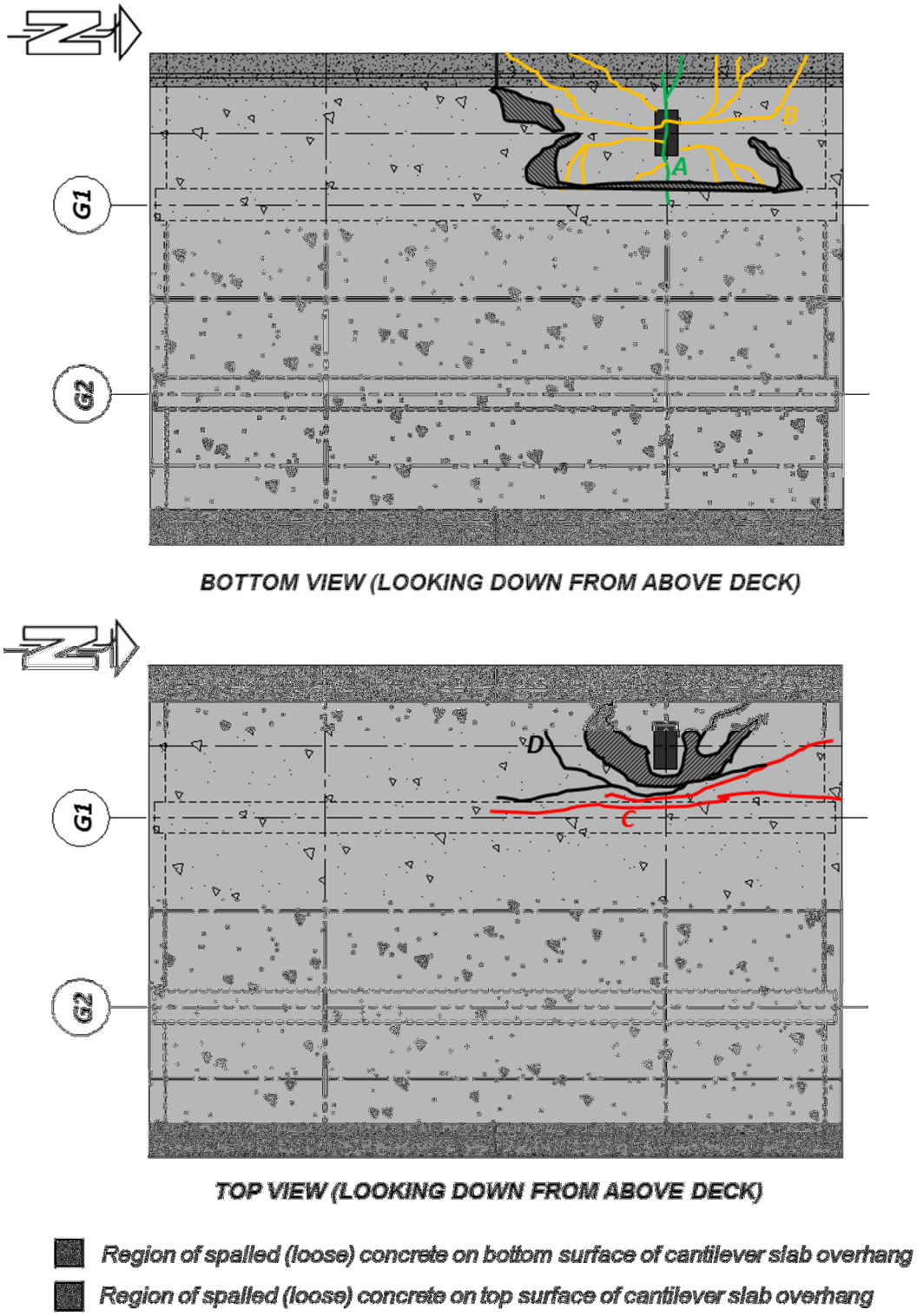

Figure 4-49: Crack patterns for the cantilever section with GFRP reinforcement subjected to static monotonic loading

and were first present at the higher loads just prior to failure. Photographs of the cracks on the top and bottom of the deck slab observed during the static test conducted on the cantilever with steel reinforcement are shown in Figure 4-50. The photographs in Figure 4-51 illustrate the cracking patterns seen during the static test conducted on the cantilever with GFRP reinforcement.

Figure 4-50: Photograph illustrating top and bottom crack patterns for the cantilever section with steel reinforcement subjected to static monotonic loading

Figure 4-51: Photograph illustrating top and bottom crack patterns for the cantilever section with GFRP reinforcement subjected to static monotonic loading

4.3.2 Static Load versus Crack Widths

During the test on the cantilever with steel reinforcement, the load was removed at 300 kN in order to relocate one of the pi gauges on the top surface of the cantilever that was measuring the longitudinal cracks described in the previous section, and a second time to place the pi gauge on the underside of the cantilever to monitor crack widths. There may be some small error in the total crack width due to the placing the pi gauges over the respective cracks. Also, it is more difficult to exactly determine at what particular load the cracks developed. At the ultimate load of 772 kN, the longitudinal cracks over the girder were recorded to be 0.64 mm and 1.05 mm in width (Figure 4-52). The transverse crack on the underside of the cantilever under the loading plate was measured to be a maximum of 0.65 mm in width at the ultimate load (Figure 4-53).

Fortunately, pi gauges used to measure crack widths on the cantilever section with GFRP were placed in appropriate locations to capture cracks as they developed with respect to applied load. The first crack that was captured was the transverse crack on the underside of the cantilever, which was initiated at an approximate load of 110 kN and increased to a maximum crack width of 2.85 mm just prior to failure (Figure 4-54). The pi gauges located over the girder indicated that one of the cracks over the girder developed at approximately 430 kN and grew to a maximum width of 0.98 mm at the ultimate load of 487 kN (Figure 4-55). The second longitudinal crack over the girder, based on the load verses crack width curve, most likely occurred at approximately 240 kN.

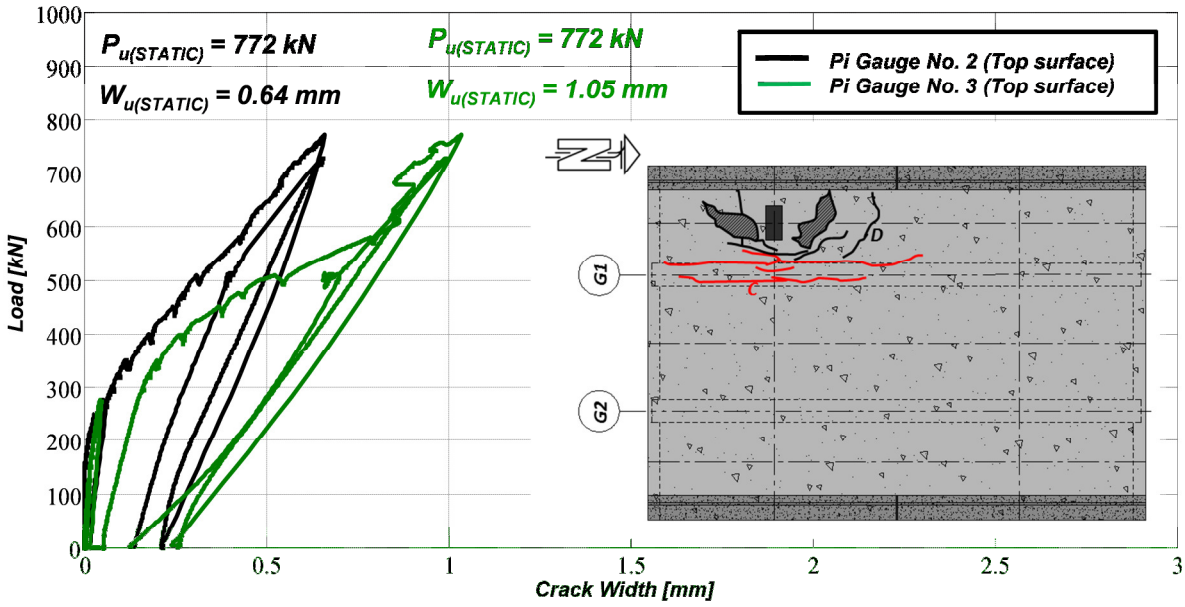

Figure 4-52: Plot of load versus underside transverse crack width for the cantilever section with steel reinforcement subjected to static monotonic loading

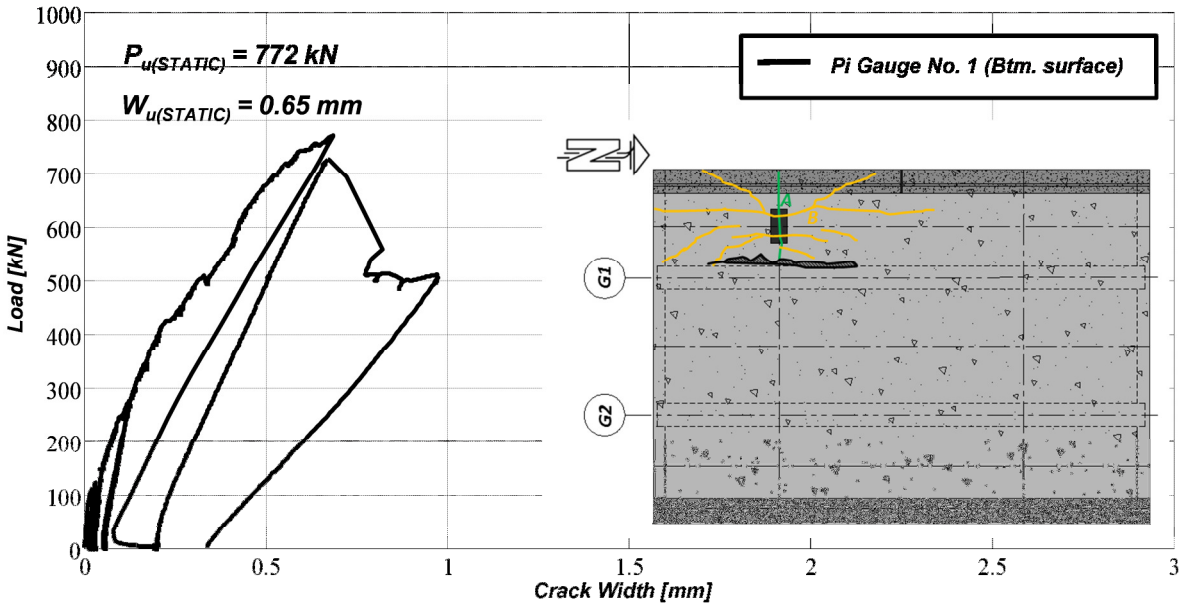

Figure 4-53: Plot of load versus top longitudinal crack widths for the cantilever section with steel reinforcement subjected to static monotonic loading

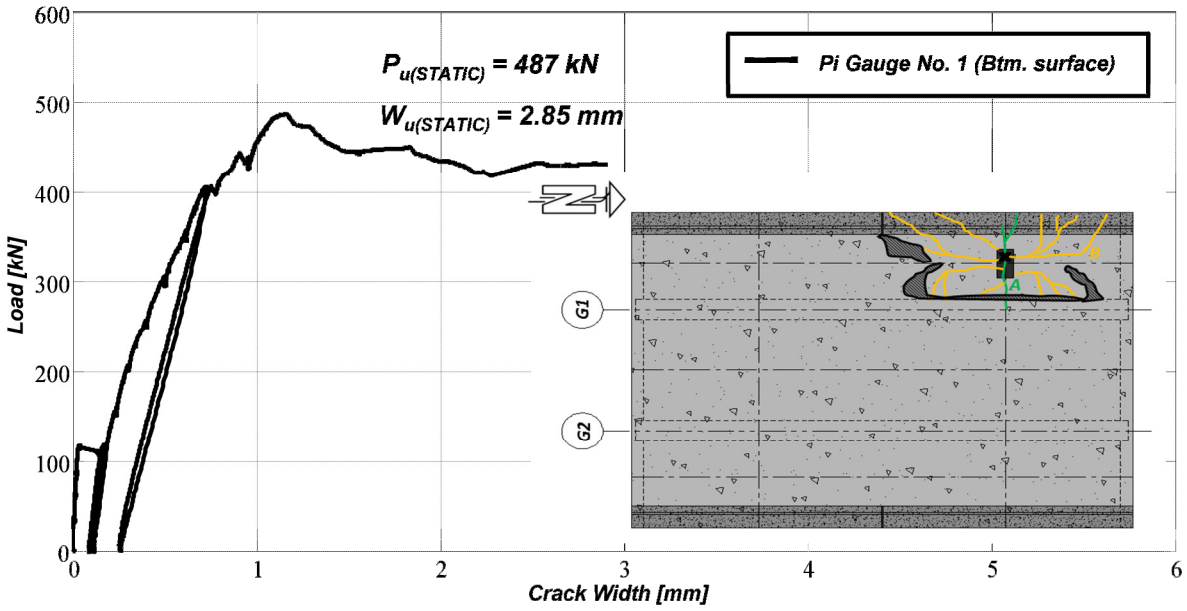

Figure 4-54: Plot of load versus underside transverse crack width for the cantilever section with GFRP reinforcement subjected to static monotonic loading

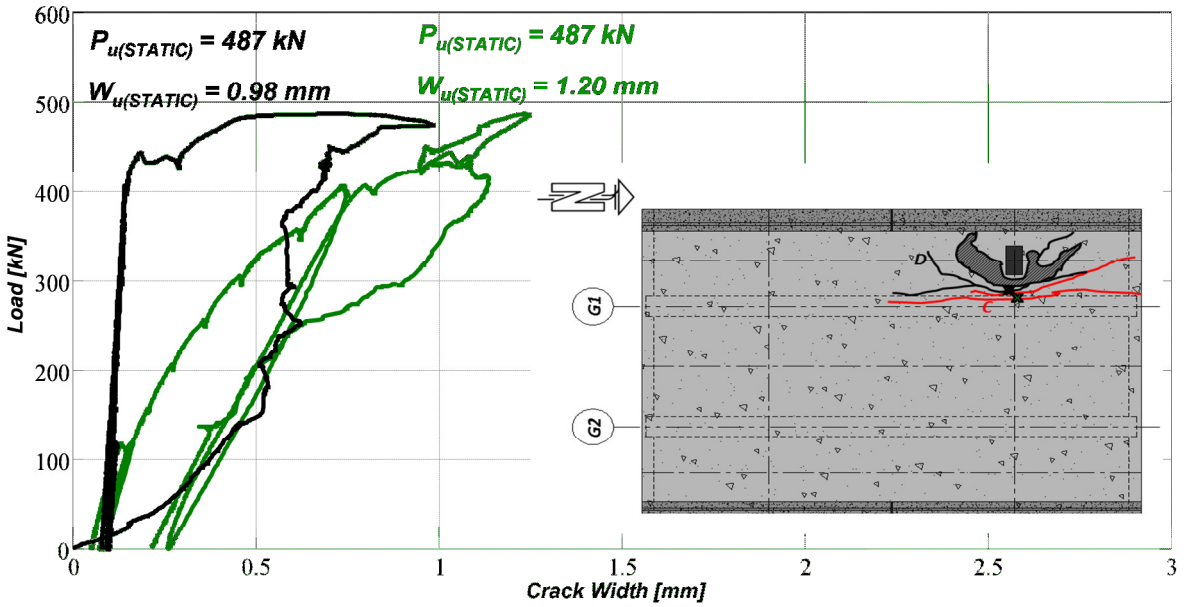

Figure 4-55: Plot of load versus top longitudinal crack widths for the cantilever section with GFRP reinforcement subjected to static monotonic loading

4.3.3 Crack Mapping under Fatigue Loads

The fatigue testing of both cantilever sections revealed the same four types of cracks, all similar in pattern and location to the cracks observed from the static testing carried out earlier. The first cracks to appear were the transverse cracks below the loading plate on the underside of the cantilever slab. Like the static tests conducted earlier, these cracks were visible between loads of 115 and 130 kN and are labeled as crack type "A" (Figure 4-56 and 4-57). Radial cracks, labelled type "B", originating from the underside of the slab below the loading plate were the second cracks observed during the first cycle of the fatigue tests. The transverse crack and radial cracks were the types of cracks that grew in width throughout the loading history and will be discussed in the following sections. Longitudinal cracks over the girder were the third crack to appear and are labelled type "C" in Figure 4-56 and 4-57. The fourth type of crack to develop, identified as crack type "D", were circumferential cracks that created a semi-circular pattern around the loading plate and many of these cracks did not develop until later on in the loading history (Figures 4-56 through 4-57). The circumferential cracks did not exhibit a semi-circle as tight to the loading plate as those seen in the static tests. Top and bottom photographs of the cracks observed during the fatigue test conducted on the cantilever with steel reinforcement are shown in Figure 4-58. The photographs in Figure 4-59 illustrate the cracking patterns seen during the fatigue cyclic test conducted on the cantilever with GFRP reinforcement.

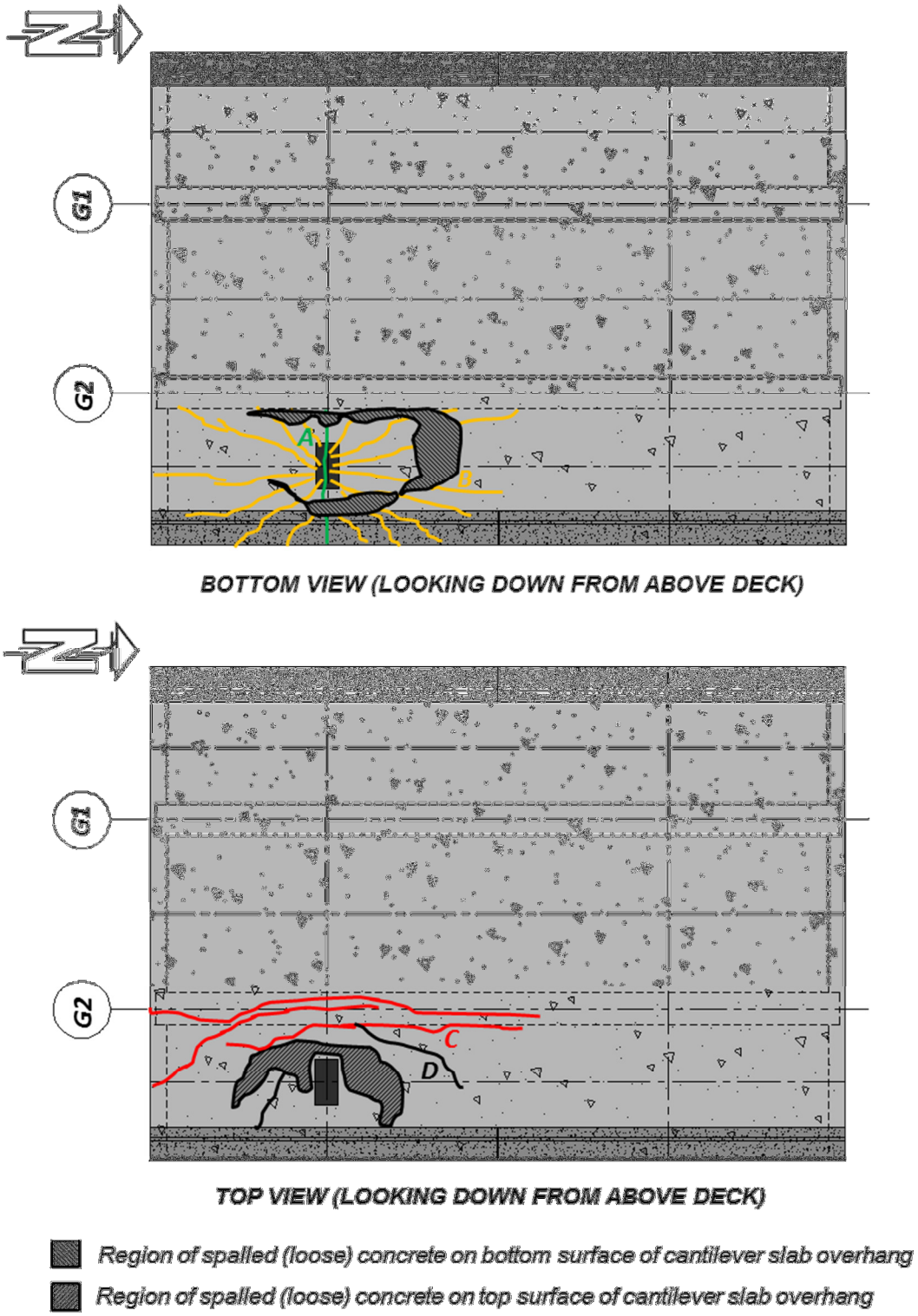

Figure 4-56: Crack patterns for the cantilever section with steel reinforcement subjected to fatigue cyclic loading

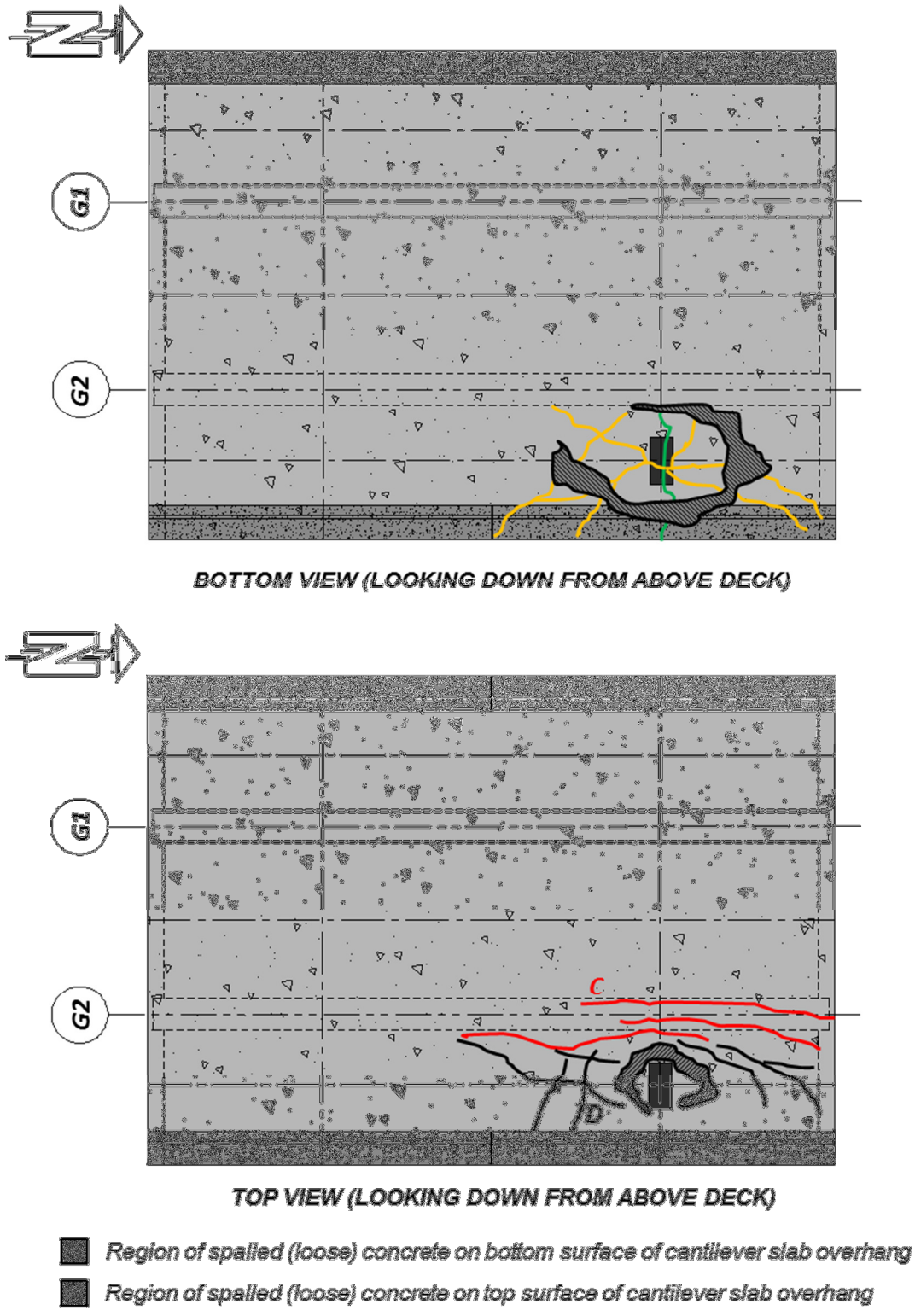

Figure 4-57: Crack patterns for the cantilever section with GFRP reinforcement subjected to fatigue cyclic loading

Figure 4-58: Photograph illustrating top and bottom crack patterns for the cantilever section with steel reinforcement subjected to fatigue cyclic loading

Figure 4-59: Photograph illustrating top and bottom crack patterns for the cantilever section with GFRP reinforcement subjected to fatigue cyclic loading

4.3.4 Fatigue Load versus Crack Widths

At the ultimate load crack widths of 0.64 and 1.05 mm were measured over the girder center-line for the cantilever section with steel reinforcement under static monotonic loading conditions. The crack widths observed over the girder after completing the first cycle were less than 0.10 mm and 0.20 mm. Pi gauge No. 2 showed that the longitudinal crack underneath it did not grow until failure. It increased slightly and then decreased towards the end of the fatigue life of the slab overhang (Figure 4-60(a)). The crack located under pi gauge No. 3 grew until reaching approximately 0.40 mm in width, but did not achieve crack widths observed during the static test conducted previously (Figure 4-60(b)). The transverse crack on the underside of the cantilever slab overhang proved to be the best indicator of damage and the approaching fatigue failure. The crack width after the first cycle measured about 0.10 mm and it continued to grow in width until failure. At the onset of the fatigue failure, the transverse crack on the underside of the slab overhang below the loading plate surpassed the width observed during the static test and was measured to be approximately 5.00 mm in width (Figure 4-60(c)). The crack grew to a width of almost 10.00 mm during the final cycles as the cantilever slab overhang could no longer susntain the applied load of 480 kN.

At the ultimate load longitudinal crack widths measured over the girder for the cantilever section with GFRP reinforcement were 0.98 and 1.20 mm (Figures 4-61(a) and 4-61(b)). The crack widths measured over the girder after completing the first cycle were recorded to be 0.20 and 0.60 mm. Both of the cracks widths grew throughout the following 2,000,000

cycles to reach approximately 0.50 and 1.00 mm. However, they did not reach the maximum static crack widths observed during the static tests. Upon conducting a static monotonic test to failure, the two longitudinal cracks increased in width and had crack widths of 1.30 and 1.54 mm at the ultimate load of 513 kN. As was the case with the cantilever with steel reinforcement, the transverse crack on the underside of the cantilever below the applied fatigue load proved to measure the largest in width, proving to be the best measure of damage in the slab overhang. It measured approximately 0.85 mm in width after the first cycle (Figure 4-60(c)). However, it did not increase in width during the 2,000,000 cycles. It grew to a maximum width of 3.70 mm measured at the ultimate load of 513 kN during the static test to failure after completing 2,000,000 cycles at the applied fatigue cyclic load of 305 kN.

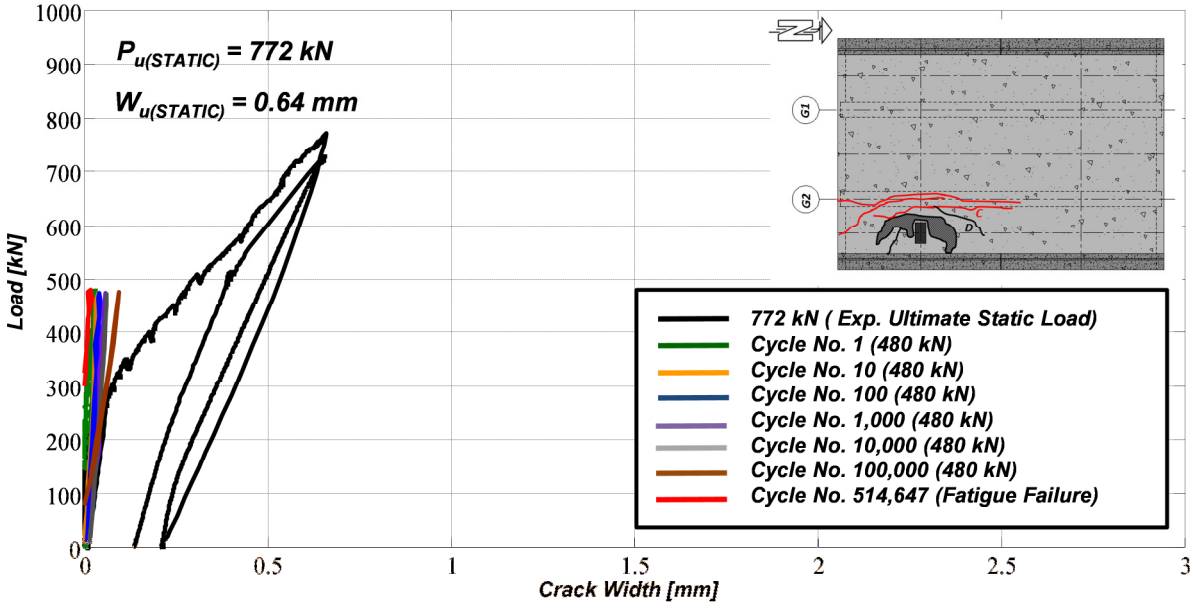

Figure 4-60(a): Plot of load versus crack width for a longitudinal crack located on the top of the deck over the girder for the cantilever section with steel reinforcement subjected to fatigue cyclic loading (Pi Gauge No. 2)

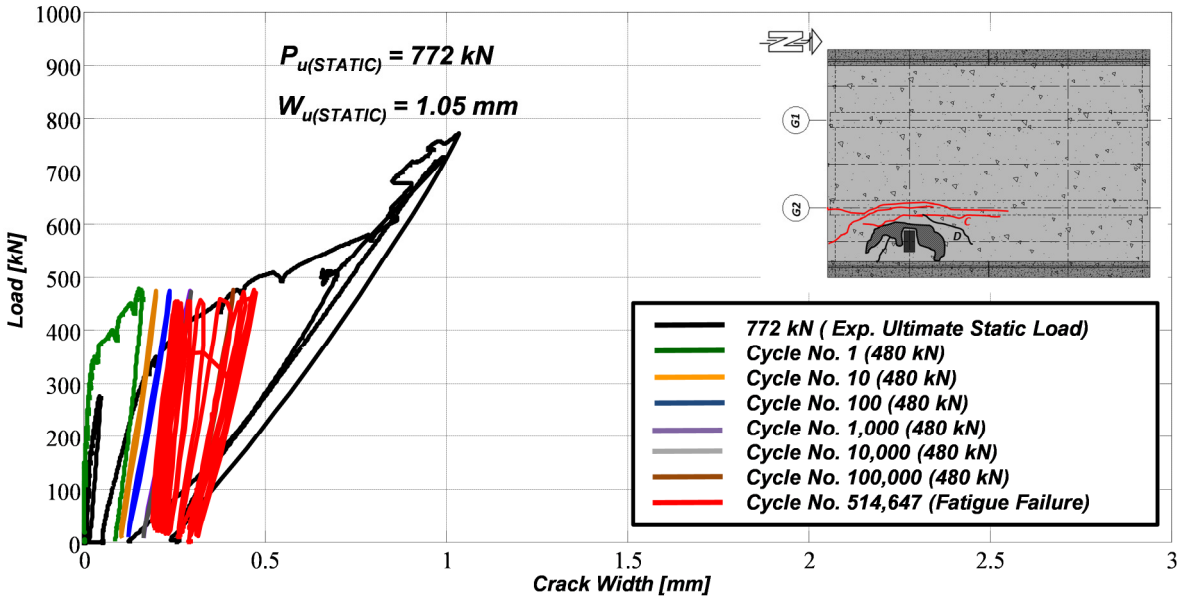

Figure 4-60(b): Plot of load versus crack width for a longitudinal crack located on the top of the deck over the girder for the cantilever section with steel reinforcement subjected to fatigue cyclic loading (Pi Gauge No. 3)

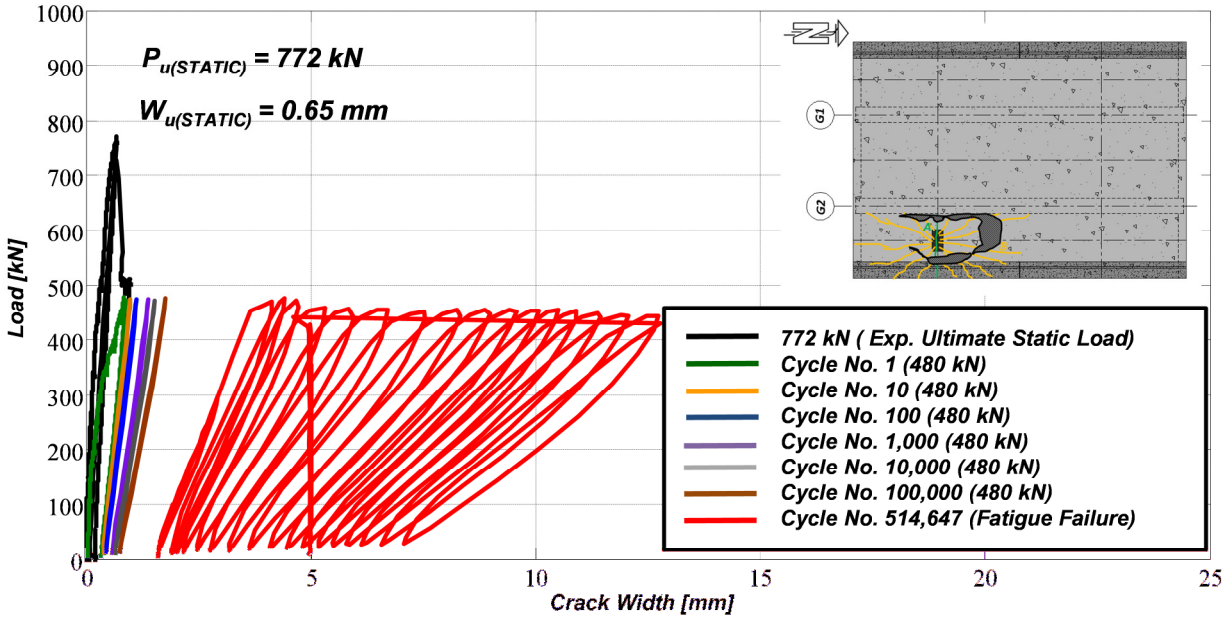

Figure 4-60(c): Plot of load versus crack width for the transverse crack located on the underside of the cantilever below the load plate for the cantilever section with steel reinforcement subjected to fatigue cyclic loading (Pi Gauge No. 1)

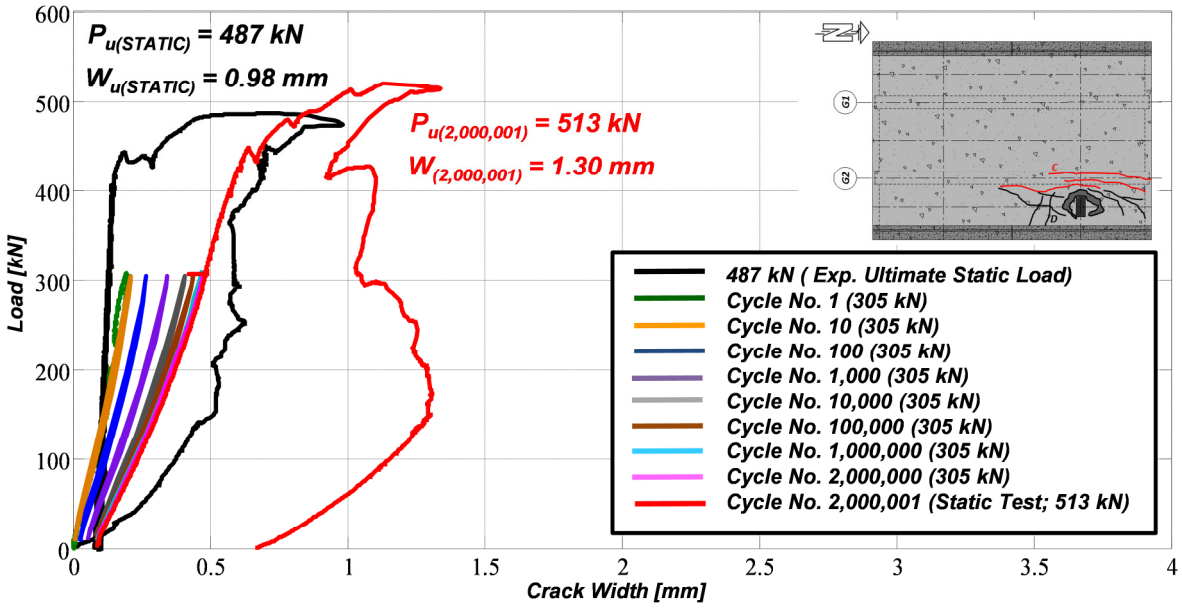

Figure 4-61(a): Plot of load versus crack width for a longitudinal crack located on the top of the deck over the girder for the cantilever section with GFRP reinforcement subjected to fatigue cyclic loading

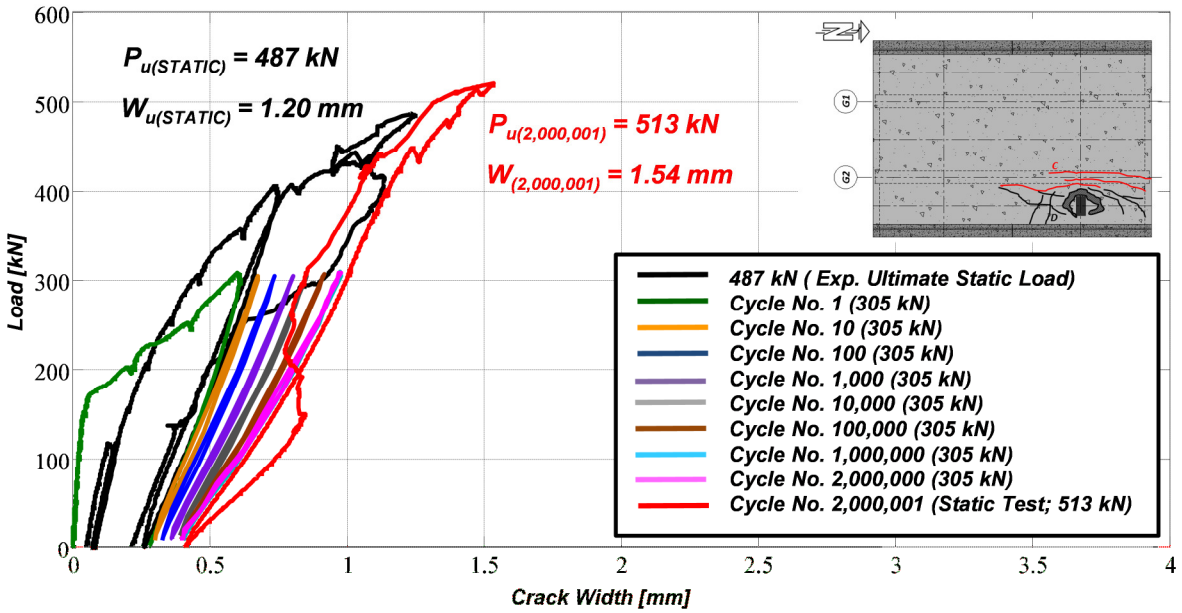

Figure 4-61(b): Plot of load versus crack width for a longitudinal crack located on the top of the deck over the girder for the cantilever section with GFRP reinforcement subjected to fatigue cyclic loading

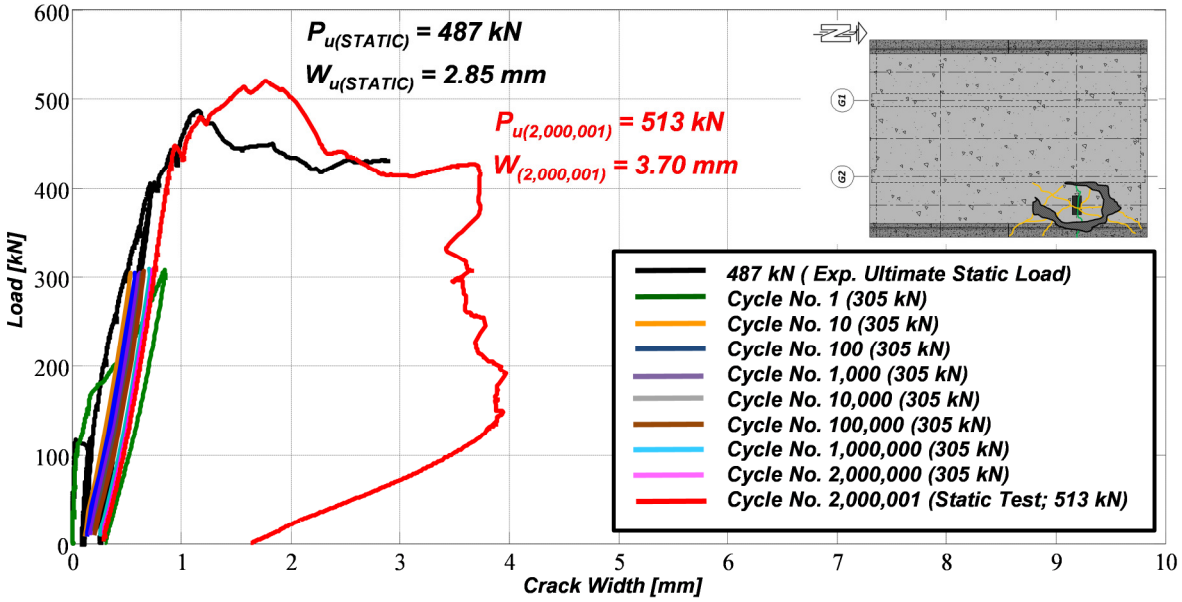

Figure 4-61(c): Plot of load versus crack width for the transverse crack located on the underside of the cantilever below the load plate for cantilever section with GFRP reinforcement subjected to fatigue cyclic loading

4.3.5 Fatigue Crack Widths versus Number of Cycles

The crack widths measured can be divided into two different components. The first component is called the absolute or maximum crack width and the second component is called the cumulative crack width. Absolute or maximum crack width for the purposes of this study is the width of a crack at any given cycle corresponding to maximum magnitude of applied load. Cumulative crack width is defined as the permanent non-recoverable crack width under any given number of applied load cycles.

An important point to note is that longitudinal cracks over the girder did not grow as much as transverse cracks on the underside of the cantilever slab overhang. It is demonstrated by the

crack widths plotted against the number of cycles required to cause failure of the cantilever sections.

The cracks over the girder for the cantilever with steel reinforcement did not increase significantly over the fatigue cycles. The maximum crack widths recorded by the pi gauges over the girder were 0.40 and 0.10 mm (Figure 4-62). However, the transverse crack on the underside of the cantilever slab overhang had steady or constant increase over the first 300,000 cycles increasing from approximately 1.00 mm to 2.00 mm when plotted on a log scale. The crack width increased from 2.00 mm to approximately 5.00 mm over the final 214,647 cycles as the cantilever section with steel reinforcement failed in punching shear caused by the fatigue cyclic loading (Figure 4-62).

Figure 4-63 indicates that the longitudinal cracks over the girder for the cantilever section with steel reinforcement had significant cumulative crack width due to the applied fatigue cyclic load throughout the 514,647 cycles prior to failure. The cracks remained fairly constant with an ultimate cumulative crack width of 0.33 mm and 0.10 mm. The transverse crack on the underside of the slab overhang showed a continuous increase in cumulative or permanent width before sharply opening up in the last 214,647 cycles as the cantilever started to fatigue, eventually failing with an ultimate crack width of 6.75 mm.

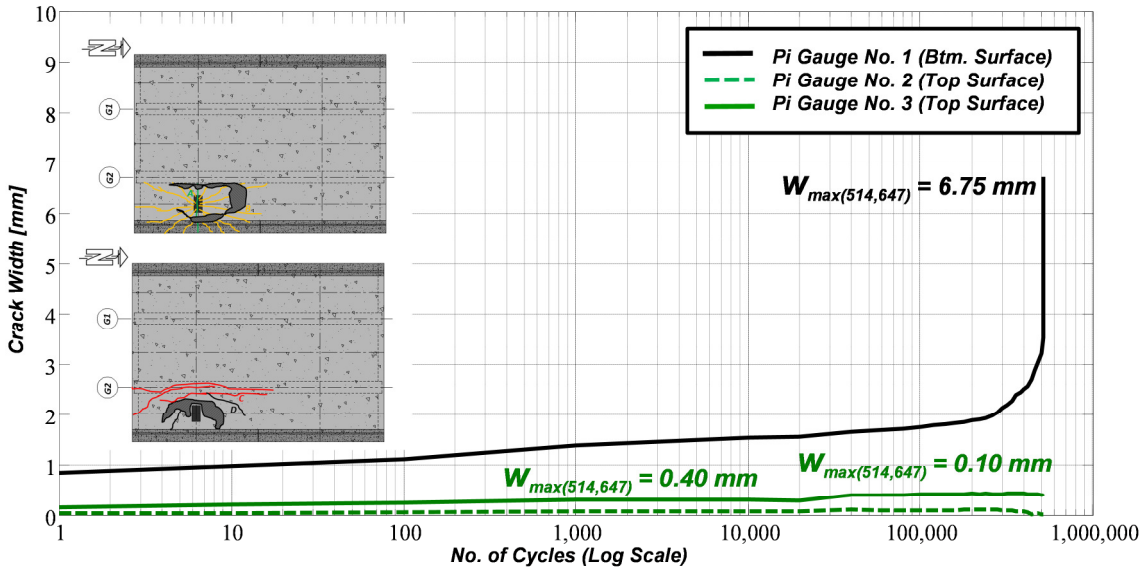

Figure 4-62: Plot of maximum crack width versus number of cycles for the cantilever section with steel reinforcement subjected to fatigue cyclic loading

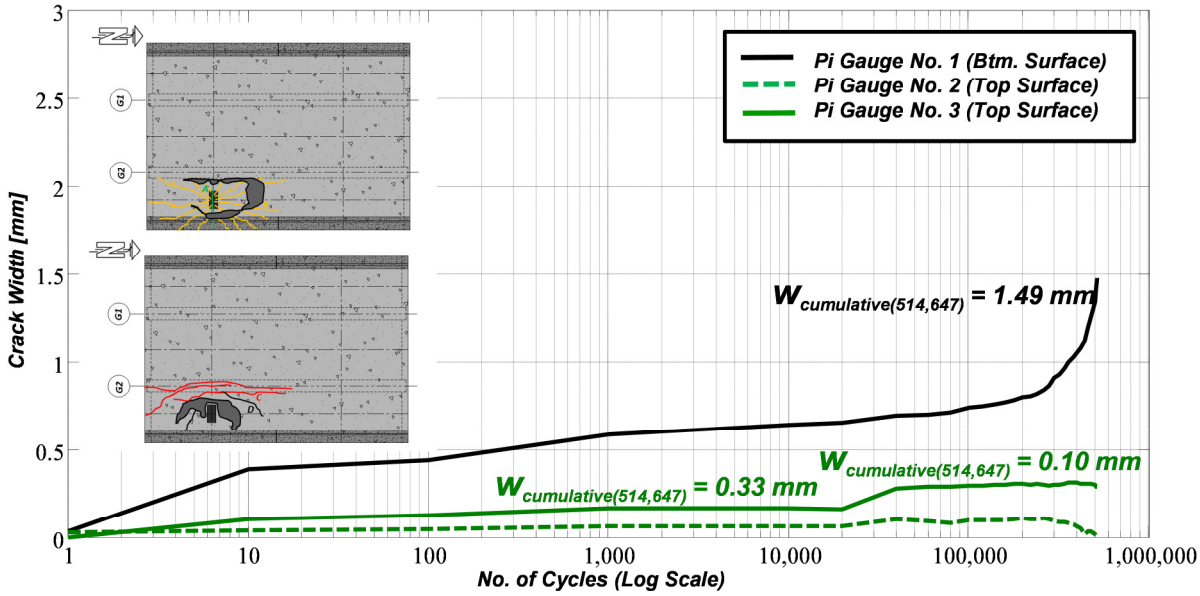

Figure 4-63: Plot of cumulative crack width versus number of cycles for the cantilever section with steel reinforcement subjected to fatigue cyclic loading

The cantilever section with GFRP reinforcement did not fail under the average applied fatigue cyclic load of 305 kN. The top longitudinal crack widths over the girder as well as the transverse underside crack width are plotted against the number of load cycles in Figure 4-64. The longitudinal cracks over the girder, like the previous fatigue test, did not grow significantly in width throughout the 2,000,000 cycles before the test was stopped. They displayed minor growth from 0.00 to 0.50 mm and 0.5 to 0.79 mm during the 2,000,000 cycles. The transverse crack on the underside of the cantilever with GFRP increased steadily from about 0.50 mm to 1.00 mm during the applied fatigue cycle load. The cumulative longitudinal crack widths measured 0.10 and 0.33 mm over the girder. The cumulative transverse crack width on the underside of the cantilever slab overhang had a width of 0.45 mm (Figure 4-65).

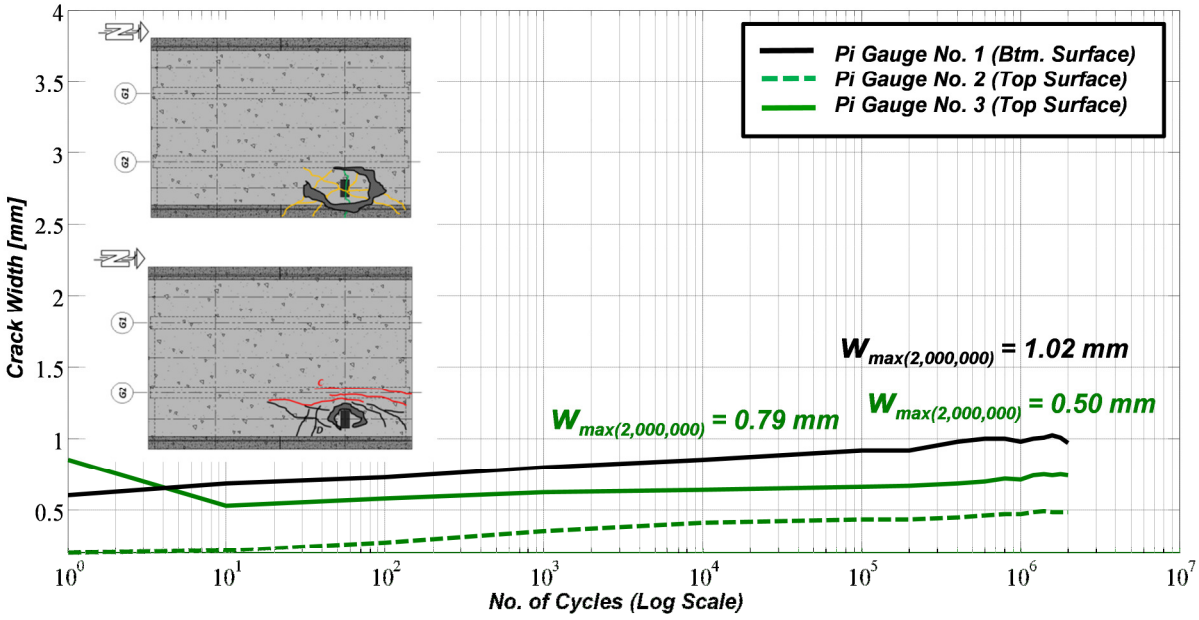

Figure 4-64: Plot of maximum crack width versus number of cycles for the cantilever section with GFRP reinforcement subjected to fatigue cyclic loading

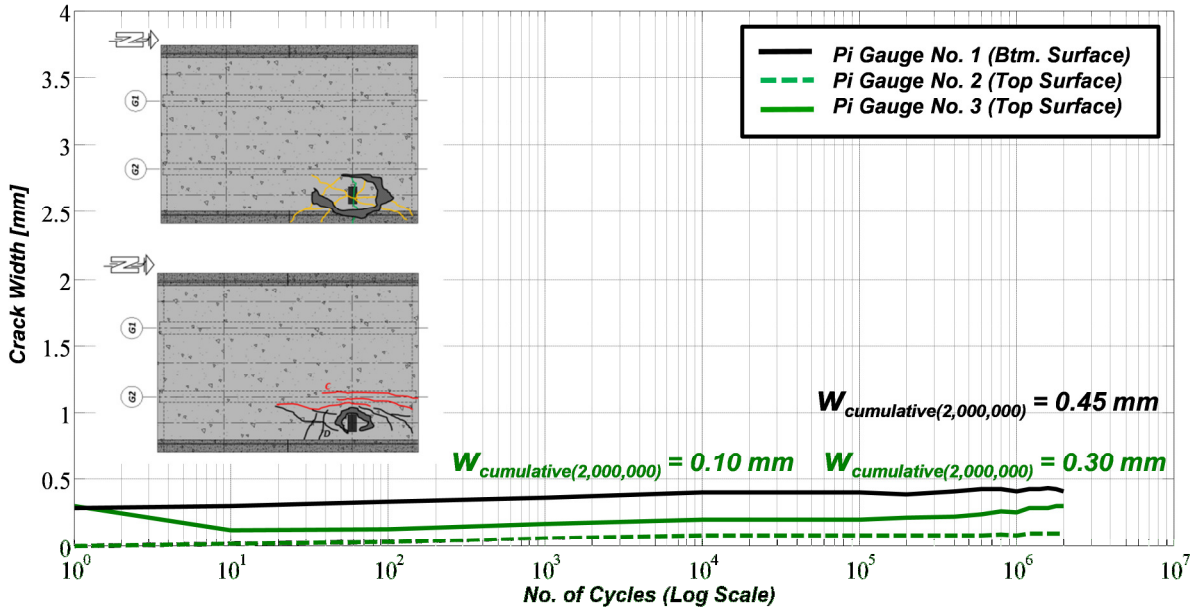

Figure 4-65: Plot of maximum crack width versus number of cycles for the cantilever section with GFRP reinforcement subjected to fatigue cyclic loading

Plots of the crack widths, described above, versus the number of completed cycles further reinforces the contention that arching action is present in edge-stiffened cantilever slab overhangs. The cracks over the girder for both cantilever sections subjected to fatigue cyclic loading gre in width slightly as the cantilevers were subjected to loads at approximately 62.0 % of their respective ultimate static loads. The transverse crack on the underside of the cantilever section with steel reinforcement located below the loading plate proved to be the best indicator of damage due to fatigue. It appeared after the first cycle and continued to grow before rapidly increasing in width to an almost identical width that was observed during the static tests just prior to failure.

4.4 Modes of Failure under Static Loads

Both cantilever sections failed in a punching shear type mode similar to that of an internal panel of a bridge deck slab. On the underside of the cantilever slab, the shape of the punch cone was semi-circular and not clearly defined in all directions. On the top of the cantilever slab, the punch cone was not as well defined as in an internal panel.

Static failure of the cantilever reinforced GFRP occurred at a static ultimate load of 487 kN. A punch angle could be measured in three directions relative to the transverses and longitudinal center lines of the applied load. The punch angle in the east direction along the transverse center line of the loading plate was determined to be approximately 32°. The punch angles along the longitudinal center line of the applied load in north and south directions were measured to be 9° and 12° respectively. Top and bottom views of the failure are shown in Figure 4-66. Figure 4-67 is a photograph taken during the demolition of the bridge deck slab and clearly shows the diagonal shear cracks representative of a typical punching shear type failure.

The cantilever with steel reinforcement failed a static ultimate load of 772 kN. Unfortunately, the punch cone was not as pronounced as it was for the cantilever with GFRP reinforcement. The punch angle could only be physically measured in the east direction along the transverse center line of the applied load and it was measured to be 33°. Figure 4-68 shows the top and bottom views of the punch cone and Figure 4-69 shows the diagonal shear cracks typical to punching shear types of failure.

Figure 4-66: Top and bottom views of punching shear type failure for the cantilever section with GFRP reinforcement subjected to a static monotonic load

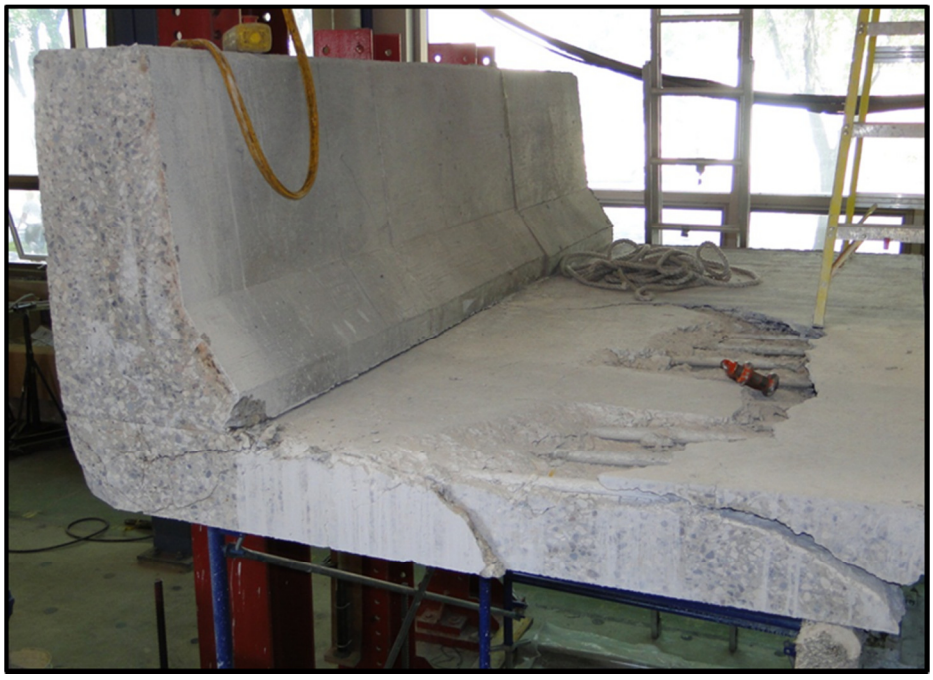

Figure 4-67: Photograph taken during demolition illustrating diagonal shear cracks representative of punching shear failure for the cantilever with GFRP reinforcement subjected to a static monotonic load

TOP OF SLAB *BOTTOM OF SLAB*

Figure 4-68: Top and bottom views of punching shear type failure for the cantilever section with steel reinforcement subjected to a static monotonic load

Figure 4-69: Photograph taken during demolition illustrating diagonal shear cracks representative of punching shear failure for the cantilever with steel reinforcement subjected to a static monotonic load

4.5 Modes of Failure under Fatigue Loads

The cantilever with steel reinforcement was the first cantilever section to be tested under fatigue cyclic loading. It failed after completing 514,647 cycles at an average applied fatigue load of 480 kN or 62.2 % of the static ultimate load of 772 kN achieved during the static test. The amount of damage was quite excessive when compared to the damage during the static test conducted on the opposite cantilever. Concrete spalling on the top surface of the cantilever was significantly greater than the quantity observed from the static test (Figure 4-70). The semi-circular punch cone on the top surface of the cantilever with steel reinforcement was larger compared to the static test. The angle of the diagonal shear cracks could only be measured in the north and west directions along the longitudinal and transverse center lines of the applied load respectively (Figure 4-71). The punch angle along the longitudinal center line of the loading plate in the north direction was 9°. The punch angle in the transverse direction towards the west direction was measured to be 27°. The observed amount of internal damage compared to the static test conducted previously was very large. Several top transverse steel bars located below the loading plate were ruptured as a result of the fatigue failure (Figure 4-72). Three of the bottom transverse steel bars were also ruptured as a result of the fatigue loading conditions (Figure 4-73).

The cantilever section with GFRP reinforcement at the opposite end of the bridge deck did not fail after achieving 2,000,000 cycles while subjected to the average applied fatigue cyclic load of 305 kN, which was 62.6 % of the ultimate static load observed earlier. A static monotonic test was conducted and the cantilever with GFRP reinforcement exhibited a

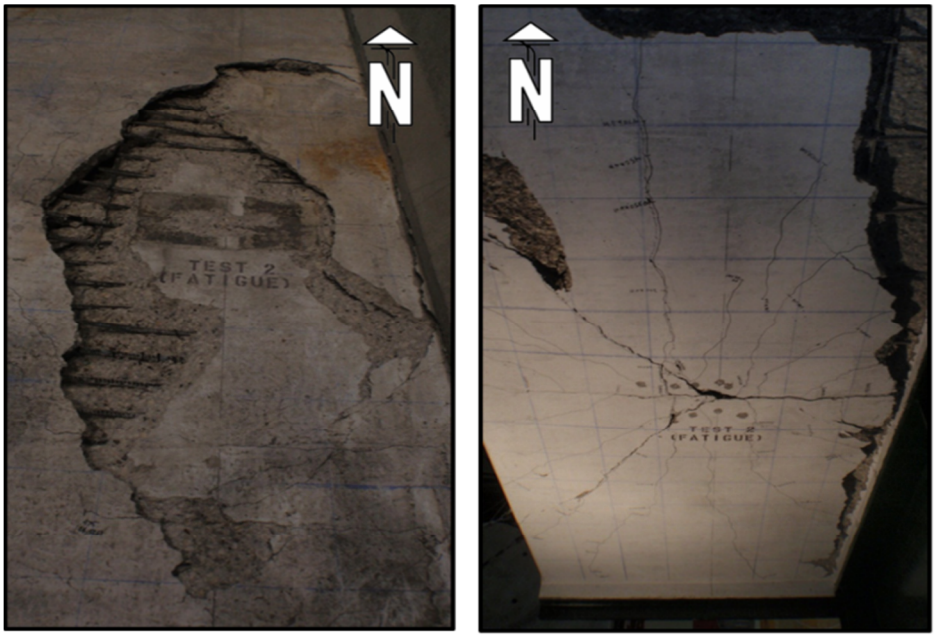

Figure 4-70: Photographs of the top and bottom views of punching shear type failure for the cantilever section with steel reinforcement subjected to a fatigue cyclic load

Figure 4-71: Photograph taken during demolition illustrating diagonal shear cracks and punch cone representative of punching shear failure for the cantilever with steel reinforcement subjected to a fatigue cyclic load

Figure 4-72: Photograph illustrating the rupture of the top transverse steel reinforcement for the cantilever with steel reinforcement subjected to a fatigue cyclic load

Figure 4-73: Photograph illustrating the rupture of the bottom transverse steel reinforcement for the cantilever with steel reinforcement subjected to a fatigue cyclic load

punching shear failure at the ultimate of 520 kN. The damage compared to the static test was much greater due to the fatigue loading conditions.

The punch cone was much more evident and pronounced compared the static test originally conducted on the opposite cantilever with GFRP reinforcement. In fact, one could say that the punch cone was experimentally identical to the one that would occur in an internal of a bridge deck slab (Figure 4-74). No rupture of the top transverse GFRP was noticed upon inspection (Figure 4-75).

TOP OF SLAB ***BOTTOM OF SLAB***

Figure 4-74: Photographs illustrating the top and bottom view of the pronounced punch cone for the cantilever with GFRP reinforcement

Three of the bottom transverse GFRP bars in the vicinity of the loading plate were ruptured (Figure 4-76). Punch angles along the transverse and longitudinal center lines of the applied load were measured. The punch angles along the longitudinal center line of the loading plate

in the north and south directions were determined and measured about 19° and 21° respectively (Figure 4-77). The punch angles in the transverse direction were calculated to be 51 ° in the east direction (towards the barrier wall) and 29° in the west direction (towards the girder).

Figure 4-75: Photograph illustrating the top view of the pronounced punch cone for the cantilever with GFRP reinforcement (no rupture of top transverse GFRP reinforcing bars)

Figure 4-76: Photographs illustrating the rupture of the bottom transverse GFRP reinforcement for the cantilever with GFRP reinforcement subjected to a fatigue cyclic load

A photograph illustrating all of the punching shear failures for the static and fatigue testing destructive testing of all cantilever sections is shown in Figure 4-78.

Figure 4-77: Photograph taken during demolition illustrating diagonal shear cracks and punch cone representative of punching shear failure for the cantilever with GFRP reinforcement subjected to a fatigue cyclic load

Figure 4-78: Photograph of the entire experimental bridge deck slab illustrating punching shear failures of the cantilever sections

5. ANALYTICAL MODELS

The chapter begins with a brief discussion and flexural analysis of the cantilever sections. It also outlines the various analytical tools that were used to model the deflections, strains, and cracking patterns under static loads. Modeling the fatigue performance of the cantilever sections included an analytical relationship for predicting the number of cycles required to fail a cantilever with edge stiffening by a traffic barrier wall subjected to a wheel load.

5.1 Flexural Analysis of the Cantilever Sections

The response or structural behaviour of cantilever slab overhangs of bridge decks subjected to loads is currently understood by engineers to be a purely flexural behaviour. These flexural effects are not limited strictly to the overhanging cantilevers, but also extend into the internal panel of bridge deck slabs (Mufti et al., 1996). This section presents the argument that the behaviour of a bridge deck cantilever slab overhang subjected to a wheel load or concentrated load *is not* purely flexural.

5.1.1 Analytical Model for Determining the Flexural Capacity of the Bridge Deck Cantilever Slab Overhangs

A computer program, ***M_r Moment Capacity*** (Tadros, 2003), was written to determine the moment capacity of reinforced concrete members and was used to determine the un-factored moment resistance for each of the cantilever sections. The program was written using the visual basic programming language and provides users with a windows type interface. The program is comprised of two major components consisting of an input screen and an output

screen. The user can input various engineering parameters such as units of measurement, dimensions of a particular cross-section, appropriate design factors, and materials properties and data pertaining to the type and quantity of reinforcement (Figure 5-1(a)).

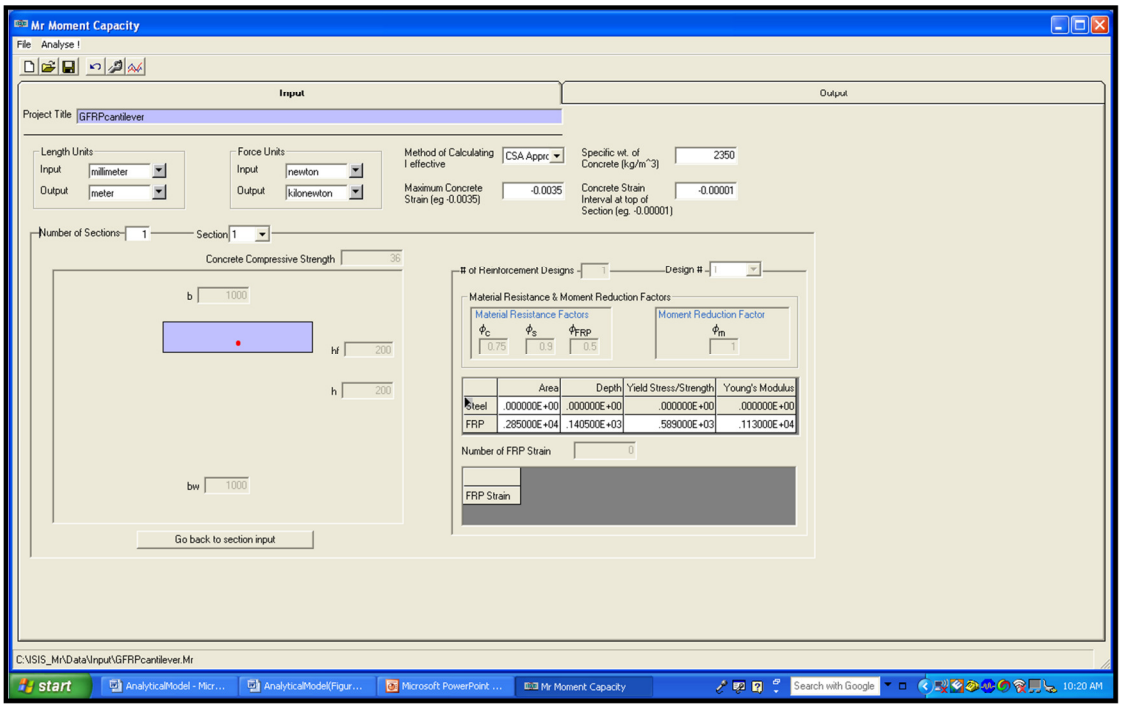

Figure 5-1(a): Screen shot of the input component of the ***M_r Moment Capacity*** program for determining the flexural moment capacity of the cantilever sections

The output component of the program provides the user with several different types of information depending on what the user specified in the input file. The program can also provide the user with the factored and un-factored moment capacity at various cross-sections along the flexural member. Analysis is based on a strain compatibility approach and the output is presented in the form of various plots including moment resistance versus concrete strain, moment resistance versus reinforcement strain, moment resistance versus neutral axis

depth, moment resistance versus curvature, and moment resistance versus effective moment of inertia (Figure 5-1(b)).

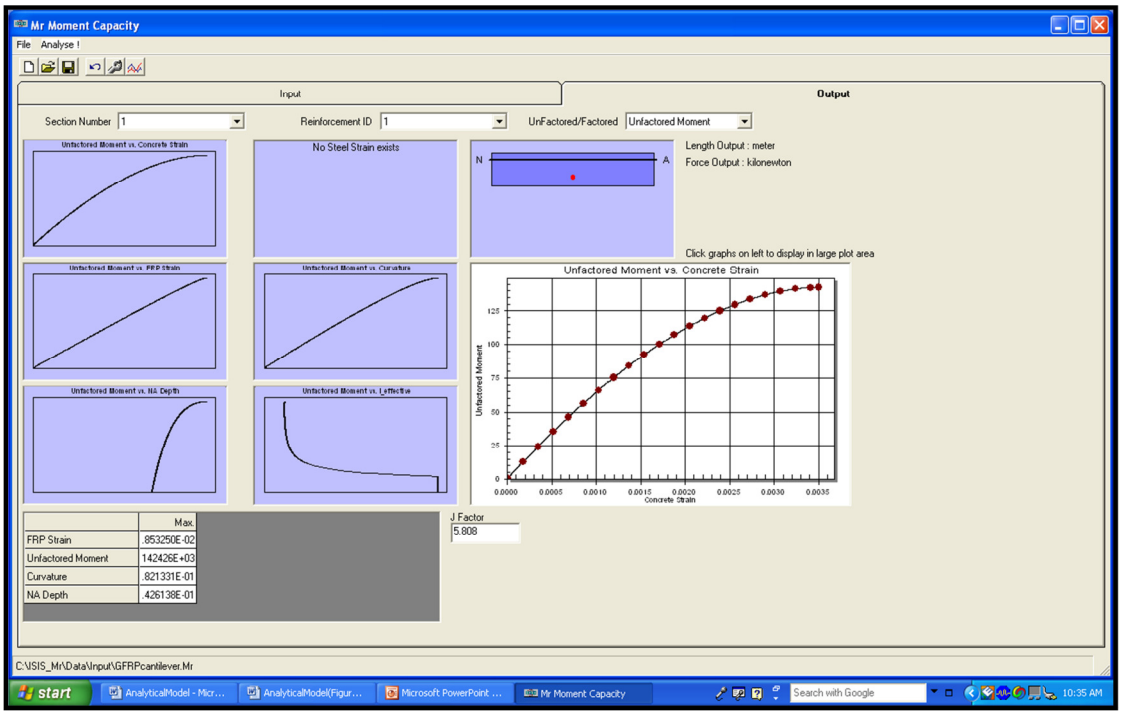

Figure 5-1(b): Screen shot of the output component of the ***M_r Moment Capacity*** program for determining the flexural moment capacity of the cantilever sections

5.1.2 Flexural Moment Resistance/Capacity of the Cantilever Sections

The ultimate un-factored moment capacity for a 1000 mm wide section of the cantilever section reinforced with steel reinforcement was determined to be 111.0 kN*m/m. The ultimate un-factored moment for the cantilever with GFRP reinforcement was established to be 124.0 kN*m/m (Figure 5-2(a)). Both cantilever sections also had corresponding strains in the concrete of 3500 με at failure. Figure 5-2(b) shows plots of the un-factored moment

resistance versus reinforcing bar strain for both of the cantilever sections. For a 1000 mm wide section of the cantilevers, flexural behaviour illustrates that the cantilever with steel was under-reinforced because the steel yielded prior to concrete crushing. On the other hand, the cantilever section with GFRP reinforcement was over-reinforced because the section exhibits concrete crushing prior to rupture of the reinforcement which would occur when the GFRP reinforcement achieves its ultimate strain of 14,050 με. It should be noted that all of the output generated from the ***M_r Moment Capacity*** program was checked using hand calculations to verify the output.

The experimental results indicated that the cantilever sections reinforced with steel and GFRP failed at the ultimate static loads of 772 and 487 kN respectively when they were subjected to a simulated wheel load. It is necessary at this point to make the following argument:

> *If the behaviour of the two edge-stiffened cantilever sections was completely and purely flexural, it is obvious that the ultimate load of the two cantilever sections reinforced with top steel and GFRP should have failed at approximately identical ultimate loads. The cantilever with GFRP had a nominal moment capacity of 124 kN*m/m and the cantilever with steel reinforcement had a nominal moment capacity of 111.0 kN*m/m Therefore, the cantilever with GFRP had 11.7 % greater nominal moment capacity than the cantilever section with steel. However, the experimental ultimate static loads indicated the cantilever with steel reinforcement achieved an ultimate load of 772 kN compared to 487 kN obtained by the cantilever*

section with GFRP. Thus, a cantilever section with an 11.7 % lower theoretical nominal moment capacity achieved a 58.5 % higher experimental ultimate load. The major difference in the observed ultimate static loads can be attributed to the significant difference in bottom transverse and longitudinal reinforcement which is discussed and confirmed in the following sections. The argument presented is that the behaviour of the edge-stiffened cantilever slab overhang, when subjected to a wheel load, is not purely flexural. A significant component of arching action is present which could not be accounted for by flexural theory.

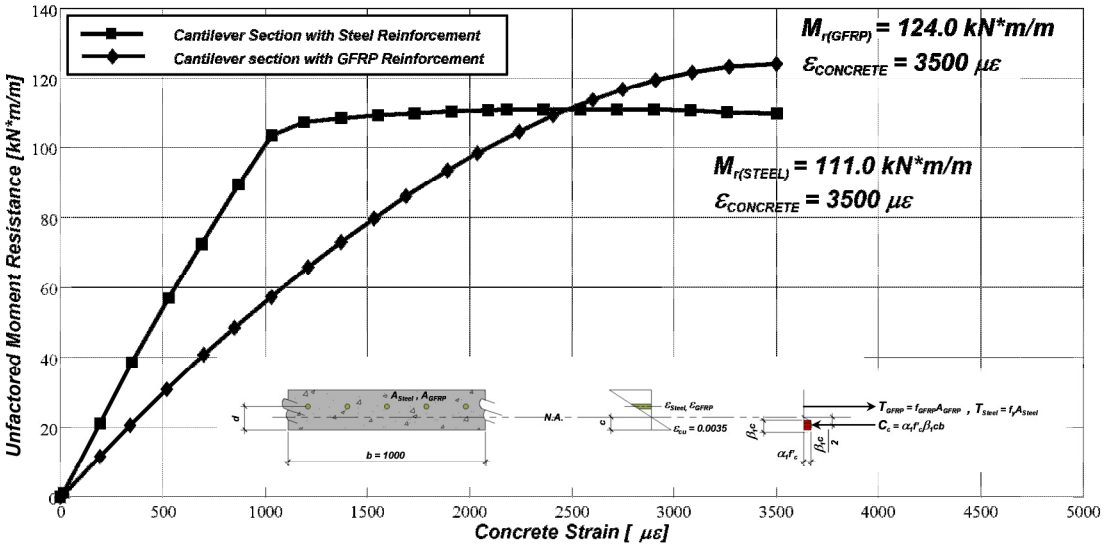

Figure 5-2(a): Plots of the un-factored moment resistance versus concrete strain for a 1000 mm wide section of the cantilever sections based on strain compatibility

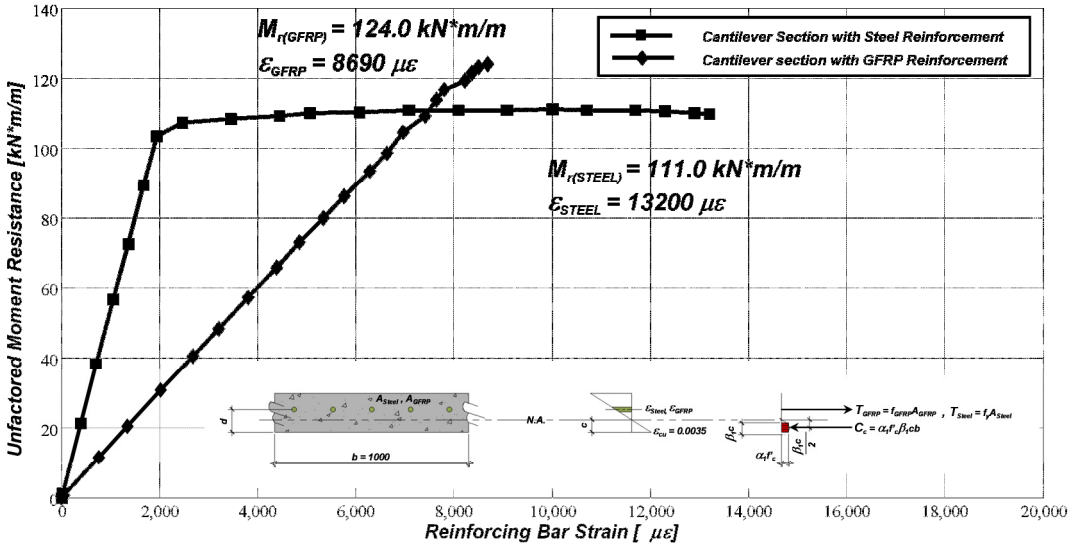

Figure 5-2(b): Plot of the un-factored moment resistance versus the reinforcing bar strain for a 1000 mm wide section of the cantilever sections based on strain compatibility

5.2 Analytical Modeling of the Behaviour of Bridge Deck Cantilever Slab Overhangs under Static Loads

Different analysis tools were required to model the theoretical behaviour of the cantilever sections under static loads. The following sub-sections discuss the models and results with respect to static deflections, top transverse reinforcing bar strains, and cracking patterns. A commercially available finite element analysis software, ***ATENA 3D*** (Cervenka et al., 2012), was used for modeling the theoretical static deflection behaviour and cracking patterns. A computer program, ***ANDECAS6*** (Mufti et. al, 2006), was used to determine the transverse negative bending moments due the concentrated or wheel load on the cantilever overhangs; this program is based on classical small deflection plate theory. Once classical flexural negative moment intensities were obtained using classical plate bending theory, strains based

on strain compatibility were determined using the computer program, ***M_r Moment Capacity*** (Tadros 2003), discussed in Section 5.1.1.

5.2.1 Analytical Model (ATENA 3D) for Determining Theoretical Deflections and Crack Patterns under Static Loads

The following sub-sections outline the specific details related to the finite element modeling of the experimental bridge deck cantilever slab overhangs. The details include geometry, concrete modeling, reinforcement modeling, and the concrete/reinforcement interaction.

5.2.1.1 Model Geometry and Boundary Conditions

The finite element model was constructed to represent the full size dimensions and structural details of the experimental bridge deck described in Chapter 3. A plan view illustrating the FEM discretization is shown in Figure 5-3(a) and a typical cross-section is illustrated in Figure 5-3(b). The black dots represent the co-ordinates input into the program to generate the two-dimensional cross-section of the model (Figure 5-3(c)). The cross-section was extruded to generate the 3-dimensional model shown in Figure 5-3(d). The mesh was generated automatically by ***ATENA 3D*** based on the input co-ordinates.

The bridge deck slab was comprised of 19,688 3-dimensional CCIso wedge elements (Figure 5-4). Each element had 15 nodes, resulting in a total of 295,320 nodes for the bridge deck slab. The barrier wall was assumed to have a perfect bond to the cantilever overhang slab and each barrier wall was comprised of 3,125 3-dimensional CCIso wedge elements.

Therefore, each barrier wall contained 50,000 nodes. The bridge deck slab was assumed to have a perfect bond to the steel supporting girders that were also automatically meshed by the program. Each girder consisted of 5,165 CCIso wedge elements, thus resulting in 77,475 nodes per girder. The girders were assumed to be fixed to the concrete blocks over their supported length (i.e. representative of the experimental deck due to the fact that the girders were post-tensioned to the blocks and the structural floor). The concrete supporting blocks were made up of 640 CCIso brick elements which each contained 20 nodes (Figure 5-5). Therefore, each concrete block contained 12,800 nodes.

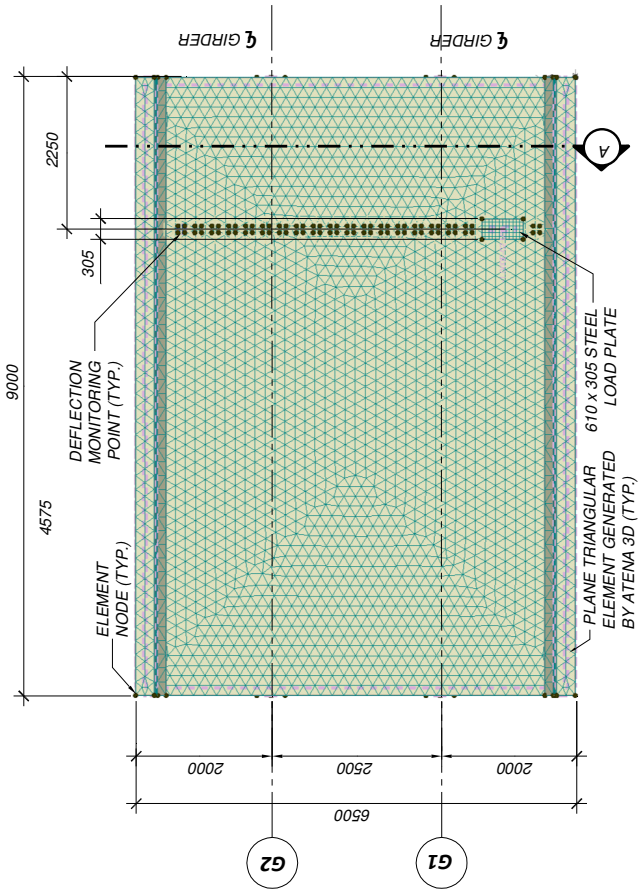

Figure 5-3(a): Plan view of finite element discretization for cantilever sections

-section A

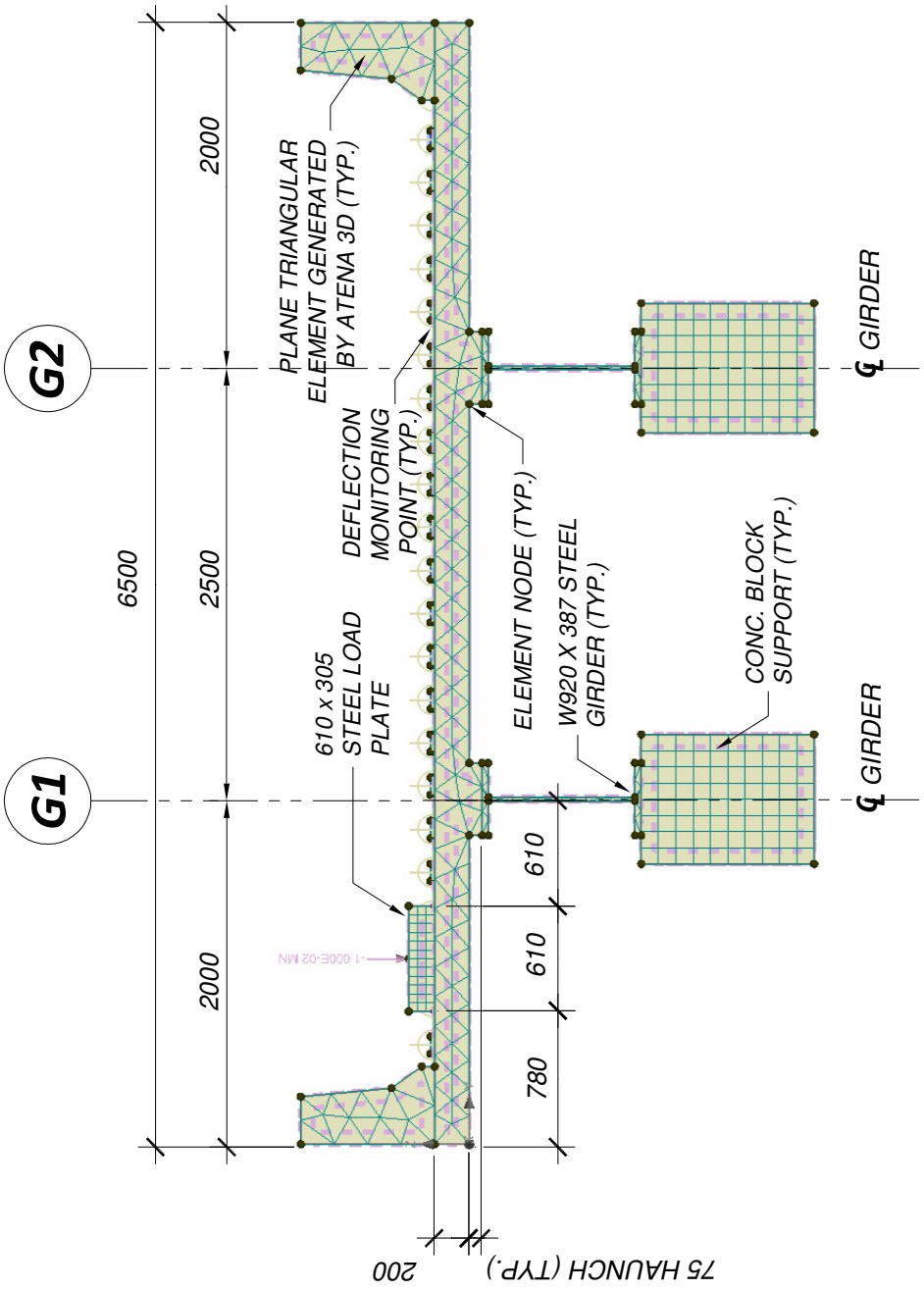
G2
G1
℄ GIRDER
℄ GIRDER
PLANE TRIANGULAR ELEMENT GENERATED BY ATENA 3D (TYP.)
DEFLECTION MONITORING POINT (TYP.)
ELEMENT NODE (TYP.)
W920 X 387 STEEL GIRDER (TYP.)
CONC. BLOCK SUPPORT (TYP.)
610 x 305 STEEL LOAD PLATE
2000
2500
2000
6500
610
610
780
200
75 HAUNCH (TYP.)

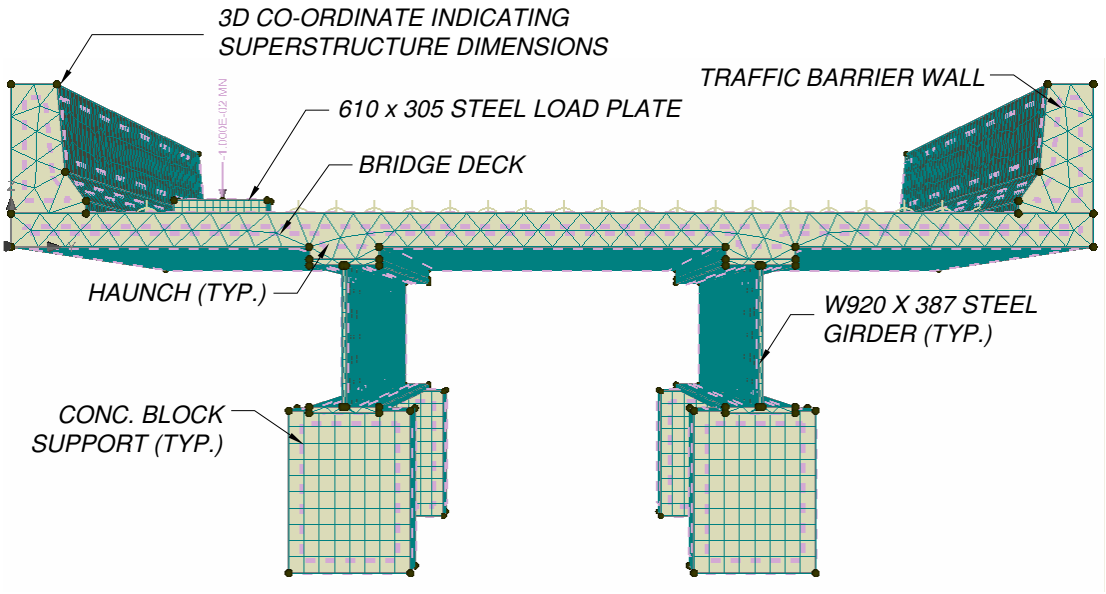

Figure 5-3(c): Perspective view of finite element discretization for the cantilever sections

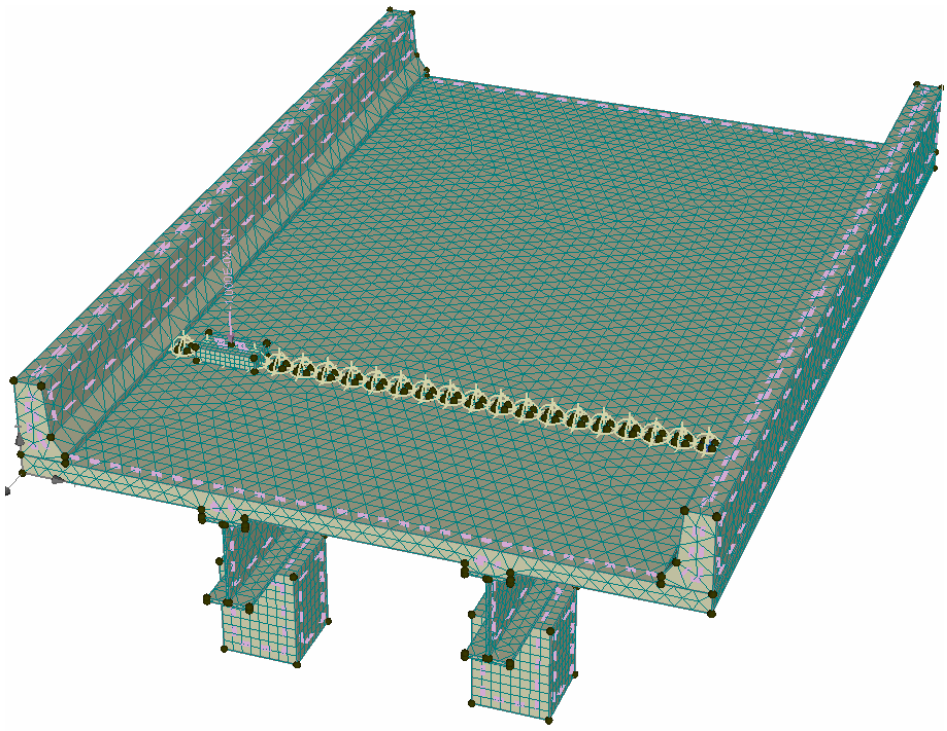

Figure 5-3(d): Isometric view of finite element discretization for the cantilever sections

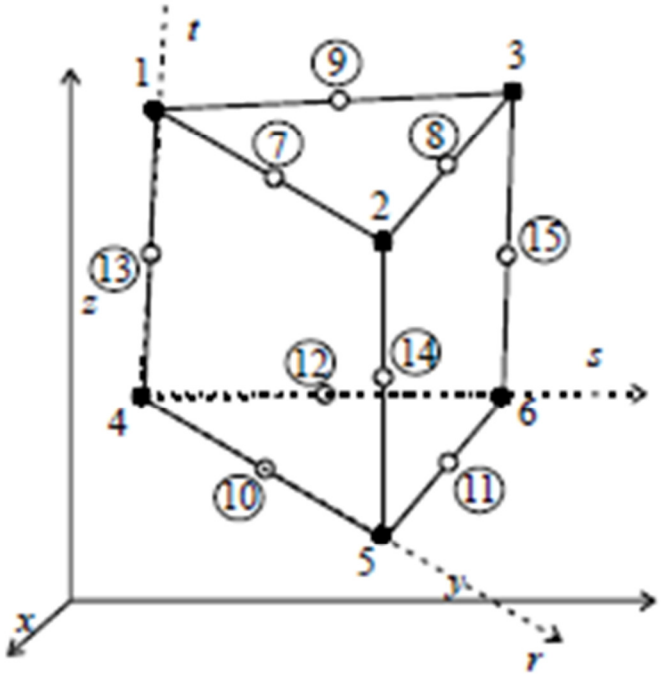

Figure 5-4: 3-dimension CCIso wedge element used in the discretization of the concrete bridge deck slab, concrete barrier walls, and steel supporting girders (Reproduction, Cervenka et al. 2007)

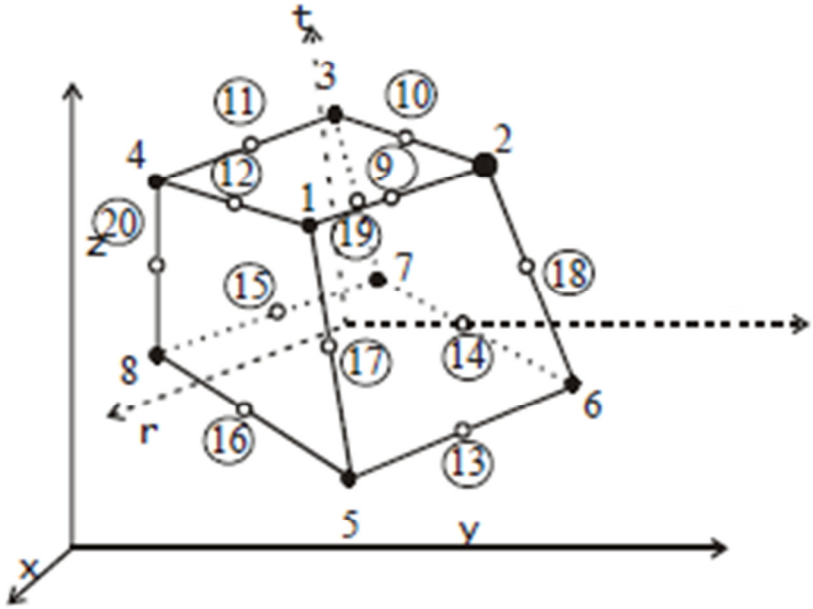

Figure 5-5: 3-dimension CCIso brick element used in the discretization of the concrete supporting blocks (Reproduction, Cervenka et al. 2007)

5.2.1.2 Concrete Modeling

The nonlinear behavior of concrete in the biaxial stress state is described by means of the so-called effective stress, σ_c^{ef}, and the equivalent uniaxial strain, ε^{eq}. The equivalent uniaxial strain is introduced in order to eliminate the Poisson's ratio effect in the plane stress state. The equivalent uniaxial strain, shown in equation 5.1 can be considered as the strain that would be produced by the stress, σ_{ci}, in a uniaxial test with modulus E_{ci} associated with the direction i (Cervenka et al., 2007). Within this assumption, the nonlinearity representing damage is caused only by the governing stress σ_{ci}. The complete equivalent uniaxial stress versus strain diagram for concrete is shown in Figure 5-6.

$$\varepsilon^{eq} = \frac{\sigma_{ci}}{E_{ci}} \tag{5.1}$$

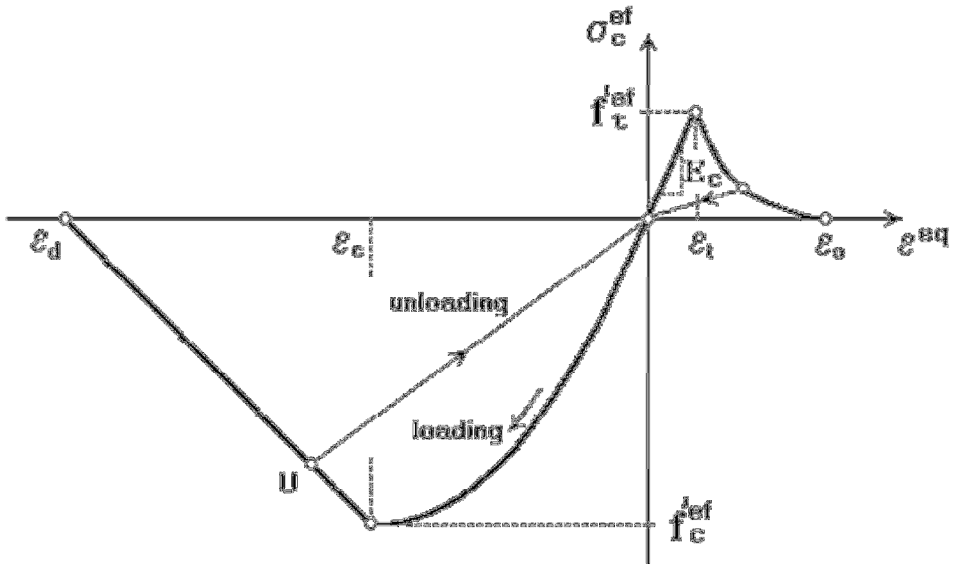

Figure 5-6: Uniaxial stress versus strain relationship for concrete modeling (Reproduction, Cervenka et al. 2007)

The peak values of stress in compression, f'^{ef}_c, and in tension, f'^{ef}_t, are calculated according to the biaxial stress state. Thus, the equivalent uniaxial stress-strain law reflects the biaxial stress state.

The biaxial stress failure criterion is used in the ATENA 3D program (Figure 5-7). In the compression-compression stress state the failure function is given by equation 5.2:

$$f'^{ef}_c = \frac{1+3.65a}{(1+a)^2} f'_c; \quad a = \frac{\sigma_{c1}}{\sigma_{c2}} \tag{5.2}$$

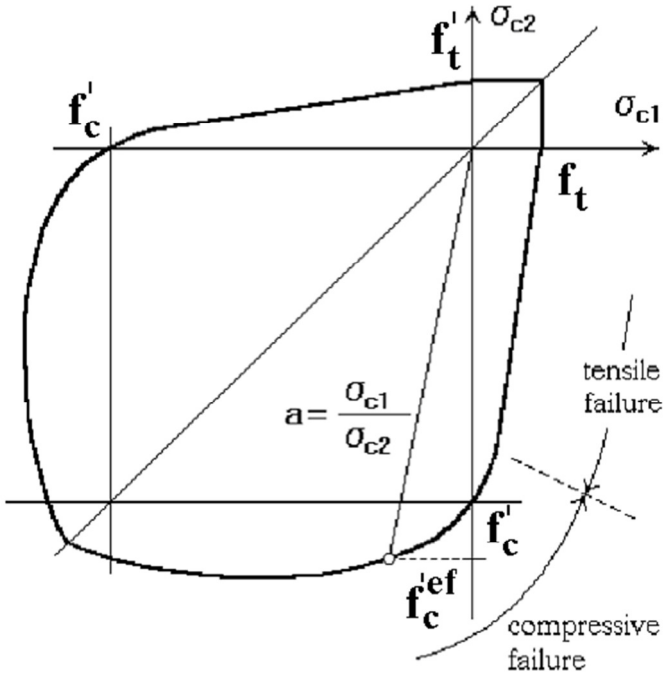

Figure 5-7: Biaxial stress failure criterion for concrete modeling (Reproduction, Cervenka et al. 2007)

Where σ_{c1} and σ_{c2} are the principal stresses in concrete and f'_c is the uniaxial cylinder strength. In the biaxial stress state, the strength of concrete is predicted under the assumption of a proportional stress path.

The fracture model is based on the classical orthotropic smeared crack formulation and crack band model where the Rankine failure criterion is used for concrete cracking, exponential tensile softening, and can be used as rotated or fixed crack model. The hardening/softening plasticity model is based on Menetrey-Willam failure surface (Menetrey et al. 1997). The model can be used to simulate concrete cracking, crushing under high confinement, and crack closure due to crushing in other material directions (Cervenka et al. 2007).

The Menetrey-Willam failure surface adopts the uniaxial compressive concrete test based on the experimental work of Van Mier (1986). The concrete stress-strain relationship is comprised of the softening descending curve is linear and the elliptical ascending part of the curve is shown in Figure 5-8 and given by the following equations:

$$\sigma = f_{co} + (f_c + f_{co})\sqrt{1 - \left(\frac{\varepsilon_c + \varepsilon_{eq}^p}{\varepsilon_c}\right)^2} \tag{5.3}$$

Where:

$$f_{co} = 2f'_t \tag{5.4}$$

$$\varepsilon_c^p = \frac{f'_c}{E} \tag{5.5}$$

$$W_d = \varepsilon_{eq}^p L_c \tag{5.6}$$

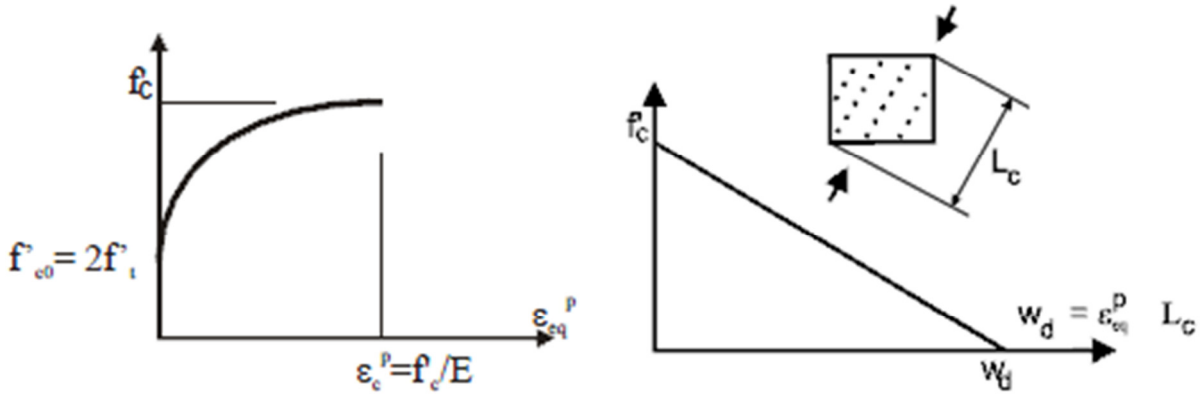

Figure 5-8: Van Mier compressive stress versus strain relationship for concrete (Reproduction, Cervenka et al. 2007)

Where f_{co} is the starting point of the non-linear curve, ε_{cp} is the value of plastic strain at the max compressive strength. The equivalent plastic strain, $\varepsilon_{eq}{}^p$, is transformed into displacements through the length scale parameter, L_c). Table 5-1 highlights the analytical model (***ATENA 3D***) default formulas for the concrete parameters and the experimentally obtained parameters that were input into the model.

A screen shot illustrating the basic parameters input for the concrete properties for both of the cantilever sections is shown in Figure 5-9.

Table 5-1: Default and experimentally obtained parameters for concrete modeling

Parameter	Formula	Experimentally obtained parameter
Cylinder strength	$f'_c = -0.85f'_{cu}$	*45.1 [MPa]*
Tensile Strength	$f'_t = 0.24f'^{2/3}_{cu}$	*3.9 [MPa]*
Initial elastic modulus	$E_c = (6000\text{-}15.5f'_{cu})\sqrt{f'_{cu}}$	*27,410 [MPa]*
Poisson's ratio	$u = 0.2$	*0.16*
Softening compression	$w_d = -0.0005$ *mm*	
Type of tension softening	*1 - exponential, based on* G_f	
Compressive strength in cracked concrete	$c = 0.8$	
Tension stiffening stress	$s_{st} = 0$	
Tension-compression funtion type	*Linear*	
Fracture energy	$G_f = 0.000025f'^{ef}_t$ *[MN/m]*	

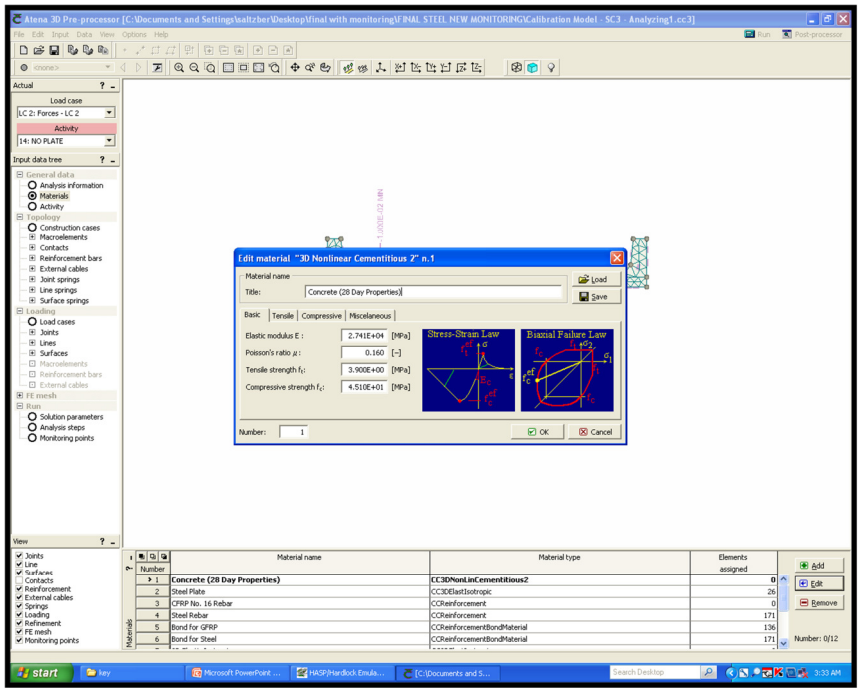

Figure 5-9: Screen shot illustrating the basic input parameters for the concrete for both cantilever sections

5.2.1.3 Reinforcement Modeling

In ***ATENA-3D***, the reinforcement can be modeled in two different forms: discrete and smeared. Discrete reinforcement is in the form of individual reinforcing bars which is modeled by finite truss elements (Cervenka et al., 2007). When the analysis begins, the program automatically breaks down each reinforcement bar into individual truss finite elements embedded into the generated mesh of the concrete solid elements. Therefore, the bar stiffness will be included in the numerical analysis. Alternatively, smeared reinforcement is a component of the composite material and can be considered either as a single (only one-constituent) material in the element under consideration or as one of such constituents. This can be done by reinforcing a macro-element in certain directions with a specific reinforcement ratio that represents actual uniform distribution of the reinforcement in the cross section. For the purpose of the analytical modeling described in this study, the internal transverse and longitudinal steel and GFRP reinforcement with the deck slab was modeled using the discrete option for reinforcement (Figure 5-10 and Figure 5-11). The internal GFRP reinforcement in the traffic barrier wall was also modeled as being discrete (Figure 5-12).

The stress-strain relationship and behaviour of the internal reinforcement can be modeled in the form of a bi-linear elastic-perfectly plastic material or a 4-segment multi-linear material. The internal steel and GFRP reinforcement was modeled as bi-linear perfectly plastic materials (Figure 5-13). Screen shots of the input parameters used for the stress-strain relationships for the steel and GFRP are shown in Figure 5-14 and 5-15.

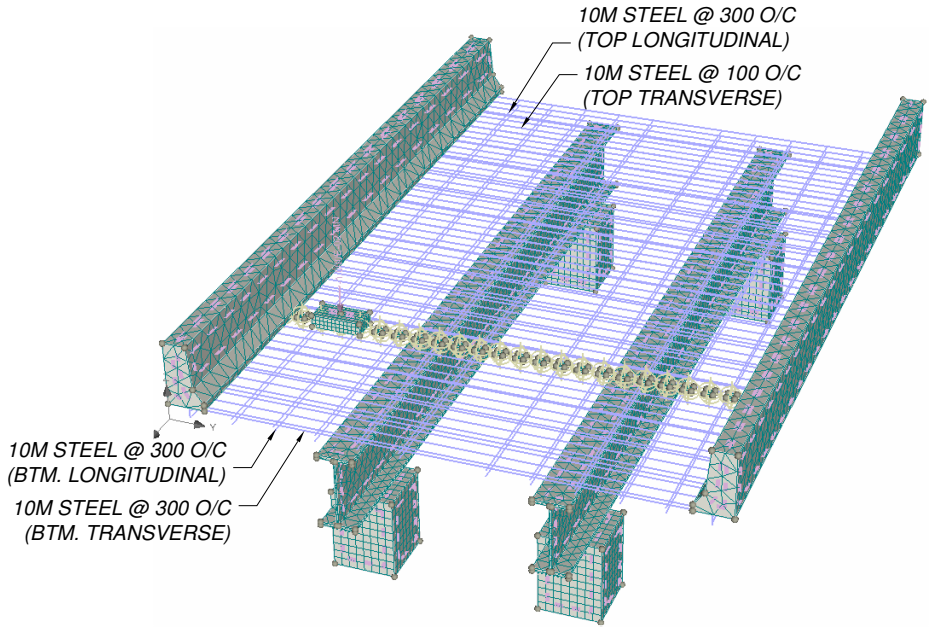

Figure 5-10: Isometric view of the discrete modeling of internal reinforcement for the cantilever section with steel reinforcement

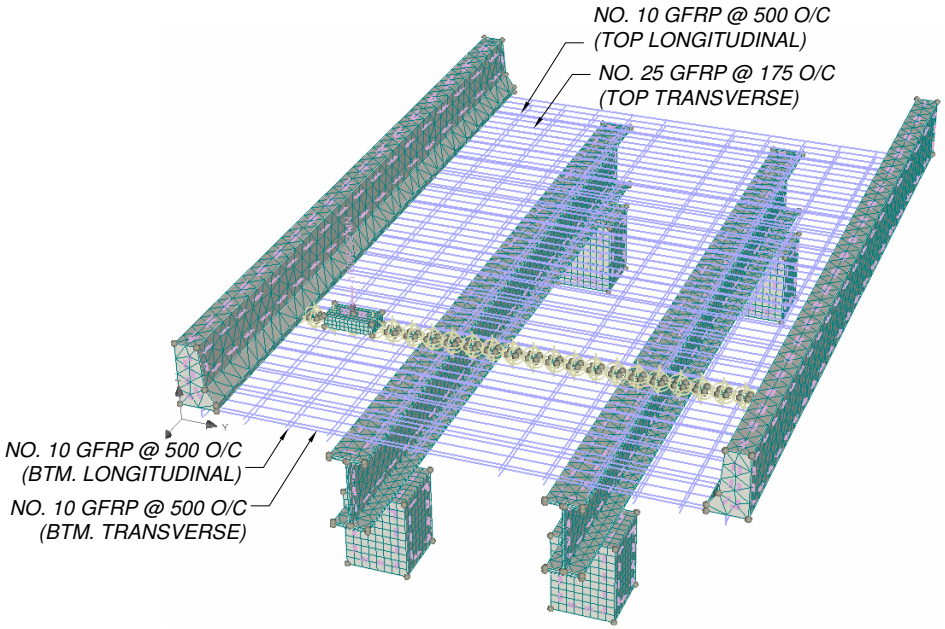

Figure 5-11: Isometric view of the discrete modeling of internal reinforcement for the cantilever section with GFRP reinforcement

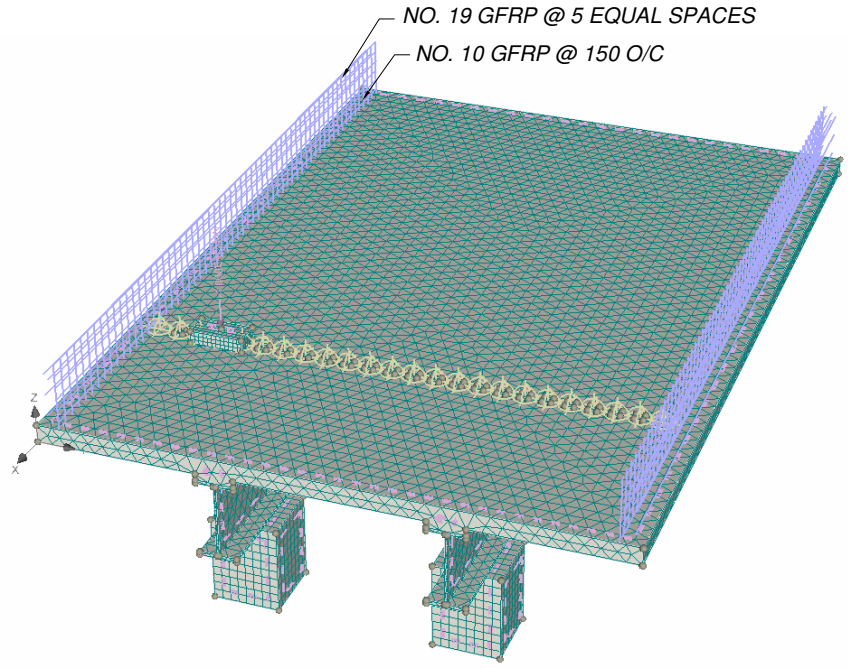

Figure 5-12: Isometric view of the discrete modeling of internal GFRP reinforcement located in traffic barrier walls

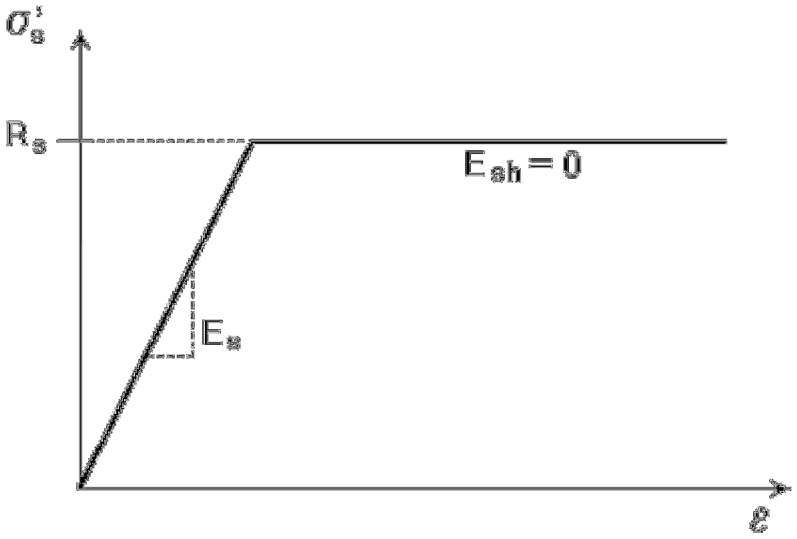

Figure 5-13: The bi-linear stress versus strain relationship as defined in ***ATENA 3D*** (Reproduction, Cervenka et al. 2007)

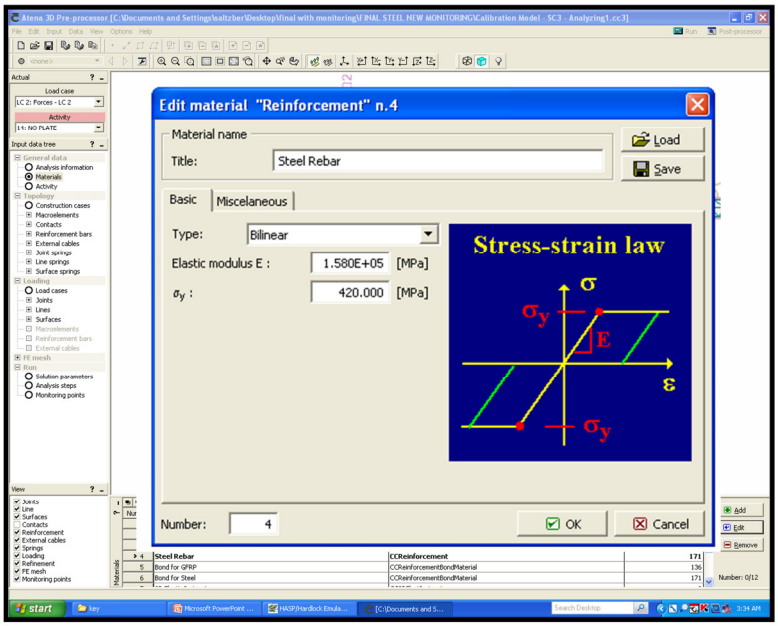

Figure 5-14: Screen shot illustrating input parameters and the bi-linear stress versus strain relationship used for theoretical modeling of the cantilever section with steel reinforcement

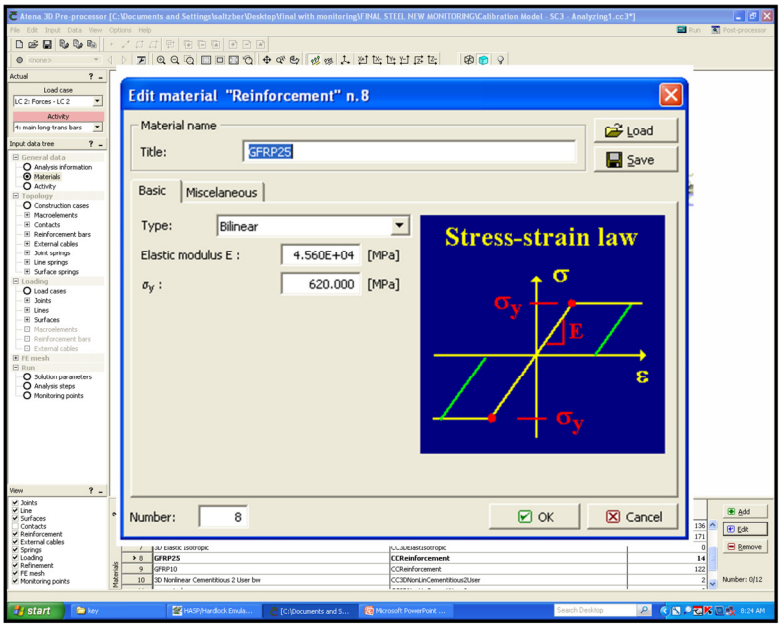

Figure 5-15: Screen shot illustrating input parameters and the bi-linear stress versus strain relationship used for theoretical modeling of the cantilever section with GFRP reinforcement

5.2.1.4 Reinforcement Bond Modeling

There are three predefined bond-slip models for reinforcement incorporated in the ***ATENA 3D*** program. However, on two of the models were applicable to this study. They are the CEB-FIB model code 1990 (Comité Euro-International du Béton, 1993) and the Bigaj model (Bigaj, 1999). There is also an option to input a general user-defined bond-slip model. For the purposes of analytical modeling, the bond-slip relationship given by the CEB-FIB model code 1990 was utilized. The bond-slip relationship is influenced by parameters such as the concrete compressive strength, reinforcement type, confinement conditions, and the quality of the surrounding concrete. The bond-slip relationship of the CEB-FIB model code 1990 is given by Equations 5.7 to 5.10 and shown in Figure 5-16.

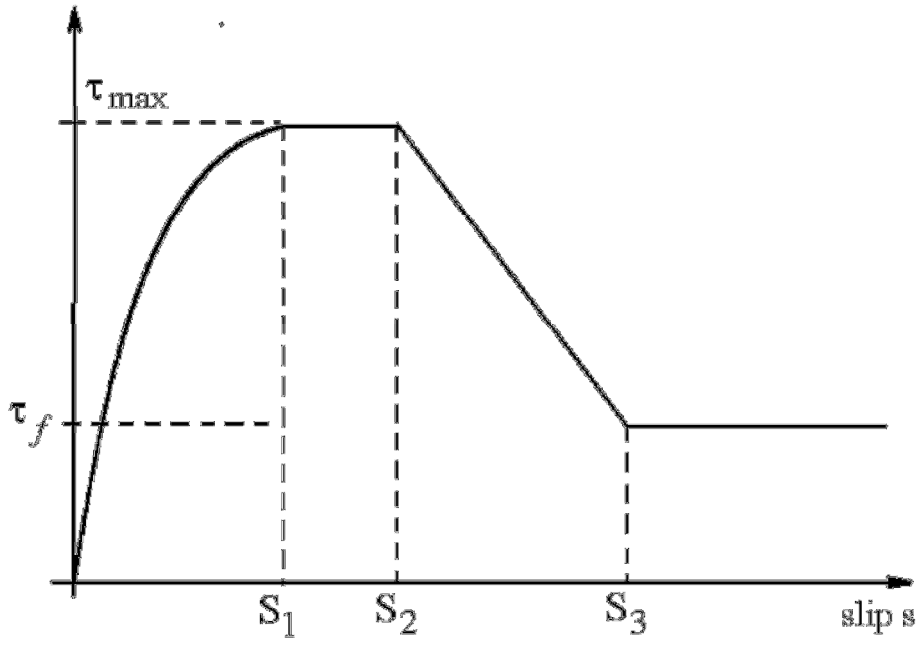

Figure 5-16: Bond-slip relationship by the CEB-FIP model code 1990 (Reproduction, Cervenka et al. 2007)

$$\tau = \tau_{max}\left(\frac{s}{s_1}\right)^{\alpha}; \quad 0 \le s \le s_1 \tag{5.7}$$

$$\tau = \tau_{max}; \quad s_1 < s \le s_2 \tag{5.8}$$

$$\tau = \tau_{max} - \left(\tau_{max} - \tau_f\right)\left(\frac{s-s_1}{s_3-s_2}\right); \quad s_2 < s \le s_3 \tag{5.9}$$

$$\tau = \tau_f; \quad s_3 < s \tag{5.10}$$

Numerical values for bond modeling parameters were input into ***ATENA 3D*** and were based on typical bond properties for conventional deformed or ribbed steel reinforcement and sand coated GFRP reinforcing bars (El-Mogy 2011, and Alves et al. 2011). The input parameters for the bond interaction for steel and GFRP are outlined in Table 5-2. Screen shots of the input parameters are shown in Figure 5-17 and Figure 5-18.

Table 5-2: Theoretical reinforcing bar bond modeling parameters

	Parameters						
	S_1 [mm]	**S_2 [mm]**	**S_3 [mm]**	**α**	**τ_{max} [MPa]**	**τ_f [MPa]**	**Remarks**
Cantilever with steel reinforcement	*0.6*	*0.6*	*1.0*	*0.4*	*11.0*	*1.9*	*Good bond*
Cantilever with GFRP reinforcement	*0.6*	*0.6*	*1.0*	*0.5*	*12.0*	*8.4*	*Good bond*

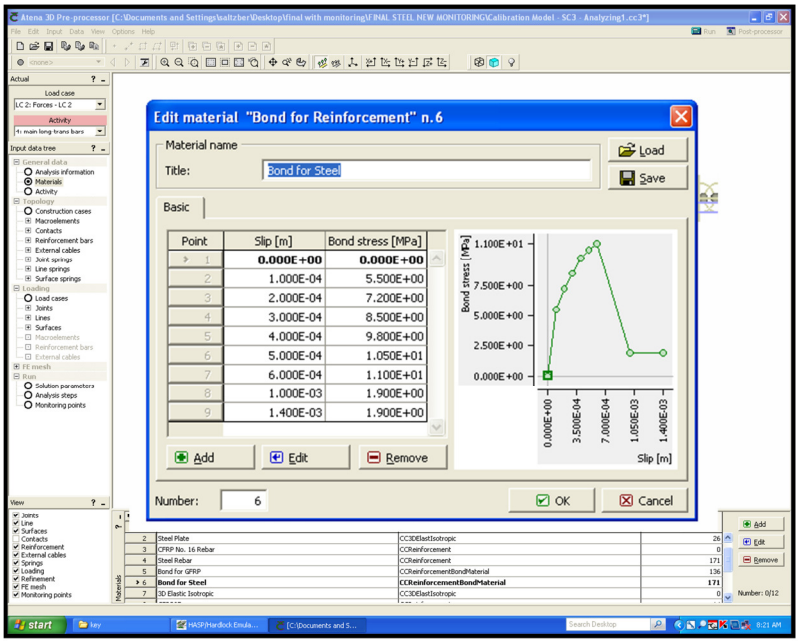

Figure 5-17: Screen shot of bond stress versus slip input parameters for the cantilever section with steel reinforcement

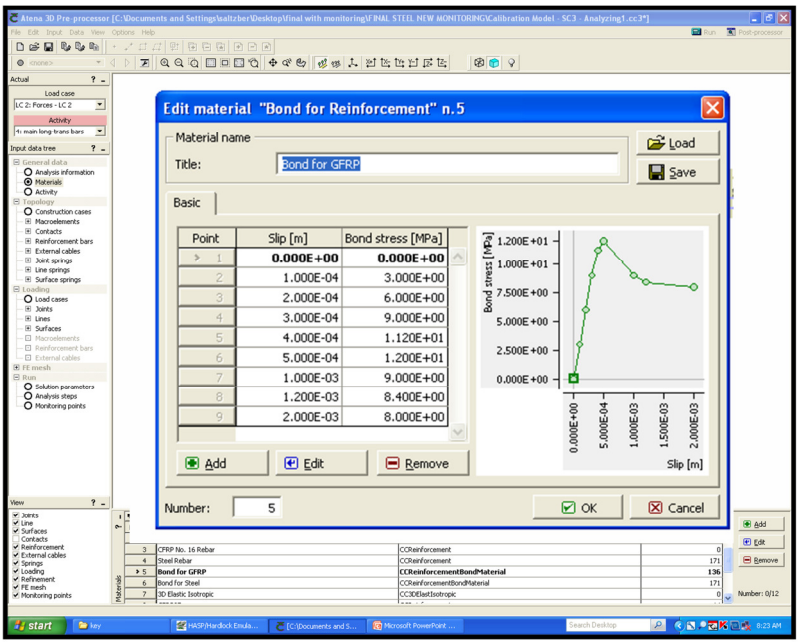

Figure 5-18: Screen shot of bond stress versus slip input parameters for the cantilever section with GFRP reinforcement

5.2.2 Analytical Static Deflection Related Results

The results produced using the finite element models are classified into two different categories. The following two sub-sections describe the theoretical static load versus deflection behaviour and the static transverse deflection profiles. The results presented are for both cantilever sections.

5.2.2 Theoretical Static Load versus Deflection Behaviour

The output file for the cantilever slab overhang reinforced with steel produced a load versus deflection relationship linear up to approximately 220 kN after which it was non-linear until reaching a theoretical ultimate load of 680 kN and a maximum deflection of 10.2 mm (Figure 5-19). The curve in Figure 5-19 is for the deflection monitoring point located at the longitudinal and transverse center of the steel loading plate. The load-deflection curve for the cantilever with model with GFRP reinforcement was similar in pattern to the cantilever with steel reinforcement. The theoretical ultimate load and maximum deflection were 520 kN and 11.8 mm respectively (Figure 5-20). Given that the transverse negative moment resistance of the two cantilever sections was approximately equal, it has been shown that the model reasonably predicted the difference in the observed experimental ultimate loads. The only logical explanation for the difference in the presented theoretical ultimate loads is accredited to the difference in the bottom transverse and longitudinal reinforcement ratios and material properties of the reinforcing bars (i.e. stiffness, modulus of elasticity, etc.).

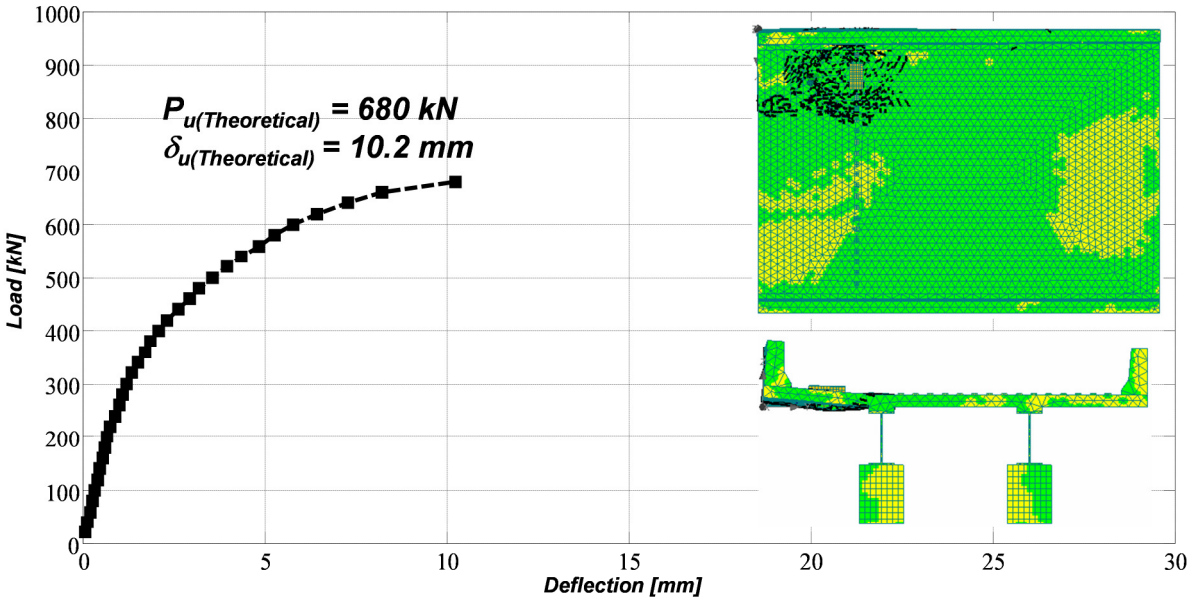

Figure 5-19: Plot of load versus theoretical deflection for the cantilever with steel reinforcement

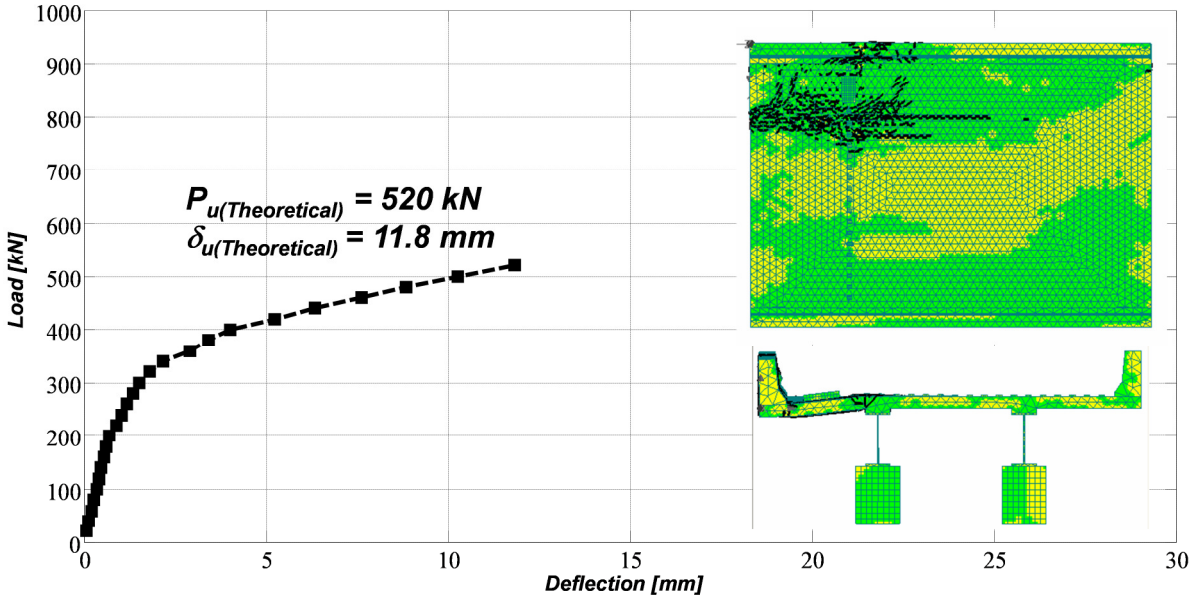

Figure 5-20: Plot of load versus theoretical deflection for the cantilever with GFRP reinforcement

5.2.3 Theoretical Static Transverse Deflection Profiles

The output file produced by ***ATENA 3D*** was used to plot the static transverse deflection profiles across the width of the bridge deck along the transverse center-line of the applied load. The maximum predicted deflection for the cantilever section with steel reinforcement occurred at the free edge of the cantilever and measured 0.62, 1.39, 4.89, and 15.7 mm for the applied loads of 100, 220, 440, and 680 kN respectively (Table 5-3 and Figure 5-21). The internal panel did exhibit a load induced influence as a result of the applied load. The internal panel had a maximum observed deflection of -0.86 mm (upwards displacement) at the theoretical ultimate load of 680 kN.

Table 5-3: Theoretical static transverse deflection profiles along the transverse center-line of the applied load for the cantilever section with steel reinforcement

Load [kN]	Transverse Distance Along Deck [mm]								
	0	625	1075	1430	2000	2750	3250	3750	4500
100	*0.62*	*0.42**	*0.31**	*0.17**	*0.00*	*-0.04*	*-0.04*	*-0.02*	*0.00*
220	*1.39*	*0.95**	*0.69**	*0.36**	*0.00*	*-0.10*	*-0.09*	*-0.06*	*0.00*
440	*4.89*	*3.36**	*2.39**	*1.16**	*0.00*	*-0.19*	*-0.16*	*-0.08*	*0.00*
680	*15.70*	*12.74**	*9.17**	*3.41**	*0.00*	*-0.86*	*-0.58*	*-0.28*	*0.00*

**Deflection values were determined using linear interpolation*

A the theoretical ultimate load, the deflection of the monitoring point located at the free edge of the test location with GFRP was greater than the observed deflection for the cantilever with steel reinforcement, which was calculated to be 19.73 mm (Table 5-4). At service loads and factored loads, the free edge deflection and the deflection below the applied wheel load are comparable in magnitude. However, at higher loads such as twice the factored wheel load, and at the ultimate load, the free edge deflection and deflection under the loading plate

are approximately twice as large compared to the cantilever with steel reinforcement measuring 10.71 and 5.68 mm respectively. The internal panel of the cantilever with GFRP reinforcement also exhibited upward displacements as a result of the applied load on the cantilever. Maximum upward displacements of -0.05, -0.05, -0.21, and -0.61 mm were predicted at the loads of 100, 220, 440, and 520 kN at a location of 2750 mm from the transverse free edge respectively (Figure 5-22). Both cantilever sections displayed a transition from positive curvature to negative curvature indicating a strong influence in the deflection behaviour as a result of the edge stiffening induced by the traffic barrier wall. The cantilever with steel reinforcement displayed a greater influence of the edge stiffening which can be accredited to the higher ultimate loads achieved as a result of the greater reinforcing ratio and material properties of the bottom transverse and longitudinal steel reinforcement.

Table 5-4: Theoretical static transverse deflection profiles along the transverse center-line of the applied load for the cantilever section with GFRP reinforcement

Load [kN]	Transverse Distance Along Deck [mm]								
	0	625	1075	1430	2000	2750	3250	3750	4500
100	*0.63*	*0.43**	*0.31**	*0.17**	*0.00*	*-0.05*	*-0.04*	*-0.03*	*0.00*
220	*1.68*	*1.13**	*0.8**	*0.41**	*0.00*	*-0.05*	*-0.09*	*-0.05*	*0.00*
440	*10.71*	*8.2**	*5.68**	*2.43**	*0.00*	*-0.21*	*-0.15*	*-0.07*	*0.00*
520	*19.73*	*15.23**	*10.57**	*4.27**	*0.00*	*-0.61*	*-0.39*	*-0.17*	*0.00*

**Deflection values were determined using linear interpolation*

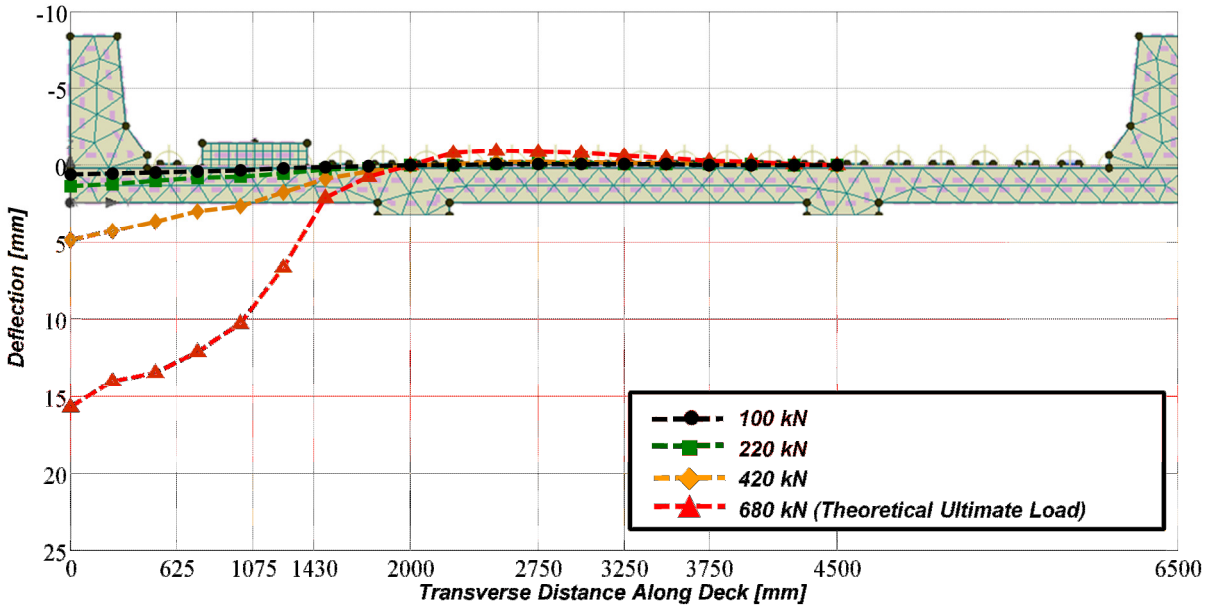

Table 5-21: Theoretical transverse deflection profiles along the transverse center-line of the applied load for the cantilever section with steel reinforcement

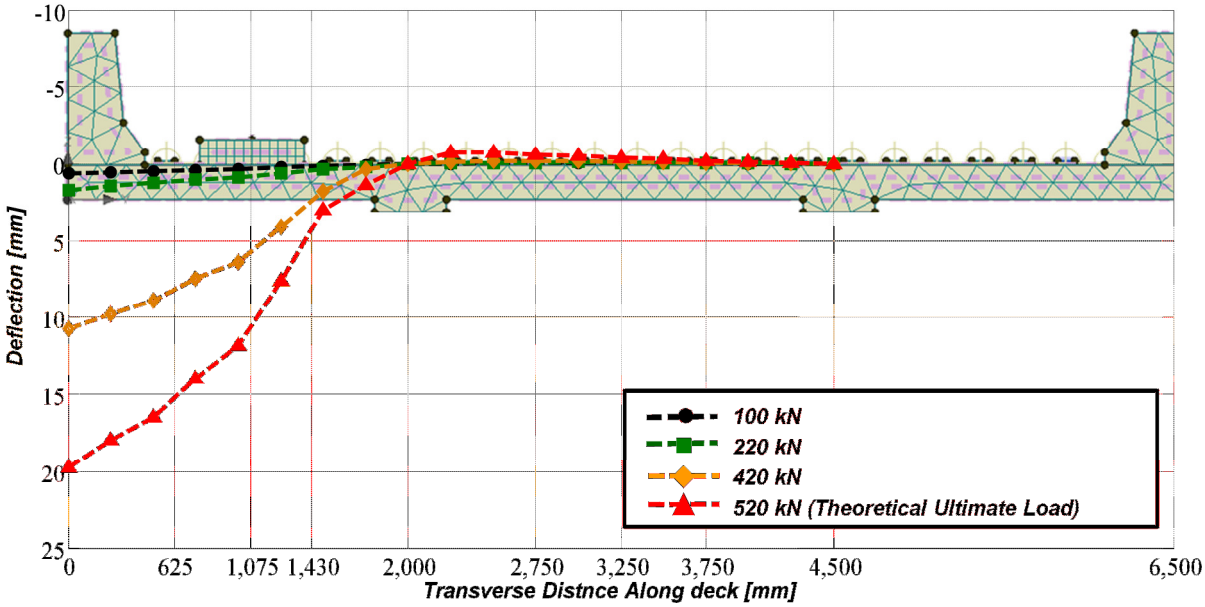

Table 5-22: Theoretical transverse deflection profiles along the transverse center-line of the applied load for the cantilever section with GFRP reinforcement

5.2.4 Theoretical Cracking Patterns

A brief discussion of theoretical cracking patterns observed from the output provided by ***ATENA 3D*** is presented in this section. It does not include a discussion of theoretical crack widths, but it is important to note that the cracking patterns predicted by the theoretical model are helpful in establishing the presence of arching action in bridge deck cantilever overhangs.

The theoretical cracking patterns for the cantilever with steel reinforcement are shown in Figure 5-23(a) and Figure 5-23(b). The theoretical ultimate top cracking pattern illustrated in Figure 5-23(a) closely resembles the cracks over the girder and circumferential cracks experimentally observed and described in Chapter 4. Cracking in the traffic barrier wall is also visible in Figure 5-23(a). Although it is difficult to distinguish exact cracking patterns generated by the FEM model, it does predict significant cracking on the underside of the cantilever slab overhang as a result of the applied wheel load. It is to suggest that the FEM model also reasonably predicts the transverse and radial cracks that were observed experimentally (Figure 5-23(b)).

Theoretical top and bottom cracking patterns for the cantilever with GFRP reinforcement also indicate cracking patterns that were observed during the experimental tests. There are some differences in the theoretical patterns that are worth noting. The theoretical top cracking patterns illustrate less circumferential cracking around the loading plate and greater cracking over the girder (Figure 5-24(a). The difference in the theoretical and experimentally

observed cracking patterns can be attributed to smaller axial stiffness in the bottom transverse and longitudinal reinforcement of the GFRP reinforced cantilever slab overhang. Greater cracking in the traffic barrier is illustrated when compared to the cantilever with steel reinforcement. However, the experimental results indicated less cracking in the barrier wall due to the lower experimental ultimate load that was observed. Again, exact cracking patterns generated from the model are hard to distinguish. However, Figure 5-24(b) indicated less cracking on the underside of the cantilever most likely due to the lower transverse and longitudinal reinforcing ratios. It is well known that lower reinforcing ratios lead to fewer larger cracks and higher reinforcing ratios, as was the case with the cantilever with steel reinforcement, result in greater cracking with smaller crack widths. Thus, it can be stated that the model reasonably predicted cracking location and patterns.

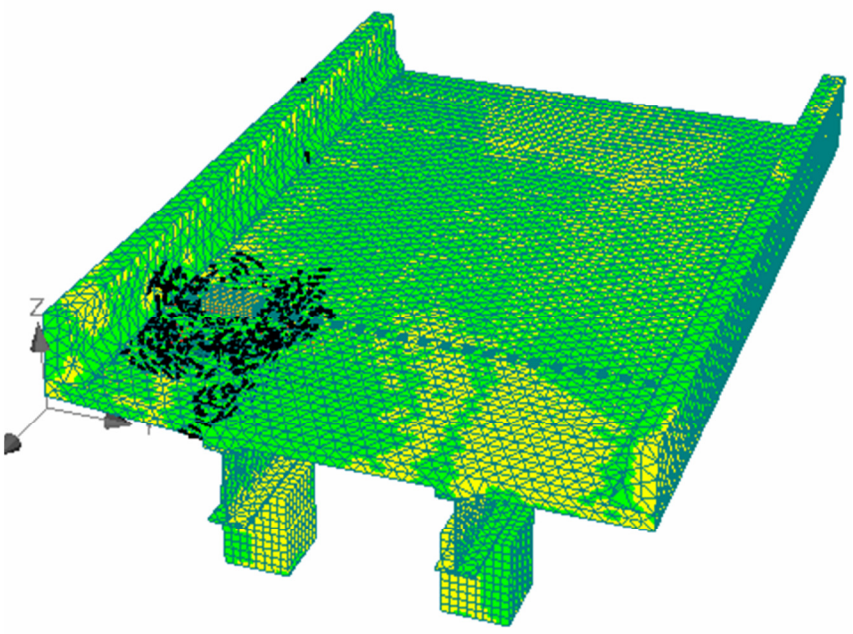

Figure 5-23(a): Top isometric view illustrating theoretical cracking patterns for the cantilever with steel reinforcement at the theoretical ultimate load

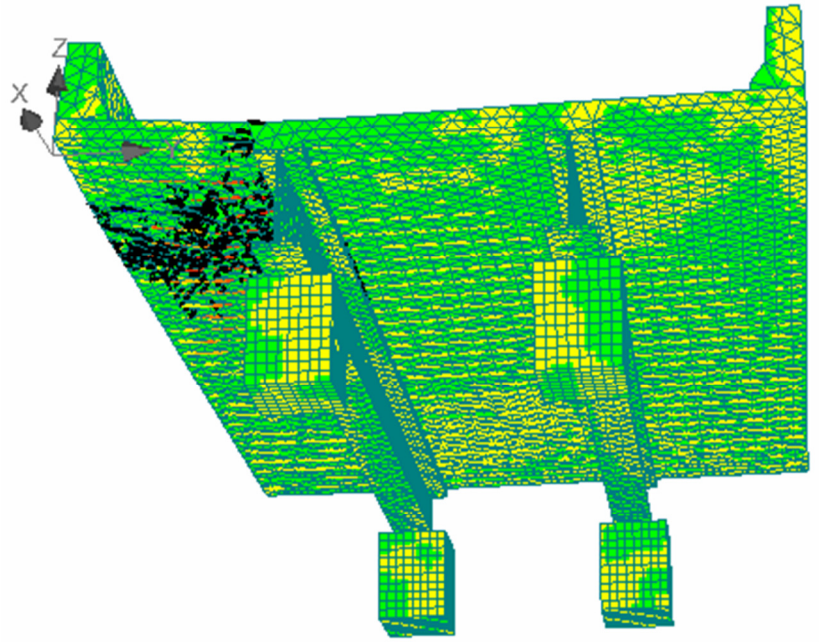

Figure 5-23(b): Bottom isometric view illustrating theoretical cracking patterns for the cantilever with steel reinforcement at the theoretical ultimate load

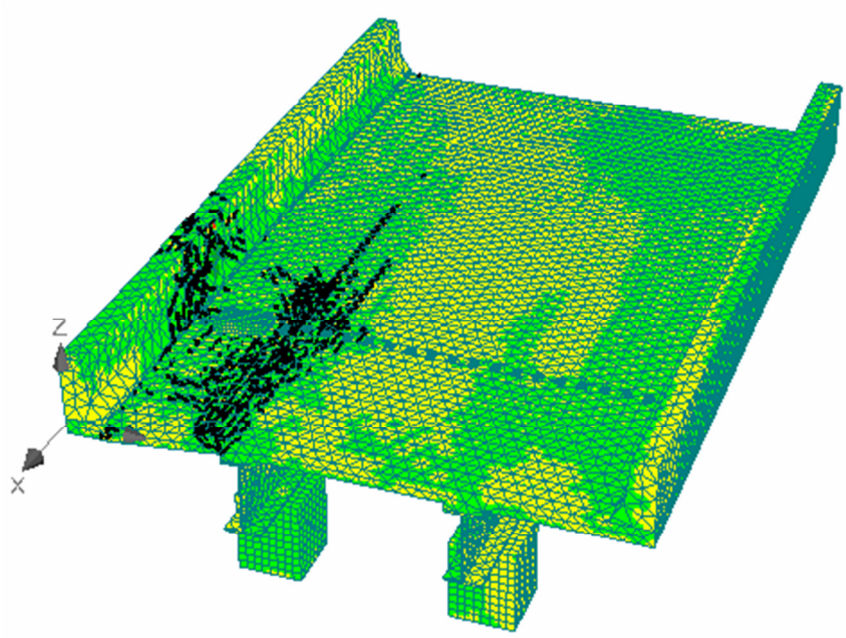

Figure 5-24(a): Top isometric view illustrating theoretical cracking patterns for the cantilever with GFRP reinforcement at the theoretical ultimate load

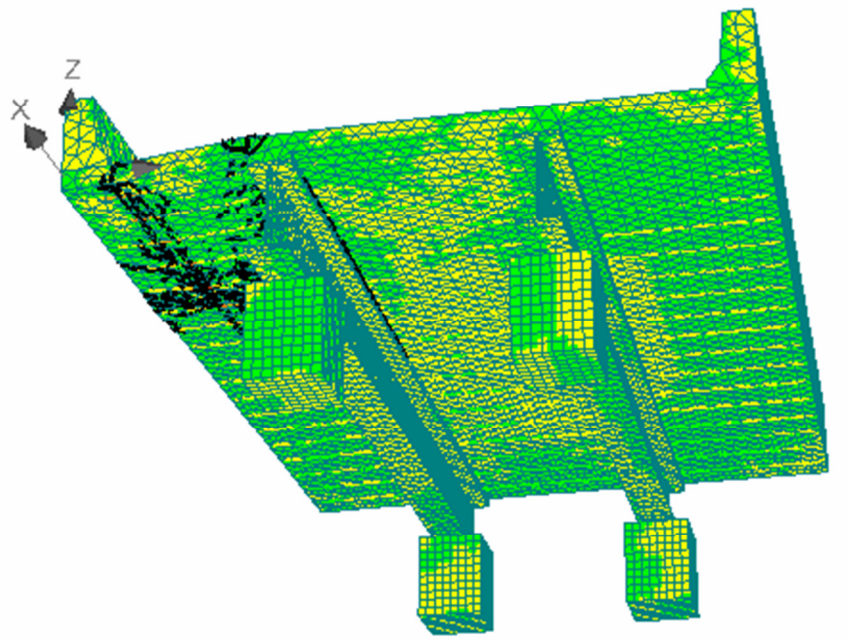

Figure 5-24(b): Bottom isometric view illustrating theoretical cracking patterns for the cantilever with GFRP reinforcement at the theoretical ultimate load

5.2.4 Analytical Models for Determining Theoretical Strains under Static Loads

Two different analytical tools were used to determine theoretical strain magnitudes for the three cantilever sections. The program ***Mr Moment Capacity*** (Tadros 2003) was used to determine strains in the top transverse bars after determining the transverse negative moment intensities resulting from the applied load on the cantilever sections using the computer program called ***ANDECAS6***.

The computer program, ***ANDECAS6,*** was used to determine the transverse negative bending moments due the load on the cantilever overhang. It is a successor of ***ANDECAS*** (***AN***alysis and ***DE***sign of ***CA***ntilever ***S***labs) and ***ANDECAS4*** and is compiled with FORTRAN 90 (Mufti et al., 2003). The program is capable of handling four different design trucks and any

other user-defined design truck. Loads that are considered in ***ANDECAS6*** consist of the weight of the barrier wall, the induced moment at the bottom of the barrier wall due to a horizontal load on the railing, the dead weight of the cantilever slab, the weight of a wearing surface, and the wheel loads located on the cantilever overhang. The program does neglect the effect of the wheel loads located in the internal panel, as required by CAN/CSA S6-06 CHBDC. The program provides the user with the factored moments along with required reinforcements, and gives the breakdown of the moments separately. ***ANDECAS6*** can perform the design of the reinforcement or simply conduct an analysis.

The program is based on the work of Bakht and Holland (1976), Dilger et al. (1990), and Mufti et al. (1993). According to these authors, the transverse bending moments of the cantilever overhang and adjacent internal panel of bridge deck slabs can be calculated from the two equations below:

For the cantilever overhang:

$$M_{yc} = -\frac{2P B_c}{\pi}\left[\frac{(c-y_c)^4}{\left[(c-y_c)^2+(B_c x)^2\right]^2}\right] \tag{5.11}$$

For the internal Panel:

$$M_{yi} = -\frac{2P B_i}{\pi}\left[\frac{c^4 (S-y_i)^4}{\left[c^2(S-y_i)^2 + S^2 (B_i x)^2\right]^2}\right] \tag{5.12}$$

where P is the concentrated load on the cantilever panel and the other notations are as defined in Figure 5-25(a) and (b). B_c and B_i are coefficients that depend on the ratios of $S_r = S/S_c$, $t_r = t_2/t_1$, $c_r = c/S_c$, and $y_r = y_c/S_c$. These coefficients are provided by Mufti et al. (1993) for conditions where the edge of the cantilever is not stiffened, such was the case with the cantilevers tested in this experimental program.

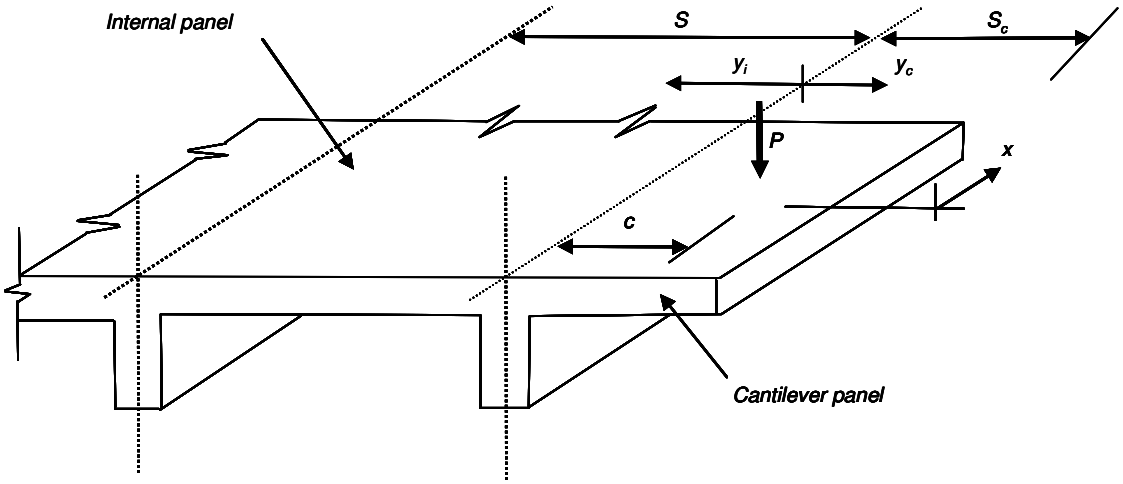

Figure 5-25(a): Configuration of a bridge deck slab subjected to a concentrated load on the cantilever overhang (Reproduction; Mufti et. Al., 2006)

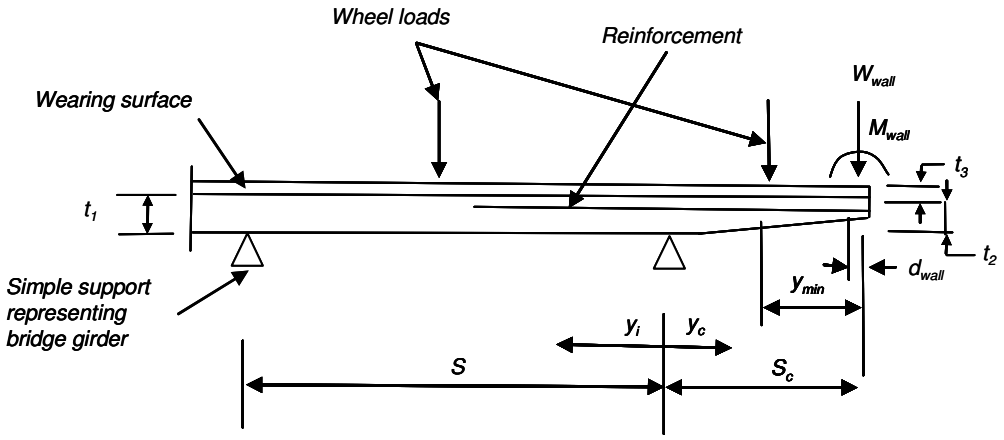

Figure 5-25(b): Definition of notations used in ***ANDECAS6***(Reproduction; Mufti et. Al., 2006)

The cantilevers were analyzed by simply placing the wheel load on the cantilever section in the same location as the experimental test (see Chapter 3 for load plate location). All of the design factors required for the input file were entered as being equal to one to ensure that the output was un-factored. The transverse negative moments were calculated for 90 kN (un-factored wheel load from an HSS 25) and 214 kN (factored wheel load including a DLA). Negative bending moments were also determined for 428, 772, and 487 kN which corresponded to twice the factored wheel load as well as the ultimate loads for the cantilever sections with steel and GFRP respectively.

*It is extremely important to note that **ANDECAS6** used linear-elastic analysis to determine the transverse negative moment intensities for the cantilever overhangs and the internal panel. Linear-elastic analysis disregards that the behaviour of the cantilevers was non-linear after the concrete developed cracks, or if the steel reinforcement yielded, or if there was any crushing of the concrete. Therefore, the*

transverse moment intensities determined using the program are only valid for the lower loads (i.e. 90 kN,) although they were calculated for the higher loads of 214, 428, 772, and 487 kN.

5.2.6 Theoretical Static Transverse Negative Moment Intensities

ANDECAS6 provided a maximum transverse negative moment of 32.6 kN*m/m for the applied load of 90 kN (typical service wheel load) at the girder-center line which diminished to 0 kN*m/m over the next adjacent girder (Table 5-5 And Table 5-6). Chapter 4 demonstrated that the first cracks to appear occurred on the underside of the cantilever slab and were visible for both cantilever sections at the approximate load of 120 to 130 kN. The transverse negative moment intensities obtained for the loads 214, 428, 487, and 772 kN are plotted in Figures 5-26 and Figure 5-27. It is noted that plate analysis assumes that the plate rigidities are independent of the load level.

Table 5-5: Theoretical transverse moment intensities along the transverse center-line of the applied load for the cantilever section with steel reinforcement

Load [kN]	Transverse Distance Along Deck [mm]								
	50	500	1000	1500	2000	2500	3250	4000	4500
90	0.0	1.0*	5.6	12.7*	32.6	20.4	9.7	2.9	0.0
214	0.0	1.0*	5.6	14.1*	51.6	31.1	15.1	4.9	0.0
428	0.0	1.0*	5.6	16.5*	84.2	49.4	24.6	8.4	0.0
772	0.0	1.0*	5.6	20.4*	136.7	78.9	39.8	14.1	0.0

**Negative moment intensities were determined using linear interpolation*

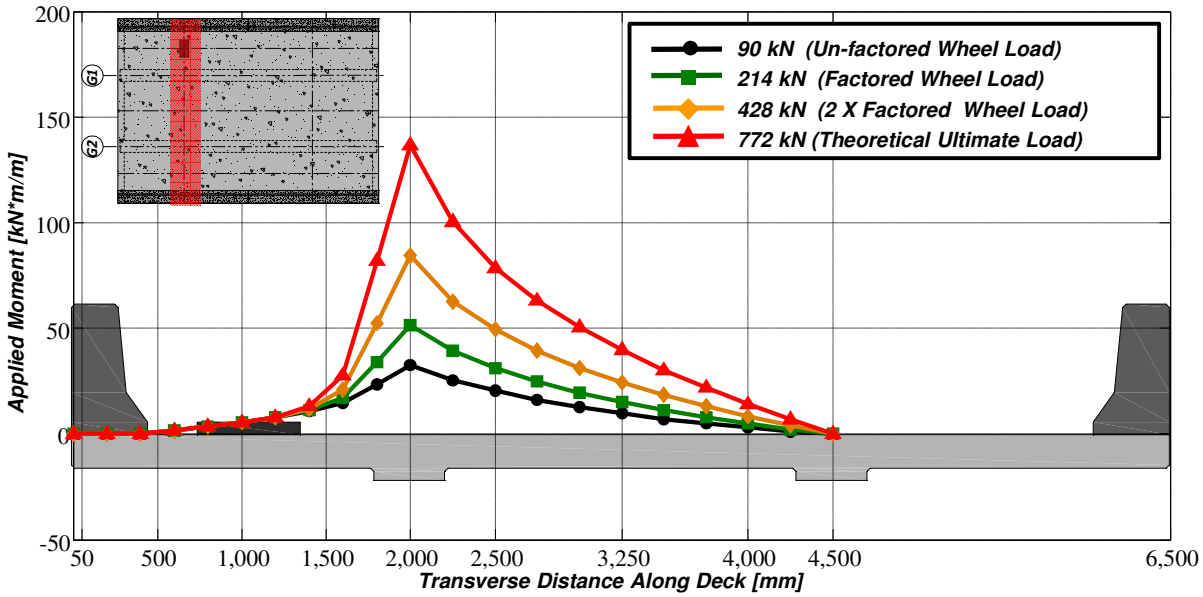

Figure 5-26: Theoretical transverse negative moment intensities for the cantilever section with steel reinforcement

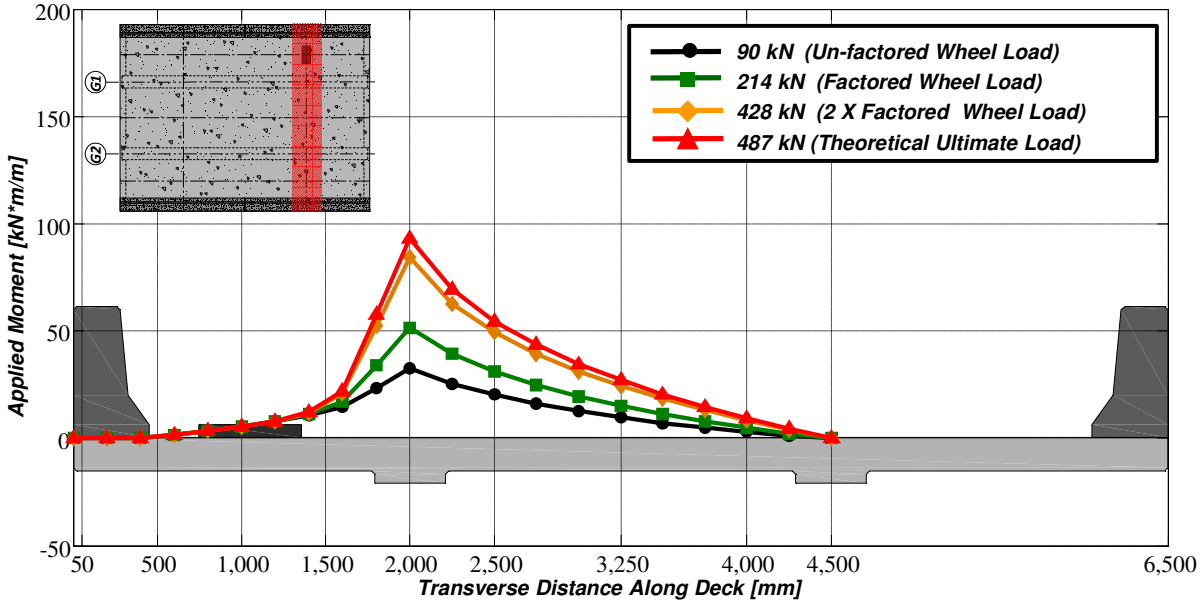

Figure 5-27: Theoretical transverse negative moment intensities for the cantilever section with GFRP reinforcement

Table 5-6: Theoretical transverse moment intensities along the transverse center-line of the applied load for the cantilever section with GFRP reinforcement

Load [kN]	Transverse Distance Along Deck [mm]								
	50	500	1000	1500	2000	2500	3250	4000	4500
90	*0.0*	*1.0**	*5.6*	*12.7**	*32.6*	*20.4*	*9.7*	*2.9*	*0.0*
214	*0.0*	*1.0**	*5.6*	*14.1**	*51.6*	*31.1*	*15.1*	*4.9*	*0.0*
428	*0.0*	*1.0**	*5.6*	*16.5**	*84.2*	*49.4*	*24.6*	*8.4*	*0.0*
487	*0.0*	*1.0**	*5.6*	*17.2**	*93.2*	*54.5*	*27.2*	*9.4*	*0.0*

**Negative moment intensities were determined using linear interpolation*

5.2.5 Theoretical Top Transverse Reinforcing Bar Strain Profiles under Static Loads

After determining the external moments under the applied loads on the cantilever overhang, the ***M_r Moment Capacity*** (Tadros 2003) program was used to determine the strains in the top transverse reinforcing bars. Once again, only the theoretical strain magnitudes were determined for the applied load of 90 kN (un-factored wheel load from an HSS 25) for both of the cantilever sections. The strain magnitudes for the applied loads of 214, 428, 487, and 772 kN, which correspond to a factored wheel load including a DLA, two times the factored wheel load, and the ultimate loads for the cantilever with GFRP and steel respectively are for illustrational purposes only.

Due to the fact that the strains for the top transverse bars are dependent upon the external moment applied to the two cantilever sections, and that the maximum transverse negative moment based on theory indicates that the maximum negative moment occurs over the girder center-line, it is obvious that the maximum theoretical strain magnitude must occur over the girder center-line. Thus, the theoretical strain magnitudes should follow the same envelope as the transverse negative moments. The maximum theoretical strain determined using the

analytical tools for the central cantilever section with steel reinforcement was 614 με over the girder center-line for the applied load of 90 kN (Table 5-7 and Figure 5-28). The maximum theoretical strain for the applied load of 90 kN for the cantilever section with GFRP reinforcement was calculated to be 2220 με (Table 5-8 and Figure 5-29). These tables and figures also show strains due to other loads.

Table 5-7: Theoretical top transverse reinforcing bar strain profiles obtained from theoretical moment intensities along the transverse center-line of the applied load for the cantilever section with steel reinforcement

Load [kN]	Transverse Distance Along Deck [mm]								
	50	500	1000	1500	2000	2500	3250	4000	4500
90	*0*	*19**	*105*	*239**	*614*	*384*	*182*	*54*	*0*
214	*0*	*19**	*105*	*265**	*969*	*584*	*285*	*92*	*0*
428	*0*	*19**	*105*	*310**	*1583*	*928*	*462*	*158*	*0*
772	*0*	*19**	*105*	*383**	*13200*	*1483*	*747*	*265*	*0*

**Strain magnitudes were determined using linear interpolation*

Table 5-8: Theoretical top transverse reinforcing bar strain profiles obtained from theoretical moment intensities along the transverse center-line of the applied load for the cantilever section with GFRP reinforcement

Load [kN]	Transverse Distance Along Deck [mm]								
	50	500	1000	1500	2000	2500	3250	4000	4500
90	*0*	*69**	*381*	*863**	*2220*	*1390*	*658*	*195*	*0*
214	*0*	*69**	*381*	*958**	*3508*	*2113*	*1030*	*333*	*0*
428	*0*	*69**	*381*	*1121**	*5730*	*3360*	*1673*	*573*	*0*
487	*0*	*69**	*381*	*1166**	*6343*	*3704*	*1850*	*639*	*0*

**Strain magnitudes were determined using linear interpolation*

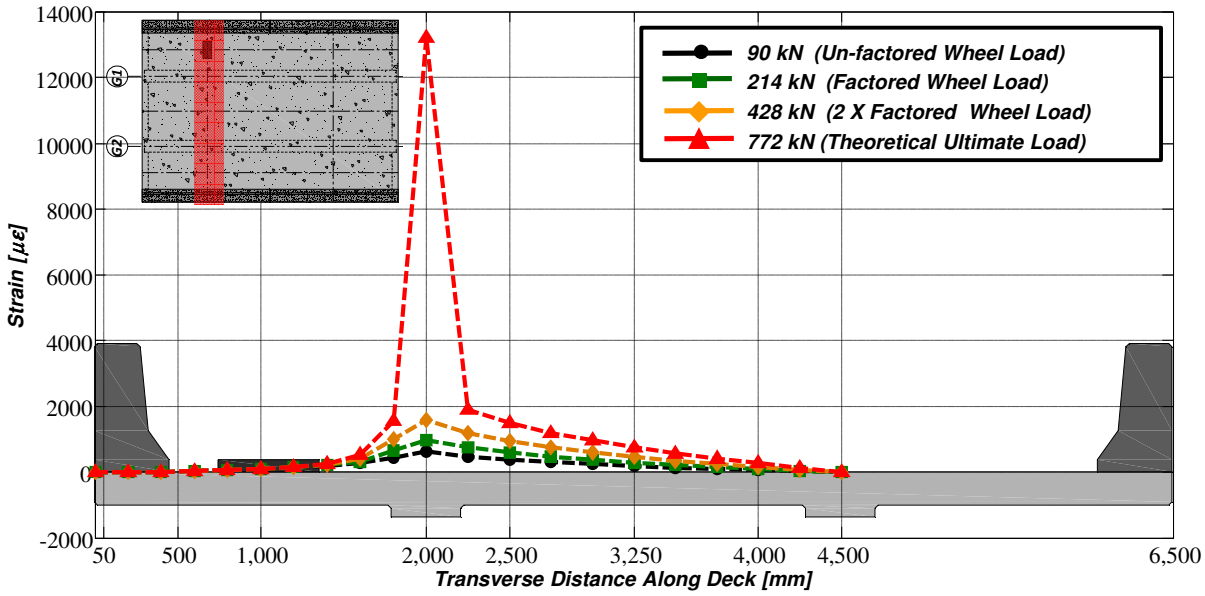

Figure 5-28: Theoretical top transverse reinforcing bar strain profiles obtained from theoretical moment intensities along the transverse center-line of the applied load for the cantilever section with steel reinforcement

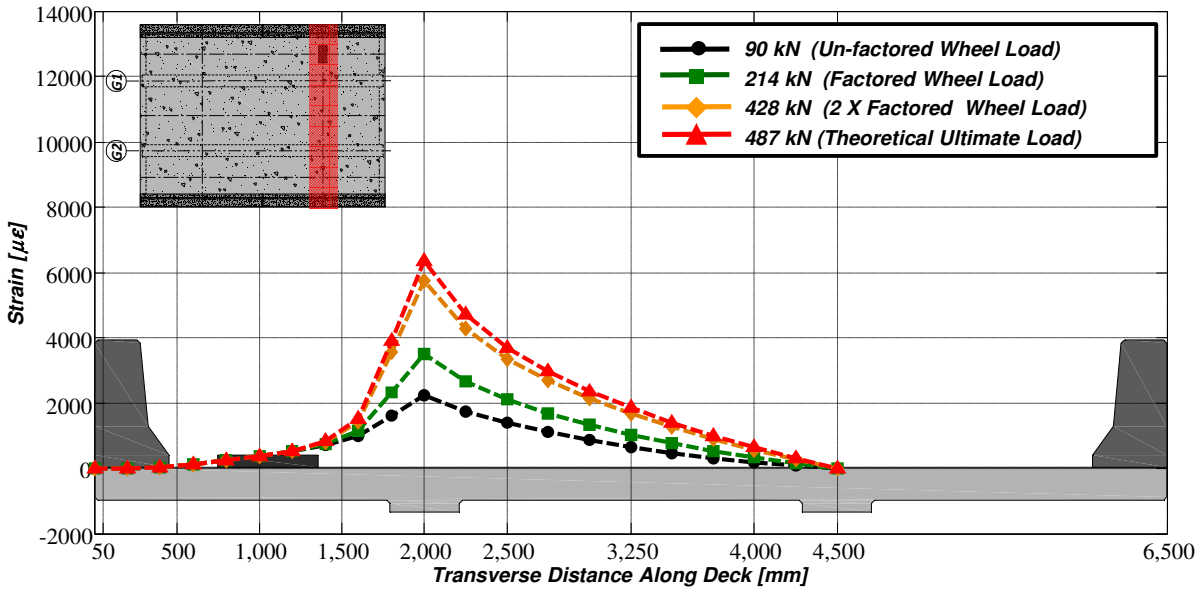

Figure 5-29: Theoretical top transverse reinforcing bar strain profiles obtained from theoretical moment intensities along the transverse center-line of the applied load for the cantilever section with GFRP reinforcement

5.3 Analytical Model Verification and Comparison to Experimental Static Test Results

A comparison of the theoretical and experimental results is made in the following three sub-sections. Experimentally obtained test results and theoretical results generated by finite element modelling using ***ATENA 3D*** are discussed and compared with respect to the load versus deflection and the transverse deflection profiles under static loads. Experimental and theoretical strain related results produced from strain compatibility are presented and discussed for the two cantilever test locations as well.

5.3.1 Comparison of Analytical and Experimental Load versus Deflection Curves under Static Loads

It should be noted that the reference point used for generating the load-deflection curves generated by the analytical model ***ATENA 3D*** was 1000 mm from the longitudinal free edge of the cantilever. Therefore, there may be a small error in the comparison between the experimental and theoretical deflections because the transverse distance between monitoring point and the displacement transducer used during the experiment differed by 75 mm. However, this error shall be considered negligible because it is a fair assumption that the deck slab below the load plate deflected uniformly due the stiffness of the steel loading plate.

The experimentally observed ultimate static load of the central cantilever section with steel reinforcement was 772 kN. The ultimate load predicted by ***ATENA 3D*** was 680 kN which was -11.9 % less than the experimentally observed static ultimate load at the center-line of the loading plate (Figure 5-30). The stiffness of the cantilever with steel reinforcement was

over-estimated throughout the entire loading history. Near failure, the maximum deflection estimated using the program was 10.2 mm compared to the observed deflection of 16.7 mm resulting in an under estimate of -6.5 mm or -38.9 %.

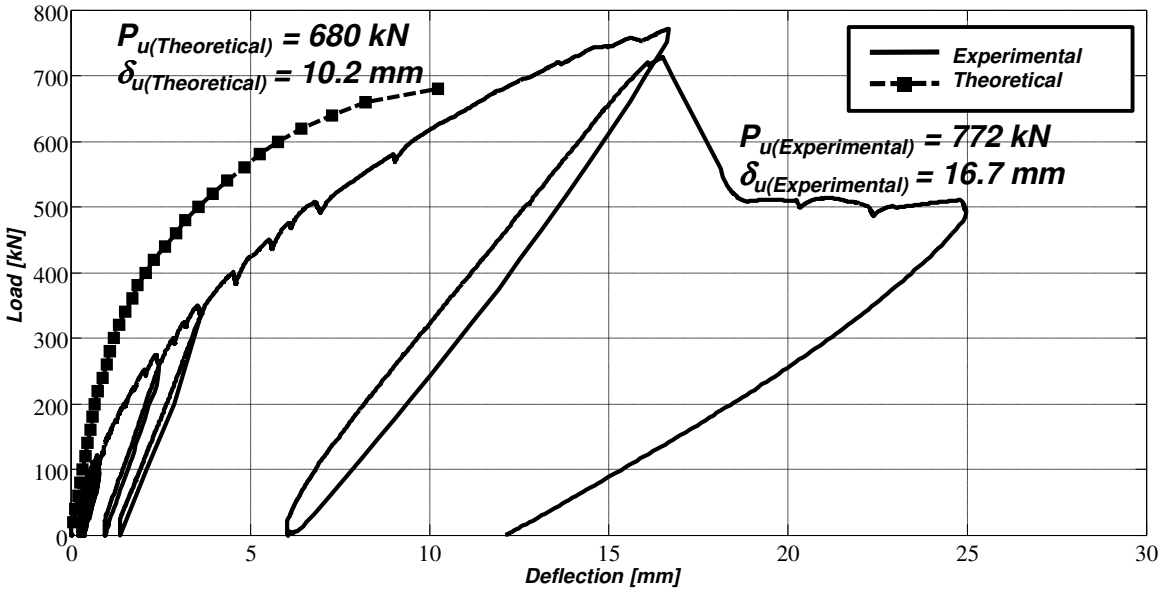

Table 5-30: Comparison of experimental and theoretical load versus deflection curves for the cantilever section with steel reinforcement subjected to static monotonic loading

The program predicted an ultimate load and a maximum deflection of 520 kN and 11.8 mm for the cantilever with GFRP reinforcement (Figure 5-31). The stiffness in the linear elastic range was over estimated, but or predicted that in the non-linear portion of the curve the slopes of the theoretical and experimental curves were in relatively close agreement. The displacement for the cantilever section with GFRP reinforcement was over estimated by 0.9 mm or 8.3 %. The projected theoretical ultimate load for the cantilever section with GFRP was over estimated by 33 kN or 6.8 %. ***ATENA 3D*** was able to accurately predict the load versus deflection relationship for the cantilever section with GFRP reinforcement.

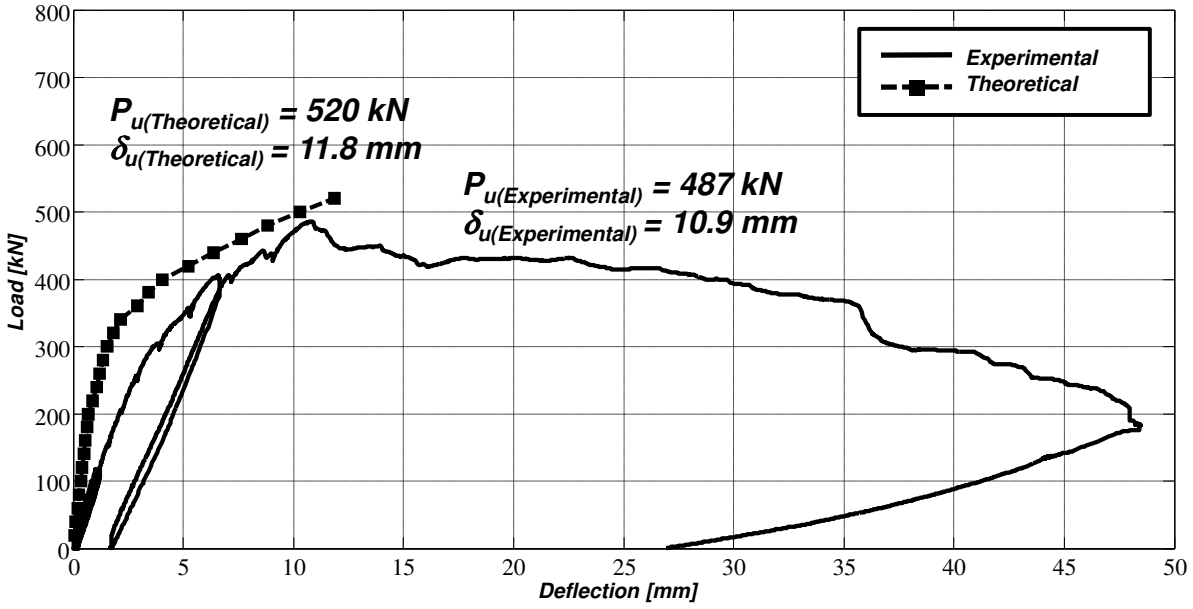

Table 5-31: Comparison of experimental and theoretical load versus deflection curves for the cantilever section with GFRP reinforcement subjected to static monotonic loading

5.3.2 Comparison of Analytical and Experimental Transverse Deflection Profiles under Static Loads

It should be noted that the FEM nodes did not correspond exactly with the displacement transducer locations. Therefore, in order to make a direct comparison between the experimentally observed displacements and deflections at the FEM deflections, the two nodes closest to the LVDT location were interpolated linearly. It is also important to note that the load steps chosen for the modeling were in increments of 20 kN. Therefore, there may be small errors in deflection profile magnitudes due to small differences in the experimental load and theoretical load magnitudes.

The ***ATENA 3D*** finite element software modeled the experimentally observed transverse deflection patterns for the cantilever section with steel reinforcement reasonably well. For the load of 90 kN (un-factored wheel load from an HSS 25), the program under-estimated the deflection of the longitudinal free edge by -26.2 % (Table 5-9). At first glance, based on percent differences, it seems that the finite element program did not accurately predict upward deflections in the internal panel for the cantilever with steel reinforcement at service loads. However, due to the small experimentally observed and theoretically predicted deflection magnitudes, it is very easy to calculate large discrepancies or differences when comparing deflection magnitudes of the order of tenths or hundredths of a millimeter. Therefore, it is reasonable to state that the FEM analysis reasonably predicted transverse deflection profiles at lower loads such as service loads and factored loads. Figure 5-32 shows a comparison of static transverse deflection profiles for the loads of 90, 214, 428, and 772 kN for the cantilever with steel reinforcement. Based on the plotted profiles it can be seen that the FEM analysis under estimated deflection magnitudes in the vicinity of the loading plate and in the internal panel. Although ***ATENA 3D*** under estimated the experimentally observed transverse deflections with accuracies ranging from approximately -26.0 % to -45.0 % in the vicinity of the load plate, it did predict negative curvature patterns under the load plate which indicate the presence of arching action.

Table 5-9: Comparison of experimental and theoretical static transverse deflection profiles along the transverse center-line of the applied load for the cantilever section with steel reinforcement

Load [kN]	Transverse Distance Along Deck [mm]								
	0	**625**	**1075**	**1430**	**2000**	**2750**	**3250**	**3750**	**4500**
90 (Experimental)	*0.84*	*0.27*	*0.48*	*0.03*	*0.00*	*0.01*	*-0.01*	*-0.01*	*0.00*
100 (Analytical)	*0.62*	*0.42**	*0.31**	*0.17**	*0.00*	*-0.04*	*-0.04*	*-0.02*	*0.00*
% Difference	*-26.19*	*55.56*	*-35.42*	*466.67*	*0.00*	*-500.00*	*300.00*	*100.00*	*0.00*
214 (Experimental)	*2.65*	*1.67*	*1.64*	*0.51*	*0.00*	*-0.02*	*-0.08*	*-0.05*	*0.00*
220 (Analytical)	*1.39*	*0.95**	*0.69**	*0.36**	*0.00*	*-0.10*	*-0.09*	*-0.06*	*0.00*
% Difference	*-47.55*	*-43.11*	*-57.93*	*-29.41*	*0.00*	*400.00*	*12.50*	*20.00*	*0.00*
428 (Experimental)	*7.46*	*6.05*	*5.14*	*1.93*	*0.00*	*-0.44*	*-0.55*	*-0.28*	*0.00*
440 (Analytical)	*4.89*	*3.36**	*2.39**	*1.16**	*0.00*	*-0.19*	*-0.16*	*-0.08*	*0.00*
% Difference	*-34.45*	*-44.46*	*-53.50*	*-39.90*	*0.00*	*-56.82*	*-70.91*	*-71.43*	*0.00*
772 (Experimental)	*21.32*	*19.60*	*16.68*	*5.21*	*0.00*	*-2.63*	*-2.74*	*-1.69*	*0.00*
680 (Analytical)	*15.70*	*12.74**	*9.17**	*3.41**	*0.00*	*-0.86*	*-0.58*	*-0.28*	*0.00*
% Difference	*-26.36*	*-35.00*	*-45.02*	*-34.55*	*0.00*	*-67.30*	*-78.83*	*-83.43*	*0.00*

**Deflection values were determined using linear interpolation*

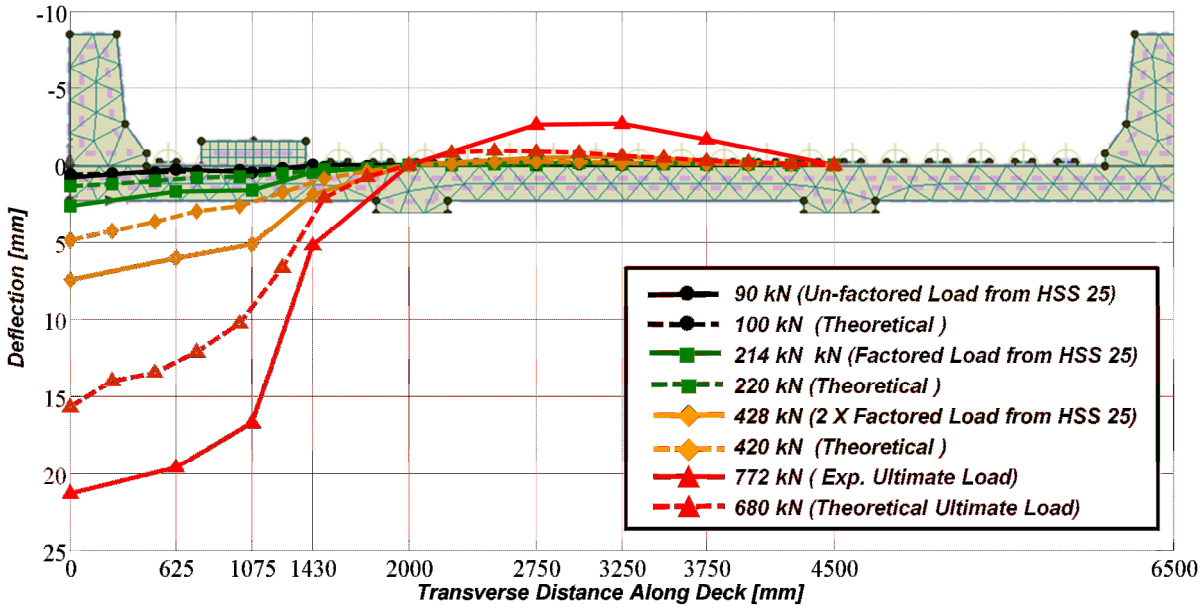

Table 5-32: Comparison of experimental and theoretical transverse deflection profiles along the transverse center-line of the applied load for the cantilever section with steel reinforcement subjected to static monotonic loading

ATENA 3D under-estimated the transverse deflection profiles for the cantilever section with GFRP reinforcement for the loads of 90 and 214 kN in the vicinity of the loading plate by approximately -50.0 to -60.0 % (Table 5-10 and Figure 5-33). In the internal panel, percent differences can again be misleading because of the small differences in experimentally observed and theoretically calculated values. At the higher loads approaching the experimental ultimate load, it predicted deflection magnitudes with greater accuracy in the cantilever with steel reinforcement. In the vicinity of the loading plate it only under predicted deflection magnitude by 2.6 %. In the internal panel, percent differences are again large; however the actual differences are relatively small in magnitude.

Table 5-10: Comparison of experimental and theoretical static transverse deflection profiles along the transverse center-line of the applied load for the cantilever section with GFRP reinforcement

Load [kN]	Transverse Distance Along Deck [mm]								
	0	**625**	**1075**	**1430**	**2000**	**2750**	**3250**	**3750**	**4500**
90 (Experimental)	*1.52*	*0.69*	*0.77*	*0.20*	*0.00*	*0.00*	*0.00*	*-0.01*	*0.00*
100 (Analytical)	*0.63*	*0.43**	*0.31**	*0.17**	*0.00*	*-0.05*	*-0.04*	*-0.03*	*0.00*
% Difference	*-58.55*	*-37.68*	*-59.74*	*-15.00*	*0.00*	*500.00*	*400.00*	*200.00*	*0.00*
214 (Experimental)	*4.05*	*2.83*	*2.32*	*1.00*	*0.00*	*-0.02*	*0.01*	*-0.01*	*0.00*
220 (Analytical)	*1.68*	*1.13**	*0.80**	*0.41**	*0.00*	*-0.05*	*-0.09*	*-0.05*	*0.00*
% Difference	*-58.52*	*-60.07*	*-65.52*	*-59.00*	*0.00*	*150.00*	*-1000.00*	*400.00*	*0.00*
428 (Experimental)	*11.12*	*9.41*	*8.16*	*3.19*	*0.00*	*-0.81*	*-0.37*	*-0.02*	*0.00*
440 (Analytical)	*10.71*	*8.20**	*5.68**	*2.43**	*0.00*	*-0.21*	*-0.15*	*-0.07*	*0.00*
% Difference	*-3.69*	*-12.86*	*-30.39*	*-23.82*	*0.00*	*-74.07*	*-59.46*	*250.00*	*0.00*
487 (Experimental)	*13.57*	*12.08*	*10.85*	*4.07*	*0.00*	*-1.11*	*-0.51*	*-0.02*	*0.00*
520 (Analytical)	*19.73*	*15.23**	*10.57**	*4.27**	*0.00*	*-0.61*	*-0.39*	*-0.17*	*0.00*
% Difference	*45.39*	*26.08*	*-2.58*	*4.91*	*0.00*	*-45.05*	*-23.53*	*750.00*	*0.00*

**Deflection values were determined using linear interpolation*

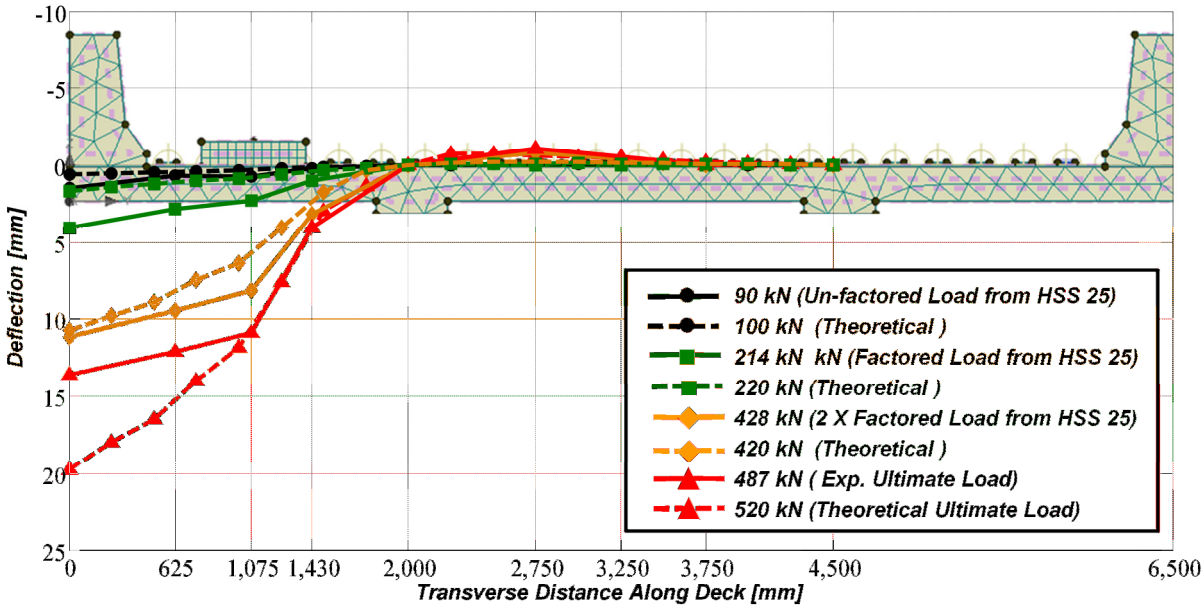

Table 5-33: Comparison of experimental and theoretical transverse deflection profiles along the transverse center-line of the applied load for the cantilever section with GFRP reinforcement subjected to static monotonic loading

Some major observations can be made by directly comparing the experimental and theoretical transverse deflection profiles across the width of the deck and along the center-line of the loading plate for both cantilever sections. At the lower loads, such as 90 kN (un-factored wheel load from an HSS 25) and 214 kN (factored wheel load including DLA from an HSS 25), the analytical model ***ATENA 3D*** predicts the transverse deflection patterns reasonably well but under-estimates the deflections for the cantilever and internal panel. Experimentally observed profiles indicated that the cantilever makes the transition from positive curvature to negative curvature in the proximity of the loading plate. The program also predicted this behaviour. Therefore, the FEM reasonably well predicts the experimentally observed deflections which indicating a strong presence of arching action in the cantilever slab overhangs.

5.3.3 Comparison of Theoretical and Experimental Top Transverse Reinforcing Bar Strains under Static Loads

A direct comparison between the experimentally observed strain values and theoretically determined magnitudes along the top transverse reinforcing bars is only discussed for the applied loads of 90 kN. Although cracking on the underside of the cantilever slab first became present at loads of approximately 120 to 130 kN, theoretical strain comparisons for the top transverse reinforcing bars at factored loads is briefly discussed. A comparison between the theoretical and experimental strain magnitudes above 214 kN is not discussed because ***ANDECAS6*** used linear-elastic analysis to determine the transverse negative moment intensities. Therefore, the strain values along the transverse length of the deck cannot be elastic and are presented for illustrational purposes only.

Theoretical strains, obtained using ***ANDECAS6*** and M_r, for both cantilever sections and the applied load of 90 kN were significantly different. Table 5-11 and the strains plotted in Figures 5-34 clearly indicate that small deflection plate theory and flexural analysis do not accurately predict the observed experimental strains in the top transverse reinforcing bars under static loads for the cantilever with steel reinforcement. The percent differences shown in the tables are so large they cannot be considered as practical evaluations. They are simply for illustrational purposes to demonstrate the large discrepancy between the experimentally observed strains and theoretical strains obtained using flexural theory. Thus, confirming the cantilever slab overhangs response to a wheel load was not flexural. The slab exhibits strong arching action in its response to a concentrated wheel load.

Table 5-11: Comparison of experimental and theoretical top transverse reinforcing bar strain profiles along the transverse center-line of the applied load for the cantilever section with steel reinforcement subjected to static monotonic loading (service loads)

Load [kN]	Transverse distance along deck [mm]								
	50	500	1000	1500	2000	2500	3250	4000	4500
90 (Experimental)	4	6	-25	7	33	28	12	4	1
90 (Analytical)	0	23	105	239	614	384	182	54	0
% Difference	-	300.3	-523.0	3486.5	1757.5	1262.1	1379.2	1267.2	-

Note: Transverse reinforcing bar theoretical strain magnitudes for the transverse distances of 500 and 1000 mm from the free edge were determined using linear interpolation

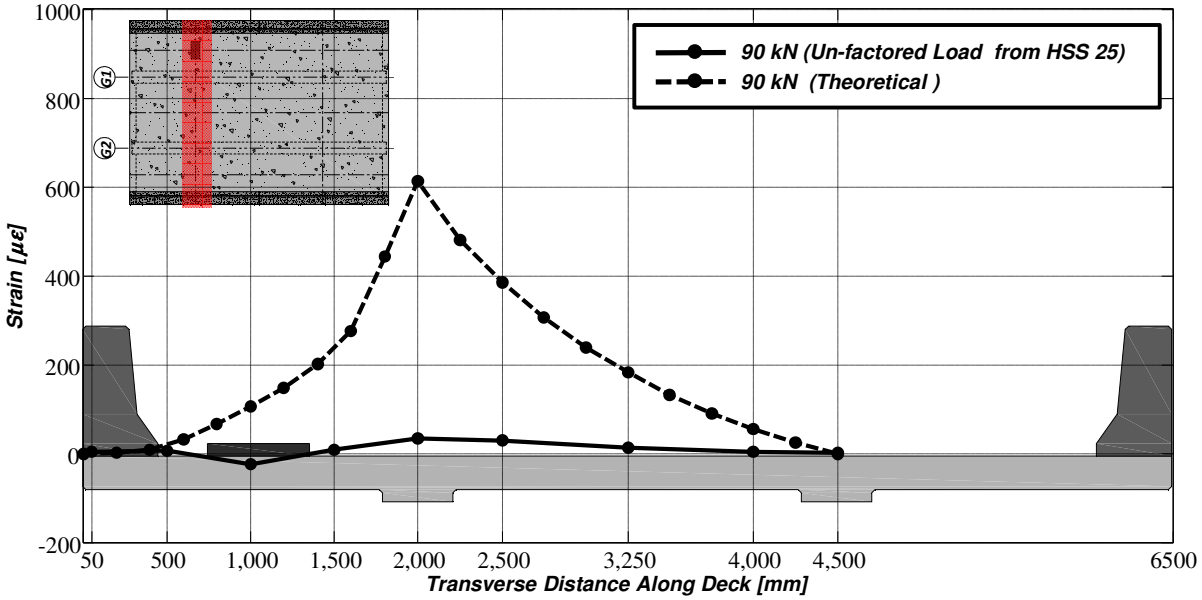

Figure 5-34: Comparison of experimental and theoretical top transverse reinforcing bar strain profiles along the transverse center-line of the applied load for the cantilever section with steel reinforcement subjected to static monotonic loading (service loads)

Table 5-12 and Figure 5-35 confirm the difference between the theoretically determined and experimentally observed strains in the top transverse reinforcing bars over the girder center-line for the cantilever with GFRP reinforcement. The cantilever section with GFRP also

demonstrated the significant difference between experimentally observed strains and theoretically calculated strains. The theoretical strain value for the applied load of 90 kN was 5886.0 % or 2183 με greater than experimentally observed magnitudes over the girder. The consistency in the difference between the theoretically determined and experimentally observed strain values for both cantilever sections strongly indicates that the behaviour of the cantilevers is strongly influenced by arching action.

Table 5-12: Comparison of experimental and theoretical top transverse reinforcing bar strain profiles along the transverse center-line of the applied load for the cantilever section with GFRP reinforcement subjected to static monotonic loading (service loads)

Load [kN]	Transverse distance along deck [mm]								
	50	500	1000	1500	2000	2500	3250	4000	4500
90 (Experimental)	*3*	*1*	*-24*	*1*	*37*	*20*	*8*	*4*	*0*
90 (Analytical)	*0*	*69*	*381*	*863*	*2220*	*1390*	*658*	*195*	*0*
% Difference	*-*	*6800.0*	*-1684.0*	*86200.0*	*5886.0*	*6819.7*	*8300.7*	*4472.2*	*-*

Note: Transverse reinforcing bar theoretical strain magnitudes for the transverse distances of 500 and 1000 mm from the free edge were determined using linear interpolation

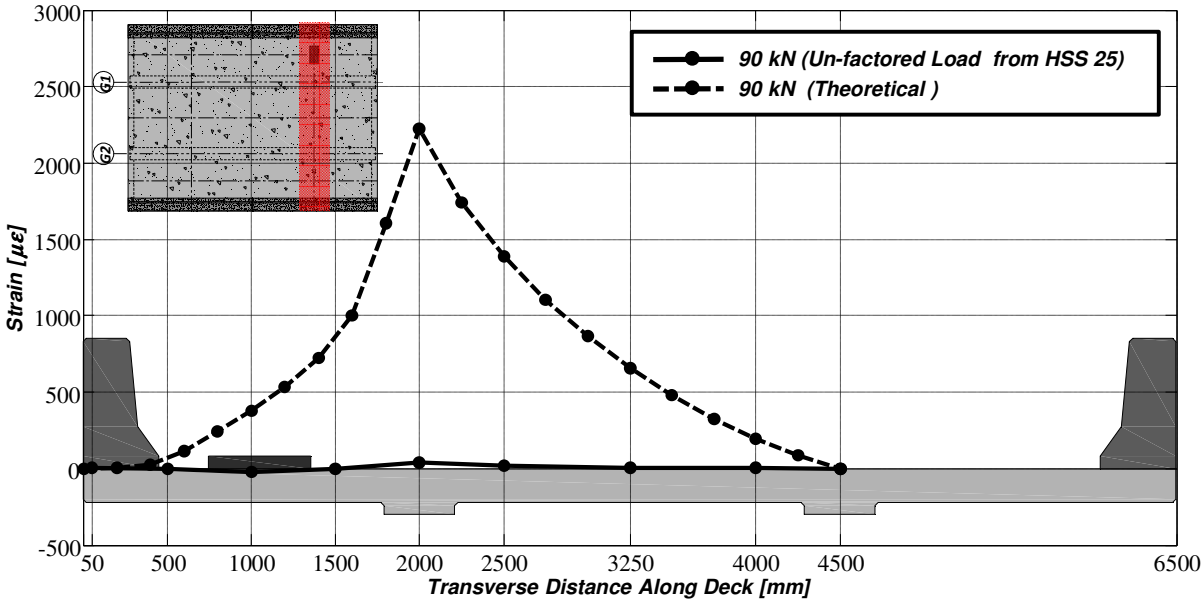

Figure 5-35: Comparison of experimental and theoretical top transverse reinforcing bar strain profiles along the transverse center-line of the applied load for the cantilever section with GFRP reinforcement subjected to static monotonic loading (service loads)

It is shown in Table 5-13 and plotted in Figure 5-36 as well as Table 5-14 and Figure 5-37 that the experimentally observed strains in the top transverse reinforcement provided in the internal panel are negligible. Flexural theory suggests that the strains in the internal panel should have been much greater as well. Theoretical strain values, based on purely flexural analysis, indicate that the bars should have been subjected to significantly higher strain magnitudes. The strains located in the first half of the internal panels span cannot be ignored. However strains in the top transverse bar beyond this point are negligible and are not predicted by flexural analysis. Hence confirming that the cantilever slabs response to concentrated wheel loads predominantly is arching action.

Table 5-13: Comparison of experimental and theoretical top transverse reinforcing bar strain profiles along the transverse center-line of the applied load for the cantilever section with steel reinforcement subjected to static monotonic loading

Load [kN]	Transverse distance along deck [mm]								
	50	500	1000	1500	2000	2500	3250	4000	4500
90 (Experimental)	4	6	-25	7	33	28	12	4	1
90 (Analytical)	0	23	105	239	614	384	182	54	0
% Difference	-	300.3	-523.0	3486.5	1757.5	1262.1	1379.2	1267.2	-
214 (Experimental)	12	9	-95	-5	104	71	26	6	-1
214 (Analytical)	0	23	105	265	969	584	285	92	0
% Difference	-	160.8	-210.0	-5396.6	835.1	724.9	1002.8	1344.7	-
428 (Experimental)	77	9	-95	43	875	536	79	14	-8
428 (Analytical)	0	23	105	310	1583	928	462	158	0
% Difference	-	169.1	-210.2	628.5	80.8	73.1	484.7	1003.6	-
772 (Experimental)	139	21	311	2166	1912	1402	206	18	-36
772 (Analytical)	0	23	105	383	13200	1483	747	265	0
% Difference	-	11.4	-66.3	-82.3	590.4	5.8	263.1	1400.3	-

Notes: *Transverse reinforcing bar theoretical strain magnitudes for the transverse distances of 500 and 1000 mm from the free edge were determined using linear interpolation*
Transverse reinforcing bar theoretical strain magnitudes for the loads of 214, 428, and 772 kN are not valid and are for illustration purposes only

Table 5-14: Comparison of experimental and theoretical top transverse reinforcing bar strain profiles along the transverse center-line of the applied load for the cantilever section with GFRP reinforcement subjected to static monotonic loading

Load [kN]	Transverse distance along deck [mm]								
	50	500	1000	1500	2000	2500	3250	4000	4500
90 (Experimental)	3	1	-24	1	37	20	8	4	0
90 (Analytical)	0	69	381	863	2220	1390	658	195	0
% Difference	-	6800.0	-1684.0	86200.0	5886.0	6819.7	8300.7	4472.2	-
214 (Experimental)	18	-1	-78	-28	132	29	24	9	0
214 (Analytical)	0	69	381	958	3508	2113	1030	333	0
% Difference	-	-5190.5	-591.2	-3545.9	2552.4	7212.1	4257.3	3779.6	-
428 (Experimental)	267	194	387	112	794	787	43	19	0
428 (Analytical)	0	69	381	1121	5730	3360	1673	573	0
% Difference	-	-64.4	-1.5	899.1	622.1	327.1	3760.5	2968.3	-
487 (Experimental)	384	198	892	1328	1332	1013	50	24	0
487 (Analytical)	0	69	381	1166	6343	3704	1850	639	0
% Difference	-	-65.1	-57.3	-12.2	376.3	265.8	3581.9	2598.0	-

Notes: *Transverse reinforcing bar theoretical strain magnitudes for the transverse distances of 500 and 1000 mm from the free edge were determined using linear interpolation*
Transverse reinforcing bar theoretical strain magnitudes for the loads of 214, 428,and 487 kN are not valid and are for illustration purposes only

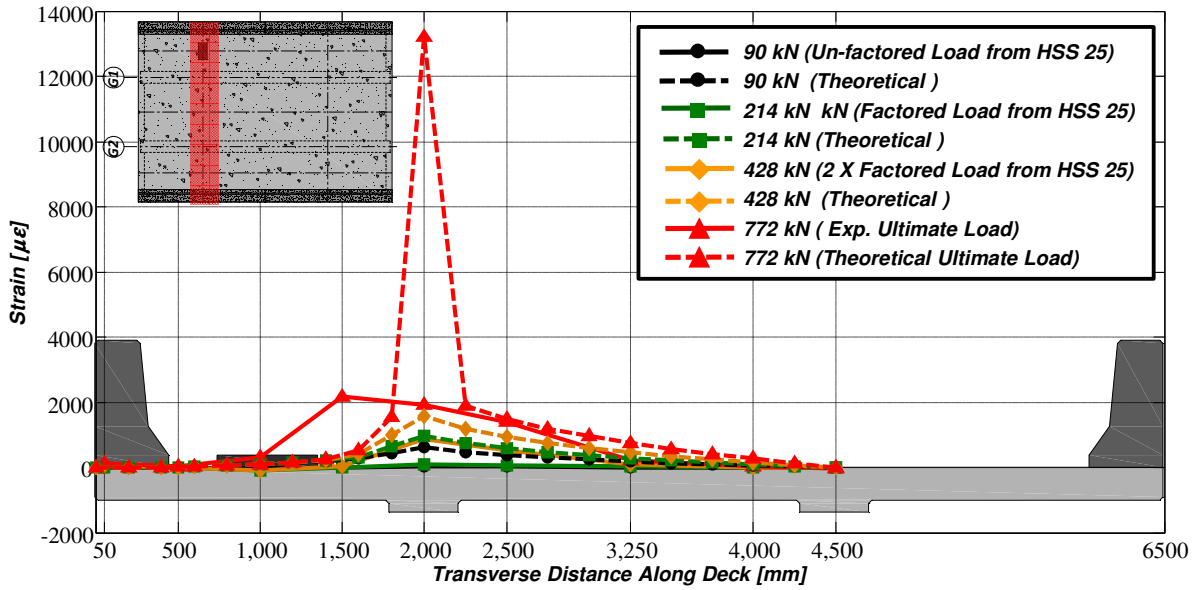

Notes: *Transverse reinforcing bar theoretical strain magnitudes for the loads of 214, 428, and 772 kN are not valid and are for illustration purposes only*

Figure 5-36: Comparison of experimental and theoretical static top transverse reinforcing bar strain profiles along the transverse center-line of the applied load for the cantilever section with steel reinforcement

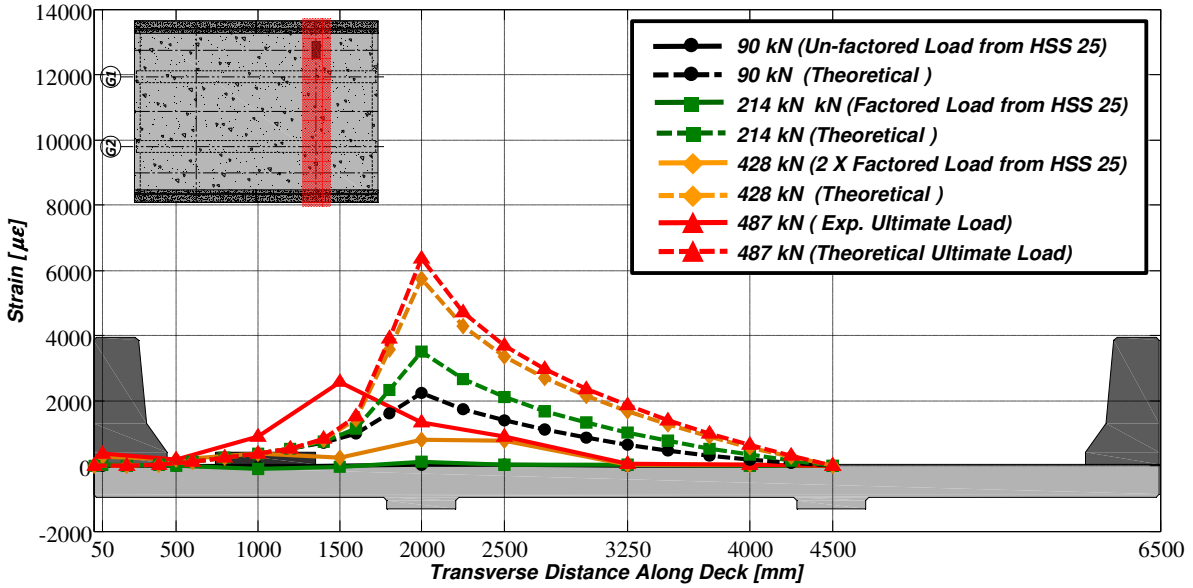

Notes: *Transverse reinforcing bar theoretical strain magnitudes for the loads of 214, 428, and 487 kN are not valid and are for illustration purposes only*

Figure 5-37: Comparison of experimental and theoretical static top transverse reinforcing bar strain profiles along the transverse center-line of the applied load for the cantilever section with GFRP reinforcement

5.3 Model for Estimating the Fatigue Life of the Cantilever Sections

Fatigue tests conducted on the internal panel of a second-generation steel free bridge deck (Memon, 2005) resulted in an equation for predicting the strength of a steel-free bridge deck. The equation was a modification of a load and number of cycles to failure relationship developed from rolling wheel tests conducted on full-scale reinforced and un-reinforced bridge decks (Matsui et al., 2001). The equation derived by Memon (2005) is written as:

$$n = 10^{\sqrt[c]{\frac{1}{P/P_u}-1}} \tag{5.13}$$

where n is the number of cycles to failure at the applied load P, P_u is the ultimate static load, and c is a constant determined from fatigue tests. In the absence of a fatigue curve obtained from experimental testing the value of c can be taken conservatively as 5.0. The values of c determined for the internal panel of a second generation steel-free bridge deck were 5.737 and 5.405 for a bottom crack control mat of GFRP and CFRP respectively. The fatigue behaviour of un-stiffened cantilever sections with top transverse GFRP and steel tested by Klowak (2007) and highlighted in Chapter 2, was very similar to that reported by Memon (2005). The same relationship was used to estimate the fatigue life of those two cantilever sections. Klowak (2007) reported that the ratio of applied load and the ultimate static load (P/P_u) was 0.633 for the cantilever section with top transverse GFRP reinforcement and indicated and that the cantilever section failed after completing 104,775 cycles. Thus, the constant c was determined to be 6.592. The un-stiffened cantilever section with top

transverse steel reinforcement, tested by Klowak (2007), specified that the ratio of applied load to the ultimate static load *(P/P_u)* was 0.595. The cantilever section failed after completing 422,517 cycles at 59.5 % of the static ultimate load of 301 kN. Therefore, the constant c for the cantilever with top transverse steel reinforcement was calculated to be 6.882 (Klowak, 2007). For the purposes of fatigue modeling the edge-stiffened cantilevers sections with steel and GFRP tested in the research program described in this thesis, Equation 5.13 was adapted and the constant *c* was modified for the two different cantilever sections.

5.3.1 Estimating the Fatigue Life for the Cantilever Section with Steel Reinforcement

The experimental results outlined in Chapter 4 for the cantilever section with steel reinforcement show that the ratio of applied load divided to the ultimate static load *(P/P_u)* was 0.622 and that the cantilever section failed after completing 514,647 cycles. Taking the log of both sides of Equation 5.13the the following expression for the constant *c* is obtained:

$$c = \frac{Log_{10} n}{\sqrt{\frac{1}{P/P_u} - 1}} \tag{5.14}$$

Inputting the number of cycles and the ratio of applied load and the static ultimate load *(P/P_u),* determined experimentally, in the above expression it is shown that for the cantilever section with steel reinforcement:

c = 7.327; cantilever section with steel reinforcement

Therefore, the equation for determining the number of cycles required cause a fatigue failure in an edge-stiffened cantilever slab overhang, with top and bottom 15M deformed steel reinforcement spaced and 300 mm in the longitudinal and transverse directions, is given by:

$$n = 10^{7.327\sqrt{\frac{1}{P/P_u}-1}} \tag{5.15}$$

Using Equation 5.15 and inputting different ratios of the applied load and the ultimate static load *(P/P_u)*, a S-N curve was generated. It can be used to estimate the number of cycles required to fail a cantilever with the steel reinforcement outlined in Chapter 3 (Table 5-15 and Figure 5-38).

Practically speaking, any applied wheel load lower than 50 % of the ultimate static capacity of the cantilever with steel reinforcement will not have an influence on fatigue life. Equation 5.13 illustrates that small changes in the applied load have pronounced or significant effects on fatigue life of bridge deck cantilever slabs that exhibit arching action. For example, if the applied load was increased from 50 to 60 % the fatigue life of the cantilever would be reduced by a factor of 22. If an applied load of 428 kN (two times the factored design wheel load) were applied to an edge-stiffened cantilever slab overhang reinforced with steel, it would have to undergo approximately 3.7 million cycles prior to fatigue failure. Considering loads of 90 and 214 kN (service wheel loads and factored design wheel loads) it is shown that loads of these magnitude would essentially have no influence on the fatigue life of an edge stiffened cantilever slab overhang reinforced with steel.

Table 5-15: Estimate of the number of cycles required to fail a cantilever with steel reinforcement subjected to fatigue cyclic loading

Applied Load (P) [kN]	Applied Load/Ultimate Static Load (P/P_u) [kN/kN]	No. of Cycles to Failure
772	*1*	*1.00E+00*
733	*0.95*	*4.80E+01*
695	*0.9*	*2.77E+02*
656	*0.85*	*1.20E+03*
618	*0.8*	*4.61E+03*
579	*0.75*	*1.70E+04*
540	*0.7*	*6.26E+04*
502	*0.65*	*2.38E+05*
463	*0.6*	*9.60E+05*
428	***0.55***	***3.70E+06***
425	*0.55*	*4.24E+06*
386	*0.5*	*2.12E+07*
347	*0.45*	*1.26E+08*
309	*0.4*	*9.41E+08*
270	*0.35*	*9.66E+09*
232	*0.3*	*1.56E+11*
214	***0.28***	***6.78E+11***
193	*0.25*	*4.91E+12*
154	*0.2*	*4.51E+14*
116	*0.15*	*2.77E+17*
90	***0.12***	***1.48E+20***
77	*0.1*	*9.57E+21*
39	*0.05*	*8.66E+31*
0	*0*	∞

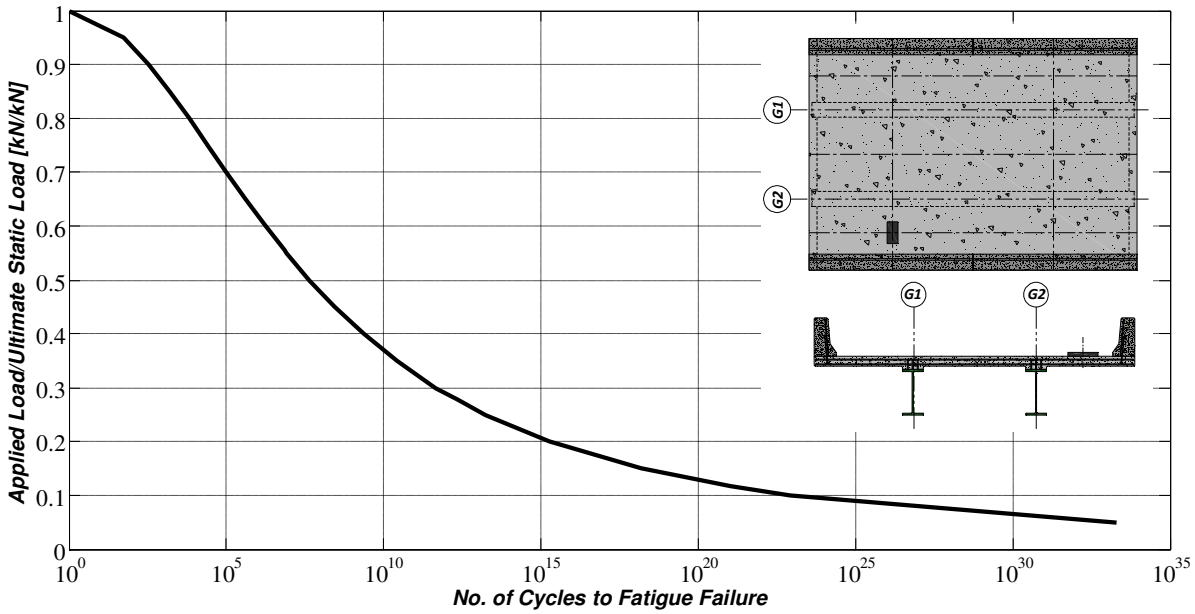

Figure 5-38: Plot of ratio of the applied load divided the ultimate static load versus number of cycles to required to fail a cantilever with steel reinforcement subjected to fatigue cyclic loading

5.3.2 Estimating the Fatigue Life for the Cantilever Section with GFRP Reinforcement

Experimental results outlined in Chapter 4 for the cantilever section with GFRP reinforcement specified that the ratio of applied load and the ultimate static load (P/P_u) obtained from the static destructive test was 0.626. The cantilever section successfully completed 2,000,000 cycles subjected to a fatigue cyclic load of 305 kN. Upon achieving 2,000,000 cycles, a static destructive test to failure was conducted and the cantilever with GFRP reinforcement failed in punching shear at an ultimate load of 513 kN. Therefore, if the assumption is made that the previous 2,000,000 cycles did not have an effect on the ultimate static load, the ratio of applied load and the ultimate static load (P/P_u) obtained from cycle 2,000,001 was 0.595.

It is important to note that the estimate for fatigue life shown in equation 5.13 is based on an important assumption that the geometry of the cantilever slab (i.e. deflections, strains, and resulting crack widths) are the same for both static and fatigue loading conditions. Therefore, a fatigue failure will occur when fatigue deflections, strains, and crack widths approach the ultimate deflections, strains, and crack widths obtained under static loads.

Upon reviewing Figure 4-12 In Chapter 4, it can be shown that the deflection under the steel loading plate had increased to 10.26 mm at the applied cyclic load of 305 kN. The maximum deflection recorded at the ultimate load of 487 kN during the initial static test was measured to be 10.9 mm. The transverse crack on the underside of the cantilever had grown to approximately 0.8 mm after completing 2,000,000 cycles (Figure 4-64). The ultimate transverse crack width measured at the initiation of the punching shear failure observed during the static test conducted earlier was approximately 1.2 mm. Based on the experimentally observed fatigue deflections and crack widths it is fair to state that the cantilever with GFRP reinforcement may have been approaching fatigue failure. It has been determined that unless a deck slab has surpassed at least 85 % of its fatigue life that previous fatigue cycles do not influence the residual static punching shear capacity (Edalatmanesh and Newhook, 2013). Based on the observed residual static capacity of the cantilever section with GFRP reinforcement (i.e. 513 kN) after completing 2,000,000, and findings reported on by Edalatmanesh and Newhook, (2013), for steel or corrosion-free deck panels, it can also be strongly argued that the cantilever section with GFRP reinforcement must have only been subjected to less than 85 % of its fatigue life. Employing engineering judgment, two conservative estimated constants are presented for the two different observed static ultimate

load capacities observed during testing. Thus, a conservative assumption that the deck with GFRP reinforcement failed after achieving 2,000,000 cycles will be used for the purposes of this thesis and for generating an approximate fatigue life estimation relationship.

Substituting 2,000,000 cycles and ratio of applied load divided by the static ultimate load *(P/P_u)* for the initial ultimate static load of 487 kN determined experimentally in the Equation 5.14, the constant *c* for the cantilever section with GFRP reinforcement becomes:

c = 8.157; cantilever section with GFRP reinforcement (Ultimate static load of 487 kN)

Therefore, the number of cycles required to fail a cantilever with the GFRP reinforcement described in Chapter 3, is expressed as:

$$n = 10^{8.157\sqrt{\frac{1}{P/P_U}-1}} \tag{5.16}$$

If the static ultimate load of 513 kN is used, assuming that the previous 2,000,000 cycles had no detrimental effect on the observed residual ultimate static load obtained during cycle 2,000,001, the constant c for the cantilever with GFRP reinforcement is calculated to be:

c = 7.630; cantilever section with GFRP reinforcement (Ultimate static load of 513 kN)

Therefore, the number of cycles required to fail a cantilever with the GFRP reinforcement described in Chapter 3, may alternatively be expressed as:

$$n = 10^{7.630\sqrt{\frac{1}{P/P_U}-1}} \tag{5.17}$$

The latter of the two equations is more conservative when estimating the fatigue life. It must also be noted that these equations are presented as a conservative estimate of the fatigue of a cantilever with GFRP reinforcement described in Chapter 3. However, they may not be an accurate representation because the cantilever section did not fail under fatigue loading conditions. It can only be stated with certainty, based on other research findings, that the cantilever slab overhang was subjected to less than 85 % of its fatigue life based on experimentally observed data. It cannot exactly be determined how much less than 85 % of its fatigue life it was subjected to. The tables and figures illustrated are a conservative estimate of fatigue life.

By substituting different ratios of applied load divided by the ultimate static load *(P/P_u)* into Equation 5.16 and 17, two different S – N or fatigue life estimation curves were generated. They may be used to estimate the number of cycles required to fail a cantilever with the particular reinforcing scheme described in Chapter 3 (Table 5-16, Table 5-17 as well as Figure 5-39).

Like the cantilever section with top transverse steel, any applied cyclic load lower than 55 % of the ultimate static capacity of the cantilever with top transverse GFRP will not have an influence on fatigue life. Utilizing Equation 5.17 it is shown that small changes in the applied load cause significant changes to the fatigue life. For instance, if the applied load was increased from 55 to 65 %, the fatigue life of the cantilever would have been reduced by a factor of 18. Again, it is extremely important to note that these equations for a cantilever slab overhang reinforced with GFRP are only rough approximations of the fatigue life.

Table 5-16: Estimate of the number of cycles required to fail a cantilever with GFRP reinforcement subjected to fatigue cyclic loading (Ultimate static load of 487 kN)

Applied Load (P) [kN]	Applied Load/Ultimate Static Load (P/P_u) [kN/kN]	No. of Cycles to Failure
487	*1*	*1.0000E+00*
463	*0.95*	*7.4361E+01*
438	*0.9*	*5.2360E+02*
428	***0.88***	***2.0553E+07***
414	*0.85*	*2.6707E+03*
390	*0.8*	*1.1981E+04*
365	*0.75*	*5.1221E+04*
341	*0.7*	*2.1878E+05*
317	*0.65*	*9.6739E+05*
292	*0.6*	*4.5726E+06*
268	*0.55*	*2.3894E+07*
244	*0.5*	*1.4355E+08*
219	*0.45*	*1.0421E+09*
214	***0.44***	***1.4848E+13***
195	*0.4*	*9.7779E+09*
170	*0.35*	*1.3065E+11*
146	*0.3*	*2.8842E+12*
122	*0.25*	*1.3438E+14*
97	*0.2*	*2.0606E+16*
90	***0.18***	***2.8471E+22***
73	*0.15*	*2.6154E+19*
49	*0.1*	*2.9580E+24*
24	*0.05*	*3.5937E+35*
0	*0*	∞

Table 5-17: Estimate of the number of cycles required to fail a cantilever with GFRP reinforcement subjected to fatigue cyclic loading (Ultimate static load of 513 kN)

Applied Load (P) [kN]	Applied Load/Ultimate Static Load (P/P_u) [kN/kN]	No. of Cycles to Failure
513	*1*	*1.0000E+00*
487	*0.95*	*5.6291E+01*
462	*0.9*	*3.4941E+02*
436	*0.85*	*1.6041E+03*
428	***0.83***	***6.9248E+06***
410	*0.8*	*6.5313E+03*
385	*0.75*	*2.5420E+04*
359	*0.7*	*9.8857E+04*
333	*0.65*	*3.9709E+05*
308	*0.6*	*1.6977E+06*
282	*0.55*	*7.9725E+06*
257	*0.5*	*4.2658E+07*
231	*0.45*	*2.7245E+08*
214	***0.42***	***2.0926E+12***
205	*0.4*	*2.2121E+09*
180	*0.35*	*2.5000E+10*
154	*0.3*	*4.5187E+11*
128	*0.25*	*1.6427E+13*
103	*0.2*	*1.8197E+15*
90	***0.18***	***1.0085E+21***
77	*0.15*	*1.4556E+18*
51	*0.1*	*7.7625E+22*
26	*0.05*	*1.8130E+33*
0	*0*	∞

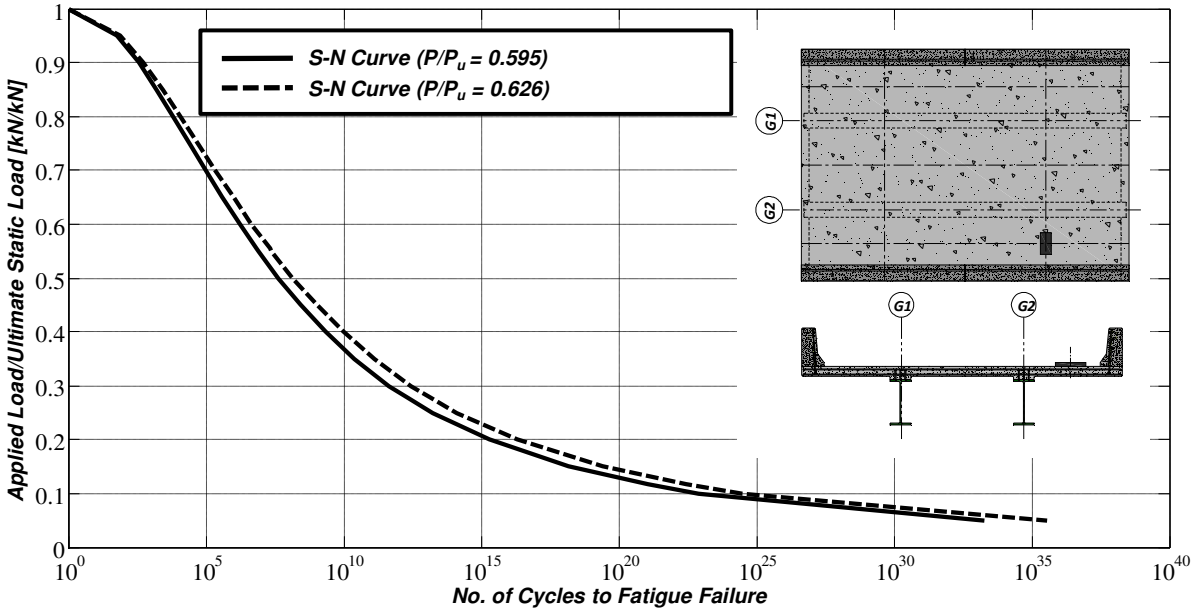

Figure 5-39: Plot of ratio of applied load divided by the ultimate static load versus number of cycles required to fail a cantilever with GFRP reinforcement subjected to fatigue cyclic loading (Ultimate static load of 487 and 513 kN)

5.3.3 Comparison of the Fatigue Life of the Cantilever Sections with Top Transverse GFRP and Steel

The cantilever with steel reinforcement was subjected to an average fatigue cyclic load of 480 kN or 62.2 % of the ultimate static load obtained from the static test conducted earlier. Therefore, the S-N or fatigue curve shown on Figure 5-39 is an accurate representation based on observed experimental data. The cantilever with GFRP was subjected to an average fatigue cyclic load of 305 kN or 62.6 % of the ultimate static load observed from the previously conducted static test to failure. It achieved 2,000,000 cycles at the calculated applied load and the ultimate static load ratio (P/P_u) of 0.626. A static test to failure revealed that the ultimate static load was 513 kN resulting in an applied load and the ultimate static load ratio (P/P_u) of 0.595. As discussed in the previous section, it was assumed that the

2,000,000 cycles did not influence the residual static punching shear capacity of the cantilever section with GFRP reinforcement.

If the higher of the two ratios for the cantilever with GFRP reinforcement is considered, it is shown in Table 5-18 and Figure 5-40 that the cantilever section with GFRP had a greater resistance to fatigue than the cantilever section reinforced with conventional steel. A ratio of applied load and the ultimate static load (P/P_u) of 0.75 leads to theoretical fatigue life 3 times greater than that of a cantilever section reinforced with steel. As the ratio of applied load and the ultimate static load (P/P_u) is reduced, the theory leads to an even greater resistance to fatigue failure for the cantilever section with GFRP reinforcement.

If higher ultimate static load for the cantilever with GFRP reinforcement is taken into account, it indicates a lower ratio of applied load and the ultimate static load (P/P_u) equal to 0.595 and a reduced fatigue life, assuming that fatigue failure occurred at 2,000,000 cycles. Therefore, at ratio of applied load divided by the ultimate static load (P/P_u) of 0.75 a more conservative theoretical fatigue life was calculated indicating that the cantilever section with GFRP reinforcement only had a theoretical fatigue life 1.5 times greater than the cantilever section with steel reinforcement. These results indicate that a 5.3 % change in the ultimate static load (could be considered experimentally identical) can influence the fatigue life by two times for a given applied load. Small decreases in static load carrying capacity can significantly reduce fatigue life when bridge deck cantilever slab overhangs are very heavily loaded. Even at lower applied load magnitudes such as design loads and service loads, small changes in ultimate static load have a very large influence on the overall fatigue performance

as fatigue life approaches infinity. However, considering the vast number of cycles required to cause fatigue failure at lower load levels, the small changes in ultimate static load will essentially or practically speaking have little influence on the fatigue life of a cantilever slab over the service life of a bridge.

The experimental test results indicated that fatigue life, under the same cyclic load (588 kN), for a conventionally reinforced deck slab with steel and a second generation steel-free deck slab with bottom GFRP were significantly different (Memon, 2005). The deck slab with external steel straps and internal GFRP failed after 420,684 cycles and the conventionally reinforced deck slab failed after only 23,162 cycles. Therefore, the fatigue resistance of the steel-free section was approximately 20 times that of the conventionally reinforced section.

Previous testing has indicated that GFRP reinforced or corrosion-free deck slabs of internal panels that exhibit arching action have superior fatigue life when compared to conventional reinforced steel deck slabs (Memon, 2005). Based on the experimental results of this research program, it has been shown that GFRP reinforced cantilever slab overhangs with arching action, have greater fatigue resistance than those reinforced with steel reinforcement. The theoretical results presented are conservative estimates because the cantilever section with GFRP reinforcement did not fail under fatigue loading conditions. It can be said with certainty that the fatigue life of a cantilever section reinforced with GFRP is at least 15 % greater than shown and possibly even greater.

Table 5-18: Comparison of fatigue life for cantilever sections with top transverse GFRP and steel reinforcement subjected to fatigue cyclic loading

Applied Load/Ultimate Static Load (P/Pu) [kN/kN]	No. of Cycles to Failure (Steel Reinforced)	No. of Cycles to Failure (GFRP Reinforced; Pu = 487 kN)	Percent Difference [%]	No. of Cycles to Failure (GFRP Reinforced; Pu = 513 kN)	Percent Difference [%]
1	*1.00E+00*	*1.0000E+00*	*0.0*	*1.0000E+00*	*0.0*
0.95	*4.80E+01*	*7.4361E+01*	*55.0*	*5.6291E+01*	*17.4*
0.9	*2.77E+02*	*5.2360E+02*	*89.1*	*3.4941E+02*	*26.2*
0.85	*1.20E+03*	*2.6707E+03*	*123.2*	*1.6041E+03*	*34.1*
0.8	*4.61E+03*	*1.1981E+04*	*160.0*	*6.5313E+03*	*41.7*
0.75	*1.70E+04*	*5.1221E+04*	*201.4*	*2.5420E+04*	*49.6*
0.7	*6.26E+04*	*2.1878E+05*	*249.4*	*9.8857E+04*	*57.9*
0.65	*2.38E+05*	*9.6739E+05*	*306.5*	*3.9709E+05*	*66.9*
0.6	*9.60E+05*	*4.5726E+06*	*376.1*	*1.6977E+06*	*76.8*
0.55	*4.24E+06*	*2.3894E+07*	*463.3*	*7.9725E+06*	*88.0*
0.5	*2.12E+07*	*1.4355E+08*	*576.1*	*4.2658E+07*	*100.9*
0.45	*1.26E+08*	*1.0421E+09*	*727.2*	*2.7245E+08*	*116.3*
0.4	*9.41E+08*	*9.7779E+09*	*938.8*	*2.2121E+09*	*135.0*
0.35	*9.66E+09*	*1.3065E+11*	*1252.4*	*2.5000E+10*	*158.8*
0.3	*1.56E+11*	*2.8842E+12*	*1752.9*	*4.5187E+11*	*190.3*
0.25	*4.91E+12*	*1.3438E+14*	*2639.1*	*1.6427E+13*	*234.8*
0.2	*4.51E+14*	*2.0606E+16*	*4470.9*	*1.8197E+15*	*303.6*
0.15	*2.77E+17*	*2.6154E+19*	*9357.9*	*1.4556E+18*	*426.4*
0.1	*9.57E+21*	*2.9580E+24*	*30803.0*	*7.7625E+22*	*711.0*
0.05	*8.66E+31*	*3.5937E+35*	*414745.3*	*1.8130E+33*	*1992.9*
0	∞	∞	-	∞	-

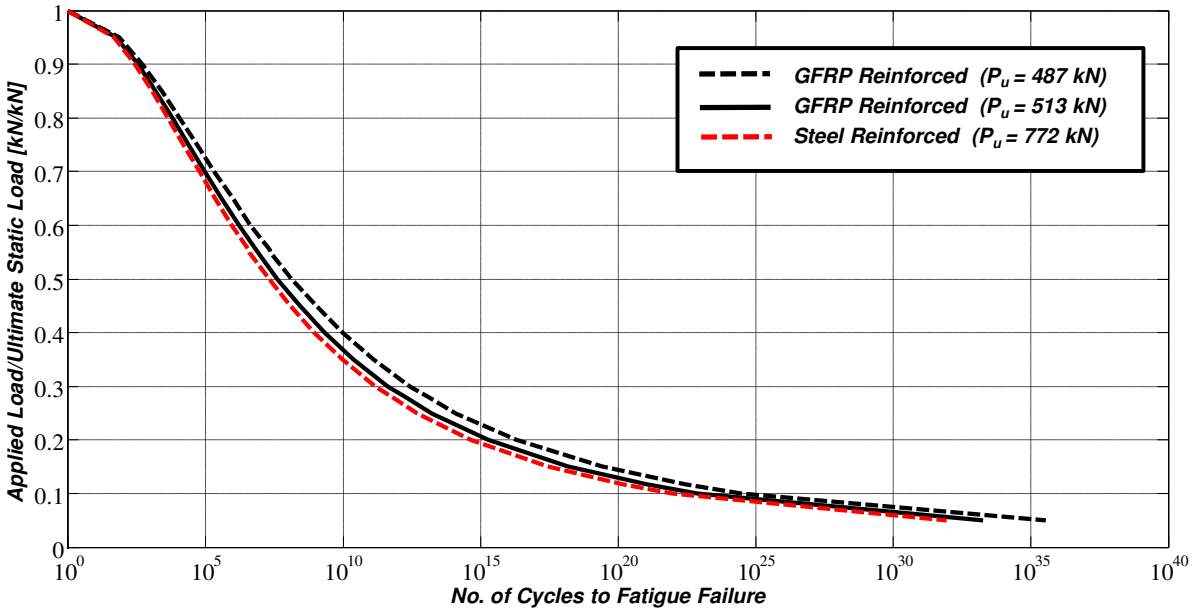

Figure 5-40: Comparison of fatigue life curves for cantilever sections with top transverse GFRP and steel subjected to fatigue cyclic loading

The fatigue curves that were generated are applicable to bridges in service. However, engineers must consider that for cantilevers or bridge decks in service that the ultimate load, $P_{u,}$ for a particular component is changing and decreasing over the its service life. A decrease in the ultimate load will usually be dictated by the environmental conditions and environmental effects such as chloride penetration into the concrete. The decrease in ultimate load will shift the fatigue or S-N curves outlined to the left for a given applied load, thus reducing the fatigue life. It is noted that under service conditions applied loads are well below a level that will affect fatigue life. A reduction in the ultimate due to environmental effects will most likely not affect the fatigue life of a cantilever similar to those tested or a particular bridge component.

6. CONCLUSIONS & RECOMMENDATIONS

Static and fatigue experimental destructive testing was conducted on a full scale model of an edge-stiffened cantilever slab overhangs of a corrosion or steel-free bridge deck to reinvestigate the behaviour of the cantilevers subjected to concentrated loads or wheel loads. Current analysis and design is based on the assumption that the response of bridge deck cantilevers to applied live loads on the cantilever overhangs is purely flexural; and that the flexural effects are not only limited to the overhangs, but also extend into the adjacent internal panel of the bridge deck slab. The model was designed according to the CAN/CSA S6-06 Canadian Highway Bridge Design Code (CHBDC) which is based on the above assumptions.

Several conclusions and recommendations can be drawn from the test results and the analytical tools used to evaluate the model. Conclusions and arguments for the presence of arching action will be discussed with respect to several of the experimentally observed parameters such as ultimate loads, deflections, strains, crack patterns and widths, barrier wall behavior, and modes of failure. Theoretical models that confirmed the experimental behavior will also be presented.

The objective of the following conclusions and recommendations is to raise the awareness that edge-stiffened bridge deck cantilever overhangs subjected to concentrated loads (such as wheel loads) dominantly behave or respond to the applied load via arching action (AA). Recommendations based on the conclusions derived from the experimental test data and analytical modeling techniques provide engineers with potential design provisions and

reinforcement reductions that may be implemented in future bridge design and construction projects.

6.1 Conclusions

6.1.1 Observed Static Ultimate Loads

The observed experimental ultimate static load was 772 kN and 487 kN for the cantilever section reinforced with steel and GFRP respectively. The factored design live load was 214 kN (CL-625 design truck; CAN/CSA S6-06 CHBDC 2006). The very large differences between the design failure loads and the actual observed failure loads, which cannot be accounted for by material resistance and design factors, clearly indicate the presence of arching action in cantilever slab overhangs. Another simple argument for the presence of arching action based on the experimentally observed ultimate static loads is that both cantilever sections (i.e. steel and GFRP) had approximately the same nominal moment resistance based on the top transvers reinforcing bars for negative moment resistance. The moment resistance for the cantilever sections with steel and GFRP reinforcement were 111.0 kN*m and 124.0 kN*m respectively. Hence, the ultimate static loads should have been a lot closer in magnitude based on a flexural response to the applied load. Analytical FEM also theoretically confirmed the experimental ultimate static loads to an accuracy of -11.9 % and 6.8 % for the cantilever section with steel and GFRP respectively. Therefore, it can be stated that that arching action played a dominant role in the observed ultimate static loads.

6.1.2 Static and Fatigue Deflections

The significant experimental and theoretical observation with respect to deflection related behavior is obvious after reviewing the static and fatigue transverse deflection profiles along the transverse center line of the applied load. Experimental static and fatigue transverse deflection profiles indicate a transition from positive curvature to negative curvature in the vicinity of the loading plate. Theoretical transverse deflection profiles confirmed the deflection profiles and transition as well. The transition in curvature in the vicinity of the loading plate can be described as looking almost like a "spoon". If pure flexure was present, only negative curvature should have been present between the external girder and loading plate. Consequently, it can be concluded that the transverse deflection profiles indicate a strong influence of the edge-stiffening provided by the barrier wall which led to arching action in the cantilever deck slab.

6.1.3 Static and Fatigue Top Transverse Reinforcing Bar Strains

Two major conclusions can be made based upon experimental test results and analytical modeling using flexural theory. Experimental top transverse strain profiles for the static and fatigue destructive testing for both cantilever sections confirmed conclusions made by Klowak (2007) regarding load induced effects in the adjacent internal panel as a result of the applied wheel load on the cantilever. Static and fatigue strains and stresses observed in the top transverse bars, provided for negative bending moments in the cantilever sections with steel and GFRP reinforcement, illustrated that the bars are not subjected to significant stress

beyond half way to the adjacent girder. Strains observed were less than 200 με indicating that strains in the top transverse bars are negligible beyond the mid-point of the span between the external and next adjacent girder. Reinforcing bars, required for flexural strength are not required beyond half the distance of the internal panel adjacent to the loaded cantilever.

Theoretical strains obtained from flexural analysis and strain compatibility did not agree with the experimentally observed strains. In fact, they were significantly different. The large discrepancy between the experimentally observed top transverse reinforcing bar strains and theoretical strains provides confirmation that an edge-stiffened cantilever slab overhang subjected to a wheel load exhibits arching action and compressive membrane forces in response to the applied load.

6.1.4 Bottom Reinforcing Bar Strains under Static and Fatigue Loads

Research findings by Klowak (2007) prompted the instrumentation of the bottom transverse and longitudinal reinforcement in both cantilever sections. Strain gauges installed on the bottom bars revealed a significant observation. Contradictory to flexural theory, the bottom transverse bars demonstrated significant tensile stresses and strains under the applied static and fatigue loads applied on the cantilever sections with both steel and GFRP. Klowak and Mufti (2007) stated that the top transverse reinforcement provided for negative moment did not play a role in the observed experimental ultimate loads due to the presence of arching action in un-stiffened cantilever slab overhangs. Their findings were based on cantilever sections that had different negative moment resistances that failed at experimentally identical

loads. In the case of this research program, it was the bottom transverse and longitudinal reinforcing ratios that differed. The cantilever with steel reinforcement contained 15M steel bars at 300 mm center to center in both directions. The cantilever with GFRP reinforcement was reinforced with No. 10 GFRP at 500 mm center to center in both the transverse and longitudinal directions. The observed experimentally different static ultimate loads and excessive tensile strains for both cantilever sections provided conclusive evidence that the axial stiffness of the bottom reinforcing bars played a major role in the observed failure loads. The cantilever with steel failed at 772 kN and displayed tensile strains in the bottom transverse bars of 3238 με at failure. The cantilever with GFRP failed at 487 kN and a maximum tensile strain of 3355 με. The presence of arching action and the difference in the bottom reinforcement ratios are the cause of the observed difference in static ultimate loads.

Fatigue test results also confirmed excessive tensile strains in the bottom transverse and longitudinal reinforcing bars for both cantilever sections. In both cases, the bottom transverse reinforcing was found to be ruptured due to fatigue loads providing conclusive evidence that the bottom transverse reinforcement aided in lateral restraint typical to arching action which led to significantly higher ultimate loads and the observed punching shear failures.

6.1.5 Top Concrete Surface Strains of the Cantilever Slab Overhang under Static and Fatigue Loads

Strains measured on the top surface of the cantilever slab overhang, obtained from a concrete strain gauge adjacent to the steel loading plate measured large compressive strains in the transverse direction for the cantilever section with GFRP reinforcement. The maximum compressive strain measured during the destructive static monotonic test to failure was -1420 με. The compressive strains observed contradicted classical flexural behaviour and indicated behaviour typical to arching action. Fatigue cyclic loading on the cantilever with GFRP reinforcement confirmed the compressive stresses present on the opposite cantilever during the static test. The cantilever with GFRP did not failure under the fatigue loading conditions. However, during the static test to failure after completing 2,000,000 cycles, large compressive strains were again observed and were measured to be -1030 με. The observed compressive strains provided additional conclusive experimental evidence and confirmed the hypothesis that arching action is present in edge-stiffened cantilever slab overhangs subjected to wheel loads.

6.1.6 Static Strain Compatibility below Loading Plate

Both strain compatibility and strains observed below the loading plate provide the strongest argument for the presence of arching action in edge-stiffened bridge deck cantilever slab overhangs subjected to a wheel or concentrated load. Flexural theory for a cantilever slab dictates that the top surface of the cantilever should be subjected to tensile stresses and strains and that the bottom surface shall undergo compressive stresses and strains. The

strains observed in the top transverse and bottom transverse reinforcing bars for both cantilever sections have already been discussed in the previous sections. However, the strains on the top surface and top and bottom transverse reinforcing bars plotted against the depth of the slab confirm strain compatibility and the assumption that plane sections remain plane. They clearly illustrate that in the vicinity of the loading plate the cantilever slab overhang is subjected to significant compressive strains on the top surface of the concrete. The top transverse bar was subjected to compressive stresses early in the loading history but then transitioned to tensile stresses as a result of cracking on the underside of the cantilever slab indicating a shift in the neutral axis. The bottom transverse reinforcing bars were only subjected to tensile strain that grew to magnitudes of a few thousand micro strains prior to a punching shear failure. The strain compatibility profiles indicated the great difference in compressive and tensile strengths of the concrete and the migration of the neutral axis as the underside of the cantilever slab cracked due to tensile stress enabling arching action or compression membrane action. The experimentally observed strain compatibility clearly identified the strong presence of arching action in edge-stiffened cantilever slab overhangs.

6.1.7 Crack Mapping and Crack Widths under static and Fatigue Wheel Loads

Static crack patterns for both cantilever sections indicated a strong presence of arching action in bridge deck cantilever slab overhangs. Crack patterns on the underside of both cantilever slab overhangs were identical to the cracking patterns typical to internal panels subjected to a concentrated load that exhibit arching or compression membrane action. Transverse cracks and radial cracks originating below the loading plate complement the observed tensile strain

magnitudes for the bottom reinforcement and the conclusion that arching action dominant factor in the behaviour of a cantilever slab overhang loaded under a wheel load. Smaller crack widths were observed on the underside of the cantilever with steel reinforcement due to the higher axial stiffness of the bottom reinforcement. Larger crack widths for the cantilever with GFRP were observed. Another interesting observation was that longitudinal cracks over the girder that would be typical to flexural behaviour were not present until loads of approximately 280 to 320 kN. If flexural behaviour governs the response to the wheel load, these cracks should have been present a lot earlier in the loading history, not to mention that the cantilever possibly should have failed prior to reaching the longitudinal cracking loads observed.

Fatigue cyclic loads applied to the cantilever section with steel reinforcement caused larger crack widths due to the excessive damage on the underside of the cantilever compared to the initial static test. Crack widths grew to magnitudes of 5.0 mm at the onset of the fatigue punching shear type failure. Longitudinal crack widths on the top surface of the cantilever with steel did not grow in width during the 514,647 cycles indicating that maximum negative moment intensities over the girder and flexure did not govern the fatigue performance and behaviour further strengthening the argument for the presence of arching action. Fatigue testing on the cantilever section with GFRP did not achieve the widths observed during the initial static test. However, the largest cracks widths were also observed on the underside of the cantilever overhang dictating that tensile stresses on the underside, below the load, are the strongest indicator of fatigue damage and the behaviour associated with arching action.

6.1.8 Static and Fatigue Barrier Wall Behaviour

Conclusive evidence that the traffic barrier walls act as edge-stiffening and improve the presence of arching action was provided via measured strains in the longitudinal GFRP reinforcing bars located in the barrier walls. The ultimate load achieved by the cantilever with steel reinforcement was great enough to induce flexural cracking in the barrier wall. The strains measured and plotted against the depth of the barrier provided strain profiles that confirmed classical engineering theory and indicated that the barrier wall carries significant load and acts as a supporting girder from above as researchers had anticipated. The lower ultimate load measured for the cantilever with GFRP reinforcement induced less flexural cracking in the barrier wall but bending strains still revealed that it provided edge-stiffening, enhanced arching action behaviour, and carried load as anticipated.

The strains measured on the longitudinal GFRP reinforcement for both cantilever sections subjected to fatigue loads confirmed the behaviour observed from the static tests previously conducted. Higher applied fatigue loads for the cantilever with steel produced cracking in the barrier and shifted the neutral axis towards the top of the traffic barrier and illustrated the assumption that plane sections remain plane. The lower applied fatigue cyclic load to the cantilever section with GFRP did not induce cracking and strains which dictated no shift in the neutral axis. All four test locations provided strong evidence to conclude that the barrier walls carry load, act as a supporting structural member from above, and enhance the presence of arching action.

6.1.9 Modes of Failure under Static and Fatigue Loads

All four cantilever test locations demonstrated punching shear failures common to arching or compression membrane action. The cantilever with steel and GFRP reinforcement failed at the ultimate load of 772 and 487 kN respectively. The cantilever with steel reinforcement failed after being subjected to 514,647 cycles at a load of 480 kN or 62.2 % of the static ultimate load obtained in initial static test. The damage due to fatigue, for the cantilever reinforced with steel, was far more excessive and included ruptured bottom transverse and top transverse reinforcing bars. The static test performed on the cantilever section with GFRP after completing 2,000,000 fatigue cycles produced the most pronounced punching shear failure and punch cone typical to arching action. Diagonal shear cracks also representative of arching action were clearly visible during the cutting required for the demolition of the test bridge deck. Hence, it can be concluded that arching action which typically results in punching shear, were the static and fatigue modes of failure.

6.2 Recommendations

6.2.1 Reduction in Top Transverse Reinforcement in the Internal Panel Adjacent to the Cantilever Slab Overhang

Experimental results and conclusions reported by Klowak and Mufti (2007) were further confirmed with static and fatigue full-scale destructive testing on two edge-stiffened cantilever slab overhangs, one reinforced with conventional steel and the other reinforced with GFRP. It can be stated with confidence that stresses and strains observed experimentally, from a total of three static and three fatigue tests conducted on unstiffened

cantilever slab overhangs as well as two static and two fatigue tests on edge stiffened cantilever slabs, are negligible beyond half the distance of the adjacent internal panel to the next supporting bridge girder (Figure 6-1). Typically, top transverse reinforcement required to resist negative moments due to loads on the cantilevers or impacts on the barrier wall is terminated at the adjacent girder from the outer most girder. There is no strength requirement for top transverse reinforcement required in this zone due to the presence of arching action. Therefore, it is recommended that the top transverse reinforcement provided in bridge deck slabs to resist negative moment as a result of wheel loads on cantilever slab overhangs be reduced to account for the presence of arching action. This recommendation may be considered for inclusion in such documents as the CAN/CSA S6-06 Canadian Highway Bridge Design Code (CHBDC) Clause 5.7.1.6.1.2. Obviously, minimum reinforcement for thermal effects, crack control, as well as shrinkage shall be provided in the regions where the reduction in top transverse may be permitted (Figure 6-1).

6.2.2 Potential Design Provisions that take into Account Arching Action (AA) or Compression Membrane Action (CMA)

The experimental test results confirmed by theoretical modeling presented in this investigation provide conclusive evidence that arching action is present in edge-stiffened bridge deck cantilever slab overhangs subjected to wheel loads. Current design practices for cantilever slab overhangs use flexural theory for design and analysis. Cantilever overhangs are designed to resist factored dead loads (self-weight of the overhang itself, asphalt overlays if required, and the self-weight of the traffic barrier walls) and factored live loads including a dynamic load allowance (DLA) for wheel loads from truck traffic. They are also designed to

resist moments that would result from an impact on the traffic barrier wall. The moment resistance required from the impact on the barrier wall is commonly the governing design criteria for the top transverse reinforcing bars.

The study presented recommends the following design provision that may be considered for inclusion in such documents as the CAN/CSA S6-06 Canadian Highway Bridge Design Code (CHBDC) Clause 5.7.1.6. Figure 6-1 summarizes the proposed design recommendations.

> *Due to the presence of arching action and compression membrane action in edge-stiffened bridge deck cantilever slab overhangs subjected to wheel loads, the cantilever slab overhang shall be designed to resist only negative bending moments caused by an impact on the traffic barrier wall if the following criteria are satisfied:*
>
> - *The bottom transverse and longitudinal reinforcement have been designed according to the empirical design method as outlined in section 8.18.4 of the CAN/CSA S6-06 CHBDC, or an alternate accepted method of design, and the bottom mat of reinforcement is also provided in the cantilever slab overhang*
> - *The traffic barrier wall and connection to the cantilever slab has been designed to resist impacts from the appropriate design vehicle*

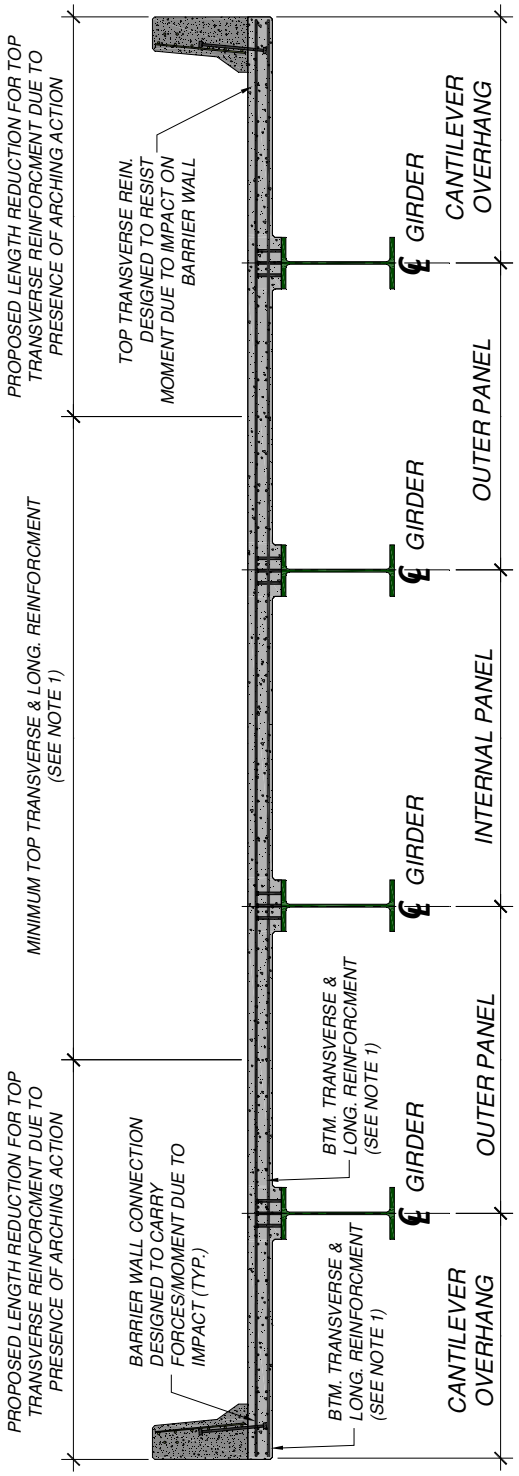

Figure 6-1: Proposed design provisions for edge-stiffened cantilever slab overhangs

NOTES:

1. *All reinforcement with the exception of the top transverse reinforcing bars in the cantilever slab overhangs (Designed to resist negative bending moments resulting from an impact on the traffic barrier) shall designed according to Clause 8.18.4 of CAN/CSA S6-06 CHBDC empirical design method or other appropriate design methods as specified by the CAN/CSA S6-06 CHBDC*

6.2.3 Further Experimental Research

Further experimental full-scale destructive testing is recommended to confirm the conclusions presented in this study. There are many factors that may influence the behavior and magnitude of arching action present in edge-stiffened cantilever slab overhangs subjected to a concentrated or wheel load. Various connections and reinforcing details between the traffic barrier wall and cantilever deck slab have been designed and implemented in practice. It is recommended that the common types of connections also be tested to confirm the findings that arching action is the dominant behaviour of a cantilever slab overhang subjected to a wheel load.

Additional full-scale testing should be carried out to investigate the potential design changes or philosophies that take into account the presence of arching action. Static and fatigue destructive testing of a cantilever slab overhang that has been designed taking into account the presence of arching action will provide practicing engineers and owners of structures confirmation that such design philosophies are valid and provide a safe and durable bridge deck slab.

6.2.3 Further Theoretical Modeling

A more detailed and in-depth theoretical investigation should be performed to further determine and understand the mechanisms that contribute to the strong presence of arching action in cantilever slab overhangs. Theoretical modeling carried out for this study

confirmed experimental results with respect to observed ultimate loads and deflection characteristics or behaviour. It is recommended that stresses and strains should be investigated in greater depth to aid in determining the magnitude of arching action present should there be a component of flexure stresses present. Perhaps the principle of superposition may be employed to investigate this recommendation. A more in-depth parametric study should also be carried out to determine which parameters influence the magnitude of arching acting present. These parameters may include cantilever span length, barrier wall connection details, and top and bottom transverse and longitudinal reinforcement ratios.

6.2.4 Proposed Demonstration Project with Civionics and Structural Health Monitoring (SHM)

An important consideration in the progress and advancement of civil engineering is to provide practicing engineers and owners of structures that use the new materials and new design concepts with assurance that they are safe, durable, and more economical than current practices. The presence of arching action in edge-stiffened cantilever slab overhangs reinforced with GFRP is an excellent candidate for a demonstration project. Therefore, it is recommended that a demonstration project that takes into account arching action in bridge deck cantilever slab overhangs, the potential design alternatives mentioned in section 6.2.1, and a complete civionics and structural health monitoring system be implemented on a real bridge structure that is in need of rehabilitation, or a new structure that is in the planning or design stage. Such a project may be implemented on a single span of a bridge in Manitoba or neighboring provinces in Canada.

REFERENCES

AASHTO (2014). *American Association of State Highway and transportation Officials, Standard Specifications for Highway Bridges*. Washington, D.C., U.S.A.

Alves, J., R., El-Ragaby, A. and El-Salakawy, E. (2011). *"Durability of GFRP Bars' Bond to Concrete Under Different Loading and Environmental Conditions"*. ASCE Journal of Composites for Construction, May-June, pp. 249-262.

Bakht, B., Aziz, T.S. and Bantusevicius, K.F. (1979). "Manual analysis of cantilever slabs of semi-infinite width". Canadian Journal of Civil Engineering. Vol. 6(2): 227 - 231.

Bakht, B. (1981). "Simplified Analysis of Edge-Stiffened Cantilever Slabs". ASCE Journal of Structural Engineering. Vol. 22: 514-523.

Bakht, B. and Agarwal, A. (1995). "Deck Slabs of Skew Bridges". Canadian Journal of Civil Engineering. Vol. 103(3): 535-550.

Bakht, B., Mufti, A.A. and Nath, Y. (2006). *ANDECAS6 User Manual - Analysis and Design of Cantilever Slabs*. ISIS Canada Research Network. Winnipeg, Manitoba, Canada.

Bakht, B. and Holland, D.A. (1976). "A manual method for the elastic analysis of wide cantilever slabs of linearly varying thickness". Canadian Journal of Civil Engineering. Vol. 3(4).

Bigaj A.J. (1999). "Structural Dependence of Rotation Capacity of Plastic Hinges in RC Beams and Slabs," PhD Thesis, Faculty of Civil Engineering, Delft University of Technology, Delft, Netherlands, 230 pp.

CAN/CSA S6-06 (2006). "*Canadian Highway Bridge Design Code (CHBDC)", Canadian Standards Association International*. Toronto, Ontario, Canada.

Cervenka, V., Jendele, L., and Cervenka, J., (2007). "ATENA Program Documentation Part 1: Theory," *Cervenka Consulting Ltd.*, Prague, Czech Republic.

Cervenka, V., Jendele, L., and Cervenka, J., (2007). "ATENA Program Documentation Part 2-2: User Manual for ATENA 3D," *Cervenka Consulting Ltd.*, Prague, Czech Republic.

Comité Euro-International du Béton, (1993). "Ceb-Fip Model Code 1990: Design Code," Thomas Telford Services Ltd, Thomas Telford House, London, UK

Desai, Y.M., Mufti A.A., Tadros, G. (2002). *FEMPUNCH – User and theoretical Manual*. ISIS Canada Research Network, Winnipeg, Manitoba, Canada.

Dilger, W.H., Tadros, G.S. and Chebib, J. (1990). "Bending moments in cantilever slabs. Developments in Short and Medium Span Bridge Engineering =90". Canadian Society for Civil Engineering. Vol. 1: 256-276. Montreal, QC, Canada.

Drysdale, R. (1982). "Behaviour of Cantilver Bridge Deck Slabs under Concentrated Loads". Research Report, McMaster University, Hamilton, Ontario, Canada.

Edalatmanesh, R. (2010). "Structural Health Monitoring Model for Fatigue Assessment in Concrete Bridge Decks". Ph. D. Thesis, University of Manitoba, Winnipeg, Manitoba, Canada.

Edalatmanesh, R., Newhook, J. (2013). *"Residual Strength of Precast Steel-Free Deck Panels"*. ACI Structural Journal, Vol. 110, No. 5, September – October, pp. 715-721.

Edalatmanesh, R., Newhook, J. (2013). *"Investigation of Fatigue Damage in Steel-Free Bridge Decks with Application to Structural Health Monitoring"*. ACI Structural Journal, Vol. 110, No. 4, July – August, pp. 557-564.

Eden, R., Eddie, D., Klowak, C., Mufti, A.A., Bakht, B. and Tadros, G., (2004). "First Application of Second-Generation Steel-Free Deck Slabs for Bridge Rehabilitation," Proceedings of the Society of Photo-Optical Instrumentation Engineers (SPIE) 11th Annual International Symposium on Smart Structures and Materials, pp. 86 - 94, San Diego, California, USA, March 14 - 18.

El-Mogy, M.A.. (2011). "Behaviour of Continuous Concrete Beams Reinforced with FRP Bars". Ph. D. Thesis, University of Manitoba, Winnipeg, Manitoba, Canada.

Hewitt, B. E., Batchelor, B. (1975). "Punching shear Strength of Restrained Slabs". ASCE Journal of Structural Division. Vol. 101. pp 1837–1853.

He, Q., Mufti, A.A. (2001). *FEMPUNCH – User and theoretical Manual*. ISIS Canada Research Network, Winnipeg, Manitoba, Canada.

Jaeger, L.G. and Bakht, B. (1990). "Rationalization of simplified methods of analyzing cantilever slabs". Canadian Journal of Civil Engineering. Vol. 17(5): 856 - 867.

Gant, K. and Newhook, J. (1999). *Wheel Load Tests on Cantilever and Internal Panels on Concrete Deck Slab on Steel Girders with and without Bottom Transverse GFRP Reinforcement - Internal Testing Report 99-01*. Dalhousie University, Halifax, Nova Scotia.

Klowak, C. (2007). "Static & Fatigue Behaviour of Bridge Deck Cantilever Overhangs Subjected to a Concentrated Load". M. Sc. Thesis, University of Manitoba, Winnipeg, Manitoba, Canada.

Lahlou, E.H. and Waldron, P. (1992). "Membrane Action in One-way Slab Strips". Proceedings of the Institution of Civil Engineers, Structures and Buildings, 94. November pp. 419-428.
Matsui, S., Tokai, D., Higashiyama, H. and Mizukoshi, M. (2001). "Fatigue Durability of Fibre Reinforced Concrete Decks under Running Wheel Load", Proceedings Third International Conference on Concrete Under Severe Conditions, CONSEC 01, Vancouver,B.C. Vol.1: 982-991

Memon, A.H. (2005). *Comparative Fatigue Performance of Steel-Reinforced and Steel-Free Concrete Bridge Deck Slabs*. (Thesis)

Menetrey, Ph., Walther, R., Zimmerman, Th., Willam, K.J., Regan, P.E. (1997). "Simulation of punching failure in reinforced concrete structures," *Journal of Structural Engineering*, 123 (5)**:** 652-659.

Mufti, A.A., Bakht, B. and Jaeger, L.G. (1993). "Moments in deck slabs due to cantilever loads". ASCE Journal of Structural Division. Vol. 119(6): 1761 - 1777.

Mufti, A.A., Bakht, B., and Jaeger, L.G., (1996). *Bridge Superstructures New Developments*. National Book Foundation, Pakistan, 1996.

Mufti, A. and Bakht, B. (2004). Technical Discussions

Mufti, A., Onofrei, M., Benmokrane, B., Banthia, N., Boulfiza, M., Newhook, J., Tadros, G., Bakht, B. and Brett, P., (2005). "Report on the Studies of GFRP Durability in Concrete from Field Demonstration Structures", Proceedings for the Third International Conference on Composites in Construction (CCC 2005), Lyon, France, July 11 - 13.

Mufti, A.A., Bakht, B., and Nath, Y. (2006). *ANDECAS6 - User and Theoretical Manual*. ISIS Canada Research Network, Winnipeg, Manitoba, Canada.

Mufti, A.A., Bakht, B., and Jaeger, L.G. (2008). "Recent Advances in Bridge Engineering." JMBT Structures research Inc.

Newhook, J.P. and Mufti, A.A., (2003). *PUNCH - User and Theoretical Manual*. ISIS Canada Research Network, Winnipeg, Manitoba, Canada.

Newhook, J., Edalatmanesh, R., (2011). *"Integrating Reliability and Structural Health Monitoring in the Fatigue Assessment of Concrete Bridge Decks"*. Structure and Infrastructure Engineering, Vol. 9, No. 7, July, pp. 619-633.

Onofrei, M. (2005). *Durability of GFRP Reinforced Concrete from Field Demonstration Structures*. ISIS Canada Research Network, Winnipeg, Manitoba, Canada.

Pultrall, Inc. (2007). "Product technical specifications." ADS Composites Group Inc., ⟨http://www.Pultrall.com⟩ (Dec. 2007).

Rizkalla, S., Mufti, A.A. (2001). *Reinforcing Concrete Structures with Fibre Reinforced Polymers - Design Manual #3*. ISIS Canada Research Network, Winnipeg, Manitoba, Canada.

Tadros, G., Bakht, B., and Muft, A. (1994). "Analysis of Egde-Stiffened Cantilver Slabs". Proceedings of Fifth Colloquium on Concrete in developing Countries. Cairo, Egypt.

Tadros, G. (2003). Visual Basic Computer Program for Flexural Analysis of Concrete Structural Members.

Van Mier J.G.M. (1986). "Multi-axial Strain-softening of Concrete, Part I: fracture," *Materials and Structures, RILEM*, 19 (111).